ADVANCING THE DEVELOPMENT OF GLUCOSE-BASED POLYCARBONATES: FROM FUNDAMENTALS TO BIOMEDICAL APPLICATIONS

A Dissertation

by

YUE SONG

Submitted to the Office of Graduate and Professional Studies of
Texas A&M University
in partial fulfillment of the requirements for the degree of

DOCTOR OF PHILOSOPHY

Chair of Committee,	Karen L. Wooley
Committee Members,	James D. Batteas
	François P. Gabbaï
	Kristen C. Maitland
Head of Department,	Simon W. North

August 2020

Major Subject: Chemistry

ABSTRACT

D-Glucose-based polycarbonates represent an attractive class of natural product-based renewable materials due to their facile syntheses, well-defined structures, tunable properties, and promising potentials in biomedical applications. This study emphasizes on advancing the development of D-glucose-based polycarbonates, also named poly(glucose carbonate)s (PGCs), by comprehensive research on fundamental structure, physicochemical property, regiochemistry, and application towards therapeutic delivery.

The fundamental aspects of the relationship between polymer structure and physicochemical property are studied with variation of glass transition temperature (T_g) as a function of the side-chain structure and molar mass for PGCs. A remarkable range of T_g values (38-125 °C) was accomplished with a various of six different alkyloxycarbonyl side chains. The impact of molar mass on T_g was investigated for two series of polymers and discrete oligomers synthesized and fractionated with precise control over the degrees of polymerization. The T_g was found to be significantly influenced by a synergistic effect of the flexibility and volume of the repeating unit side chains, as well as the chain end relative free volume.

Highly regioregular structures were observed for PGCs with carbonate side chains, whereas regioirregularity was found for PGCs with ether side-chain substituents at the 2- and 3- positions. The regiochemical details of PGC were demonstrated through a comprehensive structural investigation using a combination of 1D and 2D NMR characterizations to reveal the backbone connectivity and to demonstrate the curious side-

chain functionality-mediated regiochemical differences. Density functional theory (DFT) calculations were performed to obtain a deep understanding of the regioselectivity during organo-base catalyzed ring-opening reactions.

Lastly, the utilization of PGC in the construction of biocompatible silver-bearing nanocarriers was evaluated. This synthetic polymeric framework focuses upon effective treatment of bacterial infections by improving nanoparticle cell binding and internalization. Degradable and biocompatible polymer nanostructures of spherical, cylindrical, and 2D-platelet-like morphologies were constructed *via* crystallization-driven self-assembly (CDSA) method in aqueous solution. These nanoparticles exhibited negligible toxicity, while offering substantial silver loading capacity, extended release, and *in vitro* antimicrobial activity against uropathogenic *Escherichia coli*. In comparison to spherical analogs, cylindrical and platelet-like polymeric nanostructures engaged in significantly higher association with uroepithelial cells.

DEDICATION

To my mother and father

ACKNOWLEDGEMENTS

I would like to express my sincerest appreciation to my Ph.D. advisor Professor Karen L. Wooley, for her invaluable guidance, unreserved support, and continuous encouragement and trust throughout my graduate study at Texas A&M University, and for her passion, diligence and dedication for doing phenomenal science that continue to inspire me. It is my distinct honor to be Karen's student, and I have learned many valuable lessons from her, both academically and in life, that have furthered my growth as a scientist and as a person. She has provided me with tremendous advice and freedom to explore the fields of polymer chemistry, colloidal science and nanotechnology, taught me the skills and knowledge in scientific research, effective presentation, and scientific writing, and fully supported my research and career development as a young scientist. She has inspired me by her diligence, professionalism, enthusiasm, and kindness, that has shaped me to be the scientist I am today, and will have a long-term influence on me throughout my life.

I would also like to thank Professor François P. Gabbaï for serving on my committee and for providing support and valuable discussions during my CHEM 681 seminar presentation. I also appreciate Professors James D. Batteas and Kristen C. Maitland for their inspirational suggestions and discussions towards the completion of this dissertation while serving on my committee.

I am very grateful to have worked with many brilliant scientists throughout my Ph.D., past and present, in the Wooley research group. I would like to give special thanks

to Dr. Richen Li for his great mentorship and guidance during my Ph.D. study. I would also like to thank Dr. Lu Su, Dr. Rachel A. Letteri, and Dr. Yingchao Chen for their numerous help in my early research development and guidance for my Ph.D. study. I am very fortunate to have Mei Dong as one of my best friends and colleagues for nine years. She has been an outstanding and reliable scientist, and has always been supportive, caring, helpful, and trustful. I would also like to thank my other classmates Jessica Huang, Nari Kang, Yen-Nan Lin, Tan Nguyen, Mariela Vazquez for their friendship and encouragement. We have been through many tough moments together and have supported each other at the hardest moments. I appreciate all the past and current Wooley group members that I have interacted with at Texas A&M University, Ryan Allen, Yingchao Chen, Jeniree Flores Delgado, Benjamin Demor, Mei Dong, Mahmoud Elsabahy, Jingwei Fan, Mona Fattahi, Simcha Felder, Marco Giles, Alexis Gooch, Sarah Hancock, Xun He, Gyu Seong Heo, Jessica Huang, Ashlee Jahnke, Nari Kang, Sarosh Khan, Christopher Komatsu, Samantha Kristufek, Eric Leonhardt, Rachel Letteri, Richen Li, Soon-Mi Lim, Yen-Nan Lin, Mahsa Minaeian, Catherine Morejon-Garcia, Tan Nguyen, Shota Osumi, Ching Pang, Ami Patel, Randinu Pulukkody, Kellie Seetho, Yidan Shen, Travis Smith, Justin Smolen, Lu Su, Guorong Sun, Menaka Tandon, David Tran, Yi-Yun Tsao, Mariela Vazquez, Brooke Versaw, Kevin Wacker, Hai Wang, Fuwu Zhang, Xujia Zhong, Xiang Zhu, and Jennifer Zigmond, for the creative, hard-working, and friendly environment they created that made my experience in the WooleyLab and Ph.D. study exciting and fun. I appreciate many faculty, staff and colleagues from Texas A&M University Department of Chemistry for their help in many aspects.

I would also like to thank Professor David A. Hunstad and his group member Ms. Christina A. Collins at Washington University for their insightful discussions and more than four years of productive collaboration on the bacterial infection treatment project. I would like to thank Professor Darrin J. Pochan and his student Ms. Jee Young Lee, Professor Arthi Jayaraman and her group members Dr. Daniel J. Beltran-Villegas and Mr. Michiel G. Wessels, all from the University of Delaware, and Professor William Johnson and his student Mr. Cesar A. Ron from University of Utah for their multidisciplinary knowledgeable discussions and great patience during our DMREF collaboration of "Interface-promoted Assembly and Disassembly (IpAD) Process for Rapid Manufacture and Transport of Complex Hybrid Nanomaterials" on investigating the polymer self-assembly, simulation, and characterizations.

I gratefully acknowledge the financial support from the National Science Foundation (DMR-1507429, CHE-1610311, and DMREF-1629094), and the Robert A. Welch Foundation through the W. T. Doherty-Welch Chair in Chemistry (A-0001). Uses of Laboratory for Synthetic-Biologic Interactions (LSBI) at Texas A&M University and the Texas A&M Microscopy and Imaging Center (MIC) are also acknowledged.

Finally, I would like to express my love and gratitude to my family, for their unconditional love, understanding, and endless support for my career and life.

CONTRIBUTORS AND FUNDING SOURCES

Contributors

This work was supervised by a dissertation committee consisting of Professor Karen L. Wooley [advisor] of the Departments of Chemistry, Chemical Engineering, and Materials Science & Engineering; Professors James D. Batteas [committee member] and François P. Gabbaï [committee member] of the Department of Chemistry; and Professor Kristen C. Maitland [committee member] of the Department of Biomedical Engineering.

In Chapter II, the ESI and MALDI-TOF MS data was collected by Dr. Yohannes H. Rezenom and Mr. Michael R. Raulerson of the Department of Chemistry. The access of preparative size exclusion chromatography was supported by Professor Lei Fang of the Departments of Chemistry, and Materials Science & Engineering.

In Chapter III, the mass spectrometry data was collected by Dr. Yohannes H. Rezenom of the Department of Chemistry. The DFT calculation was performed by Ms. Xin Yang of the Department of Chemistry, supported and advised by Professor Michael B. Hall of the Department of Chemistry, and the computing resources were provided by Laboratory for Molecular Simulation (https://lms.chem.tamu.edu) and the High-Performance Research Computing Facility (http://hprc.tamu.edu) of the Department of Chemistry.

In Chapter IV, the wide-angle X-ray diffraction data was collected by Dr. Joseph H. Reibenspies of the Department of Chemistry. Mass spectrometry data was collected by Dr. Bo Wang from the Department of Chemistry.

In Chapter V, the *in vitro* epithelial cell binding, confocal and antimicrobial test data for Chapter V was provided by Professor David A. Hunstad of Departments of Pediatrics and Molecular Microbiology, and his lab member Christina A. Collins and Dr. Teri N. Hreha of the Department of Pediatrics at Washington University School of Medicine.

All other work conducted for the dissertation was completed by the student independently.

Funding Sources

Graduate study was supported by a fellowship from Texas A&M University and a dissertation research fellowship from National Science Foundation (CHE-1610311, DMR-1507429, DMREF-1629094), and the Robert A. Welch Foundation through the W. T. Doherty-Welch Chair in Chemistry (A-0001). Uses of the Texas A&M University Laboratory for Synthetic-Biologic Interactions (LSBI) and Texas A&M Microscopy and Imaging Center (MIC) are acknowledged.

Work on DFT calculation (Chapter III) was supported by the National Science Foundation (CHE-1664866) and the Robert A. Welch Foundation (A-0648). Work on the *in vitro* study of epithelial cell binding and antimicrobial test (Chapter V) was supported by National Institutes of Health (R01-DK111541 and T32-DK007126). Confocal data were generated on a Zeiss LSM880 Airyscan confocal microscope, which was purchased with support from the Office of Research Infrastructure Programs (ORIP), part of the Office of the Director, National Institutes of Health, under grant S10-OD021629.

NOMENCLATURE

AFM	Atomic force microscopy
BCP	Block copolymer
$CDCl_3$	Deuterated chloroform
CDSA	Crystallization-driven self-assembly
COSY	Correlated Spectroscopy
CuAAC	Copper(I)-catalyzed azide-alkyne cycloaddition
DBCO	Dibenzylcyclooctyne
DCM	Dichloromethane
DCTB	Trans-2-[3-(4-*t*-butylphenyl)-2-methyl-2-propenylidene]malononitrile
DFT	Density functional theory
DLS	Dynamic light scattering
DMEM	Dulbecco's Modified Eagle's Medium
DMF	*N,N*-Dimethylformamide
DMF-d_7	Deuterated *N,N*-dimethylformamide
DMPA	2,2-Dimethoxy-2-phenylacetophenone
DMSO	Dimethyl sulfoxide
DMSO-d_6	Deuterated dimethyl sulfoxide
D_2O	Deuterium oxide
DOSY	Diffusion-ordered spectroscopy

DSC	Differential scanning calorimetry
DP_n	Degree of polymerization
ESI	Electrospray ionization
FT-IR	Fourier transform infrared spectroscopy
GC(EEC)	Methyl-2,3-*O*-*n*-ethyloxycarbonyl-4,6-*O*-carbonyl-α-D-glucopyranoside
GC(EHEHC)	Methyl-2,3-*O*-2-ethylhexyloxycarbonyl-4,6-*O*-carbonyl-α-D-glucopyranoside
GC(EPC)	Methyl-2-*O*-*n*-ethyloxycarbonyl-3-*O*-propargyloxycarbonyl-4,6-*O*-carbonyl-α-D-glucopyranoside
GC(BBC)	Methyl-2,3-*O*-*n*-butyloxycarbonyl-4,6-*O*-carbonyl-α-D-glucopyranoside
GC(HHC)	Methyl-2,3-*O*-*n*-hexyloxycarbonyl-4,6-*O*-carbonyl-α-D-glucopyranoside
GC(isoBBC)	Methyl-2,3-*O*-isobutyloxycarbonyl-4,6-*O*-carbonyl-α-D-glucopyranoside
GC(neoPPC)	Methyl-2,3-*O*-neopentyloxycarbonyl-4,6-*O*-carbonyl-α-D-glucopyranoside
GC(OEHEH)	Methyl-2,3-*O*-2-ethylhexyl-4,6-*O*-carbonyl-α-D-glucopyranoside
HCl	Hydrochloric acid
HMBC	Heteronuclear multiple bond correlation
HPLC	High performance liquid chromatography

HSQC	Heteronuclear single quantum coherence
ICP-MS	Inductively coupled plasma mass spectrometry
KTFA	Potassium trifluoroacetate
MALDI-TOF	Matrix assisted laser desorption ionization-Time of flight
4-MeBnOH	4-Methylbenzyl alcohol
MIC	Minimum inhibitory concentrations
M_n	Number-average molar mass
MS	Mass spectrometry
MWCO	Molar mass cut-off
NMR	Nuclear magnetic resonance spectroscopy
NP	Nanoparticle
PBS	Phosphate buffered saline
PDGC	Poly(D-glucose carbonate)
PEG	Poly(ethylene glycol)
PGC	Poly(glucose carbonate)
PLLA	Poly(L-lactide)
ROP	Ring-opening polymerization
SCK	Shell crosslinked knedel-like
SEC	Size exclusion chromatogrphy
SPAAC	Strain-promoted azide-alkyne cycloaddition
TBD	1,5,7-Triazabicyclo[4.4.0]dec-5-ene
TEM	Transmission electron microscopy

T_g	Glass transition temperature
TGA	Thermogravimetric analysis
T_m	Melting temperature
TS	Transition state
THF	Tetrahydrofuran
UPEC	Uropathogenic *Escherichia coli*
UTI	Urinary tract infection
UV/Vis	Ultraviolet visible spectroscopy
WAXD	Wide-angle X-ray diffraction

TABLE OF CONTENTS

Page

LIST OF FIGURES

Page

LIST OF TABLES

Page

CHAPTER I

INTRODUCTION

1.1 Sustainable Functional Polymer

The pursuit of sustainable materials from renewable resources is growing and evolving at unprecedented rates. Natural product-based degradable polymers obtained from renewable resources enhance the appeal of polymeric materials by reducing environmental/biological hazards as well as the dependency on petrochemicals.[1-8] However, the current use and application of such naturally-derived polymers are still quite limited compared to petrochemically-derived polymers. Several types of polymers from renewable resources, including polyesters, polycarbonates, polyphosphoesters, and polypeptides, have been reported and utilized for a variety of applications, including hydrogel, battery, and nanomedicine.[9-12]

With an interest in developing synthetic methodologies by which to transform natural products into functional polymer materials,[8, 13] many research activities have led to development of monomers and polymers with labile backbone chemistries.[14-17] Numerous studies on the development of sugar-based polymers over the past decades have dedicated to exploring the diversity of monomer structure, functionality, different polymerization methods using well-defined chemistries, and utilization in various practical applications.[18-22] To date, sugar-based cyclic carbonate monomers of D-mannose, D-glucose, D-xylose, and deoxy-D-ribose have been studied, and their

polymers offered high degrees of functionality and regiochemical diversity for the tailoring of composition, structure, and property.

Despite advantages for introducing functionalities and modifying polymer properties (such as glass transition temperature, solubility, and crystallinity), the high hydroxyl group content of sugars often entails the use of protecting group chemistry to avoid undesired reactions during subsequent ring-opening polymerization (ROP). The synthetic routes for glucose carbonate monomers were developed and optimized within 3~4 steps from methyl 4,6-*O*-benzylidene-α-D-glucopyranoside.[23] A cyclic carbonate structure that is suitable for the subsequent ROP can be synthesized using a diol of the glucopyranoside and a carbonyl donor, such as phosgene derivatives or carbon dioxide, upon cyclocarbonation.[24-26] The six-membered cyclic carbonate is then installed in the 4- and 6-positions of glucose, with the 1-position protected by a methyl group and the 2- and 3-positions being either alkylated or carrying hydrolytically-labile and functional carbonate protecting groups.[23, 27-29] The functional side-chain protecting groups are particularly attractive, as they allow for post-polymerization chemical diversification (**Scheme I.1**). Another type of five-membered cyclic carbonate has been prepared through cyclization of the 2- and 3-positions, leaving 4- and 6-positions protecting with benzylidene group, which would afford hydrophilicity with hydroxyl groups upon deprotection.[30-31] Because of the superior performance of the six-membered D-glucose-based cyclic carbonates regarding reactivity, functionality, control of polymer molar mass and molar mass dispersity, they have been utilized frequently in versatile applications.

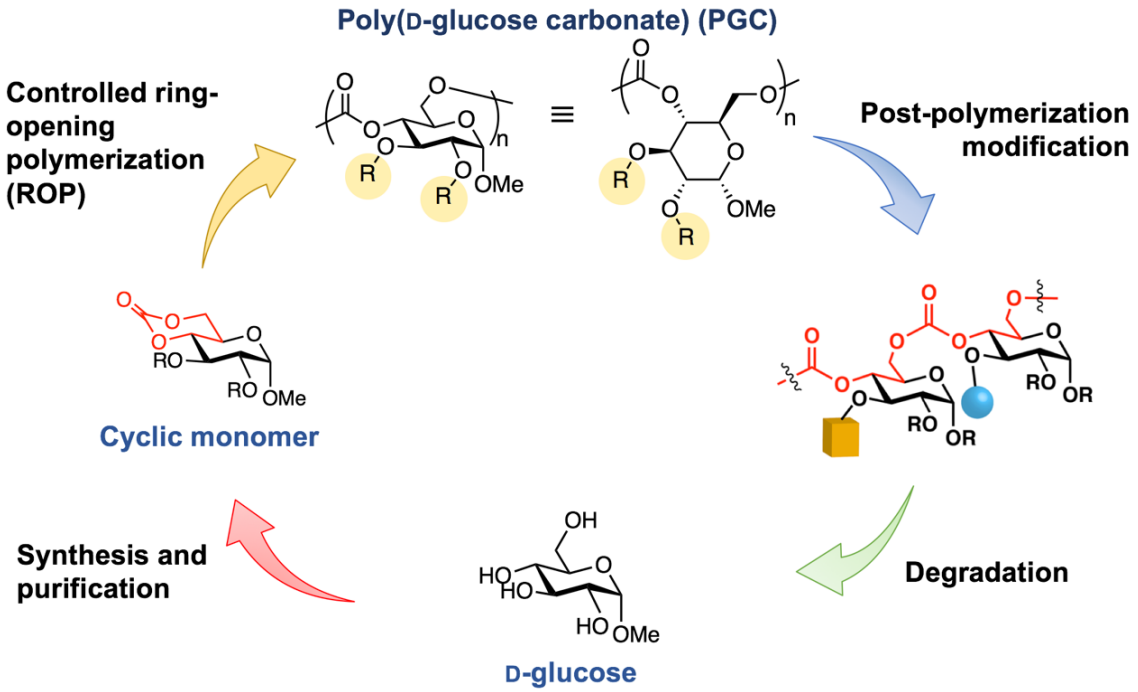

Figure I.1 Synthesis, functionalization and degradation of poly(D-glucose carbonate).

1.2 ROP and Post-Polymerization Modification

Primary approaches for the construction of well-controlled natural product-based polycarbonates lie in ring-opening (co)polymerizations (**Scheme I.2**). The alternating ring-opening copolymerizations of epoxide/carbon dioxide, pioneered by Darensbourg and Coates, offer an beneficial strategy by the use of carbon dioxide.[32-34] While various substrates have been reported to be amendable, such as limonene oxide,[35] this method essentially requires the use of air-sensitive metal complex catalysts, and often leads to the formations of five-membered byproducts and ether linkages in the resulting polymer backbones.[36] In comparison, ROPs directly from a cyclic carbonate monomer provide a versatile polymerization method that requires mild reaction conditions while rendering

living characteristics.[37-41] The guanidine organocatalyst, 1,5,7-triazabicyclo[4.4.0]dec-5-ene (TBD), has demonstrated high reactivity and excellent control of polymer molar mass and dispersity in ROPs, and has been widely applied for the polymerization of a various of cyclic monomers, such as lactide, caprolactone, phosphoester, and carbonate, in the presence of an alcohol/amine initiator.[42-48] Due to the excellent polymerization controllability and absence of metal, ROP is well-suited as a method for synthesis of a broad range of hydrolytically-labile polymers for study self-assembly properties and thereby use in delivery of small molecules for biomedical applications.

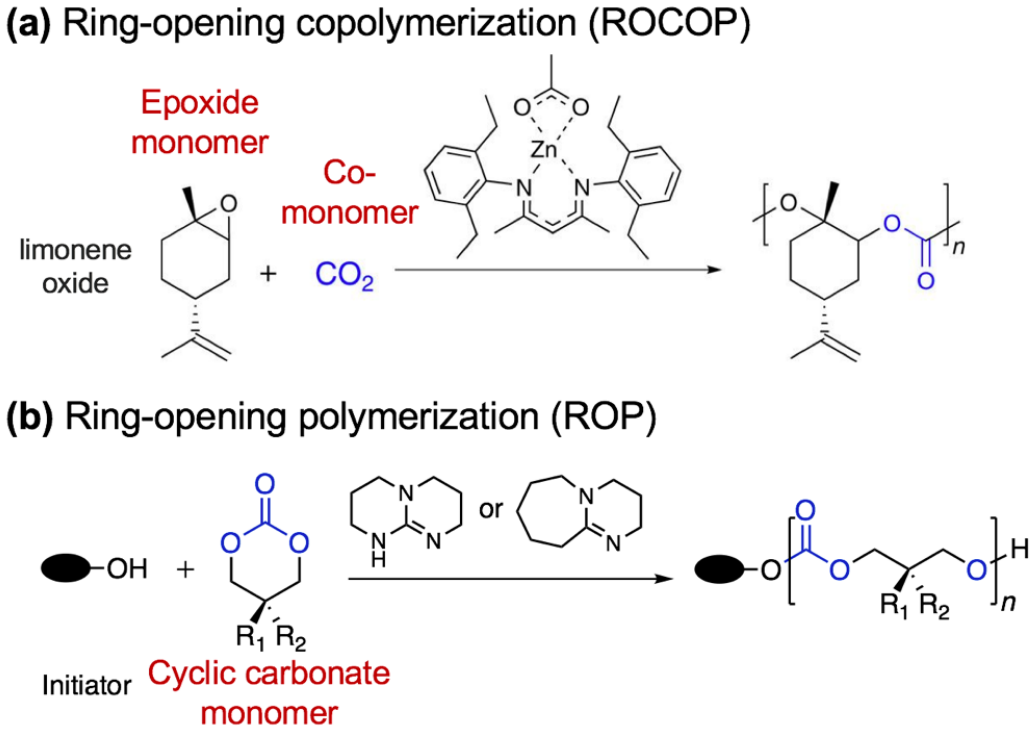

Figure I.2 Synthetic schemes of (a) alternative ring-opening copolymerizations, and (b) ring-opening polymerization.

Polymer design can start at the monomer level to have various side-chain groups or functional linkages installed, thereby affecting the structure and property of resulting polymers through the change of molar mass, dispersity, or side-chain compositions. The processes of polymerization could restrict the types of reactive functional groups present in the monomer, such as charged groups and alcohol/amine nucleophiles; therefore, post-polymerization modifications will be required to incorporate diverse functionalities in designing new synthetic pathways towards complex polymers.[49-51]

The "click" chemistry is a concept introduced by Sharpless in 2001,[52] and has demonstrated a number of success in polymer modification under various conditions over the past decades.[53] Indeed, these reactions are tolerant to a wide range of functional groups and can be carried out in a wide range of solvents. The most powerful and widely utilized click reactions in polymer chemistry are Cu(I) catalyzed azide-alkyne cycloaddition[54-56], thiol-ene/-yne (**Scheme I.3**),[57-59], Michael addition,[60-61] oxime ligation,[62-63] Diels-Alder,[64] thio-bromo,[65-67] and amine/thiol-epoxy reactions.[68-70] The use of these facile and efficient coupling reactions has enabled the design of numerous polymeric materials tailored to specific applications such as biosensors, microfluidics, and targeted drug delivery.

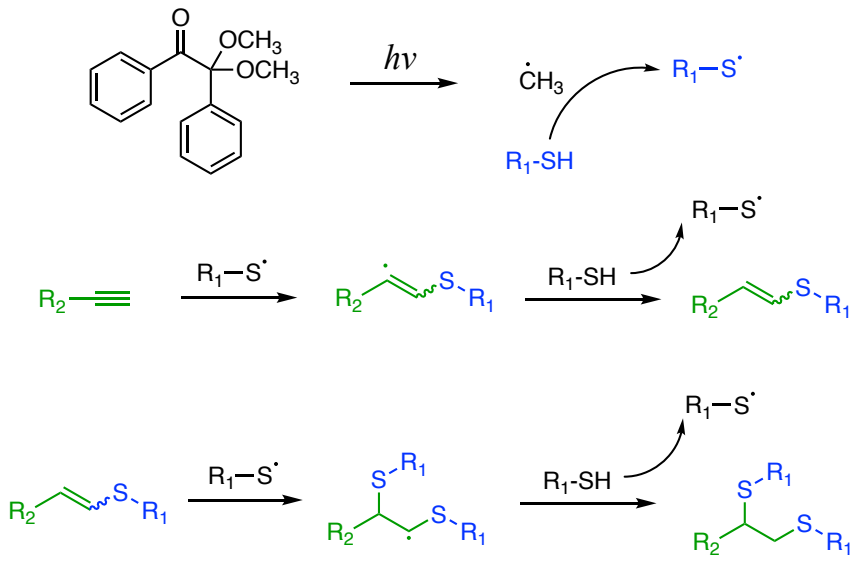

Figure I.3 Mechanism of thiol-yne click chemistry with an alkyne functional group.

1.3 Amphiphilic Block Copolymers & Self-assembly

Block copolymers with distinct hydrophilic and hydrophobic segment, or amphiphilic block copolymers, the macromolecular analogs of Nature's simple amphiphiles, are a broad class of neutral and charged polymer structures that are soluble or dispersible in water. Amphiphilic block copolymers are attractive for applications ranging from biomedicine to engineering materials due to the tunability of their chemical composition, post-polymerization functionalities, block length ratios, and molar mass. In biomedicine, amphiphilic block copolymers have established themselves as effective building blocks for the preparation of micellar nanoparticles for drug delivery.[71] Degradable nanoparticles are frequently used to improve the therapeutic effectiveness of various drugs and bioactive molecules by improving biocompatibility and reducing the accumulation of polymers.[71-76] In engineering applications, amphiphilic block

copolymers provide aqueous stability, increased elasticity, shape memory properties,[77] and stimuli responsiveness.[78] The substantial advances in biomaterials enabled by amphiphilic block copolymer structures, including polymer backbone composition, side-chain functionalities, nanoscale polymer assemblies, and macroscopic hydrogel networks, inspire the continual development of amphiphilic copolymers tailored to meet many diverse needs in nanomedicine and engineering.

One methodology used to produce hydrophilic polymers is incorporating hydrophilic moieties or hydrophilic polymer poly(ethylene glycol) (PEG) onto one of the diblock copolymer segments through selective chemical reactions upon post-polymerization modification. These hydrophilic functional groups/chains are frequently used to functionalize polymers as they are feasibly conjugated to the polymer through straightforward azide-alkyne cycloaddition or thiol-ene/thiol-yne "click" reactions. The balance of charges affords the polymer stability in solutions, provides excellent biocompatibility, and, in some cases, stimuli-responsive behavior.[79-80]

Supramolecular self-assembly techniques have provided versatile approaches by which to assemble polymer chains into well-defined three-dimensional core-shell nanostructures selectively. Block copolymer composition drives function of self-assembled NPs for delivery of small-molecule cargo.[81] Conventional micelles and vesicles constructed from hydrophilic-hydrophobic AB diblock copolymers assemble, to minimize the energetically unfavorable hydrophobe-water interactions, where the resulting structure dictated by the volume fraction of hydrophobic component.[82] This ratio of hydrophobic to hydrophilic components will affect the morphology of the assemblies,

which would significantly impact the properties and efficacy of amphiphilic block copolymers. Advances in polymer chemistry have greatly expanded the variety of morphologies of amphiphilic diblock copolymers, including cylinders/worm-like,[83-84] segmented cylinders,[85] and vesicles.[86-87] Specific nanostructure morphologies can be targeted by tuning the hydrophobic-to-hydrophilic ratio of the block copolymer, adjusting the solution conditions, or incorporating semicrystalline domains to trigger crystallization-driven self-assembly (CDSA) (**Figure I.4**).[88] CDSA is an advanced self-assembly method pioneered by Manners and Winnik,[89] and further broadened to the field of polyesters by O'Reilly and Dove for tailoring hierarchical macromolecular micelle architectures.[90]

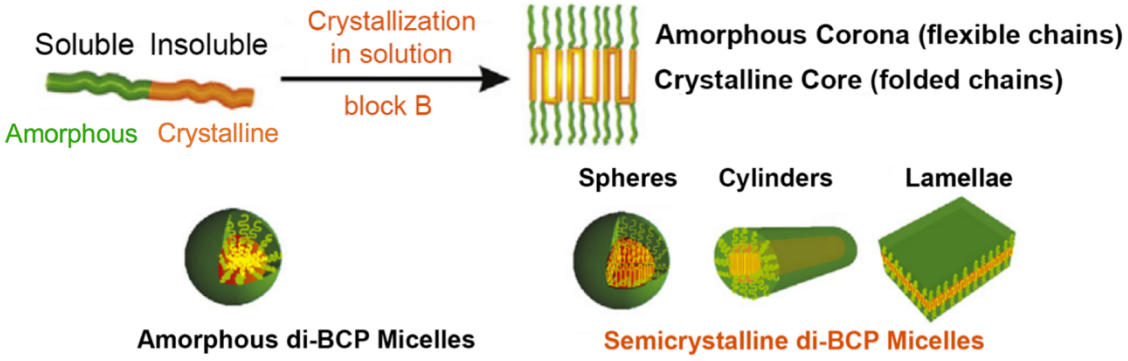

Figure I.4 Illustration of the CDSA process.[88]

1.4 Nanomedicine

The assembled polymeric micellar nanoparticles are emerging as a powerful platform and potentially excellent candidate for delivery of small molecule-cargo due to

their biocompatibility and versatile functionality (**Figure I.5**).[91-92] Polymers with varying degradation rates and mechanical properties have long been of interest for the design of biomaterials. Such materials are designed to decompose and regenerate biologically and environmentally resorbable natural products under normal or extreme conditions.[93] Among potential natural product feedstocks, naturally-derived polycarbonates have received considerable attention, as they are abundant in Nature, inexpensive, biocompatible, and exhibit considerable structural diversity.[94-95] Specifically, glucose based polycarbonates have received recent attention due to their ability to degrade into carbon dioxide, glucose and other benign small molecules.[14, 27-28, 96] Another type of biorenewable and hydrolytically degradable polymers are polyesters. For instance, polylactides are currently produced on the million-kilogram scale in the United States for packaging and clothing applications.[4]

Amphiphilic block copolymers comprising hydrophilic segment of neutral (PEG), cationic, anionic, or zwitterionic charges, and an amorphous or semicrystalline hydrophobic segment, allow for self-assembly into different morphological configurations. Among various micellar nanostructures, cylindrical block copolymer assemblies have been shown to serve as host systems for small drug molecule guests with higher loading capacities and faster rates of release than simple spherical counterparts.[97] Moreover, rod-like nanostructures have been found to have higher binding affinities to certain cells and can be internalized more rapidly and efficiently.[98-99] Such complex polymer assemblies are being developed for biomedical applications of drug delivery and pH sensing.

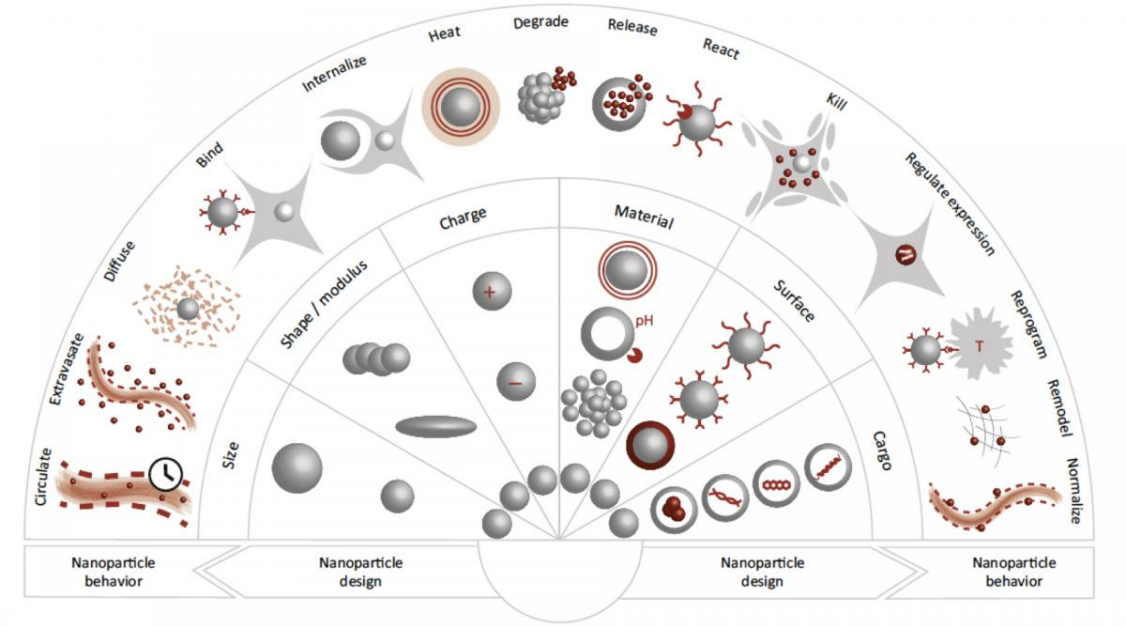

Figure I.5 Design of polymeric nanoparticles for cargo delivery.[92]

1.5 Scope of the Manuscript

In this dissertation, we seek to address the two outstanding critical challenges associated with sustainable synthetic sugar based polymers: physicochemical property tunability, backbone regiochemistry linkages, and their usage as compatible nanomaterials in biomedical applications, by using fundamental principles of organic chemistry and establishing structure-property-morphology relationships. Based on preliminary success developed by the team, we will develop highly controllable glucose-based polycarbonates through an integrated approach combining chemistry and theory. We anticipate gaining a full understanding of the structure-property-architecture relationship that can be broadened to other substrates in macromolecular community.

This dissertation will describe investigations of the synthesis, structure, property and application of functional polymers derived from D-glucose. The intent of this dissertation is to address issues of synthesis and degradability of amphiphilic block copolymers, supramolecular assembly of semicrystalline segment-containing polymers driven by crystallization process, assembly of polymers under different conditions and promoted by interfacial interactions, and design of materials for specialty biomedical applications. Moreover, the diversity and availability of nanostructured materials that possess unique, multiple properties and functions will be enhanced.

In Chapter II. fundamental studies that gain an understanding of the tunability of physical properties of PGCs are vital for optimizing their performance in extensive applications. Variation of T_g was studied as a function of the side chain structure and molar mass for linear PGCs. A remarkable range of T_g values, from 38 to 125 °C, was accomplished with six different alkyloxycarbonyl side chains. The impact of molar mass on T_g was investigated for two series of polymers and discrete oligomers synthesized and fractionated with precise control over the degrees of polymerization, with T_g variations among wide ranges of 13–125 °C and -25–38 °C for neopentyl and 2-ethylhexyl substituted PGCs, respectively, as molar mass increased from unimer to polymer. The T_g was found to be greatly influenced by a synergistic effect of the flexibility and bulkiness of the repeating unit side chain, as well as the chain end relative free volume. This work represents an important advance in the development of glucose-based polycarbonates, as materials that possess high degrees of functionalizability to be capable of exhibiting diversified physicochemical and thermal properties by simple side chain modification.

In Chapter III, the differential regiochemistries observed during ROP of cyclic carbonates derived from glucose and having carbonate *vs.* ether side chain functionalities were studied. Experimentally, highly regioselective ROP was achieved using glucose carbonate monomers with carbonate-side-chains, whereas regioirregularity was observed for polymers having ether-type side-chain substituents. Given the importance of regiochemistry in regulating polymer properties, a comprehensive experimental and theoretical study were carried out to elucidate the mechanistic origins for the curious regiochemical differences in a series of PGCs, providing structural details for the ring-opening process. Unimers and dimers from ROP initiation and propagation processes, respectively, were isolated using chromatographic techniques and identified by a combination of 1D and 2D NMR analyses. The glucose carbonate monomer with carbonate side chains exhibited regioisomeric preference of *C-O4* bond cleavage, as revealed by $^{1}H–^{13}C$ heteronuclear multiple-bond correlation (HMBC) spectroscopy, leading to the 4-to-6 polymerization direction and a head-to-tail (H–T) regioregular structure of the resulting carbonate-substituted PGC. In contrast, both *C-O4* and *C-O6* bond cleavages were observed in ROP of glucose carbonates with ether side chains, resulting in regioirregularity of the final ether-substituted PGC (**Figure I.6**). DFT calculations were carried out to understand the reactivity and regioselectivity of the reactions based on different monomer structures. Overall, this work provides a fundamental understanding of the regiochemistry of organocatalytic ROP of six-membered asymmetric cyclic glucose carbonates with varying side chain chemistry.

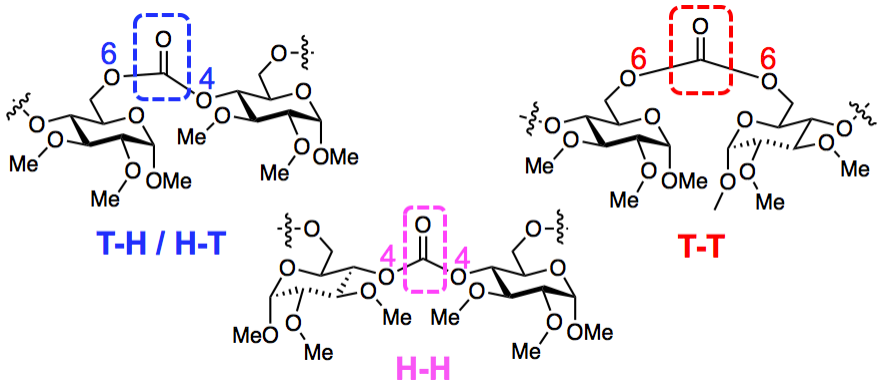

Figure I.6 Polymer regiochemistry: different types of backbone linkages.

In Chapters IV and V, fully degradable amphiphilic block polymers derived from glucose carbonate, in combination with other two natural products, L-lactide and L-cysteine, were prepared for the understanding of the supramolecular self-assembly and biomedical application as drug delivery nanocarriers (**Figure I.7**). In Chapter IV, a series of functional L-cysteine-modified diblock copolymers, poly(L-lactide)-*block*-poly(α-D-glucose carbonate)s (PLLA-*b*-PDGC-cys), was synthesized by organocatalyzed sequential ROPs of L-lactide and an alkyne-substituted bicyclic a-D-glucose carbonate GC(EPC), followed by UV-initiated thiol-yne "click" reaction with L-cysteine to render the PDGC block hydrophilic. CDSA was employed to afford nanostructures of various morphology. Incubation of the PLLA-*b*-PDGC-cys diblock copolymers in water at 65 °C for 30 h, followed by cooling to room temperature yielded spherical, cylindrical and 2D platelet-like bundled cylinder micellar nanostructures, dictated by the PLLA weight percentage in the block copolymer). ^{1}H NMR spectroscopy was employed to monitor the degradation of the materials over 100 d in aqueous solution at pH 1 and 10 at 37 °C, which allowed

for characterization of the stability of the micelles, and for determination of the hydrolytic degradability of the polymer backbone and cleavage of the side chain moieties. Electrospray ionization (ESI) and matrix-assisted laser desorption/ionization-time of flight (MALDI-TOF) mass spectrometry were used to identify the hydrolytic degradation products of the copolymers. Overall, this work broadens the scope of CDSA to functional, natural-product based degradable block copolymers (BCPs), and the polymeric nanomaterials synthesized in this work hold promise in drug and antimicrobial delivery applications, among others.

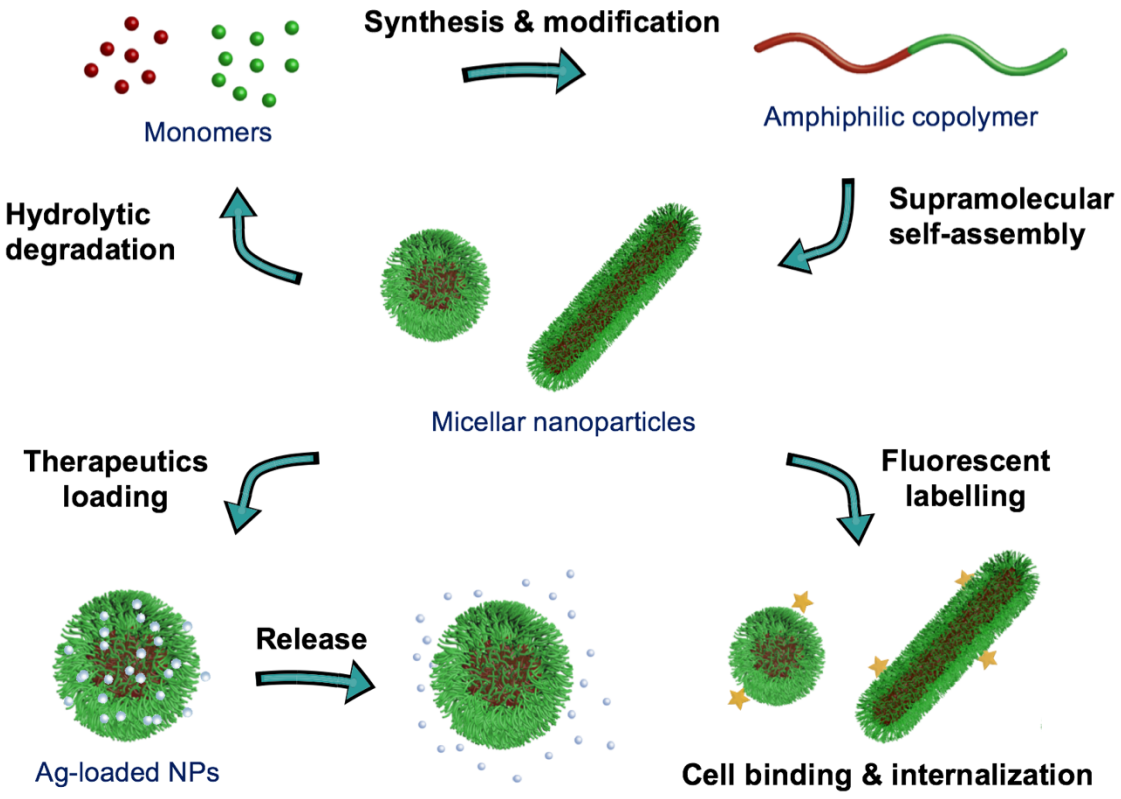

Figure I.7 Schemetic illustration of design of polymeric nanomaterials for nanomedicine applications.

The findings in Chapter IV were then applied to Chapter V to investigate the behaviors and performances of the polymers in biomedical applications. Platelet-like and cylindrical nanostructures from biocompatible sugar-based polymers were found to mimic the aspect ratio of bacteria and achieve uroepithelial cell binding and internalization, thereby improving their potential for local treatment of recurrent urinary tract infections. Polymer nanostructures that have demonstrated the ability of tunable morphology and versatile functionality, derived from amphiphilic block polymers composed of zwitterionic poly(glucose carbonate) and semicrystalline polylactide segments, were the reconstructed with conjugated fluorescent dyes to investigate their uroepithelial cell binding activities. These nanoparticles exhibited negligible cytotoxicity, immunotoxicity, and cytokine adsorption, while also offering substantial silver cation loading capacity, extended release, and *in vitro* antimicrobial activity (as effective as free silver cations) against uropathogenic *Escherichia coli*. In comparison to spherical and cylindrical analogs, platelet-like nanostructures engaged in significantly higher association (*i.e.* binding and internalization) with uroepithelial cells, as measured by flow cytometry; despite their larger size, platelet-like nanostructures maintained the capacity for cell internalization. This work establishes initial evidence of platelet-shaped nanostructures as versatile therapeutic carriers for epithelial infections.

CHAPTER II

ADVANCING THE DEVELOPMENT OF HIGHLY-FUNCTIONALIZABLE GLUCOSE BASED POLYCARBONATES BY TUNING OF THE GLASS TRANSITION TEMPERATURE*

2.1 Introduction

Development of sugar-based monomers and polymers is particularly intriguing and has been a growing area for decades due to their biocompatibility, degradability, structural diversity, and functionalization potential that enables fine tuning of their physical proprieties.[20, 100] The drive to promote the application of such materials in various fields prompted the development of a wide range of well-controlled polymerization methodologies[21, 26, 101] as well as the investigation of their fundamental properties.

The ability to modulate the physical properties of synthetic polymers is highly desirable, as they affect the behavior and performance of these materials in practical applications. The relationship between the T_g and polymer structures has been attracting enduring fundamental and practical research interest, however, such studies have not yet been explored for sugar-based renewable polymer systems. Previous research has demonstrated relatively high T_g for sugar-based polycarbonates,[27-28, 102] arising from their inherently rigid backbone containing cyclic glucose building blocks, which potentially

---

*Reprinted (adapted) with permission from "Advancing the development of highly-functionalizable glucose based polycarbonates by tuning of the glass transition temperature" by Song, Y; Ji, X.; Dong, M.; Li, R.; Lin, Y.-N.; Wang, H.; Wooley, K. L., *J. Am. Chem. Soc.* **2018**, *140* (47), 16053-16057. Copyright 2018 American Chemical Society.

limits the variety of applications of these durable materials. Therefore, tailoring and broadening the T_g range of sugar-based polycarbonate materials would further enable their usage in fields such as stretchable and self-healing materials,[103] drug delivery vehicles,[104] and soft implants/scaffolds.[105]

Variation of T_g has been extensively studied for traditional linear polymers and dendrimers, where T_g is shown to correlate with certain parameters, including molar mass,[106-107] chemical composition of the backbone,[108] steric hindrance of substituents,[109-110] side chain flexibility,[111] chain-end composition,[112] intermolecular interaction between polymer chains,[113] crosslinking density[114], and dispersity.[115] Under the guidance of polymer physics, various methods have been utilized in tailoring T_g. Mandelkern and coworkers studied the influence of side chain length on the T_g of poly(*n*-alkyl methacrylates).[116] More recently, Muñoz-Guerra, Galbis and coworkers reported the dependence of T_g on the compositions and functionality of a series of degradable linear polyesters and copolyesters from bicyclic acetalized monosaccharide monomers.[117-118] Boutevin and coworkers reported the achievement of linear and branched isosorbide-based polyhydroxyurethanes with low T_g by varying the flexibility and toughness of the polymer backbone.[119] Although the strategies for tuning T_g have been continuously explored, there has been a lack of molecular engineering directed towards the investigation of T_g on renewable polymers.

The synthesis of novel glucose-based polymers allows the structure to be tailored at the monomer level for a specific property and expands the scope of available structures beyond those found in Nature. In earlier studies, we have demonstrated the versatility of

glucose carbonate monomers and polymers with modifications of the pendent hydroxyl groups on the 2,3-*O* positions.[96, 120] In this work, we report variation of T_g for poly(glucose carbonate)s by systematically changing the alkyloxycarbonyl side chains of their constituent monomers. The dependency of T_g on molar mass was investigated within two polymer systems, both showing an exciting √-shaped plot of T_g *vs* log M_n.

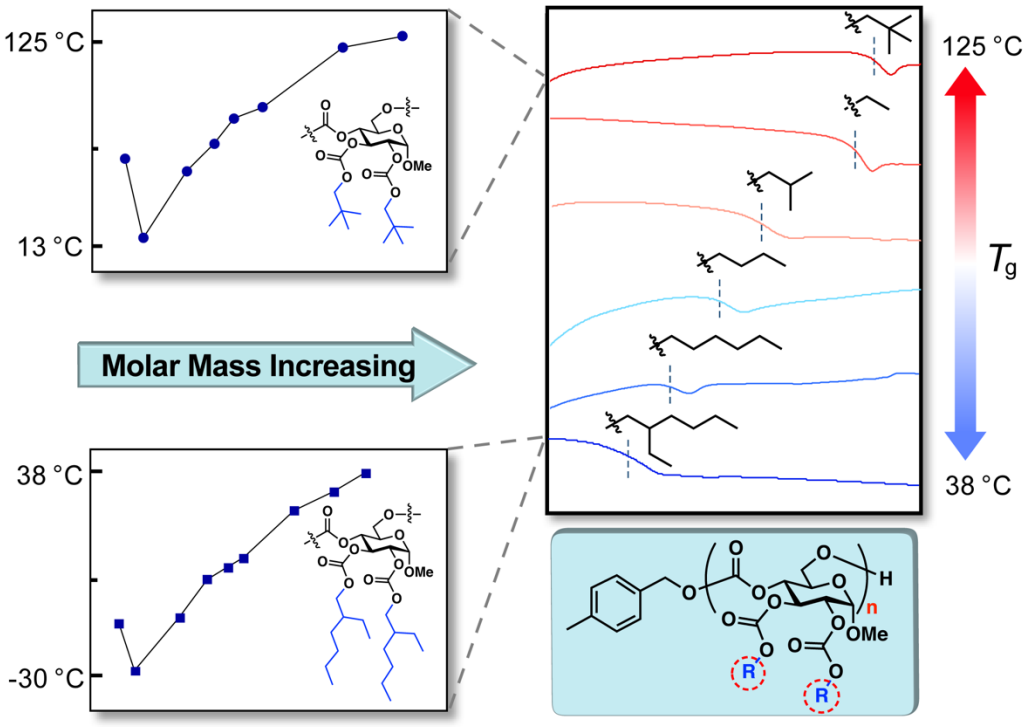

Figure II.1 Side-chain structure mediated glass transition temperatures of PGC. Reprinted (adapted) with permission from [29].

2.2 Materials and Methods

2.2.1 Materials

1,5,7-Triazabicyclo[4.4.0]dec-5-ene (TBD) and 2-ethylhexyl chloroformate were used as received from TCI America (Portland, OR). 4-Methylbenzyl alcohol was purified by recrystallization from petroleum ether and stored in a glovebox under Ar atmosphere. Amberlyst® 15 (H), ion exchange resin and *N,N,N′,N′*-tetramethylethylenediamine, 99% were purchased from Alfa Aesar, Thermo Fisher Scientific (Ward Hill, MA). Triphosgene was used as received from Oakwood Products, Inc. (Estill, SC). Dichloromethane (DCM) was purified by a solvent purification system (J. C. Meyer Solvent Systems, Inc., Laguna Beach, CA). Other reagents were used as received from Sigma-Aldrich, Co. (St. Louis, MO) unless otherwise noted.

2.2.2 Instrumentation

^{1}H NMR and ^{13}C NMR spectra were acquired on a Varian Inova 500 spectrometer interfaced to a UNIX computer using VnmrJ software. Chemical shifts were referenced to the residual solvent resonance signals. Fourier transform infrared (FT-IR) spectra were recorded on an IR Prestige 21 system (Shimadzu Corp., Japan), equipped with an attenuated total reflectance (ATR) accessory, and analyzed using IRsolution v. 1.40 software.

Size exclusion chromatography (SEC) eluting with THF was conducted on a Waters Chromatography, Inc. (Milford, MA) system equipped with an isocratic pump

(model 1515), a differential refractometer (model 2414), and a four-column set, including a 5 μm Guard column (50 × 7.5 mm), a PLgel 5 μm Mixed C column (300 × 7.5 mm, Agilent Technologies) and two Styragel® columns (500 Å and 104 Å, 300 × 7.5 mm, Waters Chromatography, Inc.). The system was equilibrated at 40 °C in THF with the flow rate set to 1.0 mL/min. Data collection and analysis were performed with Waters Breeze™ software. Molar masses were determined relative to polystyrene standards (615-442800 Da) purchased from Polymer Laboratories, Inc. (Amherst, MA). Polymer solutions were prepared at a concentration of *ca.* 3 mg/mL with 0.05 vol% toluene added as a flow marker, and an injection volume of 200 μL was used.

Preparative size exclusion chromatography (prep SEC) eluting with chloroform was conducted on a JAI LC-9230II NEXT Chromatography, Inc. (Japan) system equipped with a reciprocating double plunger pump (model P-9104B), a UV-vis 4ch NEXT detector at four wavelengths (254 nm, 280 nm, 300 nm, 330 nm), and a two-column set, including a JAIGEL-H 40P Guard column and a JAIGEL-2H-40 HPLC column. The system was equilibrated at room temperature in chloroform with the flow rate set to 14.0 mL/min. Data collection and analysis were performed with JAI Scan™ software. Polymer solutions were prepared at a concentration of *ca*. 10 mg/mL in chloroform and an injection volume of 5 mL was used.

Thermogravimetric analysis (TGA) was performed under an Ar atmosphere using a Mettler-Toledo model TGA2/1100/464 with a heating rate of 10 °C/min. Data were analyzed using Mettler-Toledo STAR^e v. 15.00a software. Glass transitions (T_g) were measured by differential scanning calorimetry (DSC) on a Mettler-Toledo

DSC3/700/1190® (Mettler-Toledo, Inc., Columbus, OH) under $N_{2(g)}$. Measurements were performed with a heating rate of 10 °C/min and analyzed using Mettler-Toledo Star^e v. 15.00a software. The T_g was taken as the midpoint of the inflection tangent of the second heating scan.

Electrospray ionization mass spectrometry (ESI-MS) experiments were performed using a Thermo Scientific Q Exactive Focus. The sample was directly infused at a flow rate of 10 μL/min. The Q-Exactive Focus HESI source was operated in full MS in positive mode. The mass resolution was tuned to 70000 FWHM at m/z 200. The spray voltage was set to 3.75 kV, and the sheath gas and auxiliary gas flow rates were set to 7 and 0 arbitrary units, respectively. The transfer capillary temperature was held at 320 °C. Exactive Series 2.8 SP1/Xcalibur 4.0 software was used for data acquisition and processing.

Matrix-assisted laser desorption ionization-time of flight mass spectrometry (MALDI-TOF MS) was performed on a microflex™ LRF mass spectrometer (Bruker Corporation, Billerica, MA) in positive linear mode. Ions were generated by a pulsed nitrogen laser (337 nm, 25 kV), and 200 laser pulses were used per spectrum. Trans-2-[3-(4-*tert*-butylphenyl)-2-methyl-2-propylidene]malonitrile (DCTB) and potassium trifluoroacetate (KTFA) were used as a matrix and cationization reagent, respectively. The sample and matrix were prepared at 1 and 26 mg/mL, respectively, in chloroform, and KTFA was prepared at 1 mg/mL in acetone. The sample solution was mixed with the matrix and KTFA at a volumetric ratio of 2:2:1, and 1 μL of the mixture was deposited onto a stainless-steel sample holder and dried in air prior to the measurement.

2.2.3 Experimental procedures

Synthesis of the bicyclic glucose carbonate monomers were performed following previously reported procedures,[27] using the corresponding alkyl chloroformates as starting materials. For simplicity, these monomers are systematically named: methyl-2,3-*O*-*n*-ethyloxycarbonyl-4,6-*O*-carbonyl-α-D-glucopyranoside GC(EEC) (**1**), methyl-2,3-*O*-*n*-butyloxycarbonyl-4,6-*O*-carbonyl-α-D-glucopyranoside GC(BBC) (**2**), methyl-2,3-*O*-*n*-hexyloxycarbonyl-4,6-*O*-carbonyl-α-D-glucopyranoside GC(HHC) (**3**), methyl-2,3-*O*-isobutyloxycarbonyl-4,6-*O*-carbonyl-α-D-glucopyranoside GC(isoBBC) (**4**), methyl-2,3-*O*-neopentyloxycarbonyl-4,6-*O*-carbonyl-α-D-glucopyranoside GC(neoPPC) (**5**), and methyl-2,3-*O*-2-ethylhexyloxycarbonyl-4,6-*O*-carbonyl-α-D-glucopyranoside GC(EHEHC) (**6**).

The monomers **1**–**5** were purified by column chromatography and recrystallization in ethyl acetate and hexanes, while monomer **6** was a liquid/wax like compound that was purified by column chromatography and extensive drying against phosphorous pentoxide under reduced pressure.

Monomer GC(BBC) (2): ^{1}H NMR (500 MHz, $CDCl_3$, ppm): δ 5.40 (dd, J = 10, 10 Hz, 1H, 3-C*H*), 5.08 (d, J = 4 Hz, 1H, 1-C*H*), 4.71 (dd, J = 10, 4 Hz, 1H, 2-C*H*), 4.53 (m, 1H, 6-CH_2), 4.33 – 4.25 (m, 1H, 6-CH_2), 4.25 – 4.09 (m, 6H, 4-C*H*, 5-C*H*, 2,3-CHOCOCH_2CH$_2$CH$_2$CH$_3$), 3.47 (s, 3H, 1-CHOCH_3), 1.71 – 1.59 (m, 4H, 2,3-CHOCOCH$_2$CH_2CH$_2$CH$_3$), 1.40 (m, 4H, 2,3-CHOCOCH$_2$CH$_2$CH_2CH$_3$), 0.94 and 0.93 (t, J = 7 Hz, 6H, 2,3-CHOCOCH$_2$CH$_2$CH$_2$CH_3). ^{13}C NMR (126 MHz, $CDCl_3$, ppm) δ 154.45, 154.04, 146.50, 97.97, 76.65, 73.63, 71.86, 69.43, 68.97, 68.94, 59.69, 56.37, 30.66, 30.62,

18.97, 18.93, 13.76, 13.73. FT-IR(ATR): 2950, 2870, 1782, 1749, 1460, 1394, 1361, 1268, 1244, 1193, 1151, 1109, 1050, 1025, 978, 931, 900, 848, 777, 656 cm^{-1}. HRMS (ESI^+) $C_{18}H_{28}O_{11}Na^+$ 443.1529, found ($M+Na^+$) 443.1515; $C_{18}H_{28}O_{11}H^+$ 421.1710, found 421.1698.

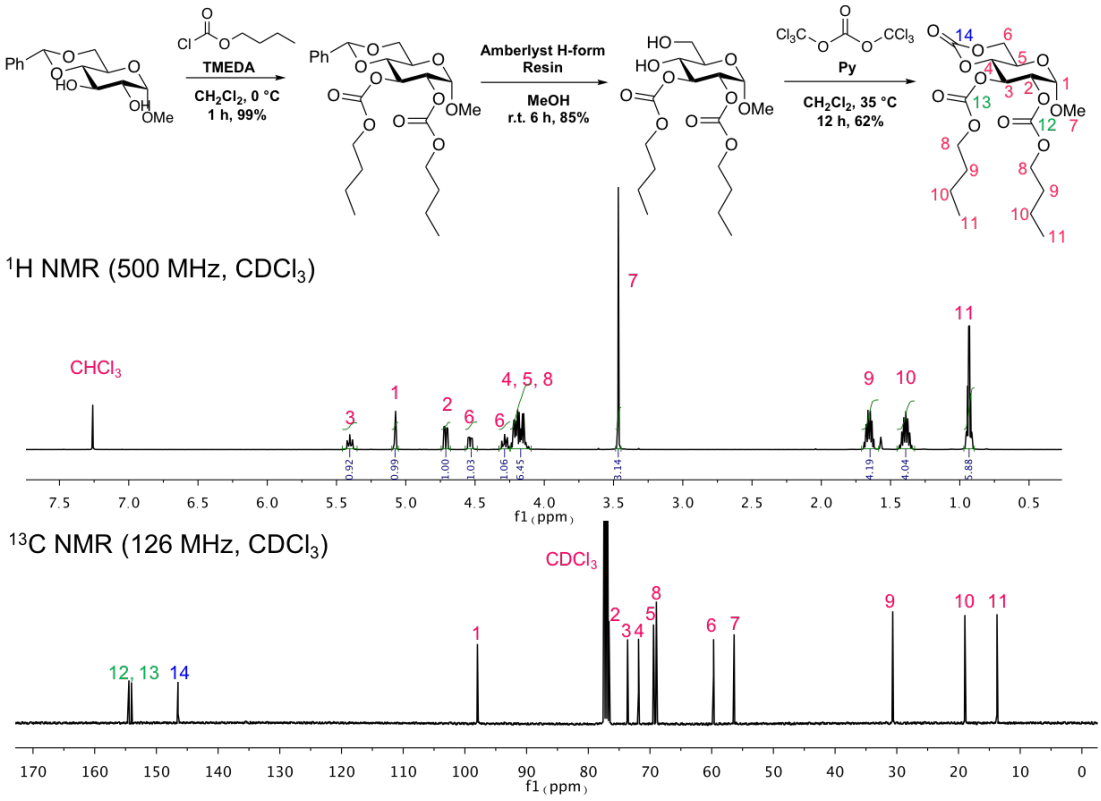

Figure II.2 ^{1}H NMR (500 MHz) and ^{13}C NMR (126 MHz) spectra of GC(BBC) (**2**) in $CDCl_3$. Reprinted with permission from [29].

Monomer GC(HHC) (3): ^{1}H NMR (500 MHz, $CDCl_3$, ppm) δ 5.40 (m, *J* = 10, 10 Hz, 1H, 3-C*H*), 5.08 (d, *J* = 4 Hz, 1H, 1-C*H*), 4.70 (dd, *J* = 10, 4 Hz, 1H, 2-C*H*), 4.57

– 4.50 (m, 1H, 6-CH_2), 4.34 – 4.25 (m, 1H, 6-CH_2), 4.25 – 4.10 (m, 6H, 4-CH, 5-CH, 2,3-CHOCOCH_2(CH$_2$)$_4$CH$_3$), 3.46 (s, 3H, 1-CHOCH_3), 1.70 – 1.59 (m, 4H, 2,3-CHOCOCH$_2$CH_2CH$_2$CH$_2$CH$_2$CH$_3$), 1.41 – 1.22 (m, 12H, 2,3-CHOCOCH$_2$CH$_2$CH_2CH_2CH_2CH$_3$), 0.88 (t, J = 7 Hz, 6H, 2,3-CHOCO(CH$_2$)$_5$CH_3). ^{13}C NMR (126 MHz, $CDCl_3$, ppm) δ 154.43, 154.02, 146.50, 97.95, 76.65, 73.62, 71.85, 69.42, 69.36, 69.26, 69.24, 59.67, 56.35, 31.49, 31.45, 28.59, 28.57, 25.39, 25.34, 22.60, 14.09, 14.08. FT-IR(ATR): 2927, 2857, 1782, 1736, 1460, 1390, 1329, 1263, 1240, 1193, 1146, 1114, 1058, 1025, 974, 908, 777, 670 cm^{-1}. HRMS (ESI$^+$) $C_{22}H_{36}O_{11}Na^+$ 499.2155, found (M+Na$^+$) 499.2145; $C_{22}H_{36}O_{11}H^+$ 477.2336, found 477.2327.

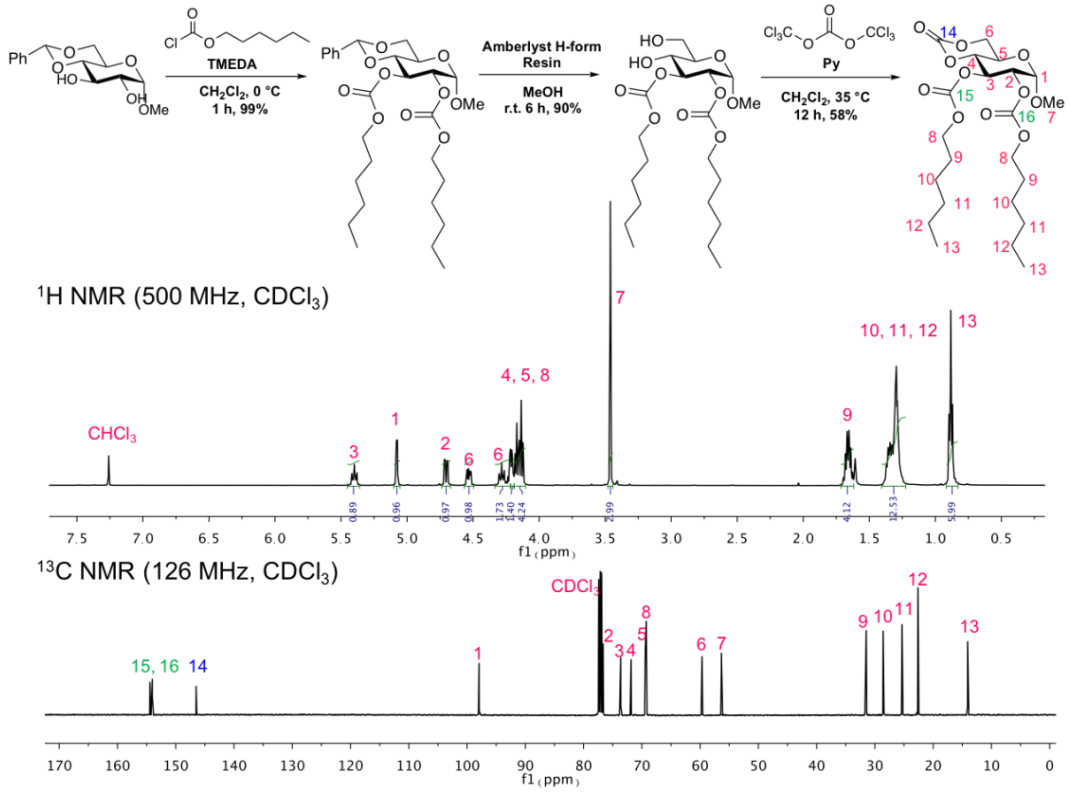

Figure II.3 ^{1}H (500 MHz) and ^{13}C (126 MHz) NMR spectra of GC(HHC) (**3**) in $CDCl_3$. Reprinted with permission from [29].

Monomer GC(isoBBC) (4): ^{1}H NMR (500 MHz, $CDCl_3$, ppm) δ 5.38 (dd, *J* = 10, 10 Hz, 1H, 3-*CH*), 5.08 (d, *J* = 4 Hz, 1H, 1-C*H*), 4.73 (dd, *J* = 10, 4 Hz, 1H, 2-C*H*), 4.54 (m, 1H, 6-CH_2), 4.34 – 4.16 (m, 3H, 6-CH_2, 4-C*H*, 5-C*H*), 4.04 – 3.88 (m, 4H, 2,3-CHOCOCH_2CH(CH_3)$_2$), 3.47 (s, 3H, 1-CHOCH_3), 1.98 (spt, *J* = 7 Hz, 2H, 2,3-CHOCOCH$_2$C*H*(CH_3)$_2$), 0.97 – 0.90 (m, 12H, 2,3-CHOCOCH$_2$CH(CH_3)$_2$). ^{13}C NMR (126 MHz, $CDCl_3$, ppm) δ 154.13, 153.84, 146.34, 97.51, 76.06, 74.50, 74.42, 73.32, 71.75, 69.06, 59.27, 55.80, 27.51, 27.46, 18.54, 18.51, 18.47, 18.46. FT-IR(ATR): 1962, 2880, 1777, 1749, 1459, 1375, 1268, 1240, 1193, 1146, 1104, 1053, 1030, 974, 894, 820, 777, 763, 670 cm^{-1}. HRMS (ESI$^+$) $C_{18}H_{28}O_{11}Na^+$ 443.1529, found (M+Na$^+$) 443.1514; $C_{18}H_{28}O_{11}H^+$ 421.1710, found 421.1698.

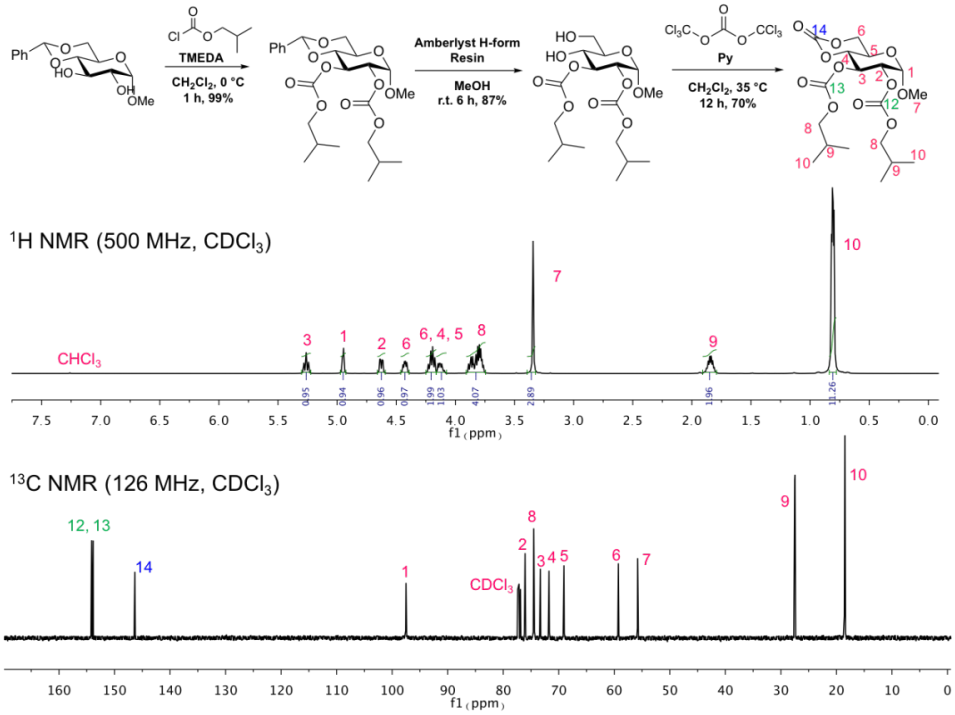

Figure II.4 ^{1}H (500 MHz) and ^{13}C (126 MHz) NMR spectra of GC(isoBBC) (**4**) in $CDCl_3$. Reprinted with permission from [29].

Monomer GC(neoPPC) (5): ^{1}H NMR (500 MHz, $CDCl_3$, ppm) δ 5.47 – 5.38 (m, 1H, 3-C*H*), 5.08 (d, *J* = 4 Hz, 1H, 1-C*H*), 4.74 (dd, *J* = 10, 4 Hz, 1H, 2-C*H*), 4.57 – 4.49 (m, 1H, 6-CH_2), 4.34 – 4.26 (m, 1H, 6-CH_2), 4.26 – 4.17 (m, 2H, 4-C*H*, 5-C*H*), 3.94 – 3.78 (m, 4H, 2,3-CHOCOCH_2C$(CH_3)_3$), 3.47 (s, 3H, 1-CHOCH_3), 0.94 and 0.93 (s, 18H, 2,3-CHOCOCH$_2$C(CH_3)$_3$). ^{13}C NMR (126 MHz, $CDCl_3$, ppm) δ 154.74, 154.29, 146.52, 98.01, 78.26, 78.22, 76.65, 73.67, 71.82, 69.44, 59.73, 56.37, 31.75, 31.74, 26.34, 26.29, 26.27. FT-IR(ATR): 2963, 2880, 1782, 1750, 1469, 1400, 1371, 1268, 1240, 1198, 1156, 1110, 1057, 1029, 983, 950, 908, 773, 679 cm^{-1}. HRMS (ESI$^+$) $C_{20}H_{32}O_{11}Na^+$ 471.1842, found (M+Na$^+$) 471.1834; $C_{20}H_{32}O_{11}H^+$ 449.2023, found 449.2016.

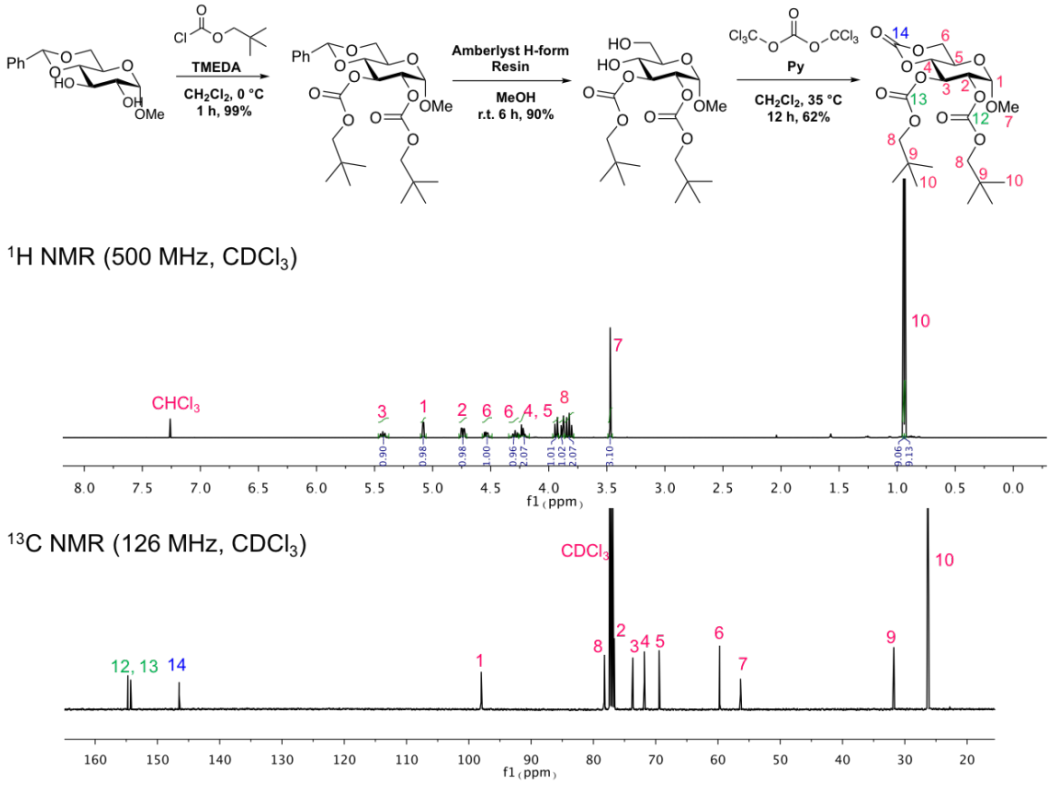

Figure II.5 ^{1}H (500 MHz) and ^{13}C (126 MHz) NMR spectra of GC(neoPPC) (**5**) in $CDCl_3$. Reprinted with permission from [29].

Monomer GC(EHEHC) (6): ^{1}H NMR (500 MHz, $CDCl_3$, ppm) δ 5.40 (dd, *J* = 10 ,10 Hz, 1H, 3-C*H*), 5.08 (d, *J* = 4 Hz, 1H, 1-C*H*), 4.71 (dd, *J* = 10, 4 Hz, 1H, 2-C*H*), 4.57 – 4.49 (m, 1H, 6-CH_2), 4.32 – 4.15 (m, 3H, 6-CH_2, 4-C*H*, 5-C*H*), 4.15 – 3.99 (m, 4H, 2,3-CHOCOCH_2CH(CH_2CH_3)$CH_2CH_2CH_2CH_3$), 3.46 (s, 3H, 1-CHOCH_3), 1.66 – 1.55 (m, 2H, 2,3-CHOCOCH_2C*H*(CH_2CH_3)$CH_2CH_2CH_2CH_3$), 1.36 - 1.25 (m, 16 H, 2,3-CHOCOCH_2CH(C$H_2$$CH_3$)C$H_2CH_2CH_2$$CH_3$), 0.88 (m, 12H, 2,3-CHOCOCH_2CH(CH_2CH_3)$CH_2CH_2CH_2$CH_3). ^{13}C NMR (126 MHz, $CDCl_3$, ppm) δ 154.61, 154.18, 146.50, 97.95, 76.64, 73.63, 71.82, 71.59, 71.55, 71.52, 69.41, 59.67, 56.34, 38.93, 38.89, 38.87, 30.24, 30.15, 30.11, 30.07, 29.01, 28.98, 28.93, 28.89, 23.57, 23.50, 23.02, 14.13, 10.98, 10.96, 10.94. FT-IR(ATR): 2960, 2925, 2869, 1755, 1460, 1383, 1264, 1242, 1194, 1140, 1243, 1187, 1145, 1103, 1046, 980, 905, 785, 765, 670 cm^{-1}. HRMS (ESI^+) $C_{26}H_{44}O_{11}Na^+$ 555.2781, found ($M+Na^+$) 555.2777; $C_{26}H_{44}O_{11}H^+$ 533.2962, found 533.2956.

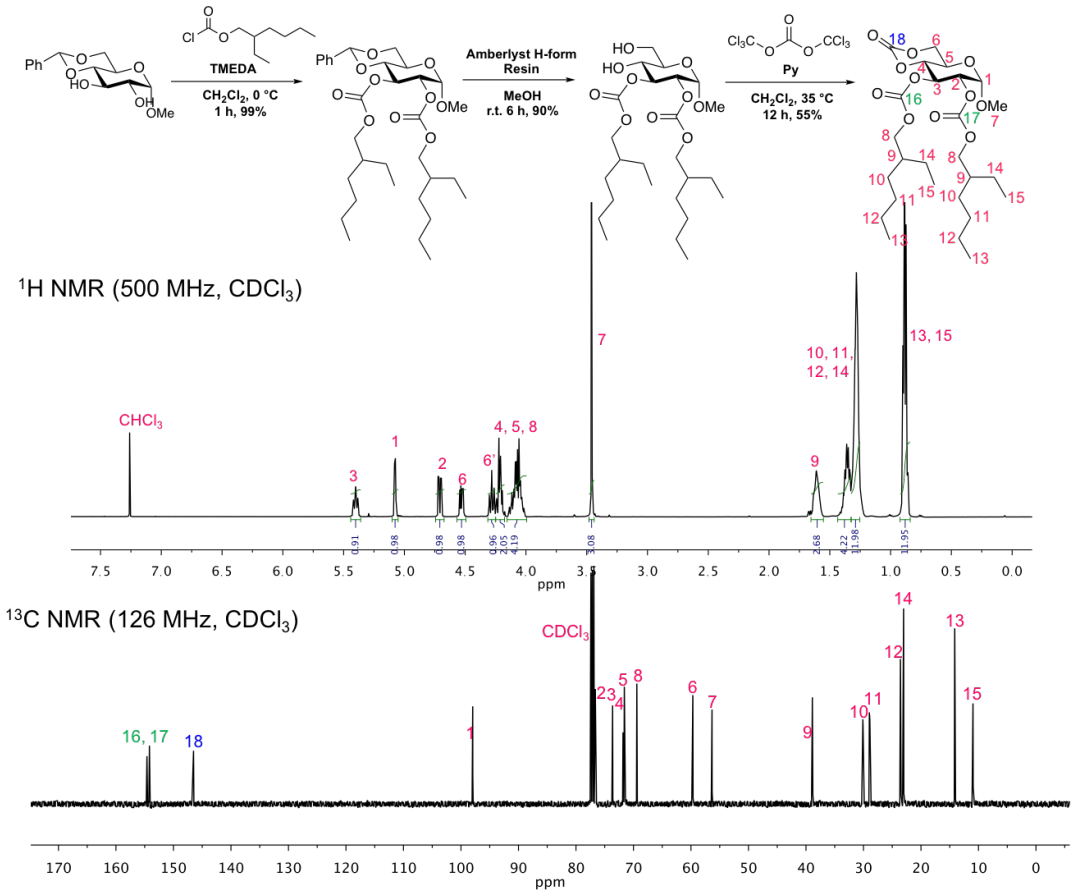

Figure II.6 ^{1}H (500 MHz) and ^{13}C (126 MHz) NMR spectra of GC(EHEHC) (**6**) in $CDCl_3$. Reprinted with permission from [29].

Synthesis of poly(α-D-glucose carbonate)s PGC(RRC) homopolymers: A solution of alkyloxycarbonyl protected glucose carbonate monomer GC(RRC) (200 mg, at predetermined equivalences) and 4-methylbenzyl alcohol (1 eq.) dissolved in *ca.* 1.0 mL of anhydrous DCM was transferred to a vial equipped with a stir bar and a rubber septum in a glovebox under Ar atmosphere, and the reaction was conducted in a -78 °C dry ice/acetone bath in a fume hood. A solution of 1,5,7-triazabicyclo[4.4.0]dec-5-ene

(TBD) (*ca.* 0.5 eq.) in 0.1 mL of anhydrous DCM was injected quickly into the vial under -78 °C. The reaction mixture was allowed to stir at -78 °C for 5 min, then quenched by adding an excess amount of acetic acid. The product was purified by precipitation from DCM into methanol three times and dried under vacuum.

PGC(BBC): ^{1}H NMR (500 MHz, $CDCl_3$, ppm) δ 7.27 and 7.16 (AB_q, J = 8 Hz), 5.33 (dd, J = 10, 10 Hz), 5.00 (d, J = 4 Hz), 4.80 (t, J = 10 Hz), 4.70 (dd, J = 10, 4 Hz), 4.32 (d, J = 11 Hz), 4.23 – 4.06 (m), 4.06 – 4.01 (m), 3.40 (s), 2.34 (s), 1.66 – 1.60 (m), 1.36 – 1.22 (m), 0.93 and 0.92 (t, J = 7 Hz). ^{13}C NMR (126 MHz, $CDCl_3$, ppm) δ 154.40, 154.34, 153.91, 96.46, 73.87, 73.60, 72.91, 68.67, 68.56, 66.89, 66.14, 55.76, 30.67, 30.65, 18.95, 18.92, 13.77, 13.75. FT-IR(ATR): 2959, 2868, 1752, 1456, 1394, 1232, 1163, 1110, 1032, 948, 846, 777 cm^{-1}. Yield: 91%. T_g = 68 °C. TGA in Ar: 270-393 °C, 87% mass loss. SEC (THF, PS standards): M_n = 15.5 kDa, $Đ$ = 1.06.

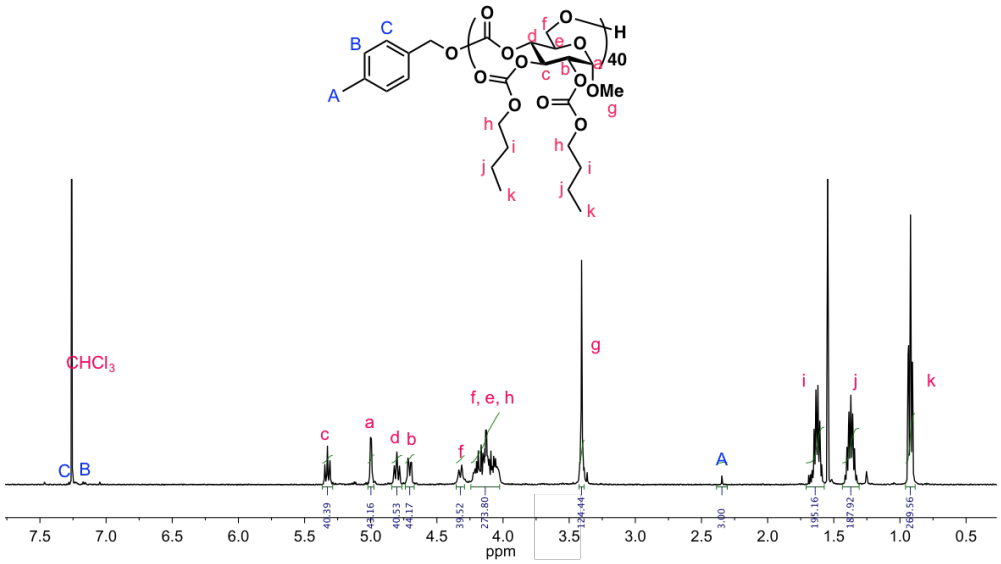

Figure II.7 ^{1}H NMR (500 MHz, $CDCl_3$) spectrum of $PGC(BBC)_{40}$. Reprinted with permission from [29].

PGC(HHC): ^{1}H NMR (500 MHz, $CDCl_3$, ppm) δ 7.27 and 7.16 (AB_q, J = 8 Hz), 5.33 (dd, J = 10, 10 Hz), 5.00 (d, J = 4 Hz), 4.80 (t, J = 10 Hz), 4.71 (dd, J = 10, 4 Hz), 4.32 (d, J = 11 Hz), 4.24 – 4.03 (m), 3.41 (s), 2.35 (s), 1.71 – 1.57 (m), 1.55 (s), 1.44 – 1.31 (m), 0.92 (t, J = 7 Hz). ^{13}C NMR (126 MHz, $CDCl_3$, ppm) δ 154.23, 154.15, 153.75, 129.19, 128.53, 96.30, 77.26, 77.00, 76.75, 73.74, 73.47, 72.77, 68.78, 68.70, 66.73, 65.96, 55.59, 31.37, 31.34, 31.19, 28.61, 28.46, 25.22, 25.20, 25.06, 22.46, 22.32, 13.95, 13.93. FT-IR(ATR): 2936, 2855, 1749, 1453, 1372, 1232, 1166, 1113, 1029, 977, 908, 778 cm^{-1}. Yield: 90%. T_g = 46 °C. TGA in Ar: 256-396 °C, 85% mass loss. SEC (THF, PS standards): M_n = 15.9 kDa, $Đ$ = 1.06.

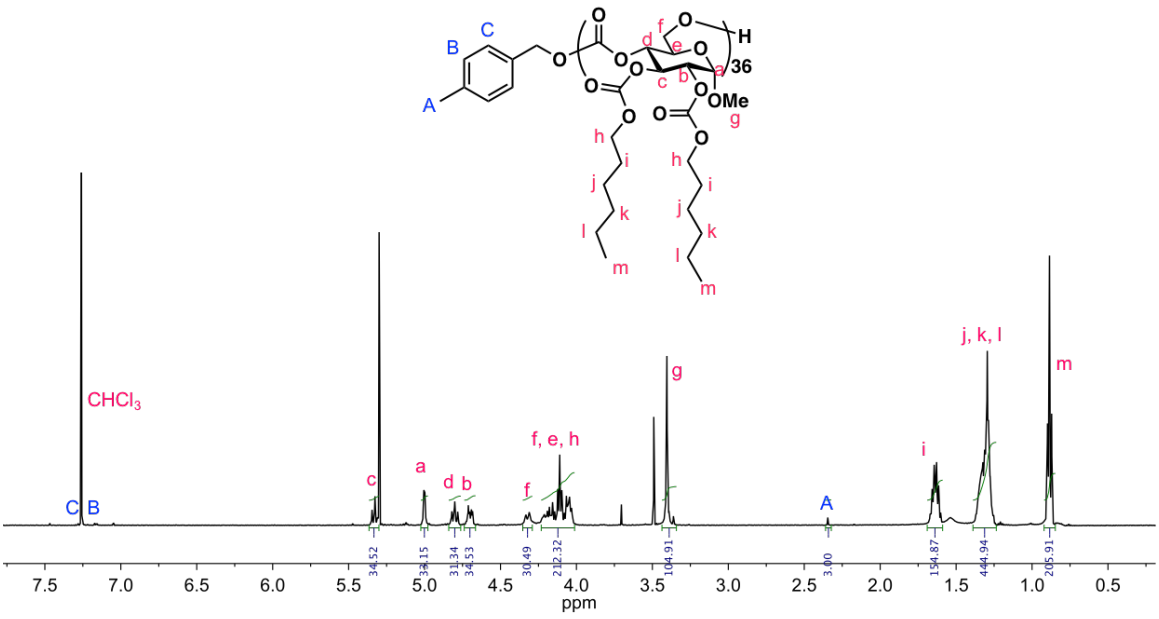

Figure II.8 ^{1}H NMR (500 MHz, $CDCl_3$) spectrum of $PGC(HHC)_{36}$. Reprinted with permission from [29].

PGC(isoBBC): ^{1}H NMR (500 MHz, $CDCl_3$, ppm) δ 7.27 and 7.16 (AB_q, J = 8 Hz), 5.38 – 5.26 (m), 5.00 (t, J = 4 Hz), 4.86 – 4.76 (m), 4.76 – 4.67 (m), 4.32 (d, J = 11 Hz), 4.20 (dd, J = 12, 6 Hz), 4.09 – 4.01 (m), 4.00 – 3.83 (m), 3.41 (s), 2.34 (s), 1.95 (m), 0.92 and 0.91 (d, J = 7 Hz). ^{13}C NMR (126 MHz, $CDCl_3$, ppm) δ 154.48, 154.40, 153.92, 129.36, 128.70, 96.47, 77.35, 74.76, 74.63, 73.88, 73.59, 72.94, 66.90, 66.18, 55.77, 27.89, 27.86, 18.94, 18.92, 18.90. FT-IR(ATR): 2959, 2876, 1751, 1459, 1378, 1231, 1169, 1110, 1035, 967, 777 cm^{-1}. Yield: 89%. T_g = 85 °C. TGA in Ar: 260-394 °C, 86% mass loss. SEC (THF, PS standards): M_n = 14.9 kDa, $Đ$ = 1.05.

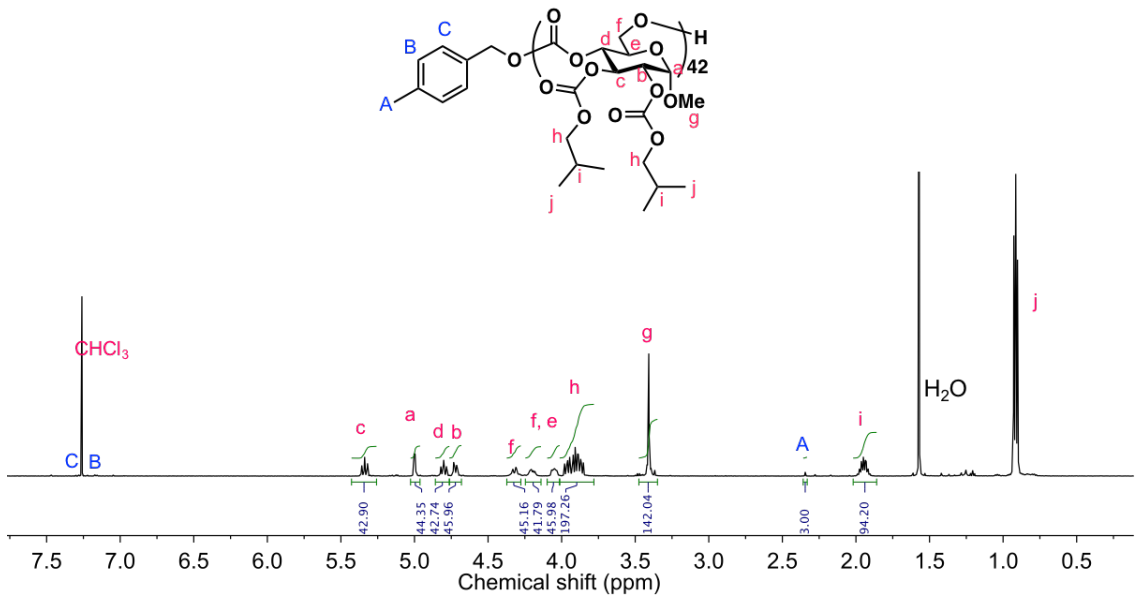

Figure II.9 ^{1}H NMR (500 MHz, $CDCl_3$) spectrum of PGC(isoBBC)$_{42}$. Reprinted with permission from [29].

PGC(neoPPC): ^{1}H NMR (500 MHz, $CDCl_3$, ppm) δ 7.28 and 7.16 (AB_q, J = 8 Hz), 5.36 (dd, J = 10, 10 Hz), 5.01 (d, J = 4 Hz), 4.80 (t, J = 10 Hz), 4.75 – 4.69 (m), 4.32 (d, J = 11 Hz), 4.19 (dd, J = 12, 6 Hz), 4.10 – 4.02 (m), 3.95 – 3.81 (m), 3.79 (dd, J = 10, 4 Hz), 3.41 (s), 3.44 – 3.33 (m), 2.35 (s), 0.93 and 0.92 (s). ^{13}C NMR (126 MHz, $CDCl_3$, ppm) δ 154.70, 154.57, 153.92, 128.71, 96.46, 77.98, 77.80, 77.35, 73.91, 73.55, 73.01, 66.90, 66.19, 55.78, 31.81, 31.72, 26.33, 26.32, 20.90. FT-IR(ATR): 2959, 2868, 1752, 1465, 1372, 1235, 1163, 1114, 1036, 958, 777 cm^{-1}. Yield: 91%. T_g = 125 °C. TGA in Ar: 266-398 °C, 89% mass loss. SEC (THF, PS standards): M_n = 15.7 kDa, $Đ$ = 1.06.

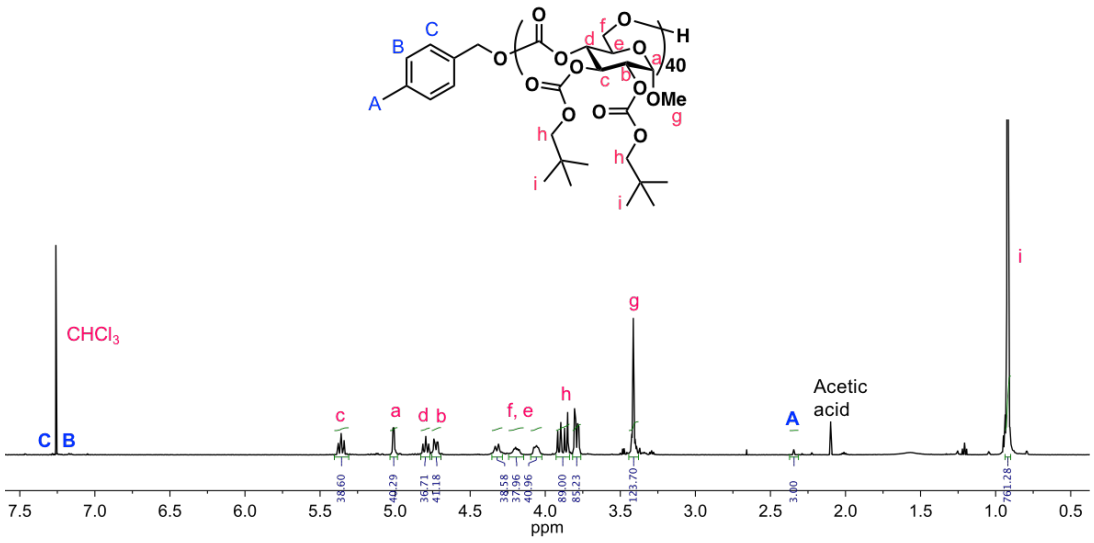

Figure II.10 ^{1}H NMR (500 MHz, $CDCl_3$) spectrum of $PGC(neoPPC)_{40}$. Reprinted with permission from [29].

PGC(EHEHC): ^{1}H NMR (500 MHz, $CDCl_3$, ppm) δ 7.27 and 7.16 (AB_q, J = 8 Hz), 5.33 (dd, J = 10, 10 Hz), 5.01 (d, J = 4 Hz), 4.79 (t, J = 10 Hz), 4.70 (dd, J = 10, 4 Hz), 4.32 (d, J = 11 Hz), 4.24 – 4.14 (m), 4.14 – 3.91 (m), 3.41 (s), 2.34 (s), 1.58 (br), 1.41 – 1.30 (m), 1.30 – 1.21 (br), 0.91 – 0.82 (m). ^{13}C NMR (126 MHz, $CDCl_3$, ppm) δ 154.58, 154.40, 153.93, 129.35, 128.69, 96.41, 77.14, 73.91, 73.62, 72.97, 71.30, 71.26, 71.17, 71.13, 66.85, 66.15, 55.75, 38.88, 30.18, 30.15, 30.11, 30.08, 29.00, 28.92, 23.54, 23.49, 23.06, 14.17, 14.16, 10.96, 10.93, 10.91. FT-IR(ATR): 2928, 2861, 1852, 1456, 1389, 1232, 1169, 1110, 1033, 967, 910, 777 cm^{-1}. Yield: 90%. T_g = 38 °C. TGA in Ar: 239-391 °C, 90% mass loss. SEC (THF, PS standards): M_n = 15.8 kDa, $Đ$ = 1.06.

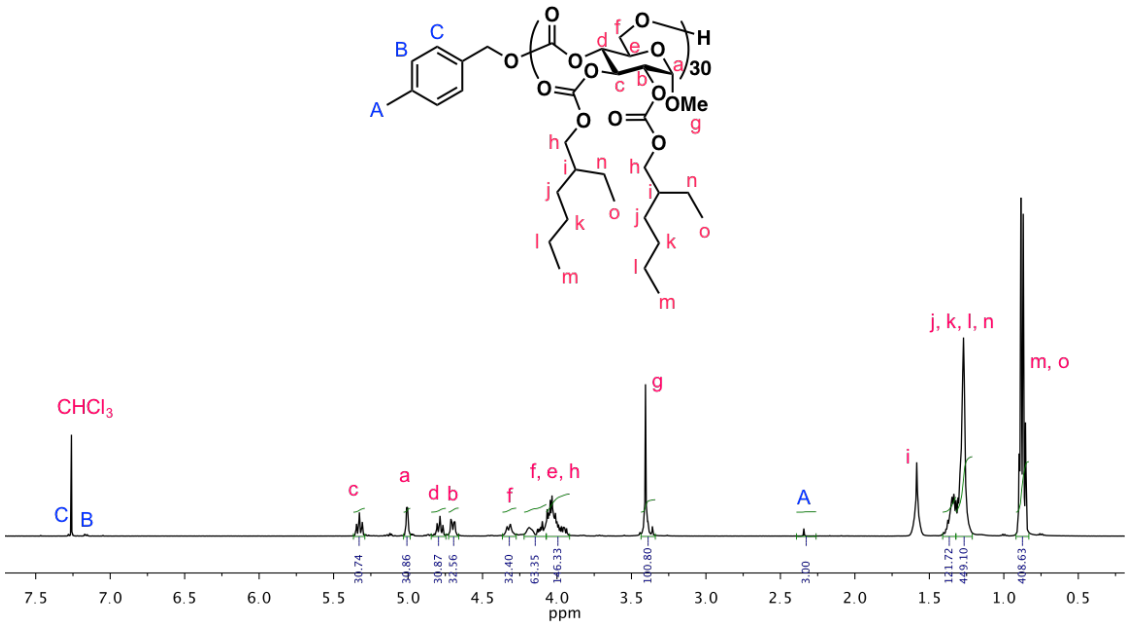

Figure II.11 ^{1}H NMR (500 MHz, $CDCl_3$) spectrum of PGC(EHEHC)$_{30}$. Reprinted with permission from [29].

Synthesis of oligomers and polymers with different molar mass of GC(neoPPC) and GC(EHEHC): Solutions of monomer and 4-methylbenzyl alcohol were dissolved in 0.5–1.0 mL of anhydrous DCM predetermined at different equivalence ratios. A solution of TBD (1% eq. of monomer) in 0.05 mL of anhydrous DCM was injected quickly into the reaction mixtures under -78 °C. After stirring for 5 min, the reaction was quenched by adding an excess amount of acetic acid. The products with DP_n > 6 were purified by precipitation from DCM into methanol three times; products with DP_n ≤ 5 were purified and separated using preparative SEC during up to 5 recycles, and dried under vacuum.

GC(neoPPC) unimer: ^{1}H NMR (500 MHz, $CDCl_3$, ppm) δ 7.28 and 7.16 (AB_q, J = 8 Hz, 4H), 5.14 (s, 2H), 5.14 (dd, J = 10, 10 Hz, 1H), 4.97 (d, J = 4 Hz, 1H), 4.72 (dd, J = 10, 4 Hz, 1H), 4.49 (dd, J = 12, 4 Hz, 1H), 4.41 (dd, J = 12, 2 Hz, 1H), 3.86 – 3.78 (m, 5H), 3.68 (dd, J = 10, 9 Hz, 1H), 3.38 (s, 3H), 2.35 (s, 3H), 0.94 and 0.93 (s, 18H). ^{13}C NMR (126 MHz, $CDCl_3$, ppm) δ 156.22, 155.58, 154.83, 138.68, 132.13, 129.40, 128.72, 128.51, 96.89, 78.13, 77.97, 76.69, 73.64, 70.13, 69.71, 69.37, 66.24, 55.57, 31.77, 31.73, 29.84, 26.33, 26.31, 26.27, 21.35. FT-IR(ATR): 3495, 2954, 2924, 2862, 1743, 1458, 1373, 1242, 1165, 1041, 980, 964, 918, 856, 787, 733 cm^{-1}. Yield: 10%. T_g = 13 °C. TGA in Ar: 164-373 °C, 81% mass loss.

GC(neoPPC) dimer: ^{1}H NMR (500 MHz, $CDCl_3$, ppm) δ 7.28 and 7.16 (AB_q, J = 8 Hz, 4H), 5.33 (dd, J = 10, 10 Hz, 1H), 5.19 – 5.09 (m, 3H), 4.99 (dd, J = 12, 4 Hz, 2H), 4.91 (dd, J = 10, 9 Hz, 1H), 4.77 (dd, J = 10, 4 Hz, 1H), 4.71 (dd, J = 10, 4 Hz, 1H), 4.50 – 4.20 (m, 4H), 4.04 (3, 1H), 3.95 – 3.76 (m, 9H), 3.76 – 3.67 (m, 2H), 3.40 and 3.39

(s, 6H), 2.35 (s, 3H), 0.96 – 0.90 (m, 36H). ^{13}C NMR (126 MHz, $CDCl_3$, ppm) δ 156.09, 155.03, 154.99, 154.84, 154.71, 154.25, 138.58, 132.17, 129.37, 128.67, 96.91, 78.04, 77.98, 77.99, 77.92, 76.63, 74.19, 73.79, 73.64, 72.99, 70.10, 69.42, 69.17, 66.97, 66.91, 65.56, 55.75, 55.61, 31.79, 31.76, 31.73, 26.35, 26.31, 26.29, 26.28, 26.25, 21.34. FT-IR(ATR): 3502, 2970, 1751, 1458, 1373, 1242, 1119, 1034, 964, 918, 864, 779, 756, 687 cm^{-1}. Yield: 19%. T_g = 50 °C. TGA in Ar: 205-369 °C, 79% mass loss.

GC(neoPPC) trimer: ^{1}H NMR (500 MHz, $CDCl_3$, ppm) δ 7.28 and 7.16 (AB_q, J = 8 Hz, 4H), 5.37 and 5.33 (dd, J = 10, 10 Hz, 2H) 5.20 – 5.07 (m, 3H), 5.03 – 4.95 (m, 3H), 4.88 (m, 2H), 4.80 – 4.67 (m, 3H), 4.47 – 4.16 (m, 6H), 4.05 (m, 2H), 3.96 – 3.67 (m, 15H), 3.43 – 3.37 (m, 9H), 2.34 (s, 3H), 0.96 – 0.89 (m, 54H). ^{13}C NMR (126 MHz, $CDCl_3$, ppm) δ 156.03, 155.00, 154.84, 154.71, 154.69, 154.65, 154.20, 153.96, 138.53, 132.25, 129.35, 128.68, 96.88, 96.64, 96.54, 78.01, 77.99, 77.93, 77.90, 77.84, 76.58, 74.21, 73.91, 73.83, 73.64, 73.51, 73.09, 72.97, 70.04, 69.44, 69.11, 67.07, 67.01, 66.89, 66.26, 65.62, 55.80, 55.71, 55.59, 31.80, 31.79, 31.76, 31.72, 31.70, 26.35, 26.31, 26.29, 21.34. FT-IR(ATR): 3502, 2963, 2878, 1751, 1558, 1466, 1373, 1242, 1119, 1034, 957, 756, 671 cm^{-1}. Yield: 28%. T_g = 65 °C. TGA in Ar: 211-377 °C, 83% mass loss.

GC(neoPPC) tetramer: ^{1}H NMR (500 MHz, $CDCl_3$, ppm) δ 7.28 and 7.16 (AB_q, J = 8 Hz, 4H), 5.37 (dd, J = 10, 10 Hz, 2H), 5.32 (dd, J = 10, 10 Hz, 1H), 5.03 – 4.95 (m, 4H), 4.92 – 4.80 (m, 3H), 4.78 – 4.68 (m, 4H), 4.48 – 4.18 (m, 9H), 4.05 (m, 3H), 3.96 – 3.75 (m, 19H), 3.42 – 3.36 (m, 12H), 2.34 (s, 3H), 0.95 – 0.90 (m, 72H). ^{13}C NMR (126 MHz, $CDCl_3$, ppm) δ 155.98, 155.00, 154.84, 154.72, 154.69, 154.69, 154.64, 154.19, 153.94, 153.92, 138.52, 132.25, 129.35, 128.68, 96.88, 96.63, 96.52, 96.51, 78.01, 78.00,

77.99, 77.89, 77.82, 76.54, 74.24, 73.94, 73.92, 73.86, 73.63, 73.49, 73.12, 73.02, 72.97, 70.04, 69.48, 69.05, 67.11, 67.04, 66.78, 66.37, 66.27, 65.61, 55.84, 55.75, 55.70, 55.58, 31.81, 31.80, 31.75, 31.72, 31.71, 26.35, 26.32, 26.30, 21.34. FT-IR(ATR): 3495, 2963, 2908, 1751, 1558, 1466, 1373, 1242, 1111, 1041, 964, 779, 664 cm^{-1}. Yield: 20%. T_g = 79 °C. TGA in Ar: 215-376 °C, 80% mass loss.

GC(EHEHC) unimer: ^{1}H NMR (500 MHz, $CDCl_3$, ppm) δ 7.28 and 7.17 (AB_q, J = 8 Hz, 4H), 5.13 (s, 2H), 5.12 (dd, J = 10, 10 Hz, 1H), 4.97 (d, J = 4 Hz, 1H), 4.71 (dd, J = 10, 4 Hz, 1H), 4.49 (dd, J = 12, 4 Hz, 1H), 4.41 (dd, J = 12, 2 Hz, 1H), 4.13 – 3.99 (m, 5H), 3.84 (m, 1H), 3.68 (m, 1H), 3.37 (s, 3H), 2.35 (s, 3H), 1.40 – 1.22 (m, 16H), 0.93 – 0.83 (m, 12H). ^{13}C NMR (126 MHz, $CDCl_3$, ppm) δ 156.18, 155.56, 154.70, 138.68, 132.12, 129.40, 128.72, 96.84, 76.71, 73.61, 71.50, 71.45, 71.30, 71.25, 70.12, 69.67, 69.41, 66.25, 55.56, 38.95, 38.91, 38.89, 30.21, 30.16, 30.15, 30.10, 29.01, 29.00, 28.94, 28.91, 23.58, 23.53, 23.06, 23.05, 21.35, 14.15, 10.99, 10.96. FT-IR(ATR): 3495, 2932, 2870, 1744, 1458, 1389, 1242, 1165, 1041, 972, 918, 787 cm^{-1}. Yield: 14%. T_g = -25 °C. TGA in Ar: 185-350 °C, 61% mass loss.

GC(EHEHC) dimer: ^{1}H NMR (500 MHz, $CDCl_3$, ppm) δ 7.28 and 7.16 (AB_q, J = 8 Hz, 4H), 5.30 (dd, J = 10, 10 Hz, 1H), 5.17 – 5.08 (m, 3H), 4.99 (dd, J = 10, 4 Hz, 2H), 4.90 (dd, J = 10, 10 Hz, 1H), 4.74 (dd, J = 10, 4 Hz, 1H), 4.68 (dd, J = 10, 4 Hz, 1H), 4.39 (d, J = 4 Hz, 2H), 4.30 (d, J = 4 Hz, 2H), 4.14 – 3.94 (m, 10H), 3.39 and 3.38 (s, 6H), 2.34 (s, 3H), 1.41 – 1.20 (m, 32H), 0.88 (m, 24H). ^{13}C NMR (126 MHz, $CDCl_3$, ppm) δ 1j56.00, 155.03, 154.92, 154.71, 154.59, 154.23, 138.57, 132.18, 129.37, 128.68, 96.87, 96.57, 76.62, 74.26, 73.78, 73.60, 72.99, 71.38, 71.33, 71.32, 71.31, 71.25, 71.20, 70.09,

69.42, 69.18, 66.91, 65.56, 55.74, 55.60, 38.95, 38.91, 38.89, 38.85, 30.21, 30.17, 30.15, 30.13, 30.10, 30.09, 29.01, 28.99, 28.96, 28.94, 28.92, 23.58, 23.52, 23.48, 23.05, 21.34, 14.15, 10.97, 10.96, 10.93. FT-IR(ATR): 3503, 2931, 2870, 1751, 1458, 1389, 1242, 1165, 1111, 1034, 972, 786 cm^{-1}. Yield: 23%. T_g = -8 °C. TGA in Ar: 190-364 °C, 82% mass loss.

GC(EHEHC) trimer: ^{1}H NMR (500 MHz, $CDCl_3$, ppm) δ 7.28 and 7.16 (AB_q, J = 8 Hz, 4H), 5.35 (dd, J = 10, 10 Hz, 1H), 5.31 (s, 2H), 5.30 (dd, J = 10, 10 Hz, 1H), 5.17 – 5.08 (m, 3H), 5.00 (dd, J = 10, 4 Hz, 2H), 4.97 (d, J = 4 Hz, 1H), 4.87 (m, 2H), 4.74 (td, J = 10, 4 Hz, 2H), 4.38 (m, 3H), 4.29 (m, 2H), 4.19 (m, 1H), 4.14 – 3.93 (m, 15H), 3.82 (m, 1H), 3.71 (m, 1H), 3.40, 3.39, and 3.37 (s, 9H), 2.34 (s, 3H), 1.43 – 1.19 (m, 48H), 0.91 – 0.82 (m, 36H). ^{13}C NMR (126 MHz, $CDCl_3$, ppm) δ 155.96, 155.00, 154.96, 154.71, 154.60, 154.58, 154.52, 154.20, 153.96, 138.53, 132.26, 129.35, 128.69, 96.86, 96.85, 96.60, 96.46, 76.55, 73.89, 73.83, 73.59, 73.54, 73.05, 73.00, 71.37, 71.31, 71.27, 71.24, 71.21, 71.19, 70.05, 69.44, 69.07, 69.06, 69.05, 67.03, 67.00, 66.84, 66.27, 65.61, 55.79, 55.70, 55.59, 38.94, 38.88, 30.16, 30.14, 30.09, 29.00, 28.95, 28.92, 23.57, 23.51, 23.06, 21.34, 14.16, 10.96, 10.92. FT-IR(ATR): 3502, 2932, 2870, 2168, 1752, 1458, 1389, 1242, 1173, 1034, 972, 779 cm^{-1}. Yield: 30%. T_g = 4 °C. TGA in Ar: 197-365 °C, 81% mass loss.

GC(EHEHC) tetramer: ^{1}H NMR (500 MHz, $CDCl_3$, ppm) δ 7.28 and 7.16 (AB_q, J = 8 Hz, 4H), 5.35 (dd, J = 10, 10 Hz, 2H), 5.30 (s, 2H), 5.29 (dd, J = 10, 10 Hz, 1H), 5.18 – 5.08 (m, 3H), 5.04 – 4.96 (m, 4H), 4.93 – 4.79 (m, 3H), 4.78 – 4.65 (m, 4H), 4.49 – 4.19 (m, 8H), 4.15 – 3.93 (m, 21H), 3.84 (s, 1H), 3.72 (s, 1H), 3.42, 3.40 and 3.37 (s,

12H), 2.35 (s, 3H), 1.43 – 1.21 (m, 64H), 0.92 – 0.84 (m, 48H). ^{13}C NMR (126 MHz, $CDCl_3$, ppm) δ 155.90, 155.00, 154.96, 154.72, 154.61, 154.60, 154.58, 154.57, 154.49, 154.19, 153.95, 153.93, 138.51, 132.27, 129.35, 128.69, 96.86, 96.60, 96.46, 76.53, 74.39, 73.94, 73.90, 73.87, 73.62, 73.59, 73.57, 73.51, 73.11, 73.01, 71.36, 71.34, 71.31, 71.28, 71.27, 71.23, 71.21, 71.18, 70.03, 69.47, 69.01, 67.07, 67.03, 66.71, 66.43, 66.35, 66.27, 65.62, 65.51, 55.82, 55.74, 55.68, 55.57, 38.94, 38.88, 30.16, 30.12, 30.09, 29.00, 28.96, 28.95, 28.92, 23.57, 23.52, 23.50, 23.06, 21.33, 14.17, 14.15, 10.96, 10.94, 10.91. FT-IR(ATR): 3502, 2932, 2870, 1751, 1458, 1389, 1234, 1173, 1034, 964, 779 cm^{-1}. Yield: 17%. T_g = 8 °C. TGA in Ar: 187-363 °C, 80% mass loss.

GC(EHEHC) pentamer: ^{1}H NMR (500 MHz, $CDCl_3$, ppm) δ 7.28 and 7.16 (AB_q, J = 8 Hz, 4H), 5.39 – 5.31 (m, 4H), 5.18 – 5.06 (m, 3H), 5.05 – 4.95 (m, 5H), 4.92 – 4.76 (m, 4H), 4.76 – 4.58 (m, 5H), 4.49 – 4.15 (m, 10H), 4.15 – 3.89 (m, 26H), 3.41, 3.40, 3.39 and 3.36 (s, 15H), 2.34 (s, 3H), 1.44 – 1.18 (m, 80H), 0.88 (m, 60H). ^{13}C NMR (126 MHz, $CDCl_3$, ppm) δ 155.88, 154.97, 154.71, 154.59, 154.56, 154.48, 154.45, 154.18, 153.95, 153.91, 138.52, 132.27, 129.35, 128.69, 96.83, 96.59, 96.44, 74.43, 74.41, 73.94, 73.88, 73.62, 73.58, 73.54, 73.50, 73.04, 73.01, 72.99, 71.31, 71.20, 71.16, 70.03, 69.48, 69.00, 67.07, 66.87, 66.67, 66.40, 66.23, 65.62, 55.79, 55.77, 55.71, 55.67, 55.56, 38.93, 38.88, 30.21, 30.15, 30.11, 30.08, 29.84, 29.00, 28.93, 28.91, 23.56, 23.50, 23.06, 21.33, 14.17, 14.15, 10.96, 10.94, 10.91. FT-IT(ATR): 2932, 2870, 1751, 1458, 1389, 1234, 1172, 1110, 1034, 964, 779, 678 cm^{-1}. Yield: 6%. T_g = 11 °C. TGA in Ar: 190-362 °C, 77% mass loss.

2.3 Results and Discussion

To evaluate the effects of side chain structure, six substituent alkyl groups: ethyl, *n*-butyl, *n*-hexyl, isobutyl, neopentyl, and 2-ethylhexyl, were studied. These side chains were installed into the glucose carbonate monomers *via* carbonate linkages following previously reported synthetic methods,[27] to introduce full hydrolytic degradability of the resulting polymers (**Figure II.12**).[48] The monomers GC(RRC) exhibited ^{13}C NMR spectroscopic signals at *ca.* 147 ppm, demonstrating the successful ring-closing with the presence of the cyclic carbonate (**Figures II.1-II.5**). Six well-defined homopolymers

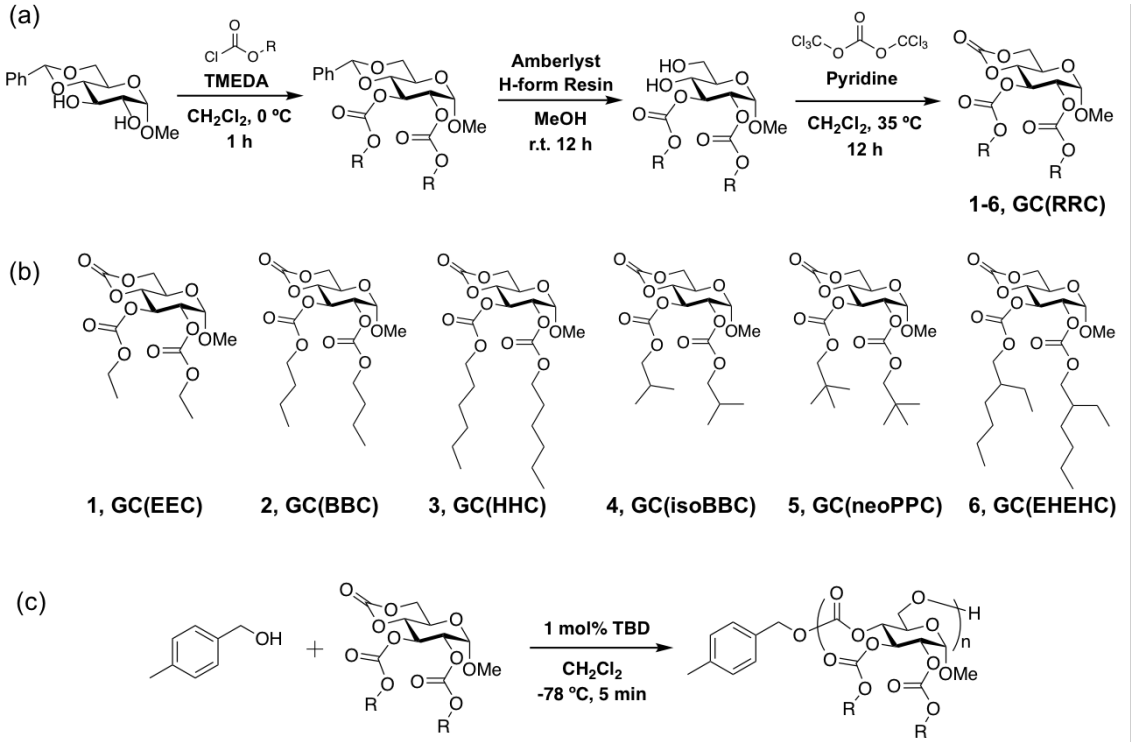

Figure II.12 (a) Synthesis of bicyclic glucose carbonate monomers GC(RRC). (b) Structures of alkyloxycarbonyl protected glucose carbonate monomers. (c) Synthesis of the polymers PGC(RRC). Reprinted with permission from [[29]].

PGC(RRC) were then produced through organocatalytic ring-opening polymerization (ROP) (**Figure II.12c**), and the products were structurally confirmed by ^{1}H NMR spectroscopy (**Figures II.6-II.10**), ^{13}C NMR spectroscopy (**Figure II.13**), Fourier-transform infrared spectroscopy (FT-IR) (**Figure II.14**), and matrix-assisted laser desorption ionization time-of-flight mass spectrometry (MALDI-TOF MS) (**Figure II.15**). The sharpness of proton resonance peaks reflected the restricted configurations of the glucose cyclic structure, as well as the regioselectivity of the polymerization during propagation steps. Only one peak corresponding to the backbone carbonate resonance at 153.9 ppm was observed from each ^{13}C NMR spectrum, further suggesting the regioregularity of PGC(RRC). Nearly equal molar masses (M_n = 15-16 kDa) and narrow dispersities ($Đ$ = 1.04-1.06) were achieved for all six PGC(RRC), as determined by size exclusion chromatography (SEC) (**Table II.1**, **Figure II.13b**,), ensuring the comparability of their thermal properties would rely upon the differences in side chain composition with little effect from differences in molar mass. The well-defined structures of these homopolymers with 4-methylbenzyl alcohol end-group functionality were also demonstrated by MALDI-TOF MS (**Figure II.15**), which revealed populations with spacing numbers in accordance with the expected repeating unit values (*i.e.* 364.1 m/z for PGC(EEC), 420.2 m/z for GC(BBC) and GC(isoBBC), 476.2 m/z for GC(HHC), 448.2 m/z for GC(neoPPC), and 532.3 m/z for GC(EHEHC)). High thermal decomposition temperatures at 330–345 °C as measured by thermogravimetric analysis (TGA) (**Figure II.14**), indicated the thermal stability of these glucose-based polycarbonates.

Table II.1 Data for PGC(RRC) with Different Alkyloxycarbonyl Side Chains. Reprinted with permission from [29].

Entry	Polymer[a]	$M_{n,\,SEC}$[b] (kDa)	$Đ$[b]	T_g[c] (°C)	T_d[d] (°C)
1	$PGC(EEC)_{51}$	16.0	1.04	120	332
2	$PGC(BBC)_{40}$	15.5	1.06	68	330
3	$PGC(HHC)_{36}$	15.9	1.06	46	335
4	$PGC(isoBBC)_{42}$	14.9	1.05	85	341
5	$PGC(neoPPC)_{40}$	15.7	1.06	125	342
6	$PGC(EHEHC)_{30}$	15.8	1.06	38	345

[a] Repeating units were calculated based on ^{1}H NMR spectroscopic analysis.
[b] $M_{n,\,SEC}$ and $Đ$ were measured by SEC
[c] T_g was measured by DSC, performed with a heating rate of 10 °C/min.
[d] T_d was measured from the onset of TGA analysis, heating from 25 to 500 °C.

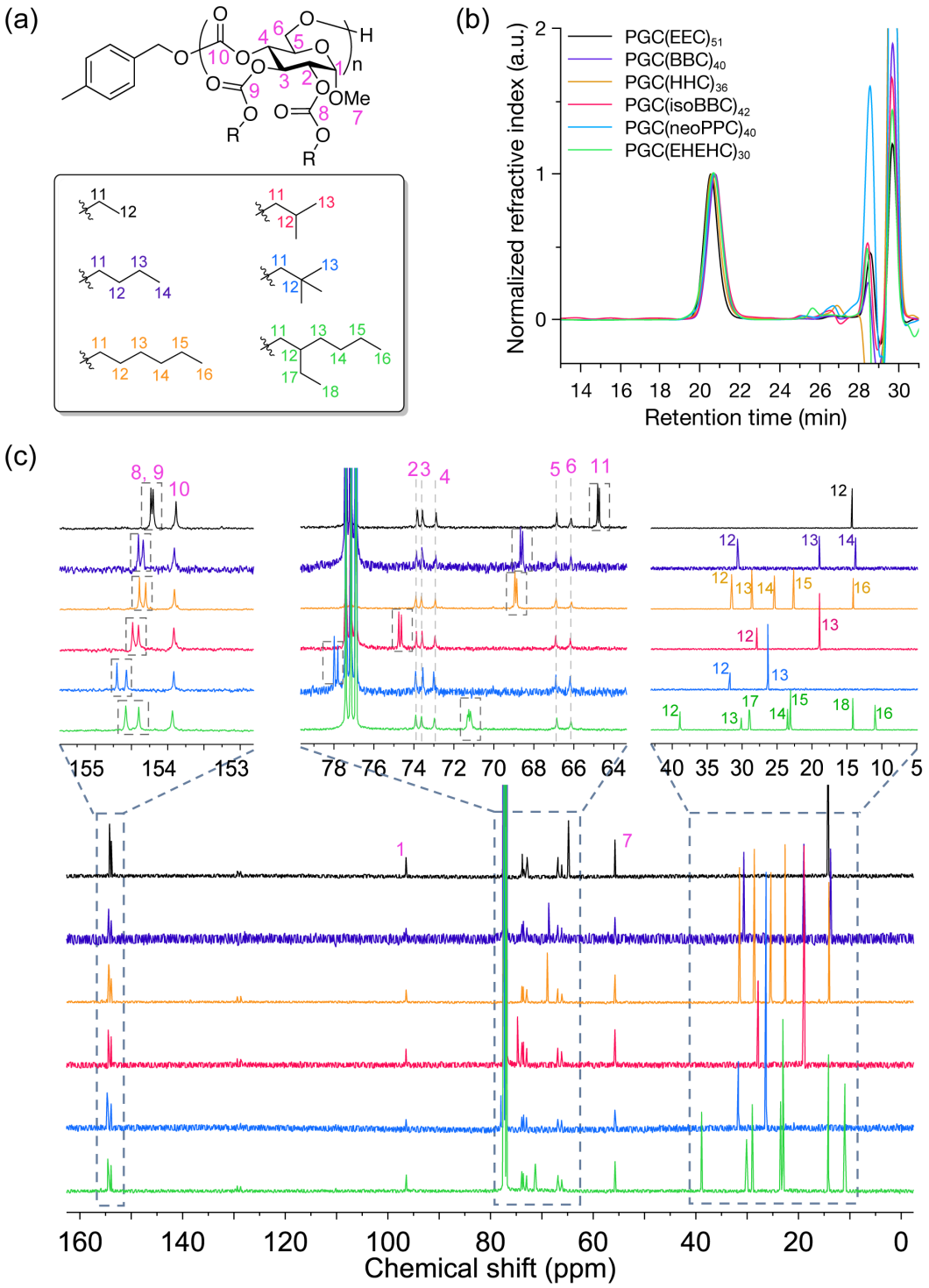

Figure II.13 (a) Structures of PGC(RRC), (b) SEC chromatograms (THF as eluent, 1.0 mL·min^{-1}), and (c) ^{13}C NMR (126 MHz, $CDCl_3$) spectra of PGC(RRC). Reprinted with permission from [29].

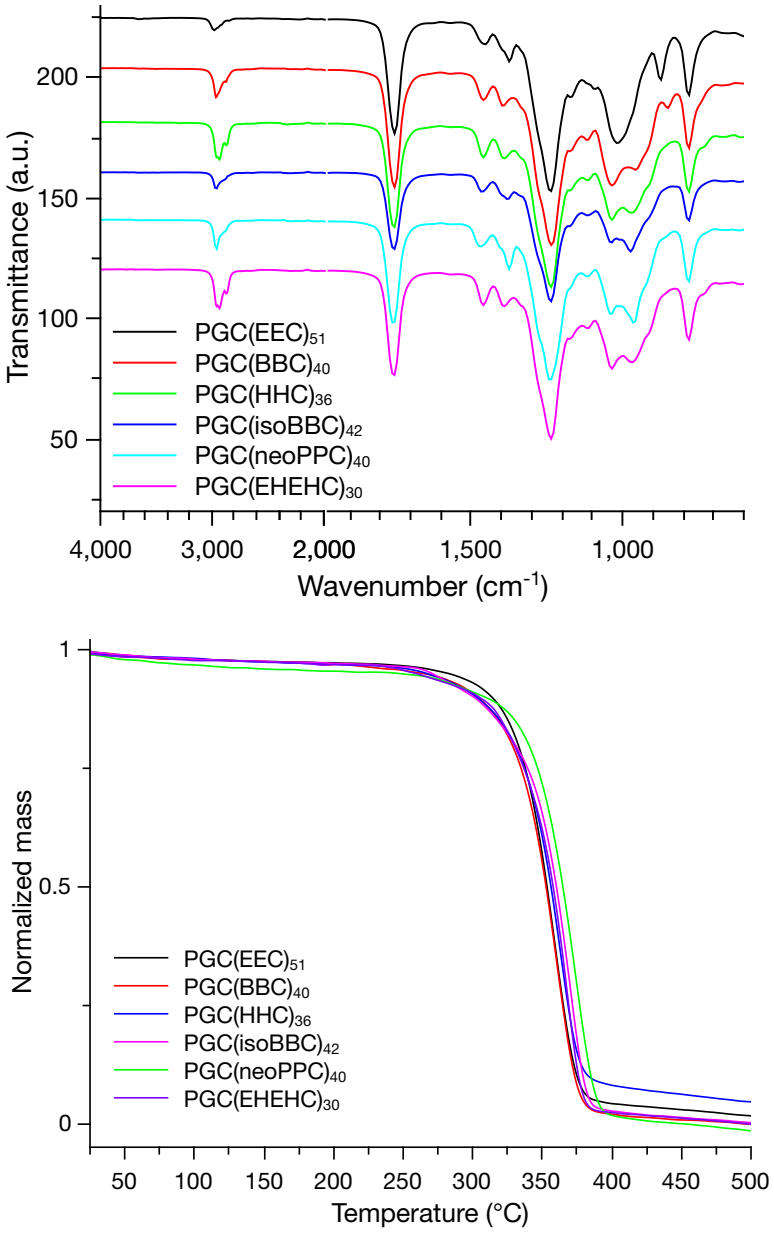

Figure II.14 FT-IR(ATR) spectra (top) and TGA traces (bottom, 25 – 500 °C, 10 °C/min) of PGC(RRC). Reprinted with permission from [29].

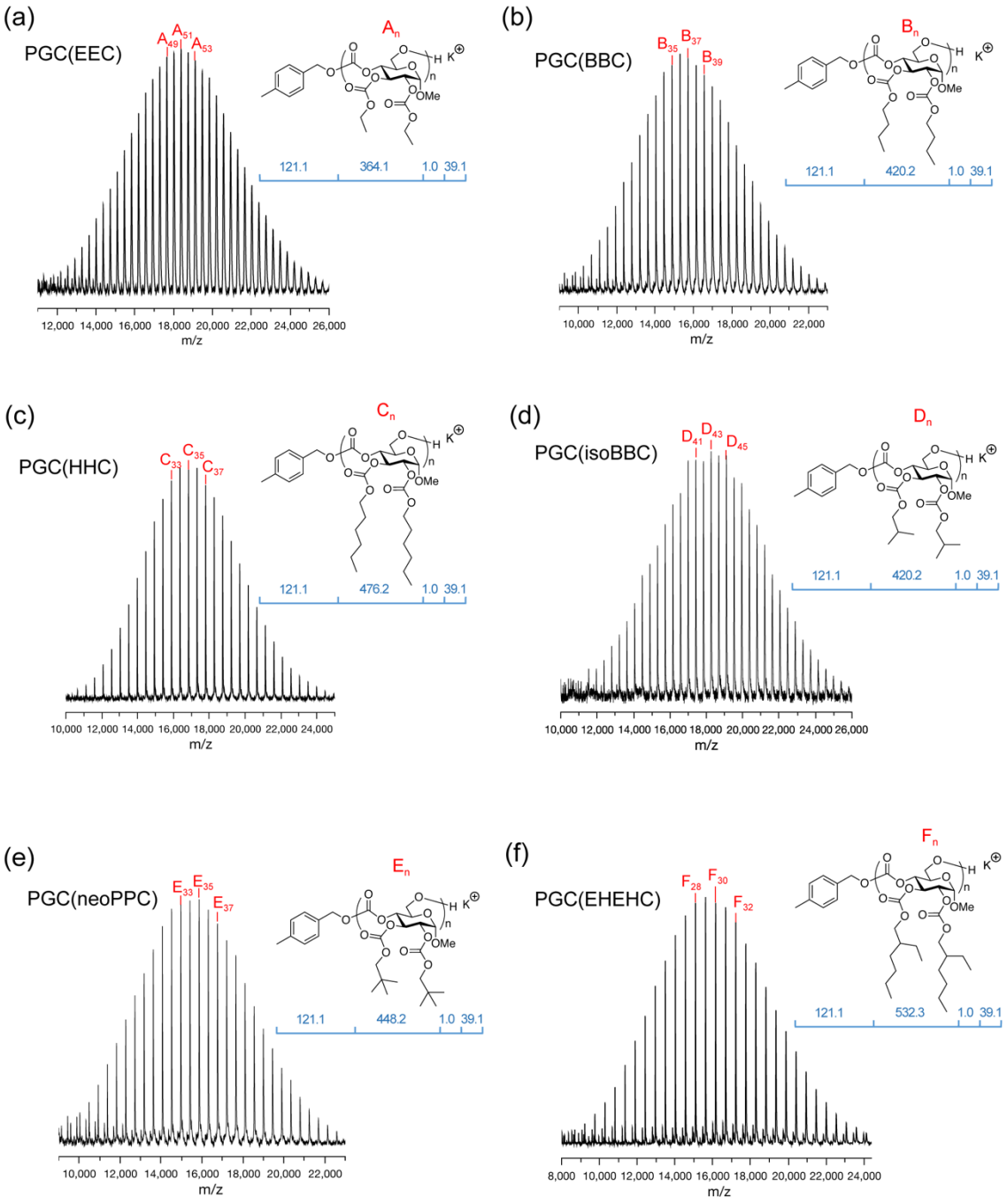

Figure II.15 MALDI-TOF MS spectra of PGCs: (a) PGC(EEC)$_{51}$, (b) PGC(BBC)$_{40}$, (c) PGC(HHC)$_{36}$, (d) PGC(isoBBC)$_{42}$, (e) PGC(neoPPC)$_{40}$, and (f) PGC(EHEHC)$_{30}$. DP_n values were calculated by ^{1}H NMR spectroscopy. Reprinted with permission from [29].

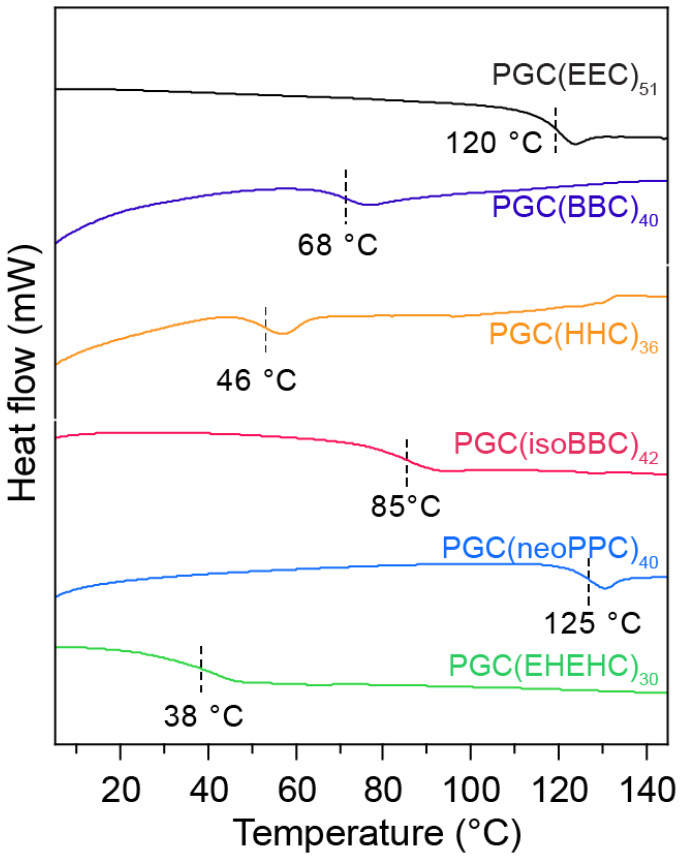

Figure II.16 DSC thermograms of PGC(RRC) (M_n = 15 – 16 kDa, $Đ \leq 1.06$). Reprinted with permission from [29].

On increasing the side chain length from ethyl to *n*-butyl to *n*-hexyl, with an elongation of only two methylene groups each step, the T_g dramatically decreased from 120 to 68 to 46 °C, as determined by differential scanning calorimetry (DSC) (**Figure II.16**). A further decrease in T_g to 38 °C was observed for PGC(EHEHC)$_{30}$, possibly due to the increased free volume created by the free rotation of the additional branched ethyl group.[121] However, an increase of the T_g to 85 °C was found for the branched isobutyl group modified PGC(isoBBC)$_{42}$, ranking between the ethyl and *n*-butyl groups,

suggesting combined effects of the chain length and branching.[111] The highest T_g of 125 °C was observed for PGC(neoPPC)$_{40}$, which can be explained by the presence of the quaternary carbon that brings in dramatic steric hindrance and rigidity.

The effect of molar mass on T_g was also investigated for two series of discrete oligomers and polymers, PGC(neoPPC) and PGC(EHEHC), which possessed the highest and lowest T_g, respectively. It is known that the T_g of polymers generally increases with increasing molar mass, which is often explained by the free volume ratio of polymer chain ends that facilitate the flexibility of a polymer chain considerably.[122] In the low molar mass range, this variation is especially pronounced, due to the prominent decrease of the ratio of chain ends with the increasing repeating units. In this system, the glucose carbonate monomers with the fused bicyclic structure were postulated to exhibit higher T_g than the corresponding ring-opened unimers, attributing to the combined effects from chain-ends and structural rigidity. To examine this hypothesis and probe the dependency of T_g on molar mass, polymers ($DP_n > 6$, $Đ < 1.10$) and oligomers were synthesized following the ROP procedure, by varying the monomer to initiator ratio. Unlike the polymer analogues, the oligomer mixture with $DP_n < 6$ is not optimal for understanding the intrinsic properties of each component.[123] Therefore, preparative SEC was used for efficient separation of the oligomer mixtures from one ROP reaction into their constituent species.

Oligo/polyGC(neoPPC)s were prepared with different monomer to initiator ratios from 2 to 20. Low dispersities of all batches were observed for the polymeric products by

Table II.2 Data for oligomers and polymers of GC(neoPPC) (Entries 7-12) and GC(EHEHC) (Entries 13-19). Reprinted with permission from [29].

Entry	Oligo/Polymer[a]	M_n[b] (Da)	$Đ$	T_g (°C)	T_d (°C)
7	$OGC(neoPPC)_1$	571	1.00	13	266
8	$OGC(neoPPC)_2$	1019	1.00	50	266
9	$OGC(neoPPC)_3$	1468	1.00	65	284
10	$OGC(neoPPC)_4$	1916	1.00	79	295
11	$PGC(neoPPC)_7$	3020	1.07	85	328
12	$PGC(neoPPC)_{20}$	8800	1.06	118	331
13	$OGC(EHEHC)_1$	655	1.00	-25	254
14	$OGC(EHEHC)_2$	1187	1.00	-8	268
15	$OGC(EHEHC)_3$	1720	1.00	4	270
16	$OGC(EHEHC)_4$	2252	1.00	8	273
17	$OGC(EHEHC)_5$	2785	1.00	11	271
18	$PGC(EHEHC)_{10}$	5360	1.06	26	304
19	$PGC(EHEHC)_{17}$	9080	1.06	32	322

[a] DP_n values for polymers were determined by SEC results. [b] M_n for discrete oligomers were calculated from DP_n.

SEC analysis (**Figure II.18a**, solid lines, **Table II.2**), while multiple peaks were found when feed ratios were set at 2 and 3, corresponding to the mixtures of oligomers with different molar mass distributions. These oligomer mixtures were then separated by

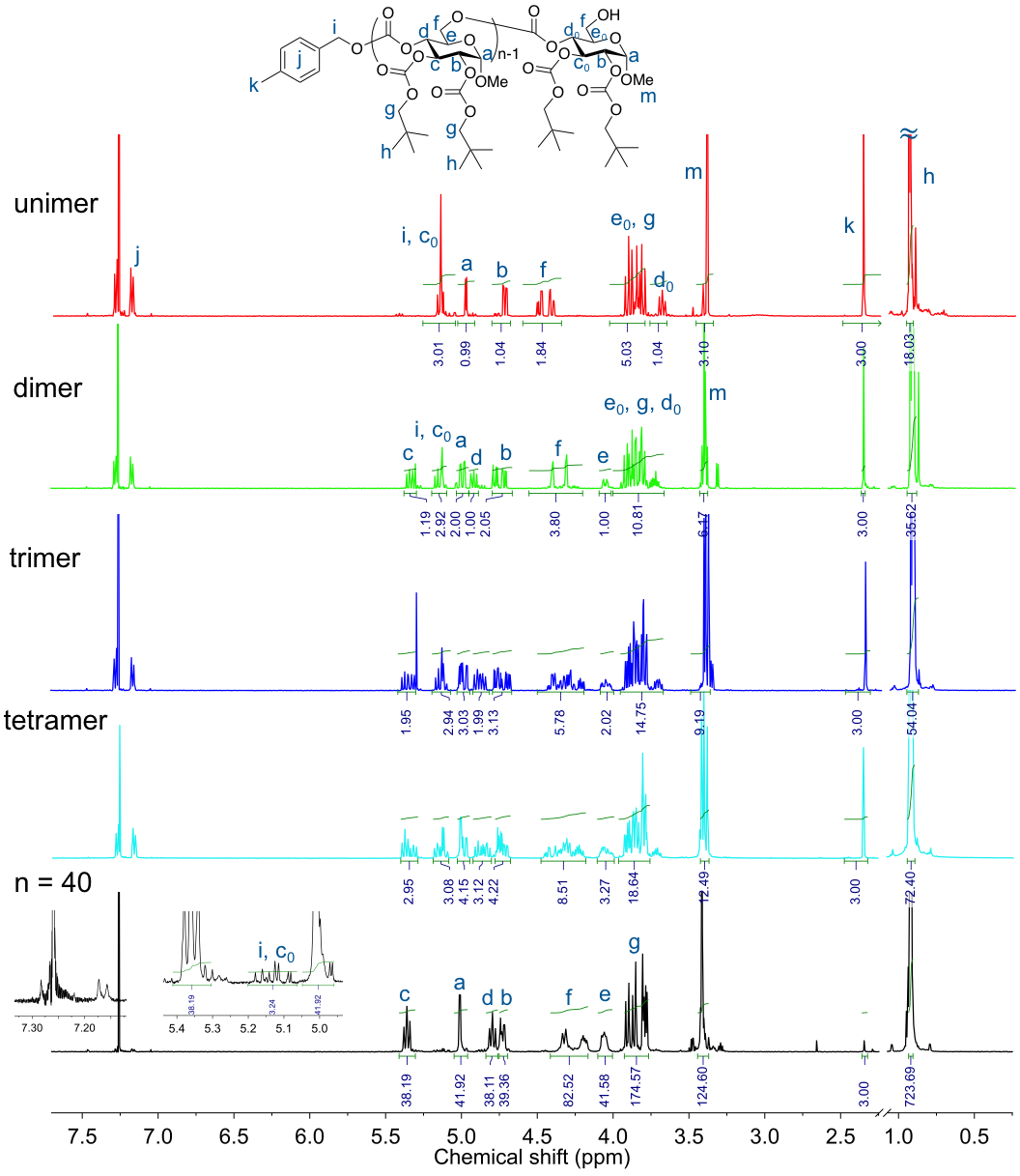

Figure II.17 ^{1}H NMR (500 MHz, $CDCl_3$) spectra of oligo/polyGC(neoPPC). Reprinted with permission from [29].

preparative SEC (chloroform as eluent), affording pure discrete oligomers as verified by analytical SEC chromatograms (**Figure II.18a**, dashed lines). MALDI-TOF MS spectra also reinforced their purity unambiguously, with m/z values corresponding to the expected

structures, and separation of *ca.* 448.2 m/z correlating with the GC(neoPPC) repeating unit. ^{1}H NMR spectroscopic analysis of the discrete oligomers provided insights into subtle structural changes as the size of the oligomer increased (**Figure II.17**).

With progression from the unimer to tetramer of GC(neoPPC), relative intensities of the glucose proton resonances (3.75–5.40 ppm region) increased when compared with the chain-end proton resonances at 2.35, 7.17, and 7.28 ppm, with integration numbers closely correlating to the oligomer DP_n. The T_g of each discrete oligomer ($DP_n < 5$) and polymer ($DP_n > 6$) of GC(neoPPC) were then measured using DSC from 0 to 150 °C at 10 °C/min, and a variation over 100 °C was observed. With the evolution from unimer to polymer ($DP_n = 40$), the free volume ratio of the chain ends decreased, leading to a rising trend of T_g from 13 °C to 125 °C. Interestingly, the GC(neoPPC) monomer behaved as an outlier of the trend line, with a T_g value of 57 °C, which is higher than the corresponding monocyclic ring-opened unimer and dimer. The fact that T_g strikingly decreased by 44 °C once the ring-opening occurred supported our hypothesis concerning the impact of the rigid fused bicyclic structure of the monomer. A special √-shaped plot was shown for T_g *vs.* log M_n, and a linear correlation was found for T_g *vs.* M_n^{-1}, which is explained by the Flory-Fox theory,[124] with an exception of the monomer (**Figure II.18d-e**). Although the T_g plateau point was difficult to be precisely identified within the given molar mass range in **Figure II.18d**, the intercept in **Figure II.18e** suggested that the T_g value extrapolated to infinite molar mass is expected to be close to 125 °C ($DP_n = 40$), where the effect of chain ends is insignificant.

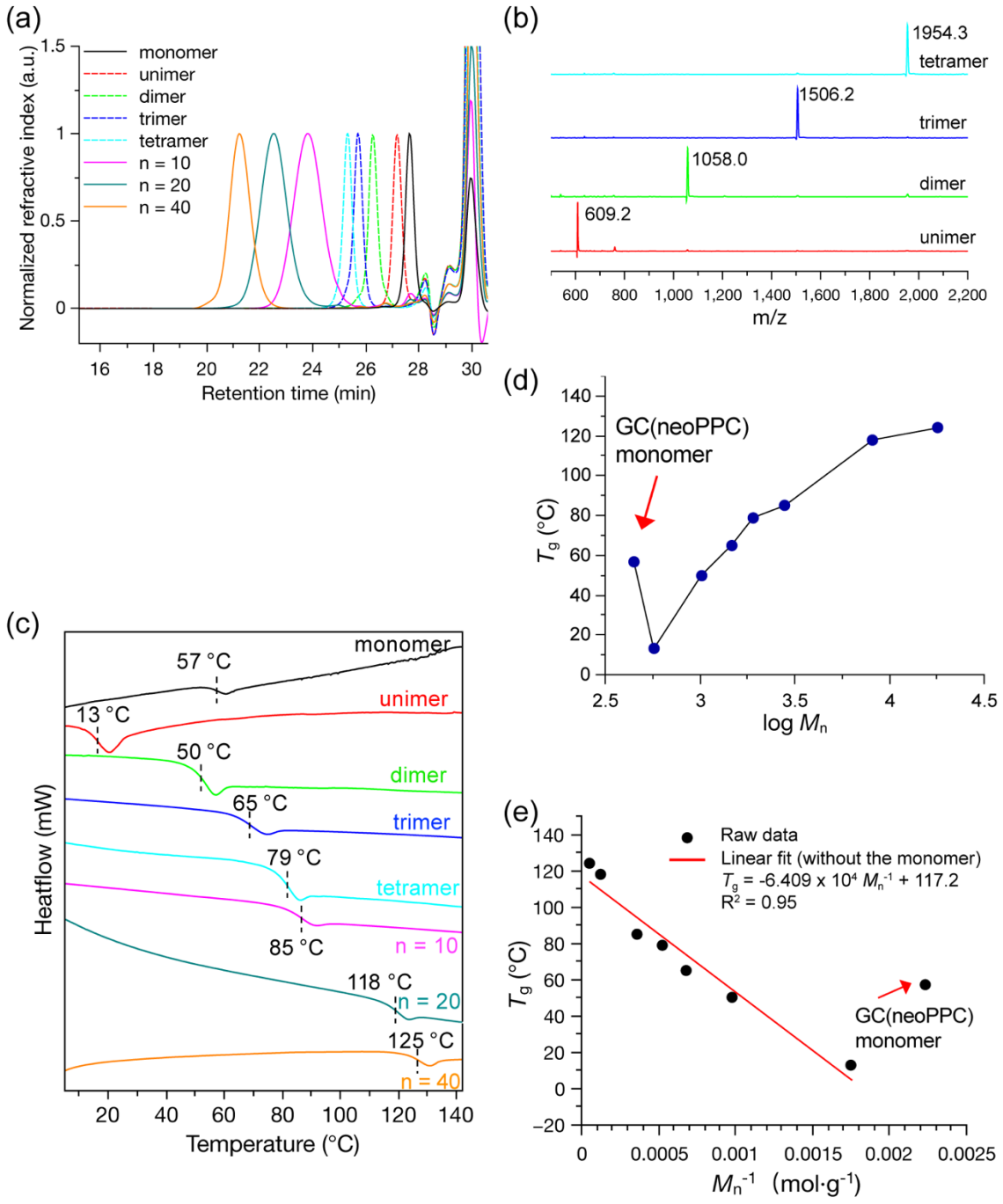

Figure II.18 Characterizations of oligo/polyGC(neoPPC). (a) SEC chromatograms, with dashed lines indicating discrete oligomers isolated by preparative SEC, (b) MALDI-TOF MS spectra of the discrete oligomers (with K^+ as the adduct ion), (c) DSC thermograms of monomer, oligomers, and polymers, and plots of (d) T_g *vs.* log M_n, and (e) T_g *vs.* M_n^{-1}. Reprinted with permission from [29].

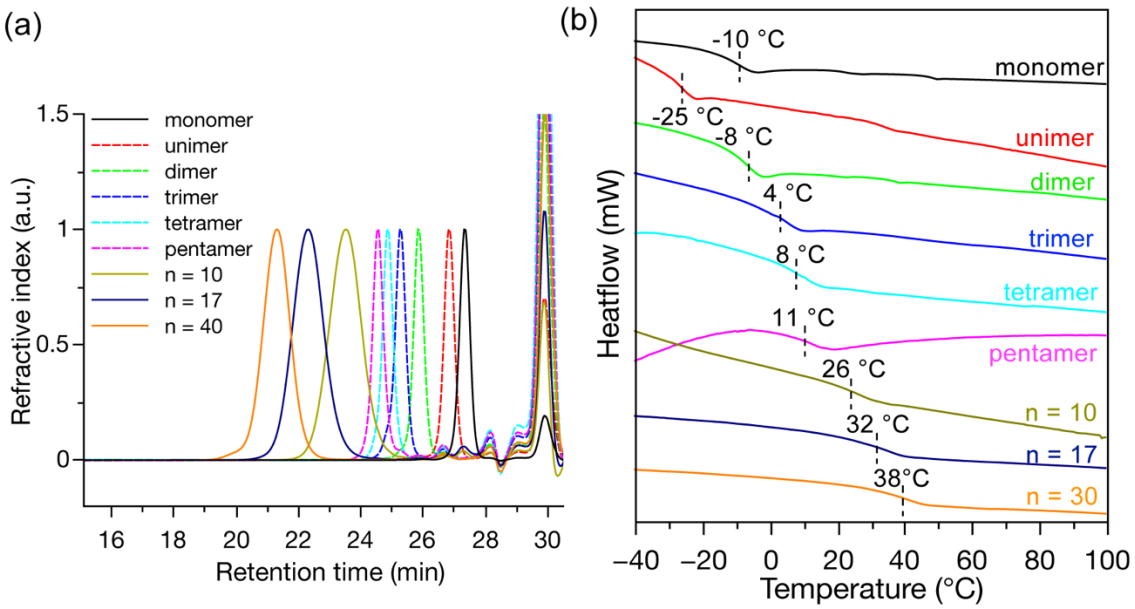

Figure II.19 (a) SEC chromatograms (dash lines: discrete oligomers isolated from preparative SEC), and (b) DSC thermograms of oligo/polyGC(EHEHC) of different molar mass. Reprinted with permission from [29].

To verify the generality of this trend in the glucose-based polycarbonate system, the study was extended to a PGC(EHEHC) series, which exhibited the lowest T_g among the six polymer analogues. Oligo/polyGC(EHEHC) was prepared in the same manner as for PGC(neoPPC), and structurally confirmed by SEC (**Figure II.19**), ^{1}H NMR spectroscopy, and MALDI-TOF MS. Similar trends of T_g progression from monomer to oligomer to polymer were also discovered. The bicyclic monomer with flexible side groups displayed low T_g at -10 °C, which decreased to -25 °C for the monocyclic ring-opened unimer, and increased gradually up to 38 °C with the chain elongation to DP_n = 30. The plots of T_g *vs.* log M_n and M_n^{-1} (**Figure II.20**) indicated the plateau of T_g at *ca.* 38 °C for PGC(EHEHC). Combining together the results of PGC(neoPPC) and

PGC(EHEHC), the general thermal property trends have been validated for poly(glucose carbonate)s.

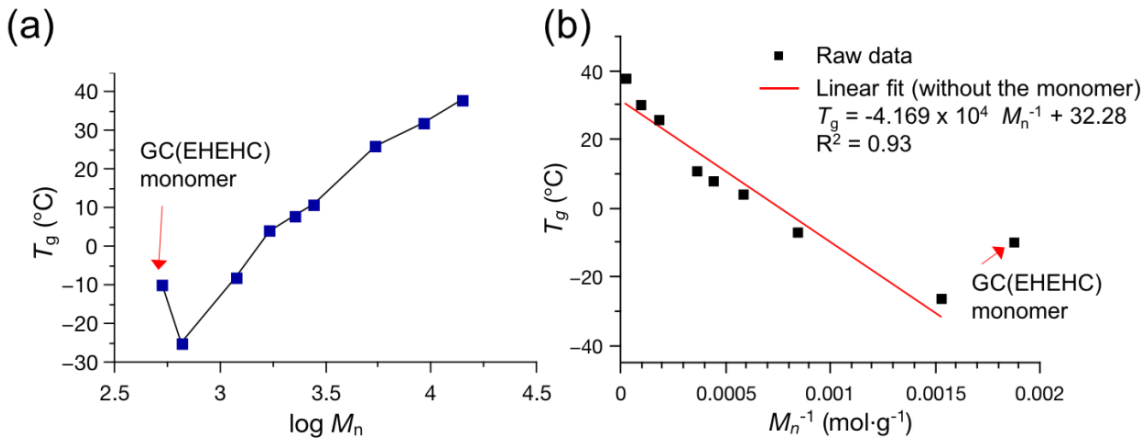

Figure II.20 Plots of (a) T_g *vs.* log M_n and (b) M_n^{-1} of oligo/polyGC(EHEHC). Reprinted with permission from [29].

2.4 Conclusions

In summary, variation of glass transition temperature of poly(glucose carbonate)s has been successfully achieved *via* control over the side chain structure and molar mass. A wide T_g range from 38 to 125 °C was achieved by varying the alkyloxycarbonyl protecting groups, of which the trend was rationalized by free volume evolution with the comprehensive effects derived from side-chain steric hindrance and flexibility. The two polymers at both ends of the trend were further evaluated for understanding the

relationship of T_g with molar mass. T_g variations with molar mass, among wide ranges of 13–125 °C and -25–38 °C for PGC(neoPPC) and PGC(EHEHC), respectively, are both well fitted to the Flory-Fox theory. It is especially interesting to note the enormous decrease of T_g from bicyclic monomers to monocyclic ring-opened unimers in both situations, which provided strong demonstration of the rigidity loss with ring-opening of the six-membered glucose carbonate ring. Future studies will be directed towards the utilization of these sustainable glucose-based polycarbonates with different T_g as high-performance materials in extensive applications.

2.5 Perspectives

The tuning of T_g for PGC materials can also be achieved by synthesis of copolymers, including both statistic and block copolymers constructed from PGC(neoPPC) and PGC(EHEHEC), for which the T_g is expected to be tunable within 38 – 125 °C by adjusting the ratios between the high and low T_g contents.

Exploring the effects of polymer T_g in various fields is of broader impacts and interests. For example, the T_g of PGC(EHEHC) studied in this work is 38 °C for M_n = 15 kDa, close to room temperature/human body temperature, holding promise for utilization in thermo-sensitive hydrogels or biomedical applications.

Moreover, preliminary studies were also conducted to understand the stiffness of nanoparticle core for the morphology change in solution. The self-assembly behaviors of these PGCs with different side-chain structure and T_g were tested, being incorporated into

amphiphilic diblock copolymers as the hydrophobic segments. A series of amphiphilic block copolymers of PGC(RRC)-*b*-PGC(cys) (PGC(cys): cysteine functionalized zwitterionic hydrophilic segment) were synthesized with nearly the same overall polymer length and hydrophobic-to-hydrophilic molar ratios. The self-assembly of the resulting polymers were then evaluated by characterizing the size and shape of the assembled nanoparticles in nanopure water at *ca.* 1 mg/mL. As indicated from TEM and DLS (**Figure II.21**), the polymers with a core segment of low T_g demonstrated the lowest average diameters of the assembled micelles. PGC(HHC)$_{35}$-*b*-PGC(cys)$_{60}$ and PGC(EHEHC)$_{38}$-*b*-PGC(cys)$_{60}$ both self-assembled into very small spherical micelles with D_{av} of 10-13 nm (determined by TEM imaging on copper coated carbon grid), and hydrodynamic diameters (D_h) (intensity) of 18-21 nm (determined by DLS), despite their larger side-chain volumes among others. AFM characterization on mica surfaces (**Figure II.22**) also demonstrated the same NP size and morphology. In comparison, the PGC(BBC)$_{35}$-*b*-PGC(cys)$_{60}$ with a higher hydrophobic segment T_g of 68 °C showed a slightly larger size of the nanoparticle by DLS with a D_h (intensity) of 26 ± 17 nm. Much larger spherical micelles of this series were observed for the assemblies from PGC(isoBBC)$_{35}$-*b*-PGC(cys)$_{60}$, presenting a D_{av} of 13 ± 2 and a D_h (intensity) of 220 ± 210 nm, likely due to the high T_g of the micellar core (T_g = 85 °C).

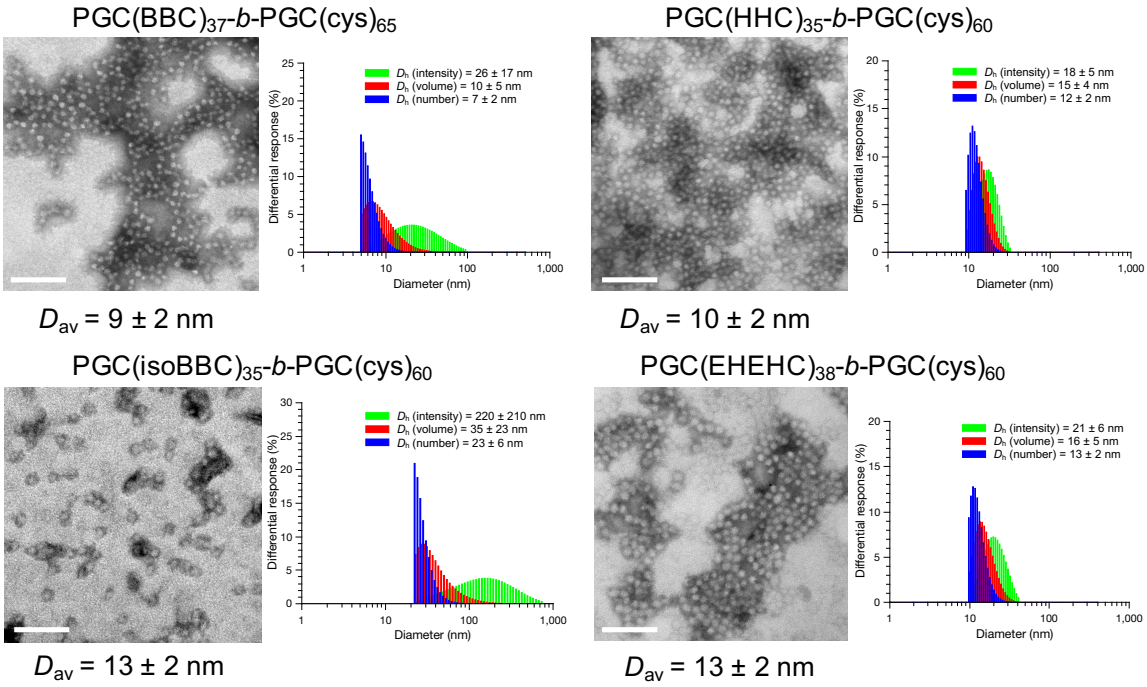

Figure II.21 TEM and DLS of PGC(RRC)-*b*-PGC(cys). R: *n*-butyl, *n*-hexyl, isobutyl, 2-ethylhexyl. Scale bars: 100 nm. Samples negatively stained with PTA (1%).

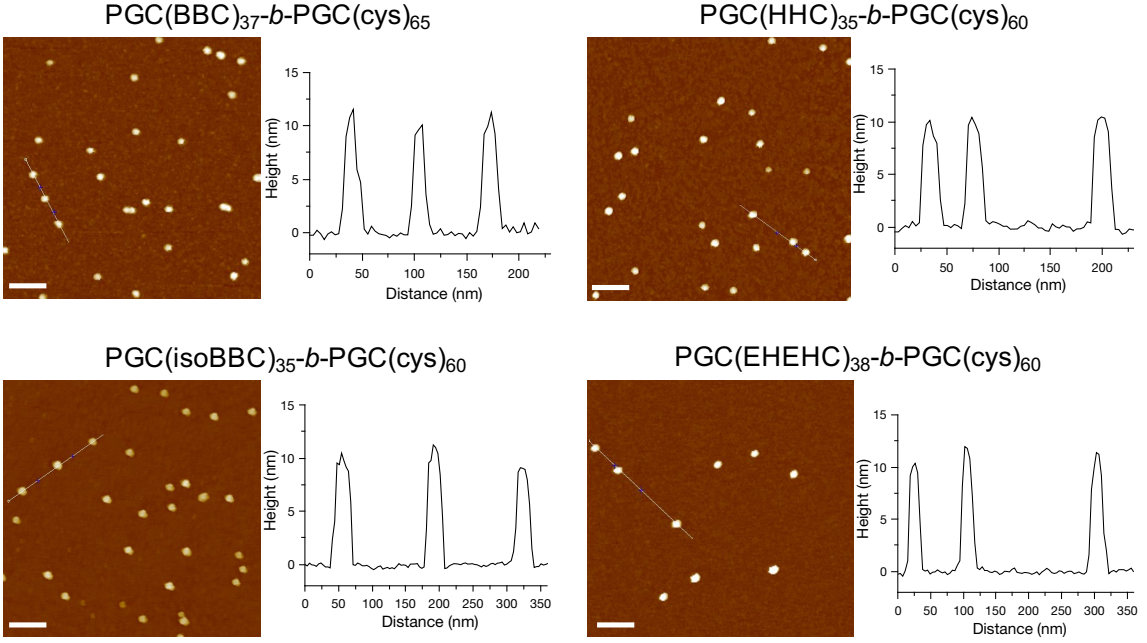

Figure II.22 AFM images and height profiles of PGC(RRC)-*b*-PGC(cys). R: *n*-butyl, *n*-hexyl, isobutyl, 2-ethylhexyl. Scale bars: 100 nm.

Interesting self-assembled polymeric nanoparticles were found for PGC(neoPPC)$_{40}$-*b*-PGC(EPC)(cys)$_{70}$, showing the formation of both small spherical particles and cylindrical (bundles) particles, demonstrated by both AFM and TEM imaging (**Figure II.23**). This phenomenon is similar to what has been observed in Chapter IV for the crystallization-driven self-assembly of poly(L-lactide)-containing diblock copolymers; however, the assembly process for the fully-glucose-based polymers were conducted at room temperature. And the crystallinity of the five polymers were examined using WAXD (**Figure II.24**). Further studies on these polymers would help improve the understandings of the physicochemical property effect in colloidal chemistry and broaden the scope of CDSA to sugar-based polymers.

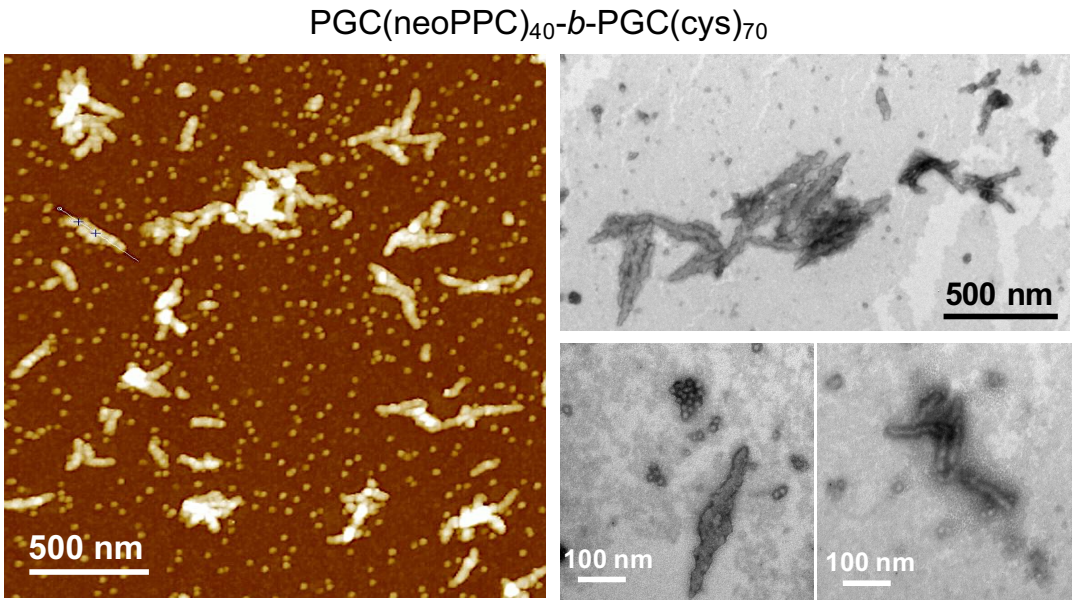

Figure II.23 AFM and TEM images of PGC(neoPPC)$_{40}$-*b*-PGC(EPC)(cys)$_{70}$, forming cylindrical nanoparticles.

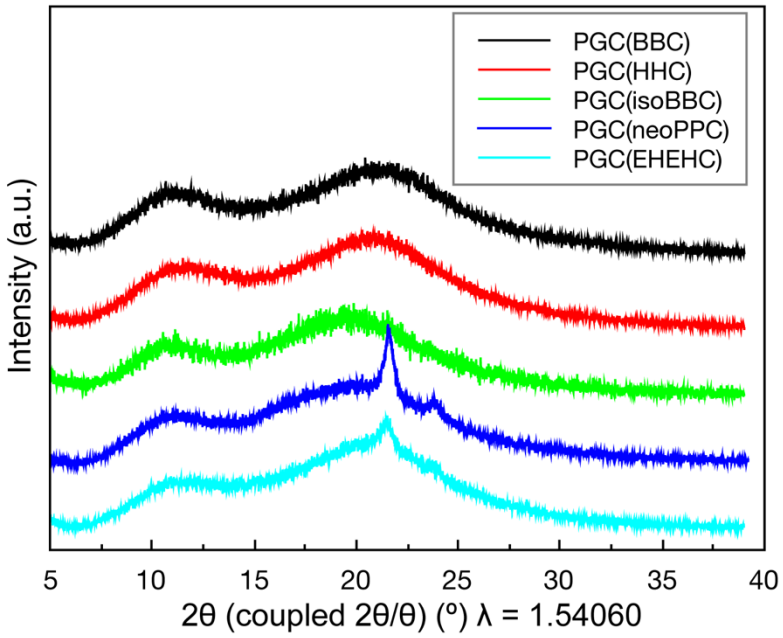

Figure II.24 WAXD diffractograms of the five amphiphilic block copolymers.

CHAPTER III

INVESTIGATION OF THE INVOLVEMENT OF SIDE-CHAIN FUNCTIONALITY IN THE MEDICATION OF REGIOSELECTIVITY DURING RING-OPENING POLYMERIZATION OF GLUCOSE CARBONATES

3.1 Introduction

Renewable sugar-based polymers have gained significant attention from chemists and from the broader community, due to their sustainability, structural diversity, and their potential as alternatives to petrochemicals for commercial applications.[1-3] There have been numerous studies on the development of sugar-based polymers over the past decades, which have often been devoted to the exploration of diversified monomer structures, incorporation of functionality, expansion of polymerization methods, and utilization in various practical applications.[4-8] Among others, glucose is of great interest, owing to its natural abundancy and high degree of functionality for tailoring of physicochemical and mechanical properties. A primary strategy for the construction of well-defined glucose-based polycarbonates has involved controlled ROPs. The guanidine organocatalyst, TBD, has been applied widely for the ROP for a variety of cyclic monomers in the presence of alcohol/amine initiators, while exerting high reactivity and excellent control of polymer molar mass and dispersity.[9-16] More recently, regioselectivity has been observed using TBD during the ring-opening of cyclic carbonates and sugar-based fused-cyclic monomers.[17-18] Despite the importance of regiochemistry in directing synthesis, regulating properties, and

thereby affecting polymer performance and applications, studies have seldom focused on revealing the regiochemical structures of the complex glucose-based polymers.

Several studies have probed the regiochemistry during ring-opening reactions of cyclic molecules. Kleij and coworkers achieved the regioselective ring-opening aminolysis of substituted five-membered cyclic carbonates by using TBD as the catalyst.[18] Uryu and coworkers studied the polymerization of 3,5-anhydro-1,2-*O*-isopropylidene-α-D-xylofuranose in which a regioregular [3→5]-2,3-*O*-isopropylidene-α-D-xylofuranan polyether was afforded under various polymerization conditions with a number of Lewis acids, anionic and coordination catalysts.[19] More recently, Buchard and coworkers reported the ring-opening of D-mannose-based 4- and 6- cyclic carbonate to proceed in a regioselective tail-to-head (T–H) direction, as was confirmed through a joint experimental and computational approach.[17] Aside from a few special cases of regioselective ring-opening reactions, the formation of regioirregular polymers is quite common. For instance, Gross and coworkers reported a polycarbonate having head-to-head (H–H), head-to-tail (H–T), and tail-to-tail (T–T) backbone linkages in a statistical 1:2:1 ratio from the ROP of a D-xylofuranose-based six-membered cyclic carbonate catalyzed by Yttrium(III) tris(isopropoxide).[20]

Within the last decade, we have experimentally observed inconsistencies in the regioregularity/regioirregularity of PGCs derived from the ROP of six-membered cyclic carbonate monomers.[21-23] Regioirregular PGCs were observed having statistical H–H, H–T, T–T repeat unit connectivities from methoxy-protected glucose carbonate monomers,[21]

whereas highly regioregular polymers were identified from glucose carbonates with ethyl- and propargyl- carbonate side chains (**Figure III.1**).[22] In Mikami *et al.*,[21] we reported the regiorandom nature of methoxy-protected glucose-derived polycarbonates from TBD-catalyzed ROP of a six-membered 4,6-cyclic asymmetric carbonate, as indicated by multiple resonance frequencies attributed to the H–H, H–T, and T–T species in ^{13}C NMR spectra and confirmed by tandem MS analyses using electron transfer dissociation (ETD). In contrast, later work, Su *et al.*,[22] indicated the preparation of regioregular PGCs with ethyl and/or propargyl carbonate protecting groups on the 2- and 3-positions of the glucose carbonate. These differential regiochemisties, observed during the ROP of D-glucose-based cyclic carbonate monomers having ether *vs*. carbonate side chain functionalities, presented an exciting challenge.

To explore the origin that dictated the regiochemistry and achieve a deep understanding of the TBD-catalyzed ROP process, therefore, we investigated the early stages of polymerization through the structural characterization of glucose carbonate unimers and dimers with carbonate- or ether- side-chain functionalities. Building upon our previous report of the synthesis and isolation of discrete oligomers,[23] full characterization of these compounds was conducted to reveal the detailed structures. Theoretical DFT calculations were also applied to probe the origin of the regioselectivity.

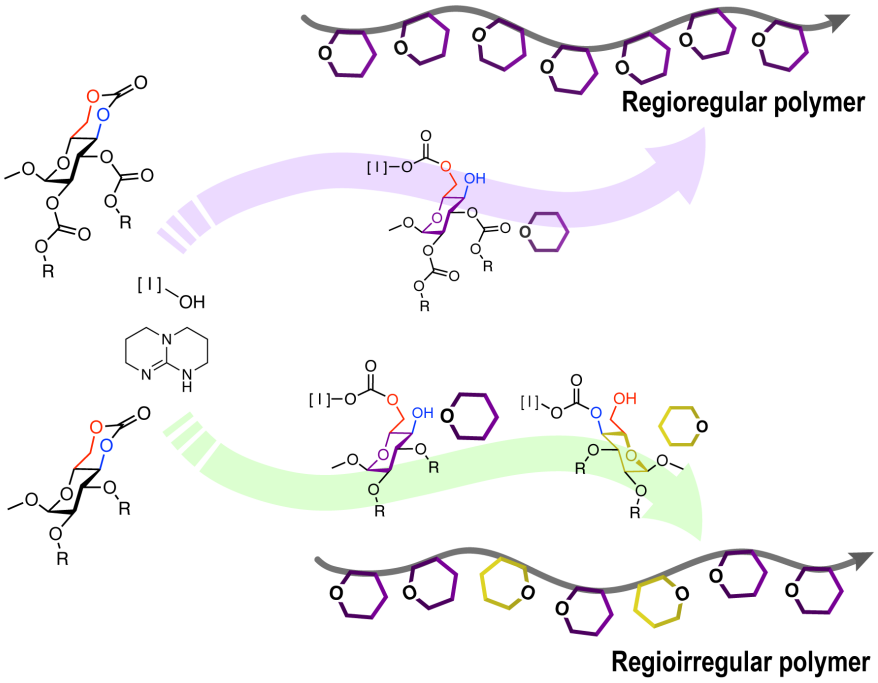

Figure III.1 ROP of glucose carbonate monomers with carbonate *vs.* ether side chain substituents, yielding regioregular and regioirregular polymers respectively.

3.2 Materials and Methods

3.2.1 Materials

1,5,7-Triazabicyclo[4.4.0]dec-5-ene (TBD) and 2-ethylhexyl chloroformate were used as received from TCI America (Portland, OR). 4-Methylbenzyl alcohol was purified by recrystallization from petroleum ether and stored in a glovebox under Ar atmosphere. Amberlyst® 15 (H), ion exchange resin and *N,N,N′,N′*-tetramethylethylenediamine, 99% were purchased from Alfa Aesar, Thermo Fisher Scientific (Ward Hill, MA). Triphosgene

was used as received from Oakwood Products, Inc. (Estill, SC). Dichloromethane (DCM) was purified by a solvent purification system (J. C. Meyer Solvent Systems, Inc., Laguna Beach, CA). Other reagents were used as received from Sigma-Aldrich, Co. (St. Louis, MO) unless otherwise noted.

3.2.2 Instrumentation

^{1}H NMR, ^{13}C NMR, COSY, ^{1}H–^{13}C HSQC and ^{1}H–^{13}C HMBC spectra were acquired on Varian Inova 500, Brucker 400, and Avance 500 spectrometers. Chemical shifts were referenced to the solvent resonance signals.

Size exclusion chromatography (SEC) eluting with THF was conducted on a Waters Chromatography, Inc. (Milford, MA) system equipped with an isocratic pump (model 1515), a differential refractometer (model 2414), and a four-column set, including a 5 μm Guard column (50 × 7.5 mm), a PLgel 5 μm Mixed C column (300 × 7.5 mm, Agilent Technologies) and two Styragel® columns (500 Å and 104 Å, 300 × 7.5 mm, Waters Chromatography, Inc.). The system was equilibrated at 40 °C in THF with the flow rate set to 1.0 mL/min. Data collection and analysis were performed with Waters Breeze™ software. Molar masses were determined relative to polystyrene standards (615-442800 Da) purchased from Polymer Laboratories, Inc. (Amherst, MA). Polymer/ oligomer solutions were prepared at a concentration of *ca.* 3 mg/mL with 0.05 vol% toluene added as a flow marker, and an injection volume of 200 μL was used.

Preparative size exclusion chromatography (prep SEC) eluting with chloroform was conducted on a JAI LC-9230II NEXT Chromatography, Inc. (Japan) system equipped

with a reciprocating double plunger pump (model P-9104B), a UV-vis 4ch NEXT detector at four wavelengths (254 nm, 280 nm, 300 nm, 330 nm), and a two-column set, including a JAIGEL-H 40P Guard column and a JAIGEL-2H-40 HPLC column. The system was equilibrated at room temperature in chloroform with the flow rate set to 14.0 mL/min. Data collection and analysis were performed with JAI Scan™ software. Polymer solutions were prepared at a concentration of *ca*. 10 mg/mL in chloroform and an injection volume of 5 mL was used.

Electrospray ionization mass spectrometry (ESI-MS) experiments were performed using a Thermo Scientific Q Exactive Focus. The sample was directly infused at a flow rate of 10 μL/min. The Q-Exactive Focus HESI source was operated in full MS in positive mode. The mass resolution was tuned to 70000 FWHM at m/z 200. The spray voltage was set to 3.75 kV, and the sheath gas and auxiliary gas flow rates were set to 7 and 0 arbitrary units, respectively. The transfer capillary temperature was held at 320 °C. Exactive Series 2.8 SP1/Xcalibur 4.0 software was used for data acquisition and processing.

Thermogravimetric analysis (TGA) was performed under an $N_{2(g)}$ atmosphere using a Mettler-Toledo model TGA2/1100/464 from 25 – 500 °C with a heating rate of 10 °C/min. Data were analyzed using Mettler-Toledo STAR^e v. 15.00a software.

Glass transitions (T_g) were measured by differential scanning calorimetry (DSC) on a Mettler-Toledo DSC3/700/1190® (Mettler-Toledo, Inc., Columbus, OH) under $N_{2(g)}$. Measurements were performed with a heating rate of 10 °C/min and analyzed

using Mettler-Toledo Star^{e} v. 15.00a software. The T_g was taken as the midpoint of the inflection tangent of the third heating scan.

3.2.3 Synthetic procedures

Synthesis of GC(OEH) monomer (Figure III.2):

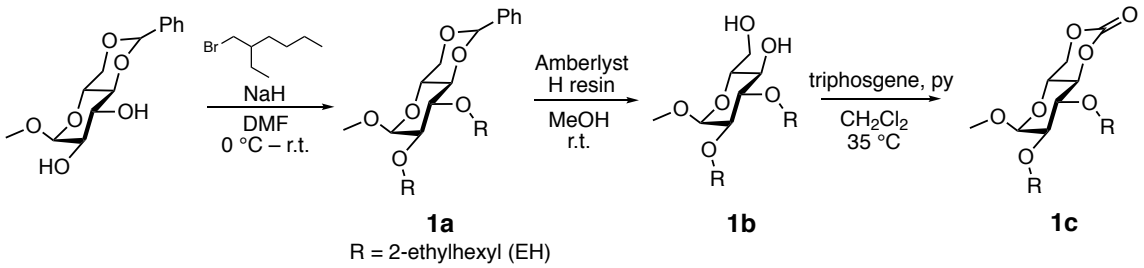

Figure III.2 Synthetic procedures for GC(OEH) monomer.

To a suspension mixture of 60 wt% NaH in mineral oil (2.3 g, 0.057 mol) in dry DMF (100 mL) was added methyl 4,6-*O*-benzylidene-α-D-glucopyranoside (2 g, 0.0071 mol) in dry DMF (30 mL) dropwise at 0 °C over 20 min and the mixture was allowed to stir at room temperature for 1 h. To the mixture was added 2-ethylhexyl bromide (6.8 mL, 0.035 mol) at 0 °C over 30 min and the mixture was allowed to stir at 0 °C for 1 h. The mixture was allowed to warm to room temperature, stirred for 22 h. The reaction was quenched by slowly adding water and extracted with dichloromethane. The collected organic layer was dried over Na_2SO_4 and concentrated under reduced pressure. The residue was purified by column chromatography (gradient ethyl acetate/hexanes) to afford the **1a** methyl-2,3-*O*-2-ethylhexylether-4,6-*O*-benzylidene-α-D-glucopyranoside (0.44 g)

as a colorless liquid. ^{1}H NMR (500 MHz, $CDCl_3$) δ 7.54 – 7.47 (m, 2H), 7.37 (m, 3H), 5.56 (s, 1H), 4.82 (dd, *J* = 4, 1 Hz, 1H), 4.30 (dd, *J* = 9, 4 Hz, 1H), 3.88 – 3.71 (m, 3H), 3.71 (dd, *J* = 7, 1 Hz, 1H), 3.68 (d, *J* = 6 Hz, 1H), 3.68 – 3.56 (m, 1H), 3.54 (m, 2H), 3.53 – 3.44 (m, 1H), 3.45 (s, 3H), 3.36 (dd, *J* = 9, 4 Hz, 1H), 1.60 – 1.47 (m, 1H), 1.51 – 1.40 (m, 1H), 1.29 (m, 19H), 0.99 (d, *J* = 6.6 Hz, 0H), 0.96 – 0.89 (m, 5H), 0.93 – 0.80 (m, 9H) ppm. ^{13}C NMR (126 MHz, $CDCl_3$) δ 137.49, 130.17, 128.48, 125.99, 101.18, 98.16, 82.23, 81.21, 78.73, 69.71, 62.71, 62.40, 61.25, 55.47, 40.24, 39.90, 31.55, 30.32, 30.21, 29.14, 28.89, 23.58, 23.45, 23.10, 22.88, 14.13, 14.10, 13.95, 11.02, 10.96 ppm.

To a solution of **1a** (0.44 g) in methanol, 2 g of Amberlyst H-from resin was added. After stirring for 12 h under ambient condition at room temperature, the mixture was filtered over celite. The obtained solution was concentrated under reduced pressure and purified by column chromatography (gradient ethyl acetate/hexanes) to afford **1b** as a colorless liquid (0.22 g). ^{1}H NMR (400 MHz, $CDCl_3$) δ 4.84 (dd, *J* = 4, 1 Hz, 1H), 3.90 (m, 2H), 3.81 (m, 1H), 3.68 (dt, *J* = 8, 4 Hz, 1H), 3.59 – 3.37 (m, 4H), 3.45 (s, 3H), 3.34 – 3.25 (m, 1H), 2.47 – 2.41 (m, 1H), 1.97 (dd, *J* = 7, 6 Hz, 1H), 1.52 (m, 2H), 1.50 – 1.39 (m, 1H), 1.42 – 1.29 (m, 5H), 1.29 (m, 8H), 0.96 – 0.85 (m, 11H) ppm. ^{13}C NMR (101 MHz, $CDCl_3$) δ 98.19, 81.35, 80.95, 73.45, 70.91, 70.80, 62.87, 55.42, 40.59, 40.47, 40.08, 30.58, 30.50, 30.42, 29.36, 29.30, 29.18, 29.12, 23.93, 23.75, 23.59, 23.28, 23.26, 23.24, 14.29, 14.26, 14.24, 11.34, 11.10, 11.08, 11.04 ppm.

To a solution of **1b** (0.22 g, 0.53 μmol) in anhydrous DCM in a 100 mL two-neck round bottom flask, pyridine (0.13 g, 1.6 μmol) was added. Triphosgene dissolved in anhydrous DCM was added dropwise *via* a syringe over 10 min. The reaction mixture

was allowed to stir at 35 °C for 10 h under $N_{2(g)}$ flow, followed by quenching with addition of $NaHCO_{3(aq)}$ slowly. The organic layer was concentrated under reduced pressure and the product was purified by column chromatography (gradient acetone/DCM) to afford **1c** methyl-2,3-*O*-2-ethylhexyl-4,6-*O*-carbonyl-α-D-glucopyranoside **GC(OEHEH)** (0.16 g) as a colorless liquid. ^{1}H NMR (500 MHz, $CDCl_3$) δ 4.82 (d, *J* = 3.5 Hz, 1H), 4.46 (dd, *J* = 10, 6 Hz, 1H), 4.19 (t, *J* = 10 Hz, 1H), 4.10 – 3.94 (m, 2H), 3.75 – 3.59 (m, 3H), 3.59 – 3.50 (m, 1H), 3.46 (s, 3H), 3.29 (dd, *J* = 9, 4 Hz, 1H), 1.55 – 1.45 (m, 2H), 1.45 – 1.19 (m, 16H), 1.01 – 0.72 (m, 12H) ppm. ^{13}C NMR (126 MHz, $CDCl_3$) δ 147.62, 99.30, 79.99, 79.93, 77.79, 77.77, 76.55, 76.53, 75.04, 75.02, 69.75, 59.76, 56.20, 53.56, 40.45, 40.40, 40.07, 40.01, 30.54, 30.47, 30.40, 30.33, 29.34, 29.29, 29.17, 29.12, 23.80, 23.72, 23.66, 23.57, 23.25, 14.25, 11.26, 11.15, 11.06, 11.01 ppm.

Polymerization of GC(OEH). A solution of GC(OEH) monomer (49.5 mg) and 4-methylbenzyl alcohol (0.26 mg, 1.0 mg/mL in DCM, 0.10 mL) were prepared in a glovebox in a vial equipped with a stir bar at 30 °C. A solution of TBD (3.2 mg/mL in DCM, 0.05 mL) was injected to the reaction mixture, and the reaction was allowed to stir at 30 °C for 6.5 h, followed by quenching by adding an aliquot of acetic acid solution. The product was purified by precipitation into methanol three times and dried under vacuum to afford the polymer as a white solid (20 mg). ^{1}H NMR (500 MHz, $CDCl_3$) δ 4.76 (d, *J* = 8 Hz), 4.57 (m), 4.41 – 4.21 (m), 4.14 (br), 3.95 – 3.79 (m), 3.68 (br), 3.52 – 3.33 (m), 3.33 – 3.22 (m), 2.34 (s), 0.96 – 0.71 (m). ^{13}C NMR (126 MHz, $CDCl_3$) δ 154.43, 97.69, 97.49, 80.61, 78.95, 78.55, 75.76, 75.19, 67.43, 67.10, 55.49, 40.46, 40.34, 40.01, 30.52, 30.42, 30.31, 29.28, 29.12, 23.68, 23.51, 23.25, 14.30, 14.26, 11.30, 11.09,

11.00, 10.86. SEC (THF, 1mL/min): 12.3 kDa, $Đ = 1.16$. $T_g = 98$ °C. TGA in $N_{2(g)}$: 230-280 °C, 98% mass loss.

Oligomerization of GC(OEH) and isolation of GC(OEH) unimers. A solution of GC(OEHEH) monomer (105 mg, 1 eq.) and 4-methylbenzyl alcohol (46 mg, 1.5 eq.) were dissolved in 1 mL of DCM in a vial equipped with a stir bar in a glovebox at 30 °C. A solution of TBD (13 mg/mL in DCM, 0.05 mL) was injected to the reaction mixture, and the reaction was allowed to stir at 30 °C for 1.5 h, followed by quenching by adding an aliquot of acetic acid solution. The product was purified and fractionated by preparative SEC to afford a mixture of regioisomeric unimers. The two regioisomeric unimers were then separated by thin layer chromatography (ethyl acetate/hexanes) and determined using 1D and 2D NMR spectroscopies.

Regioisomer A: ^{1}H NMR (400 MHz, $CDCl_3$) δ 7.28 (d, J = 8 Hz, 2H), 7.16 (d, J = 8 Hz, 2H), 5.13 (s, 2H), 4.79 (d, J = 3 Hz, 1H), 4.40 (d, J = 4 Hz, 2H), 3.91 – 3.80 (m, 1H), 3.80 – 3.73 (m, 1H), 3.58 – 3.31 (m, 8H), 3.27 (dd, J = 9, 3 Hz, 1H), 2.45 (s, 1H), 2.35 (s, 3H), 1.49 (m, 2H), 1.45 – 1.17 (m, 19H), 0.96 – 0.78 (m, 12H). ^{13}C NMR (126 MHz, $CDCl_3$) δ 155.50, 138.59, 132.30, 129.37, 128.74, 98.13, 81.28, 80.76, 80.75, 80.67, 80.66, 76.74, 76.58, 75.40, 73.57, 73.54, 70.03, 69.90, 69.21, 66.92, 55.46, 40.57, 40.46, 40.04, 40.01, 30.66, 30.65, 30.56, 30.46, 30.39, 29.85, 29.81, 29.51, 29.35, 29.29, 29.16, 29.13, 23.90, 23.88, 23.71, 23.56, 23.28, 23.26, 23.24, 21.37, 14.28, 14.26, 14.25, 11.33, 11.31, 11.09, 11.06, 11.05. HRMS (ESI^+): $C_{32}H_{54}O_8$, 589.3711 found ($M+Na^+$) 589.3700; $C_{32}H_{54}O_8NH_4^+$ 584.4157, found 584.4149.

Regioisomer B: ^{1}H NMR (400 MHz, $CDCl_3$) δ 7.17 (d, J = 8 Hz, 2H), 5.13 (m, 2H), 4.82 (d, J = 3 Hz, 1H), 4.70 (t, J = 10 Hz, 1H), 3.82 – 3.35 (m, 11H), 3.33 (dd, J = 9, 4 Hz, 1H), 2.35 (s, 3H), 1.45 – 1.12 (m, 16H), 0.96 – 0.72 (m, 12H). ^{13}C NMR (126 MHz, $CDCl_3$): δ 155.63, 138.77, 131.97, 129.47, 128.71, 128.69, 98.22, 80.78, 80.69, 78.73, 76.59, 74.82, 74.30, 70.38, 69.53, 61.33, 55.55, 40.49, 40.29, 40.03, 30.59, 30.42, 30.36, 30.24, 29.85, 29.30, 29.25, 29.15, 23.70, 23.60, 23.55, 23.26, 23.23, 21.37, 14.27, 11.24, 11.09, 11.05. HRMS (ESI^+) $C_{32}H_{54}O_8$, 589.3711 found ($M+Na^+$) 589.3699; $C_{32}H_{54}O_8NH_4^+$ 584.4157, found 584.4148.

Oligomerization of GC(OMe) and separation of GC(OMe) oligomers. A solution of GC(OEH) monomer (300 mg, 3 eq.) and 4-methylbenzyl alcohol (49 mg, 1 eq.) were dissolved in 1 mL of DCM in a vial equipped with a stir bar in a glovebox at 30 °C. A solution of TBD (34 mg/mL in DCM, 0.1 mL) was injected to the reaction mixture, and the reaction was allowed to stir at 30 °C for 30 min, followed by quenching by adding an aliquot of acetic acid solution. The product was purified and fractionated by preparative SEC to afford mixtures of regioisomeric unimers and dimers.

3.2.5 Computational details

All geometries of reactants, transition states (TSs), and intermediates were fully optimized by Gaussian 16, B.01 program.[130] The ωB97XD functional[131] was chosen as it includes a built-in dispersion correction, which has been shown to have great performance on closely related systems. The 6-31+G(d) basis set[132] was used for the molecule. In addition to that, a single p polarization was added to the two H atoms directly involved in

hydrogen bonding. Geometries were optimized in DCM solvent using conductor-like polarizable continuum (CPCM) model.[133-134] Frequency calculations at the same level of theory were carried out to verify all stationary points as minima (zero imaginary frequency) and transition states (one imaginary frequency). Cartesian coordinates of all the stationary points are available in .xyz format in the Appendix A.

3.3 Results and Discussion

Structures of discrete unimers and dimers with carbonate-side chains. Recently, we have investigated the ROP of a broad range of D-glucose carbonate monomers with varied alkyloxycarbonyl side chains; high regioselectivity persisted regardless of the length and branch/bulkiness of the side chain.[22-23] The polymer regioregularity was evidenced by only one sharp peak corresponding to the polymer backbone carbonate C=O resonating at 153.6 – 153.9 ppm in the ^{13}C NMR spectrum of the PGCs. In accordance with the ^{13}C NMR analysis, well-defined splitting patterns for the glucose monomer repeat unit protons of the side chain carbonate-protected PGCs in ^{1}H NMR analysis contrasted with typical broad peaks for regioirregular polymers, as was observed for side chain ether-protected PGCs. To agree with both the ^{13}C and ^{1}H NMR observations, possible regioisomeric forms of highly regioregular PGC include 4-to-6 (H–T) or 6-to-4 (T–H) linkages. Either would lead to regioregularity of the resulting polymers, but were indiscernible from the polymer 1D NMR spectra. However, further structural elucidation directly on the polymers, including homonuclear and heteronuclear 2D NMR

techniques, was impeded by the structural and resulting spectroscopic complexities. To reveal the regioselectivity during initiation and propagation steps, the structures of unimers and dimers were targeted. Therefore, TBD-catalyzed ring-opening reactions of D-glucose-based cyclic carbonates were conducted in the presence of 0.3-0.5 equivalences of 4-methylbenzyl alcohol (4-MeBnOH) to limit chain growth. Oligomeric samples **A1**, **A2** (derived from methyl-2,3-*O*-neopentyloxycarbonyl-4,6-*O*-carbonyl-α-D-glucopyranoside [GC(EHEHC)]), **B1** and **B2** (derived from methyl-2,3-*O*-2-ethylhexyloxycarbonyl-4,6-*O*-carbonyl-α-D-glucopyranoside [GC(neoPPC)]) (**Figure 1**) were prepared, followed by fractionation using preparative size-exclusion chromatography (SEC) to isolate sufficient quantities of pure unimeric and dimeric structures for detailed NMR analyses.

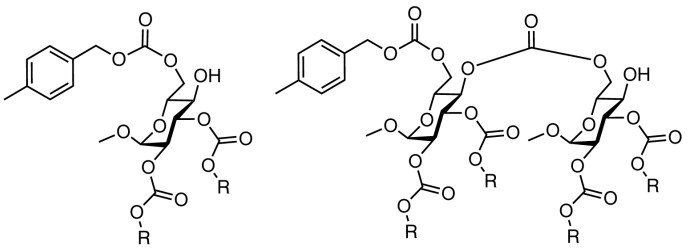

A1: R = 2-ethylhexyl
B1: R = neopentyl

A2: R = 2-ethylhexyl
B2: R = neopentyl

Figure III.3 Unimer and dimer structures of 2-ethylhexyl- (**A1** and **A2**, respectively) and neopentyl- (**B1** and **B2**, respectively) D-glucose carbonate for investigation of the ring-opening directions of monomers with carbonate-based side chain protecting groups.

Homonuclear correlation spectroscopy (COSY) (**Figures 2a**, **S1**), ^{1}H–^{13}C heteronuclear single quantum correlation (HSQC) (**Figure S2**), and ^{1}H–^{13}C heteronuclear multiple-bond correlation (HMBC) (**Figure 2b**) 2D-NMR analyses were performed to examine the structural details, thereby providing regioselective preferences of ring-opening reactions during initiation and propagation. First, each proton of **A1** was assigned by combining the results from ^{1}H NMR, COSY and HSQC. The unimer structure was found to have the *C4* position linked to a free hydroxyl group, as indicated by the COSY spectrum showing a cross peak at (3.69, 3.10 ppm), designated to the coupling of the O***H*** and C-$\boldsymbol{H}_{d}$ protons, while no cross peak between $\boldsymbol{H}_{f}$ and O***H*** was observed. Meanwhile, by HMBC, the presence of a critical $^{3}J_{\mathrm{CH}}$ coupling between the backbone carbonyl carbon and the protons on *C6* (C$\boldsymbol{H}_{f}$) at (4.43, 155.45 ppm) suggested the *C–O6* bond was retained (**Figure 2b**). The absence of J_{CH} between $\boldsymbol{H}_{d}$ proton with any carbonyl carbon further verified the cleavage of the *C–O4* bond in HSQC spectrum. The absence of correlation between the alcohol proton (f2 = 3.06 ppm) and any carbon in HSQC (**Figure S2**) gave the same conclusion. These combined results suggested that the initiation reaction of the ring-opening polymerization with 4-MeBnOH was favorable at the *C–O4* position cleavage, yielding a secondary alcohol on the *C4* position as the active chain-end for the following propagation process.

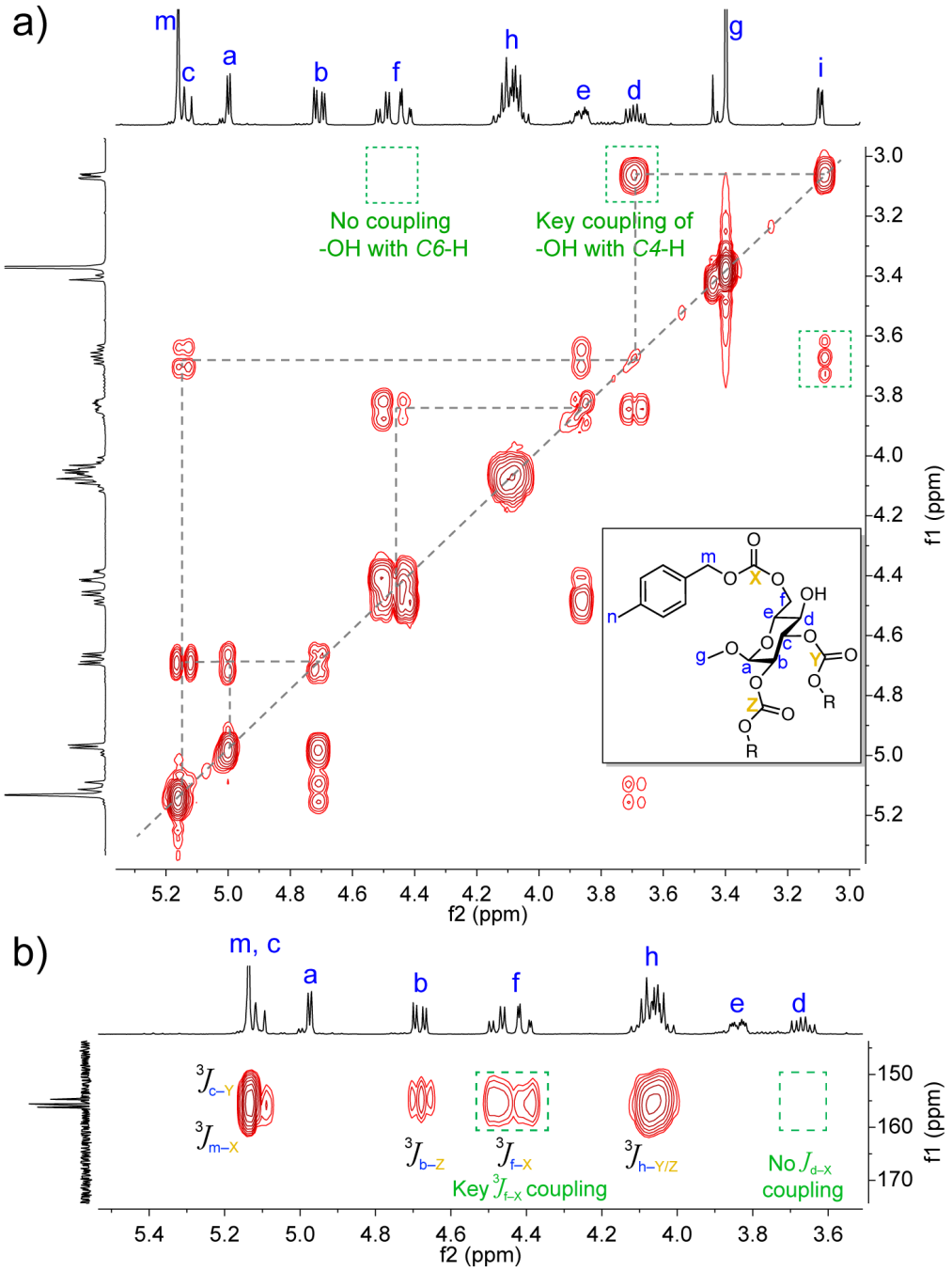

Figure III.4 ^{1}H–^{13}C HMBC spectrum (400 MHz for ^{1}H) of GC(EHEHC) unimer in $CDCl_3$, indicating preferential initiator–*O*6 linkage for initiation step when 4-methylbenzyl alcohol was used.

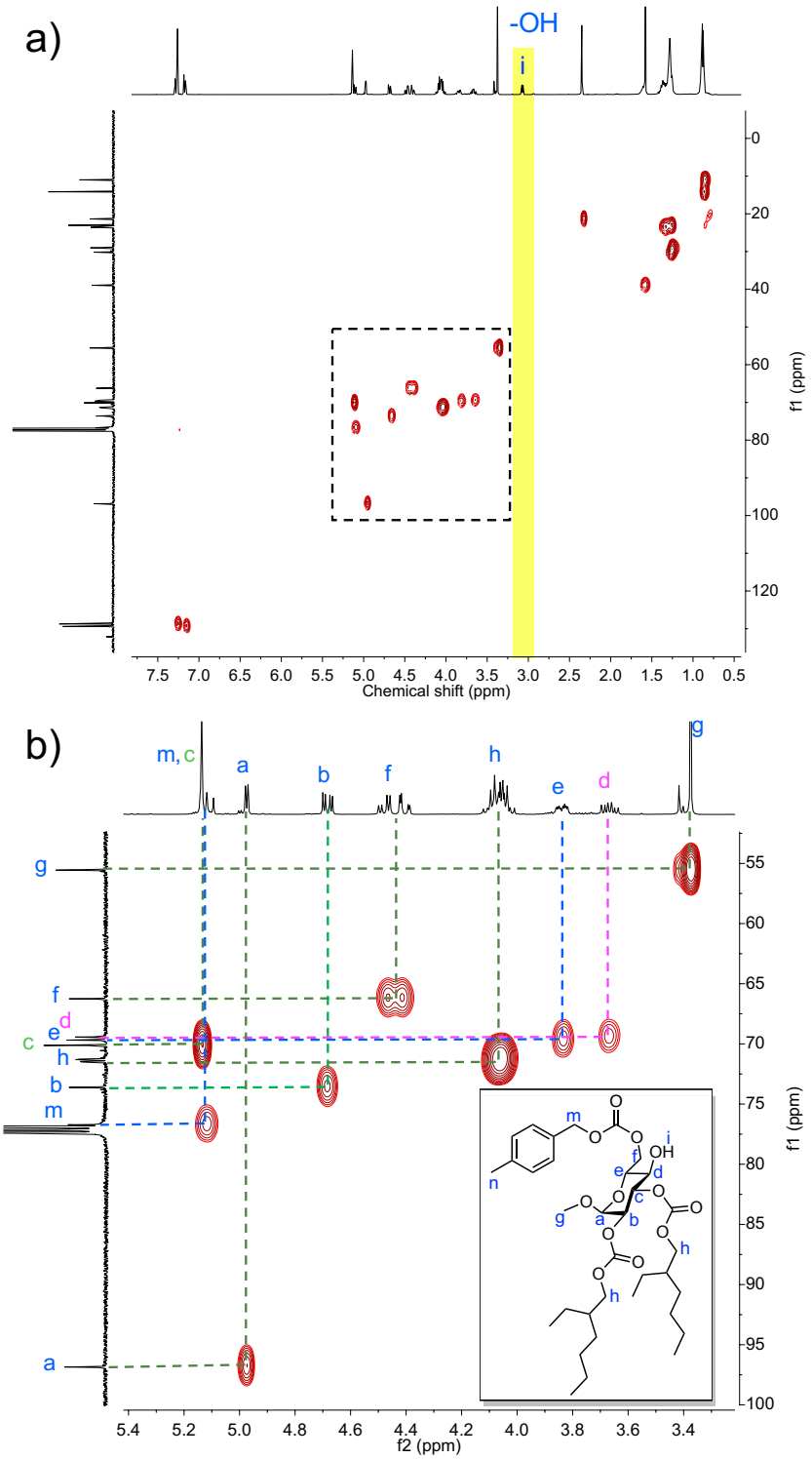

Figure III.5 ^{1}H–^{13}C HSQC spectra (500 MHz for ^{1}H) of GC(EHEHC) unimer in $CDCl_3$; (a) full-view and (b) enlarged area of the dashed box in (a).

To study whether the same regioselectivity was maintained in the following propagation process of ROP from the unimer, COSY, ^{1}H–^{13}C HSQC, and ^{1}H–^{13}C HMBC spectra of the dimer of GC(EHEHC) (**A2**) were acquired (**Figures III.6-III.7**). Similarly, two sets of proton resonances in the ^{1}H NMR that correlated to the first and second repeating units of the D-glucose carbonates were assigned before further analysis (Figure 2c). From HMBC spectroscopy, the presence of a key $^{3}J_{CH}$ coupling between the backbone carbonyl carbon of the second repeating unit ($\boldsymbol{C}_{X2}$) and the protons on *C6* ($\boldsymbol{H}_{f2}$) at (4.39, 154.81 ppm), together with the absence of the carbonyl carbon with the proton on *C4* ($\boldsymbol{H}_{d2}$, f2 = 3.72 ppm) (**Figure III.7c**), revealed the sustained *C–O6* linkage and occurance of *C–O4* cleavage in growth of the second repeating unit during the propagation process. Further evidence of this dimer connection was found by comparing the chemical shifts of the protons connected to *C4* and *C6* in both repeating units. The protons on *C6* ($\boldsymbol{H}_{f1}$ and $\boldsymbol{H}_{f2}$) in both repeating units possessed similar downfield chemical shifts at 4.30 and 4.39 ppm, respectively, indicative of their alike connections to the backbone carbonate groups. Whereas for chemical shifts of protons on *C4* ($\boldsymbol{H}_{d1}$ and $\boldsymbol{H}_{d2}$), a distinct difference was observed between the two repeating units, revealing their varied chemical environments. The more deshielded resonance of $\boldsymbol{H}_{d1}$ (4.90 ppm) was attributed to the connectivity of *C4* in the first repeating unit to a carbonate group, while *C4* in the second repeating unit was found to attach to a free hydroxyl group by comparing the chemical shift of $\boldsymbol{H}_{d2}$ (3.72 ppm) and $\boldsymbol{H}_{d}$ (3.69 ppm) of the unimer. Therefore, both of the unimer and dimer structures exhibited preference in the formation of backbone carbonate linkages

at the less sterically hindered primary position, and leaving the secondary hydroxyl group for subsequent selective propagation, affording the regioregular 6-to-4 H–T linkages. When the 2-ethylhexyl substituted side chains of the monomer was changed to neopentyl-carbonate (**B1** and **B2**), same regiochemistry was perceived based on the corresponding unime and dimer (**Figures III.8-13**). This regioselective ROP process was in agreement with recent reports by Sopeña *et al.*[127] and Gregory *et al.*[26] in the synthesis of carbamates and mannose-based polycarbonates, respectively, where the initiator attacked the cyclic carbonyl and selectively cleaved the side having a methine group.

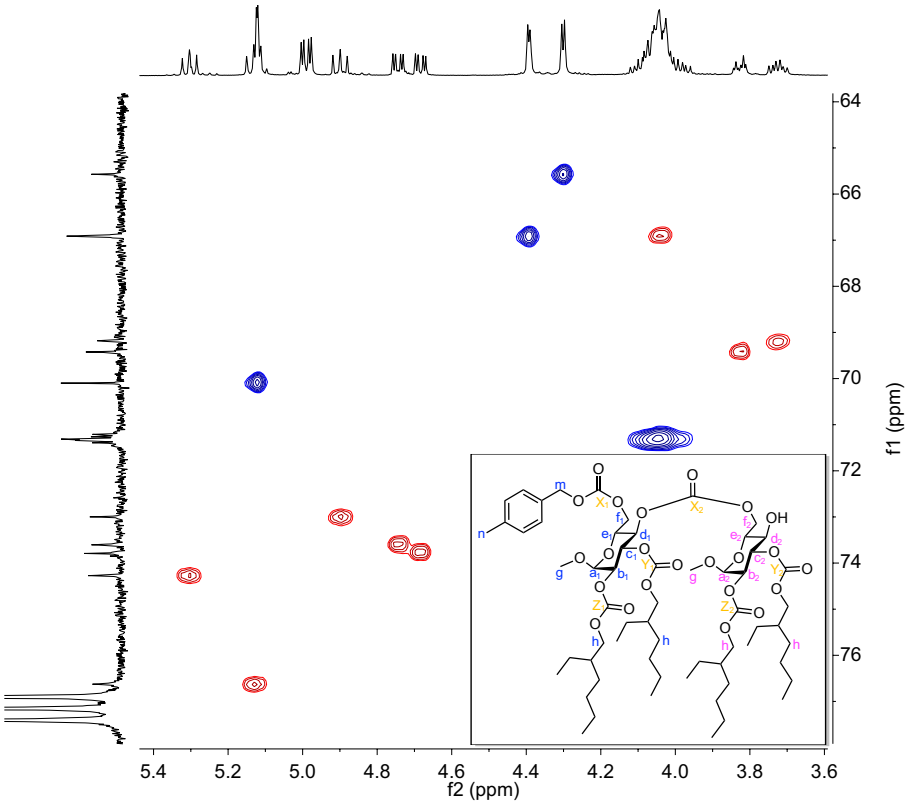

Figure III.6 $^{1}H–^{13}C$ HSQC spectra (500 MHz for ^{1}H) of GC(EHEHC) dimer in $CDCl_3$.

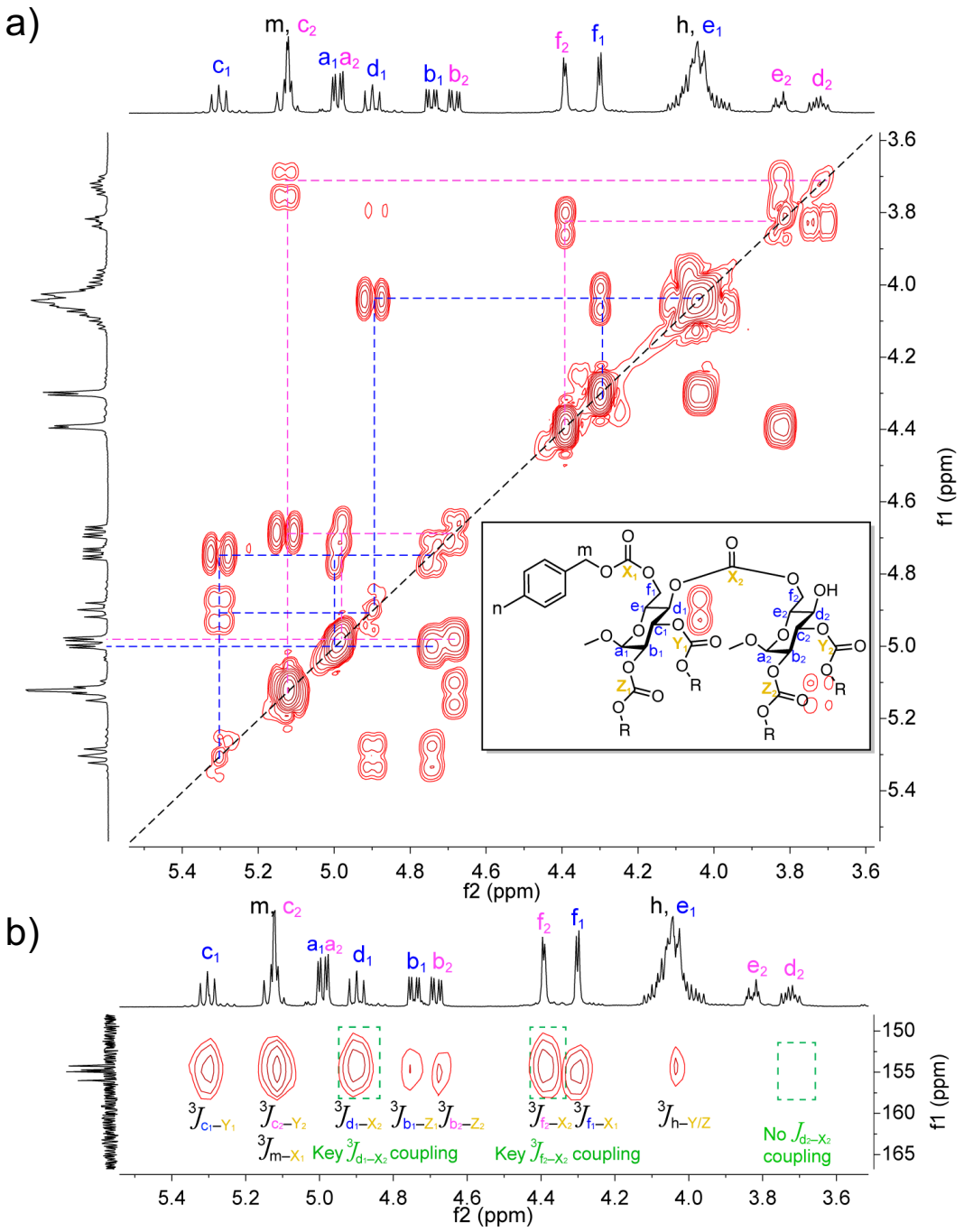

Figure III.7 Molecular structures (a), COSY (b, 500 MHz) and ^{1}H–^{13}C HMBC spectra (c, 400 MHz for ^{1}H) of GC(EHEHC) dimer in $CDCl_3$, indicating preferential *O*4-*O*6 linkage for propagation.

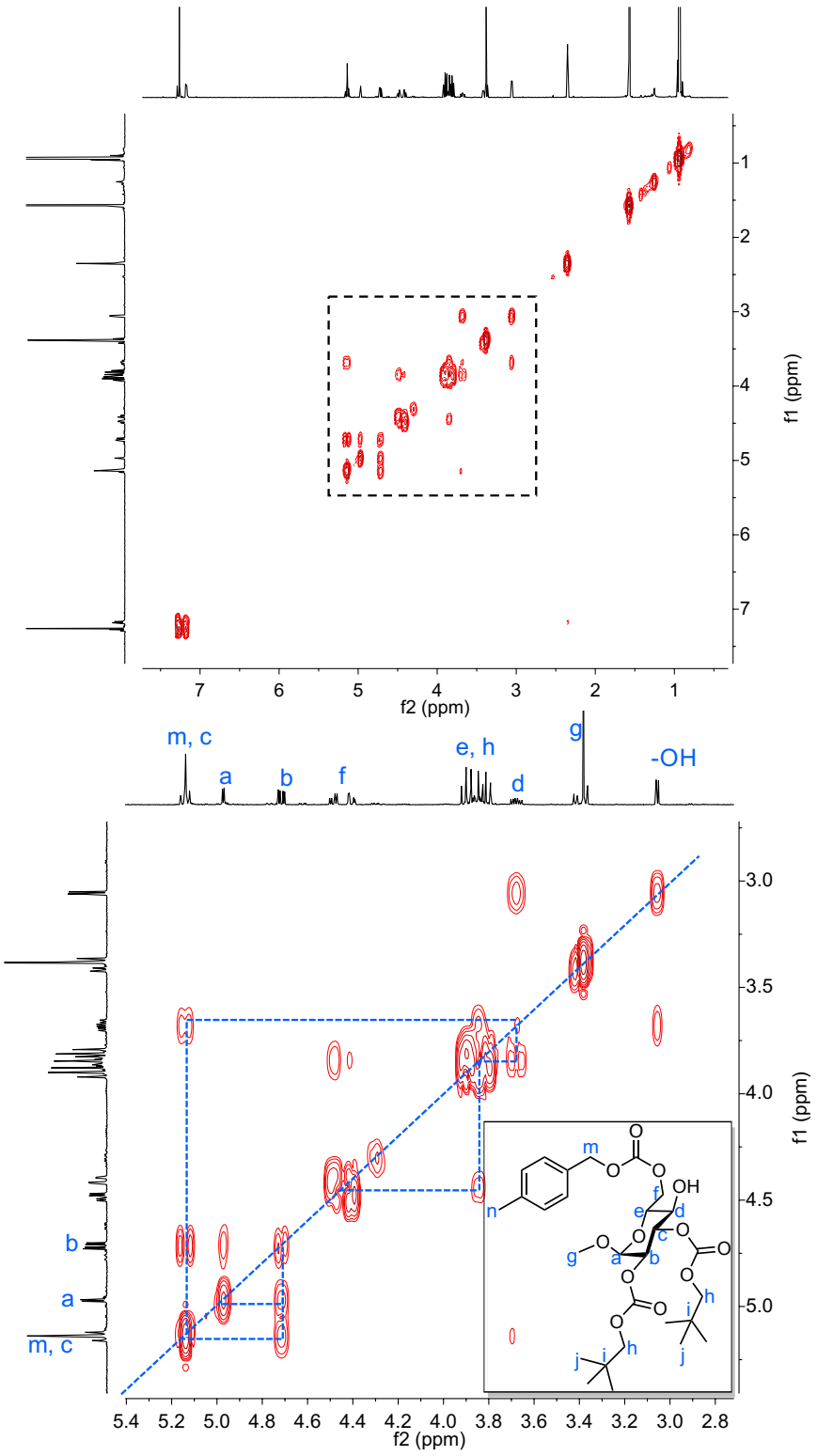

Figure III.8 COSY spectrum (500 MHz) of GC(neoPPC) unimer in $CDCl_3$.

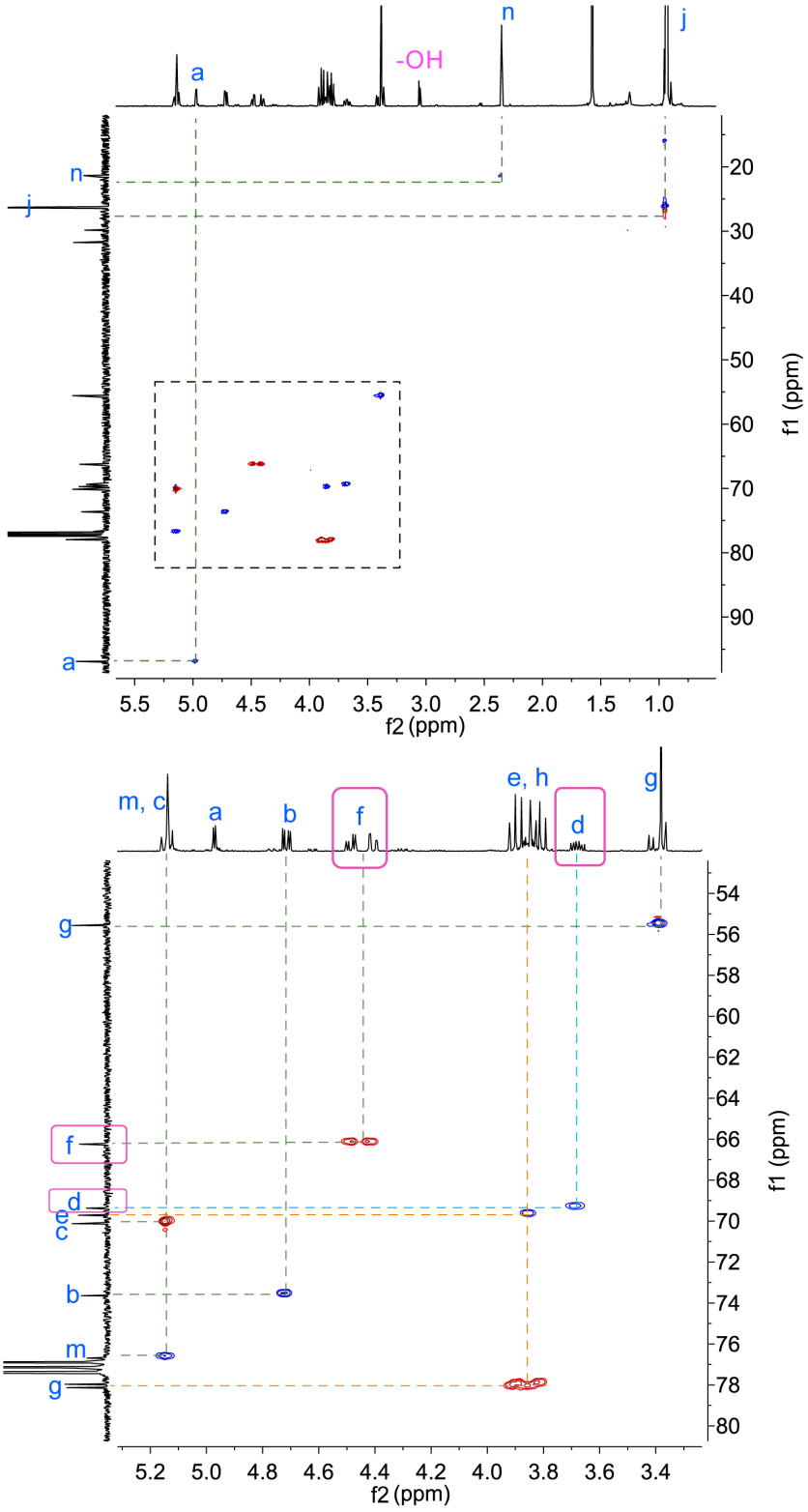

Figure III.9 ^{1}H–^{13}C HSQC spectrum (500 MHz for ^{1}H) of GC(neoPPC) unimer in $CDCl_3$.

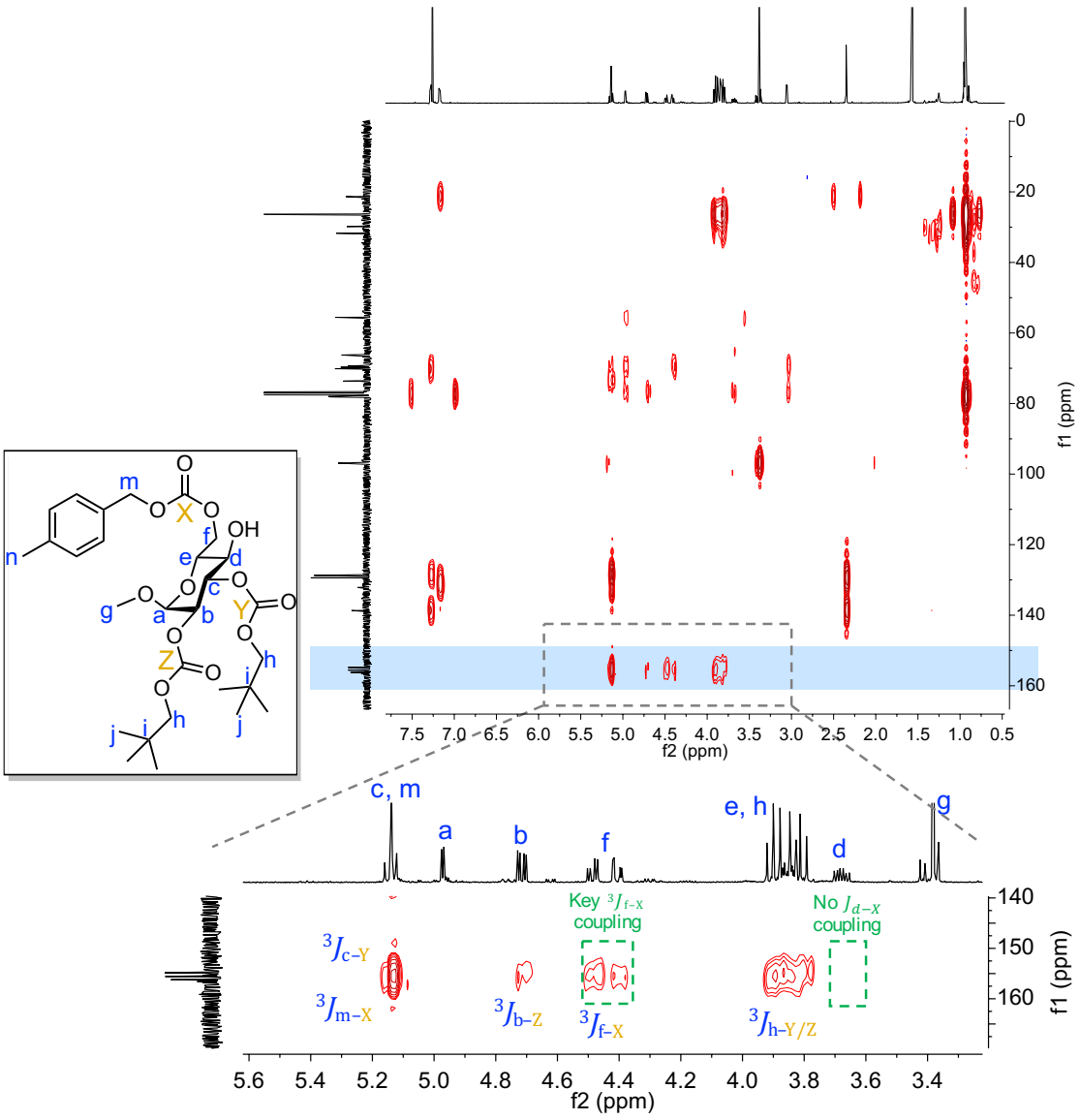

Figure III.10 ^{1}H–^{13}C HMBC spectrum (400 MHz for ^{1}H) of GC(neoPPC) unimer in $CDCl_3$.

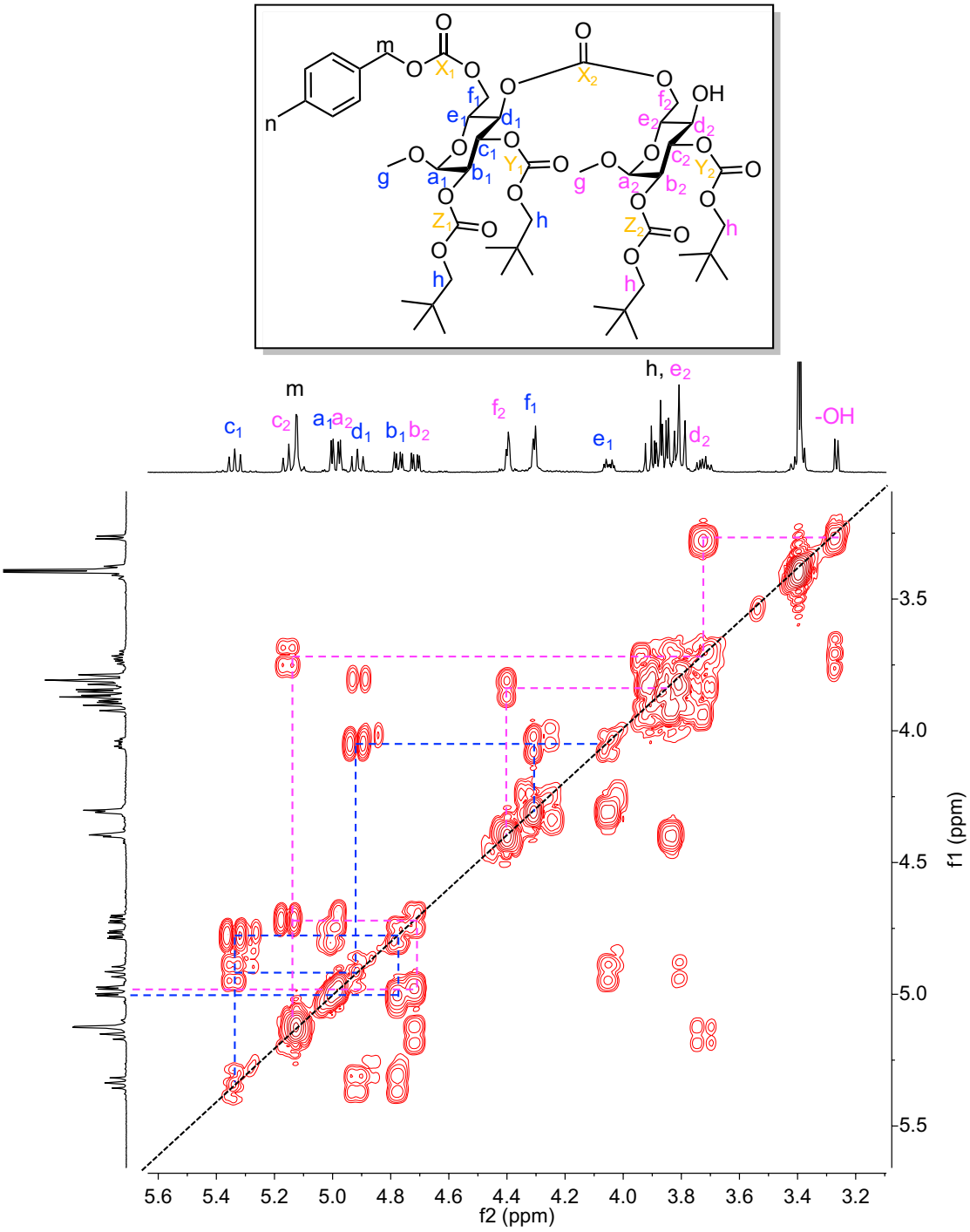

Figure III.11 COSY spectrum (500 MHz) of GC(neoPPC) dimer in $CDCl_3$.

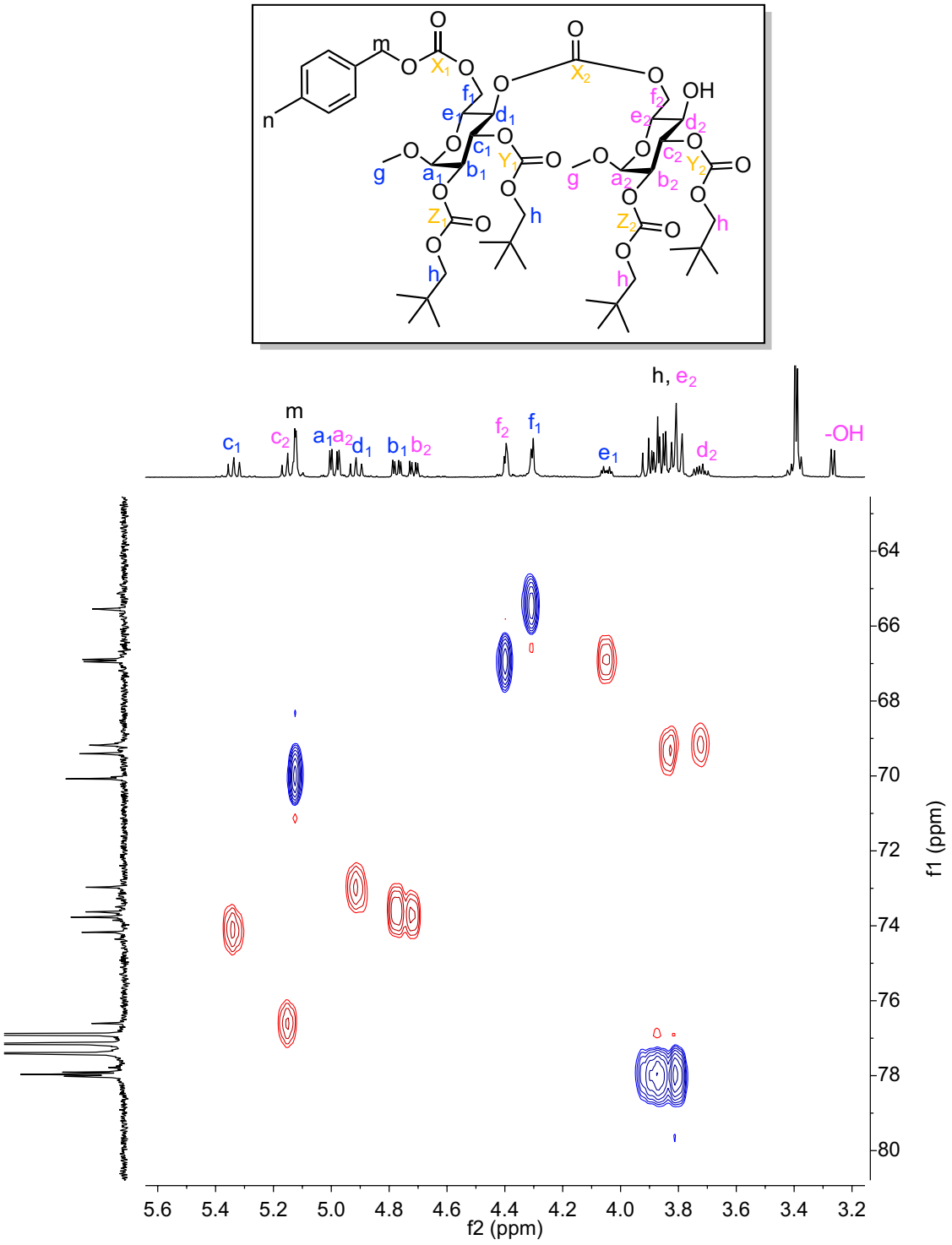

Figure III.12 HSQC spectrum (500 MHz) of GC(neoPPC) dimer in $CDCl_3$.

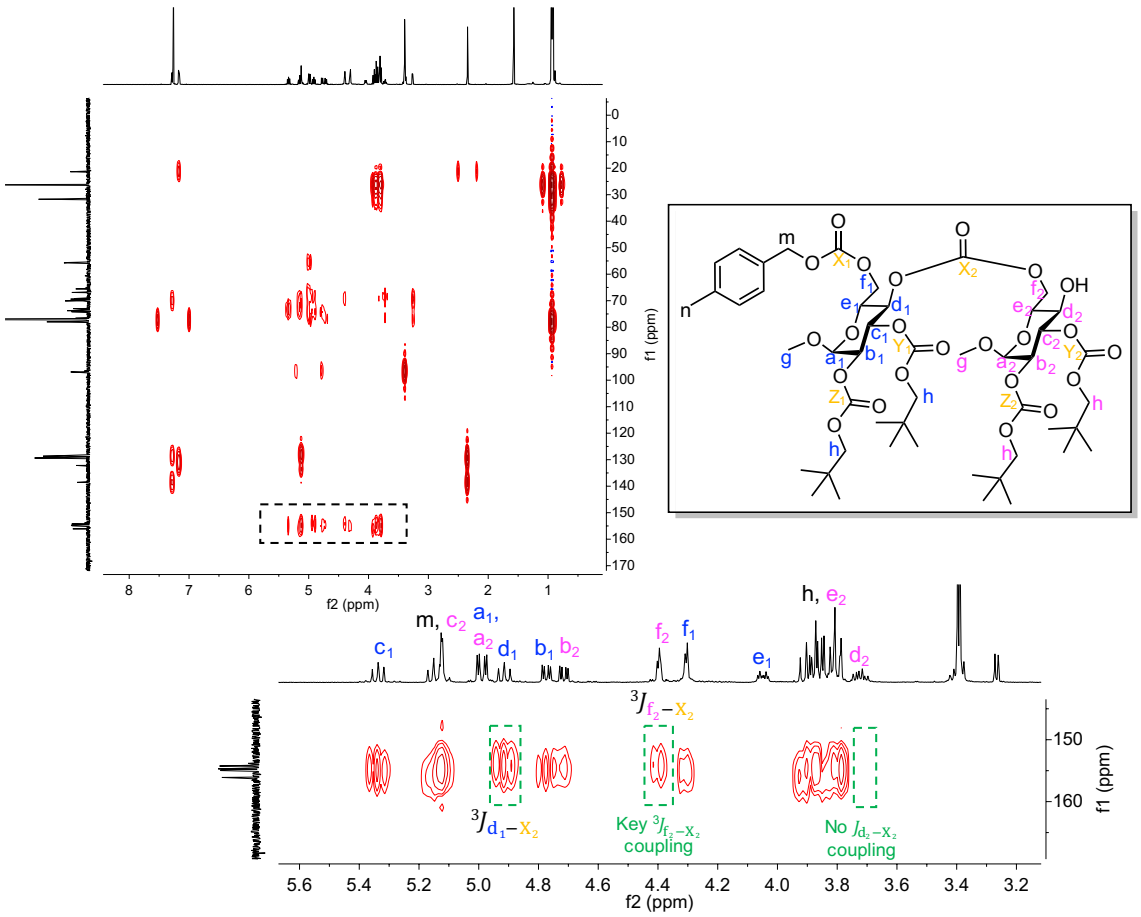

Figure III.13 HMBC spectrum (500 MHz) of GC(neoPPC) dimer in $CDCl_3$.

Synthesis and structural analyses of regioisomers with ether-side chains. To investigate whether the preference of the ring-opening reactions during initiation and propagation of alkyloxycarbonyl protected D-glucose carbonates was caused by side-chain steric hindrance, a parallel study was performed on a D-glucose-based carbonate monomer with a similar side chain structure, but an ether-linkage at the 2- and 3- positions, methyl-2,3-*O*-2-ethylhexyl-4,6-*O*-carbonyl-α-D-glucopyranoside [GC(OEH)]. The monomer was synthesized using modified procedures from previous reports (**Figure III.14**),

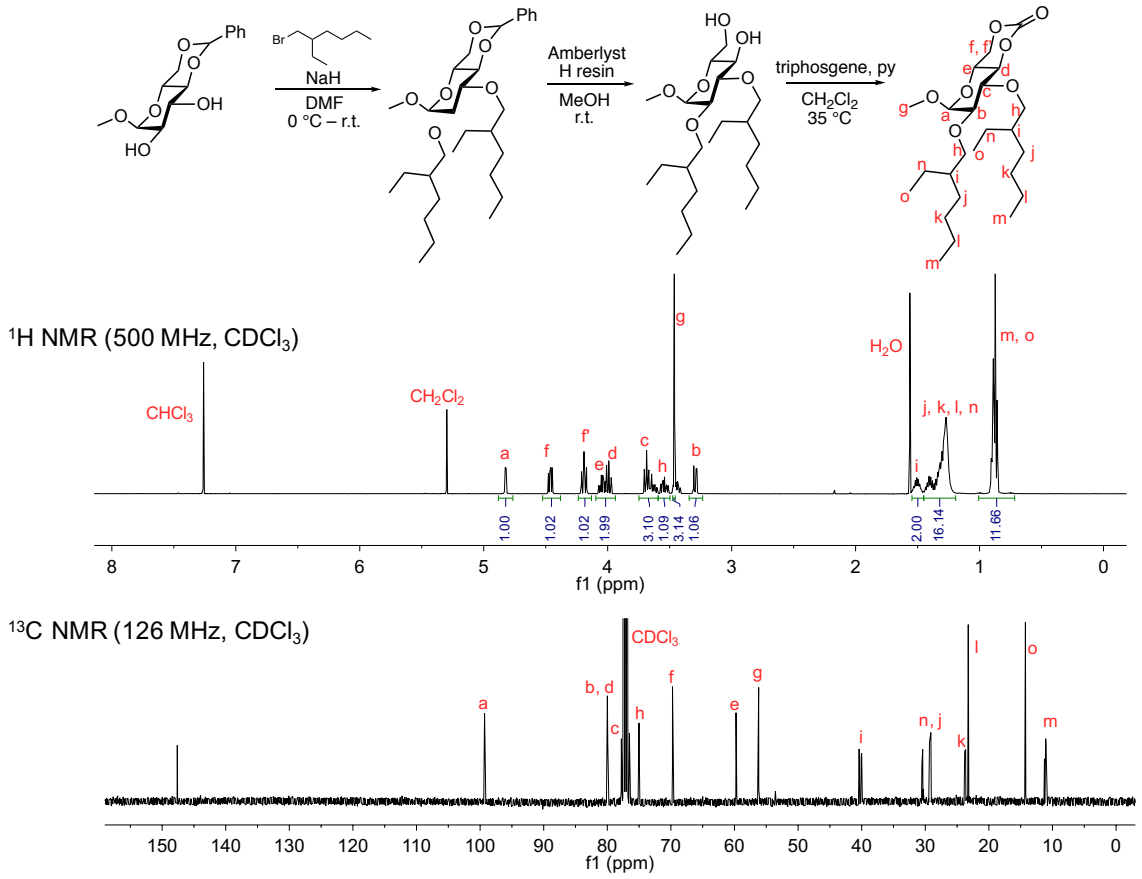

Figure III.14 Synthetic routes, ^{1}H & ^{13}C NMR spectra of GC(OEHEH) monomer.

followed by which polymer PGC(OEH) (12.3 kDa, $Đ$ = 1.16) was afforded through ROP with 4-MeBnOH and TBD at room temperature in a glovebox. Different from the ^{13}C NMR spectrum of PGC with carbonate-side chains, multiple/broad peaks at 154.0–155.5 ppm were found for this polymer ether-side chains (**Figure III.15**), suggesting the existence of a various of backbone linkages (H–H, H–T, T–T) and therefore a regioirregular polymer structure. The same analysis method was applied to further

confirm the regioirregular nature of the ROP for D-glucose-based cyclic carbonate with ether-side chains, and to probe the regioselectivity preference quantitatively. In particular,

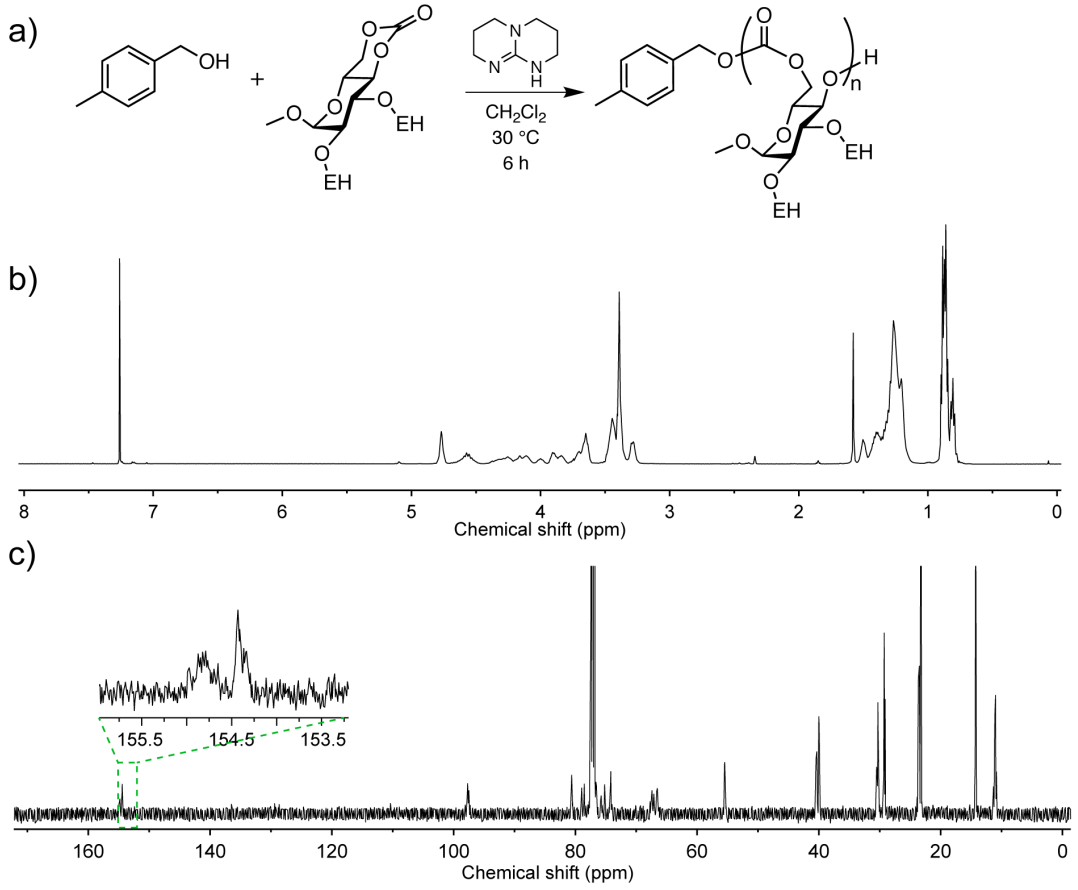

Figure III.15 (a) Polymer PGC(OEHEH); (b) ^{1}H and (c) ^{13}C NMR spectra of the polymer PGC(OEHEH) (inset: zoom in from 156 – 153 ppm)

isomeric unimers of GC(OEH) were synthesized and separated from preparative SEC, to determine their quantitative ratio, and each regioisomer was further separated and identified using a combination of 1D and 2D NMR spectroscopic characterization.

Oligomerization reaction was conducted in the same conditions as for polymerization, with 4-MeBnOH and GC(OEH) molar ratio set at 1:1. The reaction was allowed to proceed for 2 h prior to being quenched with the addition of acetic acid. Oligomers were fractionated using preparative SEC, affording a mixture of regioisomeric unimers **I** & **II** (**Figure III.16-18**). The quantitative ratio of the two regioisomers was determined from the ^{1}H NMR spectrum by comparing the integrations of the signals resonating at 4.82 *vs.* 4.79 ppm and 3.32 *vs.* 3.27 ppm, resulting in a ratio of 1:4. These two unimers with the same molar mass were then isolated using preparative thin-layer chromatography, where each fraction of the isomeric unimers was identified using high-resolution mass spectrometry (HRMS) and NMR spectroscopies. HMBC spectroscopy provided critical information to structurally distinguish these two isomeric unimers (**Figure III.19**), by differentiating couplings between the carbonyl carbon and either $\boldsymbol{H}_{\mathrm{d}}$ or $\boldsymbol{H}_{\mathrm{f}}$ proton(s). Isomer **I** presented a $^{3}J_{\mathrm{CH}}$ coupling signal between *C6* proton ($\boldsymbol{H}_{\mathrm{f}}$) with the carbonyl signal resonating at (4.40, 155.50 ppm), supported the linkage of *C–O6*. In contrast, a $^{3}J_{\mathrm{CH}}$ coupling signal of the proton on *C4* with the carbonyl carbon resonating at (4.70, 155.50 ppm) of **II** correlated the identity of **II** with the *C–O4* isomer. Taken together, with unimers of GC(OEH), the preference between the *C–O6* and *C–O4* cleavage in the ring-opening initiation step was determined to be 1:4 at the given conditions, and the dominant 6-to-4 linkage was the same as the ROP of carbonate-side chain monomers.

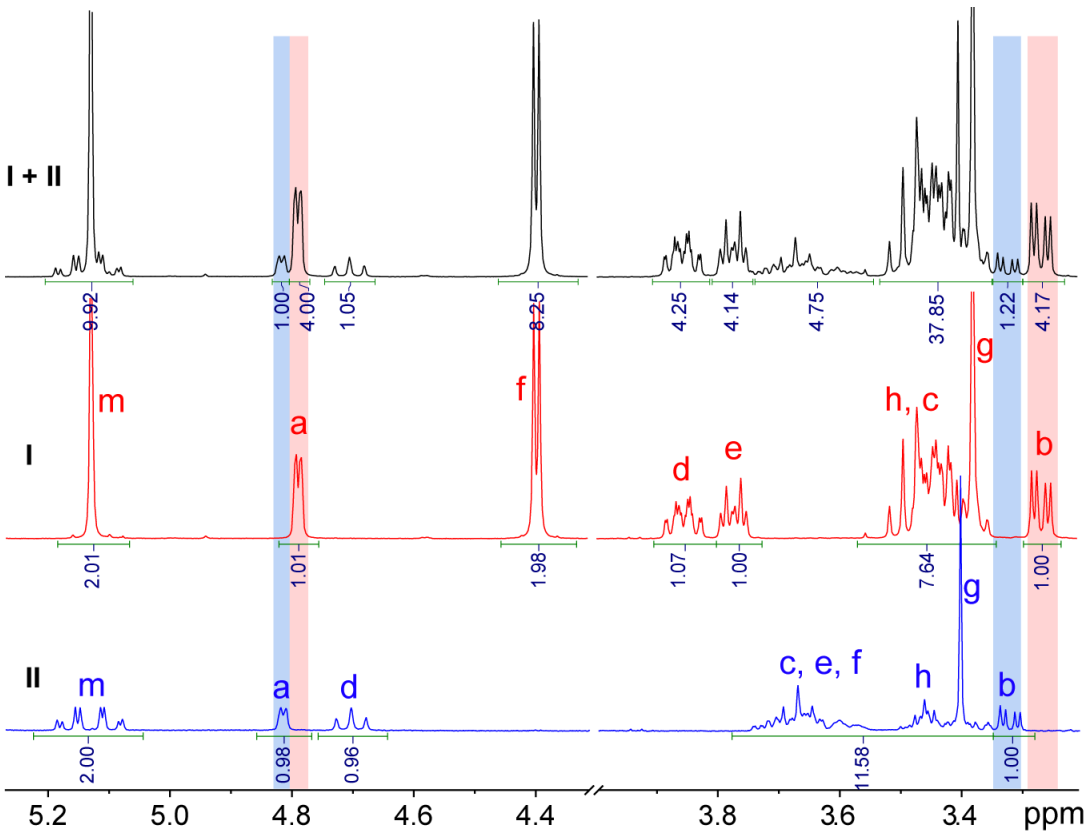

Figure III.16 (a) ^{1}H NMR (400 MHz, $CDCl_3$) spectra of a crude mixture of the unimer isomers.

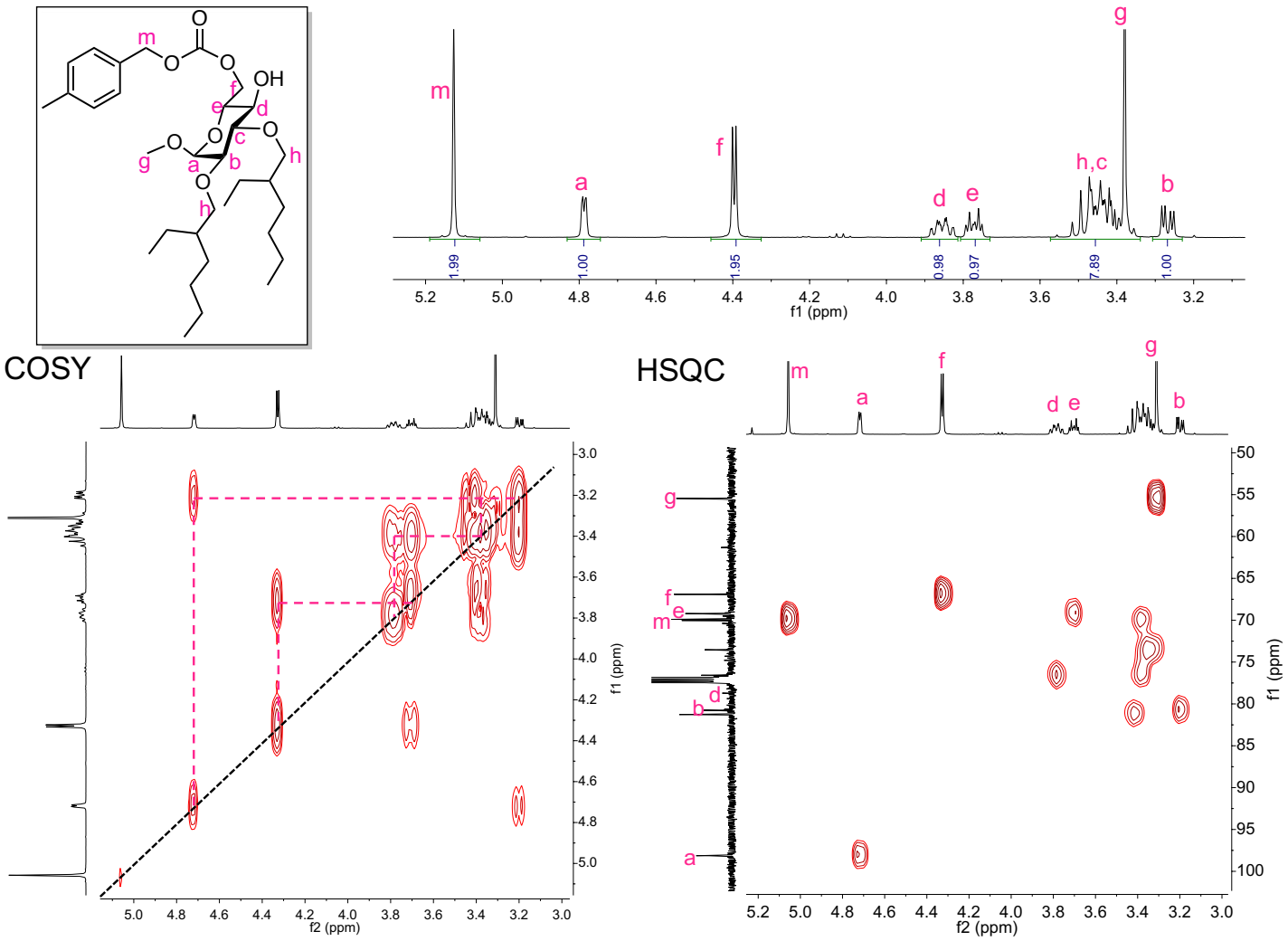

Figure III.17 ^{1}H, COSY and HSQC of GC(OEHEH) unimer regioisomer **I**.

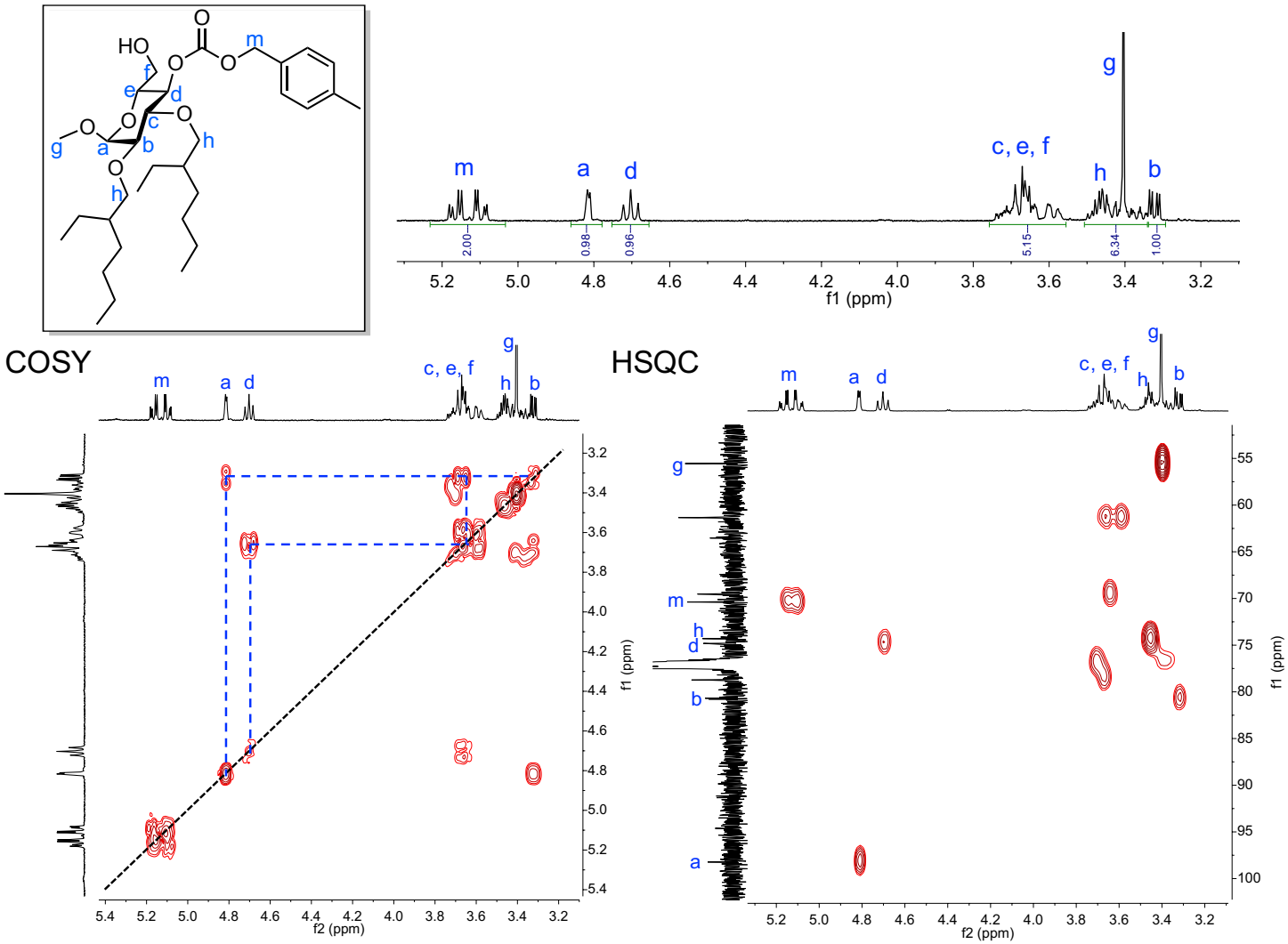

Figure III.18 ^{1}H, COSY and HSQC of GC(OEHEH) unimer regioisomer **II**.

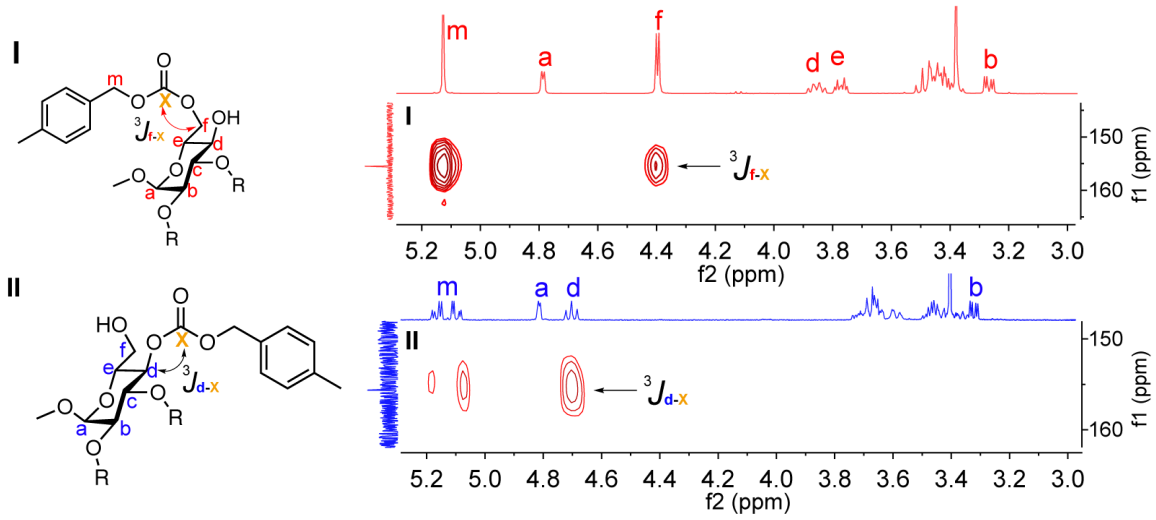

Figure III.19 HMBC spectra of GC(OEH) isomeric unimers **I** and **II**.

For the ether-substituted regioirregular PGCs, subtle differences were discovered in their initiation steps. In study of the ROP of methyl-2,3-*O*-methyl-4,6-*O*-carbonyl-α-D-glucopyranoside [GC(OMe)], a higher preference for *C–O4* cleavage of *ca.* 92% regioselectivity was found in the initiation step based on the unimer structure. Interestingly, this selectivity diminished in the propagation step when a second repeating unit was growing, as demonstrated by four distinct carbonyl signals of *ca.* 1:1:1:1 ratio, and two sets of signals attributed to aromatic initiator carbons in the ^{13}C NMR spectrum of GC(OMe) dimer (**Figure III.20**). Therefore, the regiorandom feature of PGCs with methoxy-side chains was mainly caused by the propagation process rather than the initiation step.

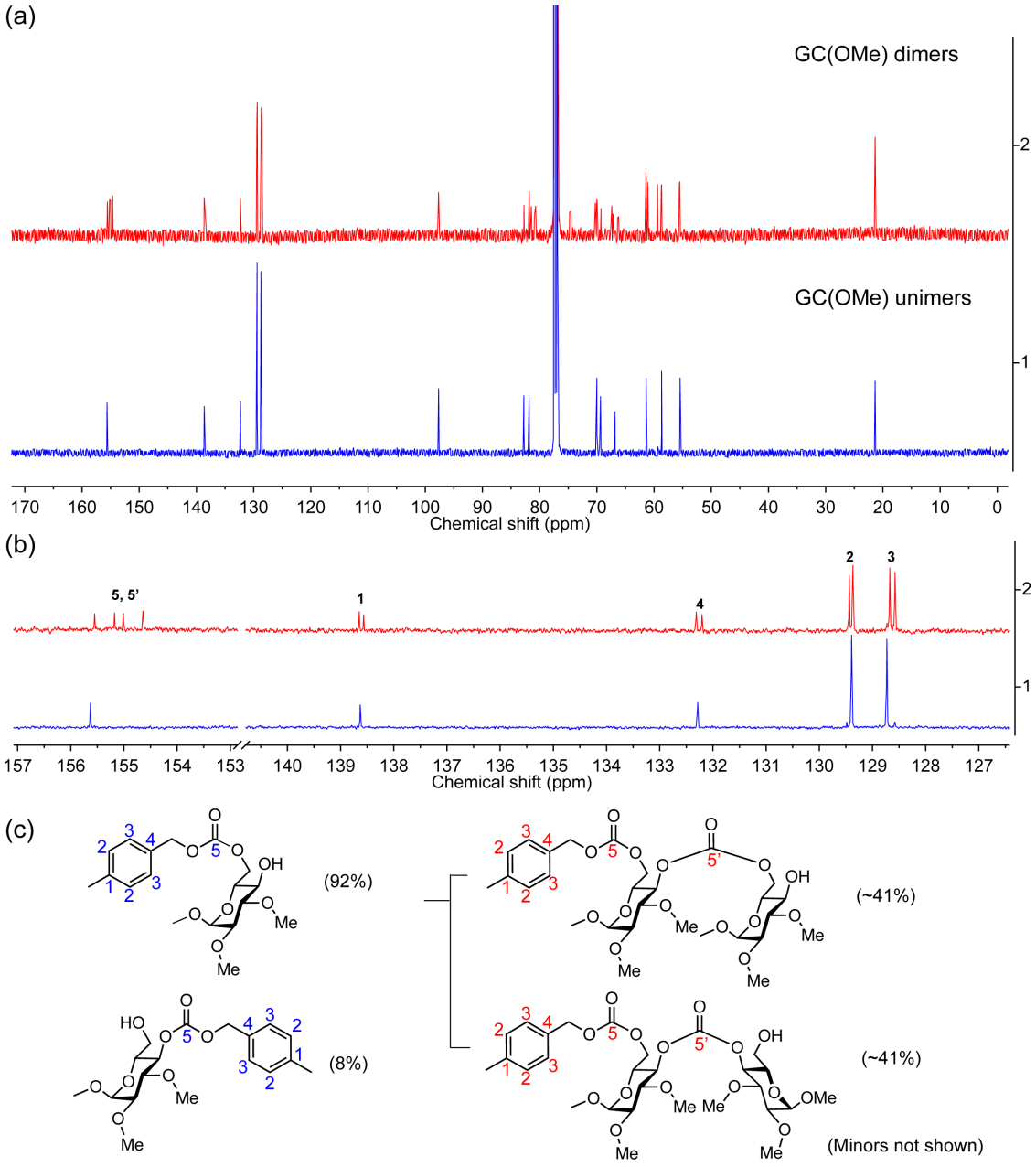

Figure III.20 (a) ^{13}C NMR (100 MHz, $CDCl_3$) of GC(OMe) unimers and dimers; (b) broadened area of the carbonyl and aromatic regions. (c) The structures of unimers and dimers.

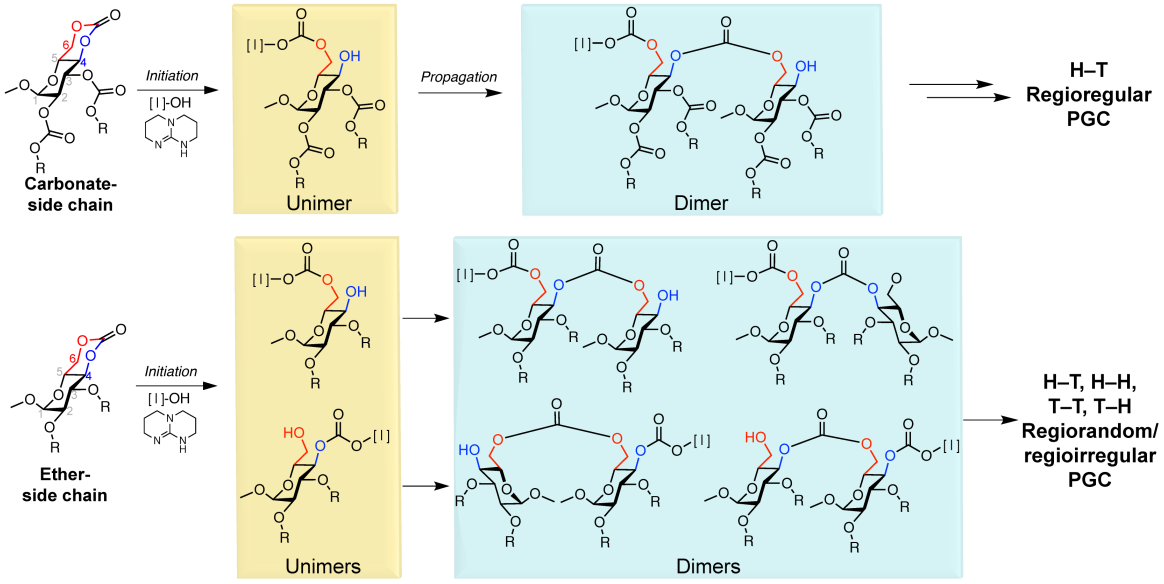

Figure III.21 Initiation and propagation of D-glucose-based cyclic carbonate with carbonate and ether side chains.

DFT calculations of the initiation step during ROP. Inspired by the work of Buchard and coworkers,[26] we investigated the initiation step during the ROP of carbonate-protected glucose carbonate with DFT calculations. In accordance with previous work on the study of ROP mechanism,[37, 135-137] the initiator and monomer undergo a simultaneous activation of bifunctional TBD through the hydrogen bonding mechanism, followed by TBD migration to activate the carbonate C–O bond and afford the growing polymeric alcohol chains (**Figure III.22**). The reference point in the energy profile was taken as the free energy sum of the monomer, TBD and 4-MeBnOH. Four different structural arrangement of the starting materials were calculated. For paths *a* and *b*, the initiator attacks *anti* to the anomeric methoxy group of the monomer, yielding a secondary alcohol chain though *C–O6* cleavage (path *a*), or a primary alcohol chain *via C–O4* cleavage (path

b). Similar mechanisms were proposed for path *c* (*C–O6* cleavage) and path *d* (*C–O4* cleavage) when the initiator attacks *syn* to the anomeric methoxy group. Due to the relative weakness of hydrogen bonds, rapid interchanges occurred among intermediates 3 (INT3) before the cleavage of C–O bonds. The smallest difference of Gibbs free energy barrier found for TS2 between *C–O6* cleavage and *C–O4* cleavage was 2.0 kcal/mol, which is sufficient to make a rate difference over an order of magnitude under the reaction condition at -78 °C (**Figure III.23**). Furthermore, the C–O distances were found to be very similar between the transition states of TS2-*a* and TS2-*b* of 1.98 Å and 1.99 Å, respectively. Noteworthy, transition state geometries of TS2-*b* and TS2-*d* were structurally more compact than TS2-*a* and TS2-*c*, comparing the *C–O6* cleavage and *C–O4* cleavage pathways (**Figure III.24**), which might assist in stabilizing the transition state in condensed phases. The transformation from INT2 to INT3 and the interchanges of configurations within INT2 and INT3 were found to be almost barrierless through the migration of TBD. Hence, the regioselectivity was primarily determined by the reaction barrier of the C–O cleavage step (TS2). The energy profile suggested that the transition states leading to *C–O4* cleavage products are more stable than the *C–O6* cleavage transition states. The *C–O4* cleavage transition states probably get stabilized by the relative compactness of their geometries.

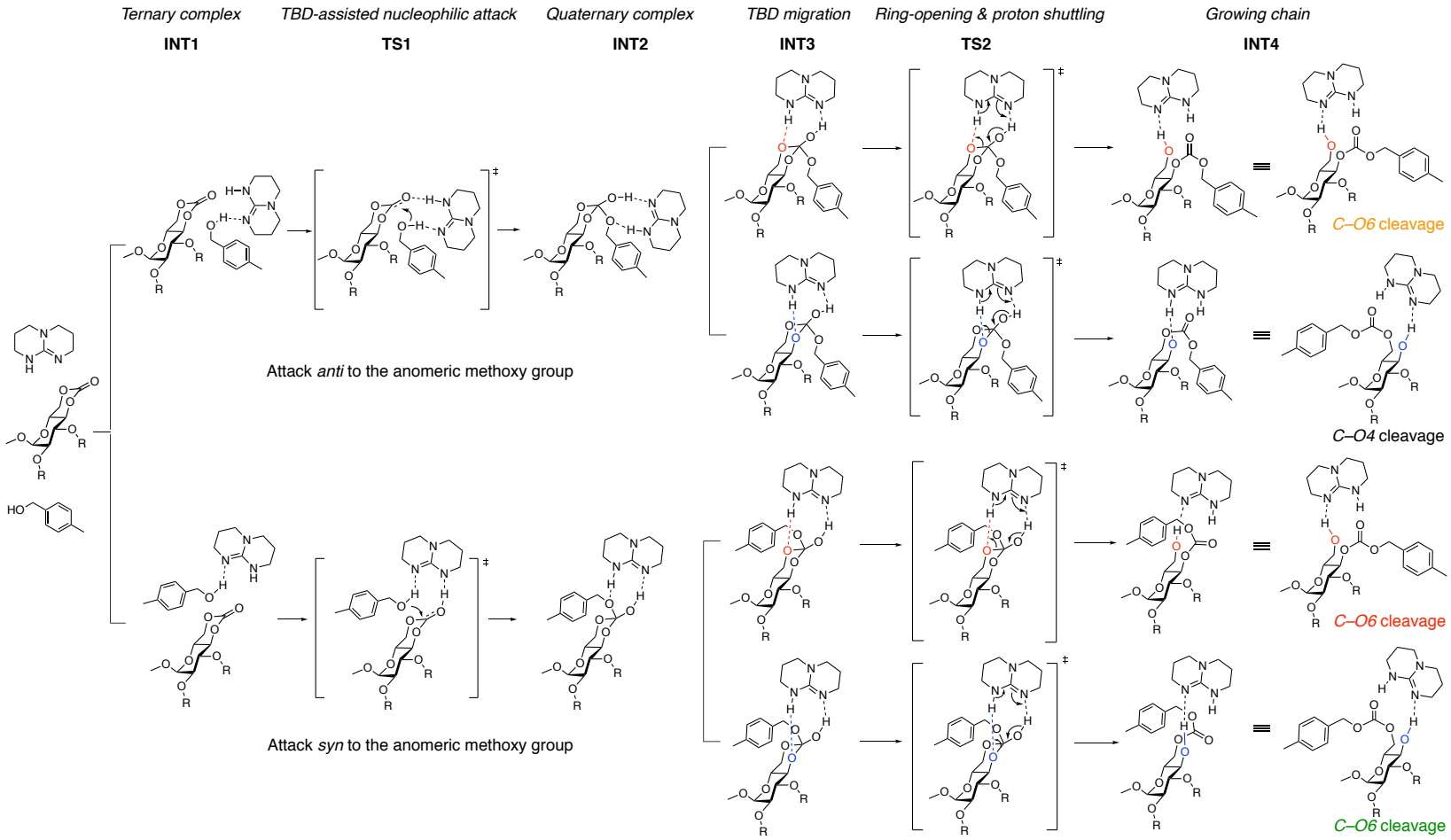

Figure III.22 Initiation step during the ROP of D-glucose-based 4-, 6- cyclic carbonate, catalyzed by TBD and initiated by 4-MeBnOH: proposed regiochemistries.

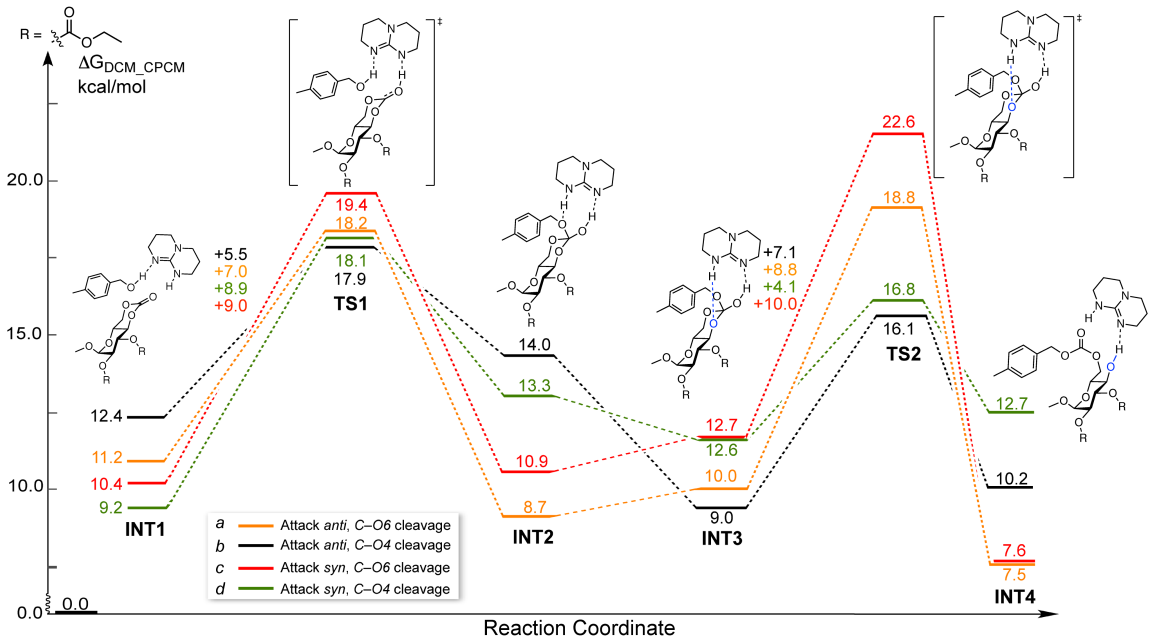

Figure III.23 Gibbs free energy profile for the ring-opening initiation of glucose carbonate monomers with R= ethyloxycarbonyl side chains, catalyzed by TBD and initiated by 4-MeBnOH.

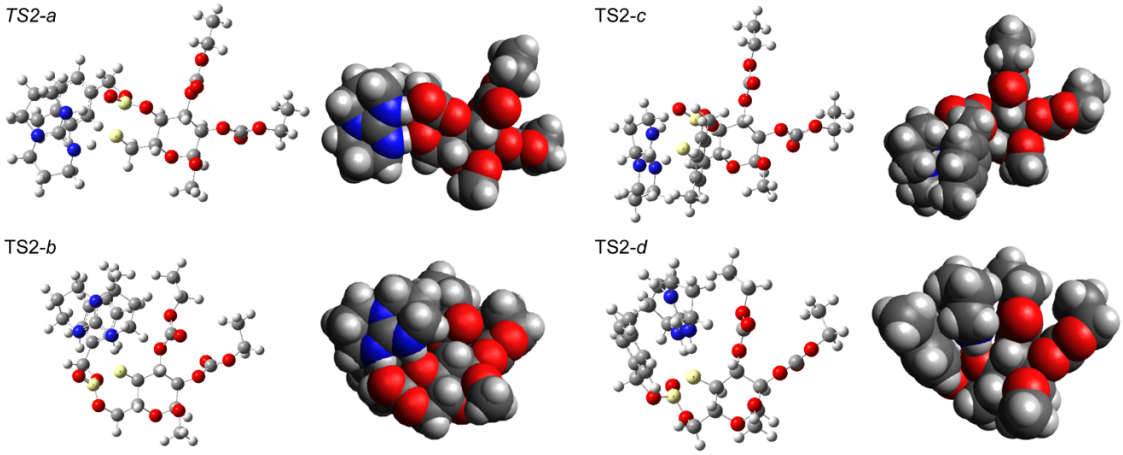

Figure III.24 Optimized geometries of the transition states in ball and stick and space-filling model: TS2-*a*: *C–O6* cleavage, f = 304.2i, TS2-*b*: *C–O4* cleavage, imaginary frequency f = 252.7i, TS2-*c*: *C–O6* cleavage, f = 229.9i, and TS2-*d*: *C–O4* cleavage, imaginary frequency f = 282.6i. The activated C and O are highlighted in yellow.

3.4 Conclusions

In summary, we have demonstrated the side-chain-modulated regioselectivity of the ROP of D-glucose carbonate through syntheses and isolation of discrete unimers and dimers and characterization of their exact structural details during the initial stages of polymerization. From a comprehensive 1D and 2D NMR analyses of the unimers and dimers of D-glucose carbonate **A1**, **A2**, **B1** and **B2**, in combined with our previous observation of distinct peaks in the ^{13}C NMR of relevant polymers, PGCs with carbonate-side chains were concluded to be exclusively 6-to-4 H–T backbone linkages throughout the polymer chains. Further, this analysis approach was extended for quantitatively determining the regioselectivity of the initiation step of the regioirregular PGC with ether substituents by comparing regioisomeric unimers of GC(OEH), and a 4:1 ratio between *C–O4 vs. C–O6* cleavage products was observed, verifying the regioirregular property of the polymers. Furthermore, it was found that the ROP of GC(OMe) possessed a regioselective initiation step while a non-selective propagation process. Lastly, the regioselectivity of the initiation step was validated by the DFT calculations, revealing the change in product distribution was most likely arising from the structural and energetic difference of the transition states at the C-O cleavage step occurred with distinct spatial arrangements of TBD relative to the activated cyclic oxygen. Overall, this work advanced fundamental understandings of the polymerization behavior and polymer regiochemistry of D-glucopyranose-based 4,6-cyclic carbonates. We anticipate the exploration of reasons behind the variation of ring-opening preferences in the ROP system will further the development of the next generation of sugar-based polymers.

3.5 Perspectives

In the proposed work, experimental studies will continue, with computational insights to be provided by DFT calculations to understand the reactivity and regioselectivity of the reactions based on different monomer structures. The regioselectivity study of the organocatalyzed ROP will be extended to five-membered cyclic glucose carbonates,[30] where effects of different acetal protecting groups on regiochemistry will be investigated. As with the xylose system, versatile protecting groups, including those derived from natural ketone or aldehyde sources, *e.g.*, carvone, cinnamaldehyde or crotonaldehyde, will be explored (beyond the benzylidene acetal used previously) to bring side chain functionality for further diversity by side chain chemical modification reactions. Moreover, the regiochemical investigations will be combined with stereochemical variation of the hexose carbohydrate core structure, to include studies of regiochemical and stereochemical effects across a platform of highly-functional carbohydrate-based polycarbonates (**Figure III.25**).

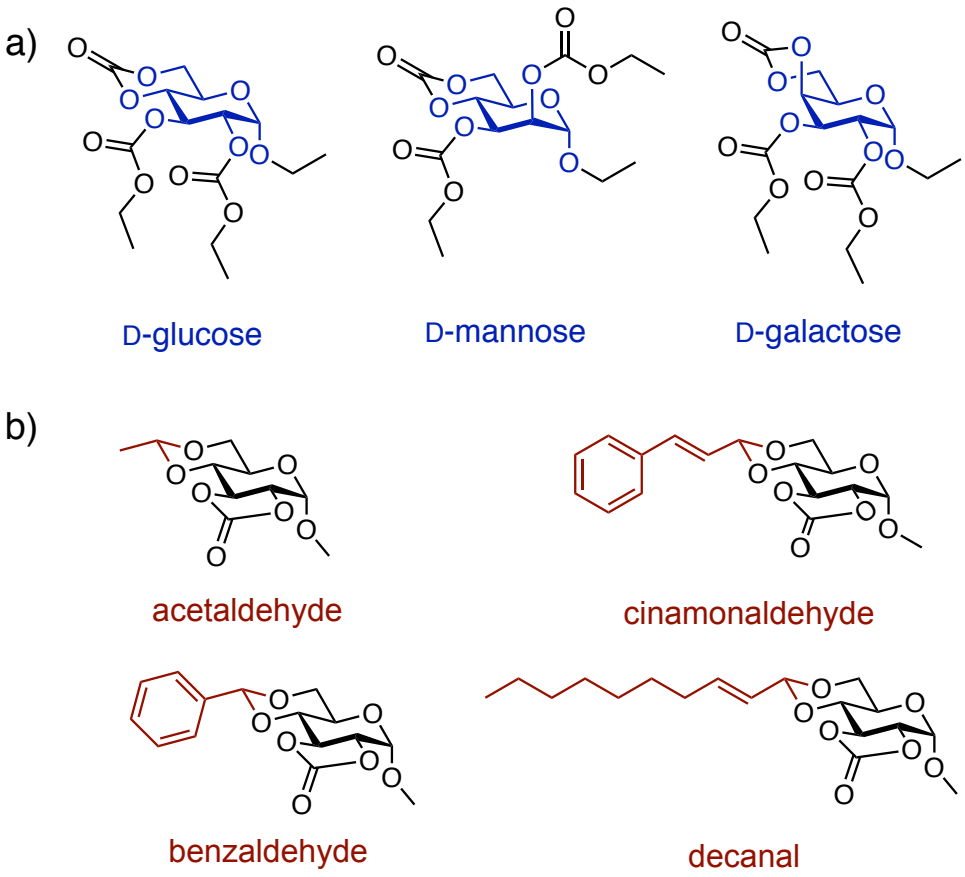

Figure III.25 (a) 4,6-Six-membered cyclic carbonate monomers derived from glucose (left), mannose (center), and galactose (right), and (b) 2,3-five-membered cyclic glucose carbonate monomers with 4,6-protecting groups derived from acetaldehyde, benzaldehyde, cinamonaldehyde, and decanal, for study of stereochemical effects on ROPs and properties of the resulting polymers, each of which will be capable of undergoing hydrolytic degradation to afford the respective carbohydrate, alcohol and carbon dioxide.

CHAPTER IV

CRYSTALLIZATION-DRIVEN ASSEMBLY OF FULLY DEGRADABLE, NATURAL PRODUCT-BASED POLY(L-LACTIDE)-*BLOCK*-POLY(A-D-GLUCOSE CARBONATE)S IN AQUEOUS SOLUTION*

4.1 Introduction

Amphiphilic block polymers are capable of self-assembly into a variety of well-defined nanostructures, including spherical and cylindrical/worm-like micelles, vesicles, disks, toroids, and others,[138-143] which are of great interest for applications in nanomedicine, environmental remediation and multiple other chemical industries. Cylindrical nanoparticles, in particular, have been investigated by many research groups in recent years,[83, 144-149] including significant contributions by the Müller group demonstrating the construction of cylindrical polymer brushes,[150] 1D hybrid nanomaterials,[151] and multi-compartment cylinders with precisely placed patches *via* hierarchical assembly of triblock terpolymer blends that have expanded the complexity and precision of block polymer solution assemblies.[152-154] The unique anisotropic and elongated shape of cylindrical nanostructures imparts notable properties, such as increased *in vivo* circulation time and altered cellular internalization pathways relative to spherical

*Reprinted (adjusted) with permission from "Crystallization-driven Assembly of Fully Degradable, Natural Product-based Poly(L-lactide)-*block*-poly(α-D-glucose carbonate)s in Aqueous Solution" by Song, Y.; Chen, Y.; Su, L.; Li, R.; Letteri, R. A.; and Wooley, K. L., *Polymer* **2017**, *122*, 270-279. Copyright 2017 Elsevier Ltd.

nanostructures (*i.e.,* spherical micelles and vesicles).[97, 155-158] Among various methods for the construction of cylindrical micelles, Manners and Winnik have pioneered crystallization-driven self-assembly (CDSA) as a powerful approach yielding living epitaxial growth characteristics and, in some cases, control of length to afford nanostructures with well-defined dimensions.[83, 88, 159-160] Unlike entirely amorphous block copolymers (BCPs), solution assembly of BCPs with a crystalline block favors the formation of micellar morphologies driven by crystallization processes, which facilitate axial alignment of polymer chains and, as a result, reduced interfacial curvature.[149] CDSA processes in aqueous solution have been expanded to include natural and degradable polymer components by the O'Reilly and Dove groups, in an elegant use of polylactide-containing diblock copolymers for the fabrication of nanoscopic cylinders with controlled length.[148, 161-164] With our interest in polymers that are fully degradable and derived from natural products, we have now built upon the substantial recent progress in assembly of BCPs *via* CDSA,[83, 148-149, 159-163, 165] to explore cylindrical and spherical micelles derived from L-lactide, L-cysteine and D-glucose.

The construction of morphologically-complex nanomaterials from fully biocompatible and degradable materials synthesized from renewable resources is of broad interest as they eliminate potential environmental hazards from accumulation of non-degradable materials.[2, 9, 22] Our group has explored poly(glucose carbonate)s, which have been receiving attention due to their potential for degradation into carbon dioxide, glucose and other small molecules.[14, 27-28, 96] Herein, a new type of amphiphilic BCP comprised of a zwitterionic hydrophilic poly(α-D-glucose carbonate) (PDGC) segment and a semi-

crystalline hydrophobic poly(L-lactide) (PLLA) segment, was constructed by ring-opening polymerization (ROP) with a metal-free catalyst.[166-167] These diblock copolymers represent a natural product-based platform, in which both blocks are hydrolytically degradable and the PDGC segment is capable of rapid and efficient functionalization *via* the alkyne groups.[58, 168-170] Specifically, post-polymerization modification by thiol-yne reaction with L-cysteine transformed PDGC into a hydrophilic PDGC-cys segment that afforded an overall amphiphilic character to the poly(L-lactide)-*block*-poly(α-D-glucose carbonate) (PLLA-*b*-PDGC-cys) block copolymers. Cylindrical and spherical nanostructures were obtained from aqueous solution assembly of PLLA-*b*-PDGC-cys, where spheres, cylinders and partially-reorganized 2D platelet-like bundled cylinder micellar nanostructures formed from BCPs with low, intermediate and high PLLA contents, respectively, and the hydrolytic degradability of both the PLLA and PDGC segments was confirmed through NMR spectroscopy and mass spectrometry studies.

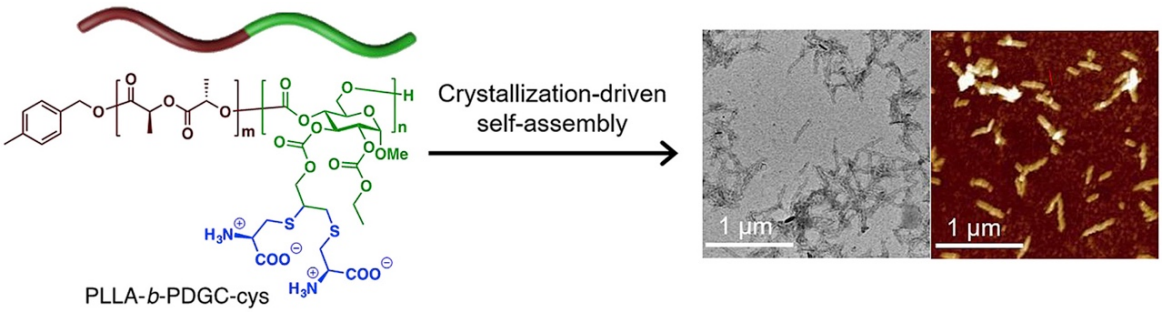

Figure IV.1 Assembly of polymers towards cylindrical nanoparticles. Reprinted with permission from [48].

4.2 Materials and Methods

4.2.1 Materials

L-Lactide was purified by recrystallization from ethyl acetate. 1,5,7-Triazabicyclo[4.4.0]dec-5-ene (TBD) was purchased from TCI chemicals. Dichloromethane (DCM) was dried using a solvent purification system (J. C. Meyer Solvent Systems, Inc., Laguna Beach, CA). Hydrochloric acid (HCl, 36.5–38.0 wt%) was purchased from Thermo-Fisher Scientific. Nanopure water (18.2 MΩ·cm) was acquired from a Milli-Q water filtration system (Millipore Corp, USA). The alkyne-substituted glucose carbonate monomer, methyl-2-*O*-ethyloxycarbonyl-3-*O*-propargyloxycarbonyl-4,6-*O*-carbonyl-α-D-glucopyranoside (D-GC(EPC)), was synthesized according to a previously published procedure [27]. All other chemicals were purchased from Sigma-Aldrich (St. Louis, MO) and used without further purification unless otherwise noted. Spectra/Por dialysis membranes (MWCO 12–14 kDa) were purchased from Spectrum Laboratories, Inc. (Rancho Dominguez, CA).

4.2.2 Instrumentation

^{1}H NMR and ^{13}C NMR spectra were recorded on either a Varian 300 or a Varian 500 spectrometer interfaced to UNIX computers using VnmrJ software. Chemical shifts were referenced to solvent resonance signals. Fourier transform infrared (FT-IR) spectra were recorded on an IR Prestige 21 system equipped with a diamond attenuated total reflection (ATR) lens (Shimadzu Corp., Japan) and analyzed using IRsolution v. 1.40 software.

Size exclusion chromatography (SEC) eluting with tetrahydrofuran (THF) was performed on a Waters Chromatography, Inc. (Milford, MA) system equipped with an isocratic pump (model 1515), a differential refractometer (model 2414), and column set comprised of a PLgel 5 μm guard column (50 × 7.5 mm), a PLgel 5 μm Mixed C column (300 × 7.5 mm, Agilent Technologies) and two Styragel® columns (500 Å and 104 Å, 300 × 7.5 mm, Waters Chromatography, Inc.). The system was operated at 40 °C with a flow rate of 1 mL/min. Data were analyzed using Breeze software from Waters Chromatography, Inc. (Milford, MA). Molecular weights were determined relative to polystyrene standards (580 to 3,250,000 Da) purchased from Polymer Laboratories, Inc. (Amherst, MA). Polymer solutions were prepared at a concentration of *ca.* 3 mg/mL with 0.05 vol% toluene as the flow rate marker; an injection volume of 200 μL was used.

Thermogravimetric analysis (TGA) was performed under N_2 atmosphere using a Mettler-Toledo instrument (model TGA/SDTA851e), with a heating rate of 10 °C/min, from 25 to 500 °C. Glass transition (T_g) and melting (T_m) temperatures were measured by differential scanning calorimetry (DSC) on a Mettler-Toledo DSC822® calorimeter (MettlerToledo, Inc., Columbus, OH), with a heating and cooling rate of 10 °C/min. Three heating and cooling cycles were conducted, from 30 to 165 °C for the L-cysteine-modified polymers and from 25 to 200 °C for the alkyne-functionalized polymer precursors. Measurements were analyzed using Mettler-Toledo Star^e v. 7.01 software. The T_g was taken as the midpoint of the inflection tangent during the second heating scan, and the T_m was taken as the maximum of the endothermic peak during the first heating scan.

Transmission electron microscopy (TEM) was performed on a FEI Tecnai F-20 electron microscope operated at 200 kV, equipped with a Gatan CCD camera. Carbon-coated copper TEM grids were pretreated with oxygen plasma to increase the surface hydrophilicity. Samples were prepared by drop-casting nanoparticle solutions (*ca.* 4 μL, 0.1 mg/mL) directly onto a grid. After 1 min, excess solution was wicked away using filter paper and the grids were allowed to dry under ambient conditions for 30 min. Uranyl acetate (1 μL, 1% aqueous solution) was then applied to the grids, which were allowed to dry in ambient conditions prior to imaging. TEM images were analyzed using ImageJ software, and 200 particles were counted from each sample to obtain the length distributions. Average nanostructure diameters were measured by counting *ca.* 50 particles.

Atomic force microscopy (AFM) was performed on a Multimode 8 system (Bruker, Santa Barbara, CA) in PeakForce Tapping® mode with ScanAsyst® image optimization software and a ScanAsyst-Air probe (k = 0.4 N/m, Bruker). Nanoparticle solutions (20 μL, 0.1 mg/mL) were deposited onto freshly cleaved mica, then excess solution was wicked away using filter paper after *ca.* 1 min and the samples were allowed to dry in ambient conditions prior to imaging. AFM images were analyzed using Nanoscope Analysis software (Bruker) to obtain the height of the nanostructures, and the average height was measured by counting 5 particles.

Wide angle X-ray diffraction (WAXD) was performed on a Bruker D8® Bragg-Brentano X-ray powder diffractometer, equipped with a 1 kW Cu tube source (1.54 Å), using an operating voltage of 40 kV and a current of 25 mA. The X-ray optics were set to

standard Bragg-Brentano para-focusing mode, with X-rays focusing on the sample from an incident beam divergence-limiting slit (1 mm) and then converging onto a position-sensitive X-ray detector (Lynx-Eye, Bruker-AXS). The sample (*ca.* 10 mg) was placed in the holder of a two-circle goniometer (d = 218 mm) in a radiation safety enclosure, and standard powder θ-2θ diffraction scans were performed at room temperature. Data collection was automated using the COMMANDER program and analyzed with EVA software (Bruker).

Electrospray ionization (ESI) mass spectrometry was performed on a Bruker amaZon SL mass spectrometer (Bruker Daltonics Inc., Billerica, MA) in both positive and negative ion modes. Matrix-assisted laser desorption/ionization-time of flight (MALDI-TOF) mass spectrometry was performed on a Voyager DE-STR mass spectrometer (Applied Biosystems, Foster City, CA) in positive linear mode. Ions were generated by a pulsed nitrogen laser (337 nm). Trans-2-[3-(4-*t*-butylphenyl)-2-methyl-2-propenylidene]malononitrile (DCTB) and potassium trifluoroacetate (KTFA) were used as the matrix and cationization reagent, respectively.

4.2.3 Synthetic procedures

Representative polymerization of L-lactide and α-D-glucose carbonate. A solution of L-lactide (77 mg, 0.54 mmol) and 4-methylbenzyl alcohol (0.1 mL, 10.9 mg/mL in DCM, 0.009 mmol) was prepared in anhydrous DCM (1.0 mL) and transferred to a vial equipped with a stir bar and a rubber septum in an argon-filled glovebox. The vial was then removed from the glovebox and connected to a Schlenk line. A solution of

TBD in DCM (0.1 mL, 15.0 mg/mL, 0.01 mmol) was injected quickly into the vial of L-lactide at -78 °C. After stirring for 2 min, a solution of the glucose carbonate monomer D-GC(EPC) (200 mg, 0.535 mmol) in DCM (1.0 mL) was added *via* syringe to the reaction mixture. The reaction was stirred for an additional 10 min at -78 °C and then quenched by addition of excess acetic acid. Precipitation from DCM into methanol three times, and drying under vacuum yielded $PLLA_{45}$-*b*-$PDGC_{45}$ a white powder (215 mg, 78%). ^{1}H NMR (500 MHz, $CDCl_3$, ppm): δ 7.21 and 7.16 (AB_q, J = 8 Hz), 5.36 (dd, J = 10, 10 Hz), 5.16 (q, J = 7 Hz), 5.03 (d, J = 4 Hz), 4.89 (dd, J = 10, 10 Hz), 4.79–4.67 (m), 4.28 (s), 4.20 (tt, J = 7, 4 Hz), 4.02 (m), 3.42 (s), 2.59 (t, J = 2 Hz), 2.35 (s), 1.58 (d, J = 7 Hz), 1.30 (t, J = 7 Hz). ^{13}C NMR (126 MHz, $CDCl_3$, ppm): δ 169.61, 154.04, 153.63, 153.54, 129.28, 128.41, 96.41, 77.24, 76.92, 76.21, 74.12, 73.49, 72.17, 69.01, 66.63, 65.67, 64.79, 55.90, 55.76, 16.65, 14.13. FT-IR: 3290, 2980, 1750, 1450, 1375, 1240, 1095, 1050, 980, 950, 880, 770, 660 cm^{-1}. SEC (THF): M_n = 14.0 kDa, $Đ$ = 1.18. T_g = 64 °C, T_m = 154 °C. TGA in Ar: 290–380 °C, 84% weight loss. The molecular weights and compositions of all polymers used in this study are provided in **Table IV.1**.

Representative thiol-yne click reaction of PLLA-*b*-PDGC with L-cysteine. A solution of $PLLA_{45}$-*b*-$PDGC_{45}$ (20 mg, 0.039 mmol alkyne), L-cysteine (47 mg, 0.39 mmol), HCl (0.2 mL) and 2,2-dimethoxy-2-phenylacetophenone (DMPA) (3.0 mg, 0.012 mmol) was prepared in *N,N*-dimethylformamide (DMF, 5 mL), deoxygenated with bubbling $N_{2(g)}$ for 5 min, and irradiated at 365 nm (1000 μJ/cm^2) for 2 h. The DMF solution was transferred into dialysis tubing (MWCO 12–14 kDa) and dialyzed against nanopure water adjusted to pH 3 with HCl at 4 °C for 36 h. The resulting solution was

then lyophilized to yield the cysteine-modified polymer as a white powder. ^{1}H NMR (500 MHz, DMF-d_7, ppm): δ 7.29 and 7.21 (AB_q, J = 8 Hz), 5.26 (q, J = 7 Hz), 5.17–5.06 (m), 4.98 (br), 4.87 (br), 4.68 (br), 4.61–4.39 (m), 4.19 (br), 3.57–3.21 (m), 2.30 (s), 1.54 (d, J = 7 Hz), 1.25 (t, J = 7 Hz). ^{13}C NMR (126 MHz, DMF-d_7) δ 170.28, 170.12, 155.10, 154.81, 154.63, 129.87, 129.02, 97.09, 81.31, 72.31, 69.77, 69.14, 69.10, 68.61, 68.57, 65.71, 65.30, 65.26, 61.76, 61.70, 61.65, 61.59, 55.98, 53.43, 46.99, 20.95, 20.93, 20.87, 20.30, 17.03, 14.55, 9.06, 9.03. FT-IR: 3680-2180, 1750, 1620, 1480, 1390, 1245, 1100, 1020, 880, 770, 630 cm^{-1}. T_g = 114 °C, T_m = 143 °C. TGA in Ar: 162–240 °C, 25% weight loss; 250–300 °C, 58 % weight loss. All other polymers were modified with L-cysteine following the same procedure, with a molar ratio of L-cysteine: alkyne: DMPA = 10:1:0.03.

CDSA of PLLA-*b*-PDGC-cys diblock copolymers. PLLA-*b*-PDGC-cys was dissolved in nanopure water at concentrations between 0.05–0.1 mg/mL and stirred overnight at room temperature. The solutions were then heated to 65 °C for 30 h to aid dissolution,[147] and then removed from heat and allowed to cool to room temperature prior to characterization by TEM and AFM. Powder samples for WAXD experiments were obtained by lyophilization.

4.3 Results and Discussion

Synthesis and characterization of the PLLA-b-PDGC-cys diblock copolymers. Sequential ROP of L-lactide and the cyclic carbonate of methyl-α-D-glucopyranoside bearing pendant ethyl- and propargyl-carbonates (D-GC(EPC)), followed

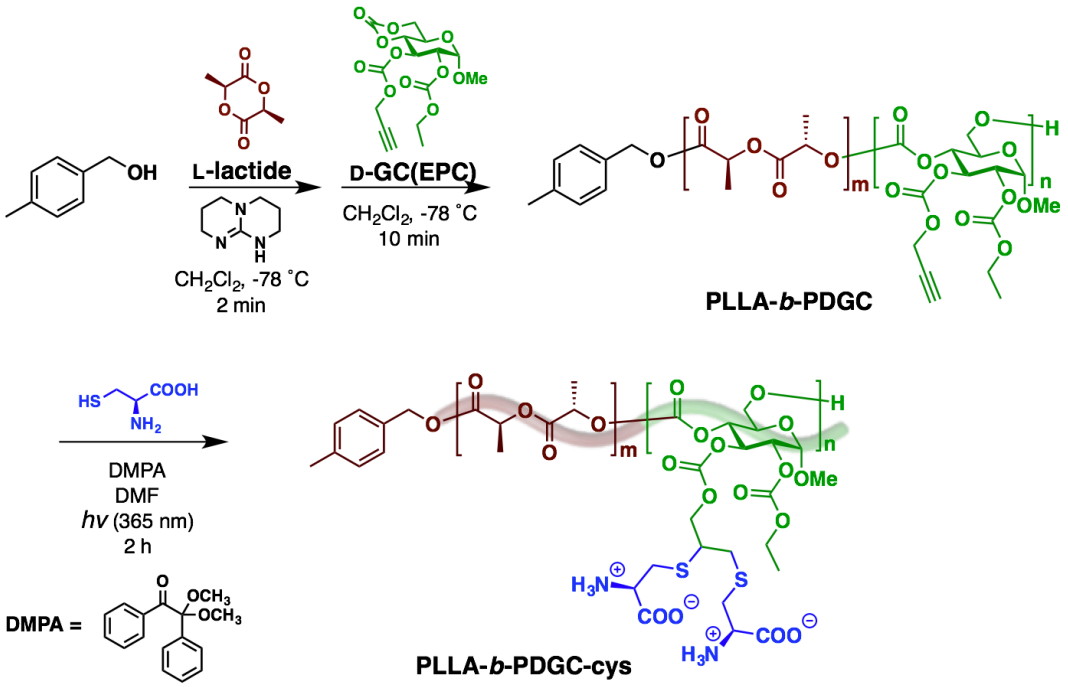

Figure IV.2 Synthesis of PLLA-*b*-PDGC-cys *via* sequential ROP of L-lactide and D-GC(EPC), followed by UV-initiated thiol-yne click modification with L-cysteine. Reprinted with permission from [48].

by post-polymerization modification of the alkyne groups with L-cysteine yielded a series of amphiphilic diblock copolymers (PLLA-*b*-PDGC-cys, **Figure IV.2**). The naturally-derived monomers, L-lactide and D-GC(EPC), were selected for their degradability and biocompatibility, with L-lactide providing crystallinity and D-GC(EPC) imparting functionality to the corresponding polymers.[27, 171] The semi-crystalline nature of PLLA micelles, while the alkyne groups of PDGC were designed to allow for versatile post-polymerization modification. Similarly as L-lactide, glucose-based cyclic carbonates are amenable to organocatalyzed ROP for the production of well-defined polymers.[14, 27-28, 96] L-Lactide was polymerized first using TBD as the catalyst, which is known for mediation of high efficiency polymerization of a variety of cyclic monomers,[166, 172-176] and

quantitative L-lactide conversion was achieved in less than 2 min. After 2–3 min, the D-GC(EPC) monomer was added to grow the PDGC block. Varying the feed ratios of the initiator and two monomers yielded PLLA-*b*-PDGC diblock copolymers **1**–**7** with different compositions and molecular weights (**Table IV.1**). Polymerizations yielding diblocks **2** and **3** employed a 1:1 molar ratio of L-lactide and D-GC(EPC), and those yielding **5** and **6** employed a 1:3 molar ratio of L-lactide and D-GC(EPC) to explore the effect of polymer molecular weight at constant PLLA contents on the sizes and morphologies of the resulting assemblies. FT-IR, ^{1}H NMR and ^{13}C NMR spectroscopies confirmed the structures and compositions of polymers **1**–**7** (**Figure IV.3**). ^{1}H NMR spectroscopy was also used to determine the number-average degrees of polymerization, by comparing the relative integrations of peak *m* (PLLA), and *a* or *h* (PDGC) to peak *r*, corresponding to the methyl group at the polymer chain end. Narrow molecular weight distributions ($Đ$ < 1.20) were observed by SEC, however, the SEC M_n values were consistently less than those derived from NMR data (**Table IV.1**), likely due to the SEC calibration against polystyrene standards.

UV-activated thiol-yne modification of the alkyne groups on the PDGC block with L-cysteine in the presence of the photoinitiator DMPA yielded amphiphilic diblock copolymers for assembly in aqueous solution. L-Cysteine was selected due to its biocompatibility and to impart a zwitterionic character to the micelle surface, which is desirable for preventing aggregation in physiological conditions and circumventing toxicity concerns associated with cationic polymers [177]. Successful addition of L-cysteine to PLLA-*b*-PDGC was achieved by employing a large excess of L-cysteine (10 equivalents

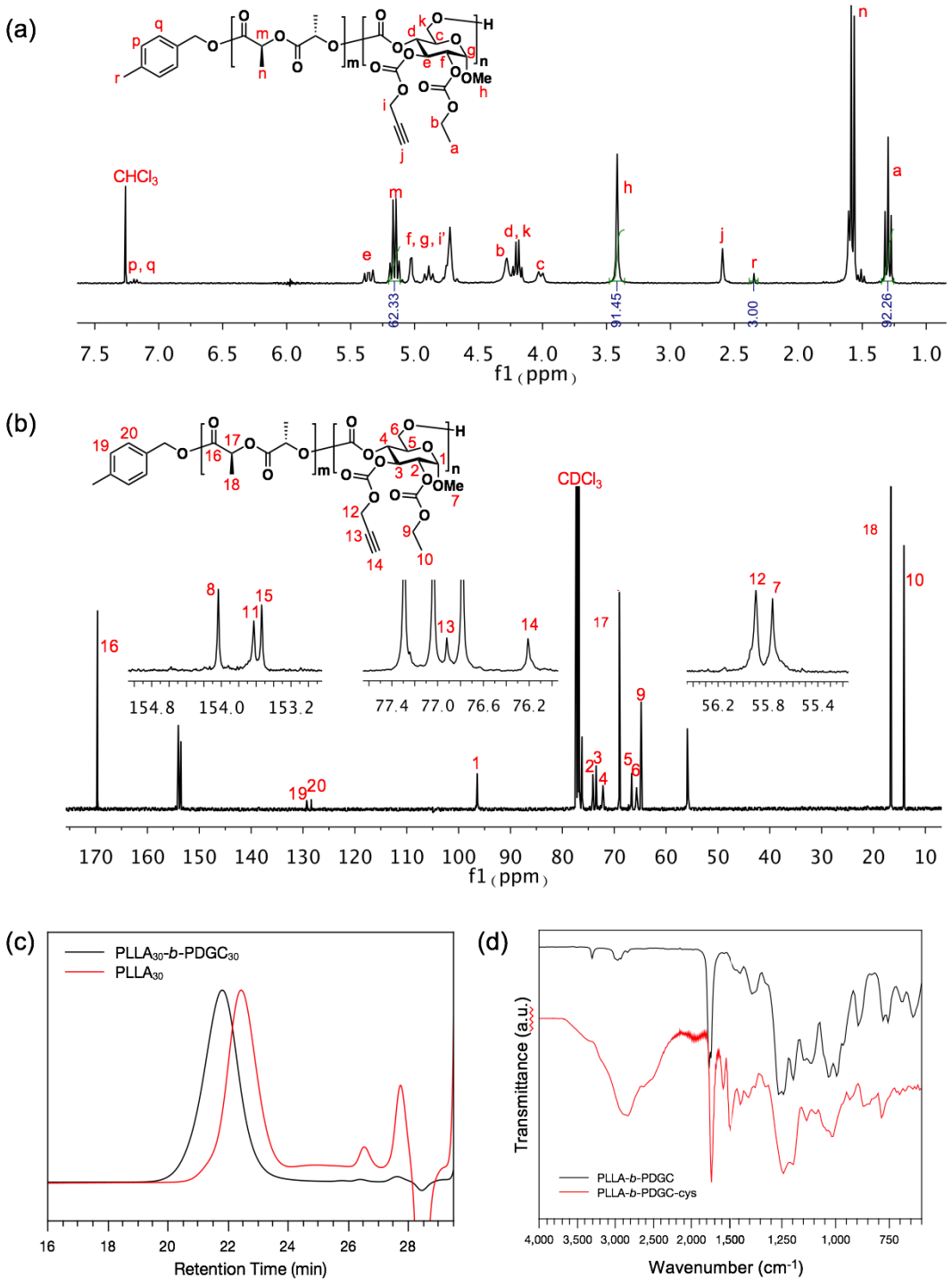

Figure IV.3 Characterization of $PLLA_{30}$-*b*-$PDGC_{30}$-cys. (a) ^{1}H NMR (300 MHz) and (b) ^{13}C NMR (126 MHz) spectra acquired in $CDCl_3$. (c) SEC traces of $PLLA_{30}$-*b*-$PDGC_{30}$ and $PLLA_{30}$. (d) FT-IR spectra of PLLA-*b*-PDGC and modified diblock copolymer PLLA-*b*-PDGC-cys. Reprinted with permission from [48].

relative to alkyne groups), and was supported by ^{1}H NMR spectroscopic analysis of the polymer in d_7-DMF, noting the appearance of cysteine proton resonances at δ 4.5, δ 4.2 and δ 3.4 ppm. FT-IR spectroscopy further revealed peaks characteristic of O-H and N-H stretching in carboxylic acid and amine groups between 3600-2300 cm^{-1} after modification (**Figure IV.3d**). The overlap of these peaks with the characteristic alkyne C-H stretching peak at *ca.* 3300 cm^{-1} complicated IR analysis of alkyne consumption, however the disappearance of the carbon resonances of the alkyne groups at δ 76.20 and 76.93 ppm indicated full conversion of the alkyne residues to thioether linkages, consistent with quantitative conversion of alkyne moieties observed in similar reactions of cysteine, cysteamine, and 3-mercaptopropionic acid with other alkyne-containing polyphosphoester (PPE)-, PLLA- and PDGC-containing diblock copolymers.[28, 178-179] Additionally, TGA indicated a two-stage decomposition, with mass loss measured between 140-162 °C and 250-300 °C (**Figure IV.4**), corresponding to the loss of cysteine moieties and the decomposition of polymer backbone, respectively, and agreeing well with the polymer compositions determined by NMR spectroscopy. For instance, TGA of $PLLA_{45}$-*b*-$PDGC_{45}$-cys measured 27% mass loss between 162-240 °C and 58% mass loss between 250-300 °C. Across the series of $PLLA_m$-*b*-$PDGC_n$-cys, the percentage mass loss at the lower temperature range (162-240 °C) increased as the value of n/m increased. Taken together, the NMR, SEC, FT-IR and TGA data indicate the successful synthesis of a series of well-defined amphiphilic diblock copolymers amenable to crystallization-driven assembly in aqueous solution, enabling exploration of the effects of composition, molecular weight, and crystallinity on solution assembly behavior.

Table IV.1 Characterization of the PLLA-*b*-PDGC and PLLA-*b*-PDGC-cys diblock copolym Reprinted (adjusted) with permission from [48].

	$M_{n,\,NMR}$[a] (kDa)	$M_{n,\,SEC}$[b] (kDa)	$Đ$[b]		M_n[c] (kDa)	M_w[d] (kDa)	PLLA (wt%)	Morphology[e]
1, $PLLA_{72}$-*b*-$PDGC_{32}$	22.3	17.3	1.08	**1'**, $PLLA_{72}$-*b*-$PDGC_{32}$-cys	30.1	32.5	34	cylinder bundles
2, $PLLA_{30}$-*b*-$PDGC_{30}$	15.6	12.7	1.12	**2'**, $PLLA_{30}$-*b*-$PDGC_{30}$-cys	22.8	25.5	19	cylinders
3, $PLLA_{45}$-*b*-$PDGC_{45}$	23.4	14.0	1.18	**3'**, $PLLA_{45}$-*b*-$PDGC_{45}$-cys	34.2	40.3	19	cylinders
4, $PLLA_{32}$-*b*-$PDGC_{52}$	24.0	16.9	1.08	**4'**, $PLLA_{32}$-*b*-$PDGC_{52}$-cys	36.6	39.5	13	cylinders
5, $PLLA_{17}$-*b*-$PDGC_{54}$	22.6	13.6	1.04	**5'**, $PLLA_{17}$-*b*-$PDGC_{54}$-cys	35.7	37.1	7	spheres
6, $PLLA_{26}$-*b*-$PDGC_{84}$	35.1	17.5	1.05	**6'**, $PLLA_{26}$-*b*-$PDGC_{84}$-cys	55.4	58.2	7	spheres
7, $PLLA_{17}$-*b*-$PDGC_{82}$	33.1	17.1	1.06	**7'**, $PLLA_{17}$-*b*-$PDGC_{82}$-cys	53.0	56.2	5	spheres

[a] Determined by ^1H NMR (500 MHz) in $CDCl_3$.
[b] Estimated relative to polystyrene standards by SEC eluting in THF.
[c] Calculated molecular weights from corresponding PLLA-*b*-PDGC NMR-derived molecular weights, assuming full conversion of alkyne groups.
[d] Calculated molecular weights from corresponding PLLA-*b*-PDGC NMR-derived molecular weights and SEC-derived $Đ$, assuming full conversion of alkyne groups.
[e] After self-assembly in nanopure water for 30 h.

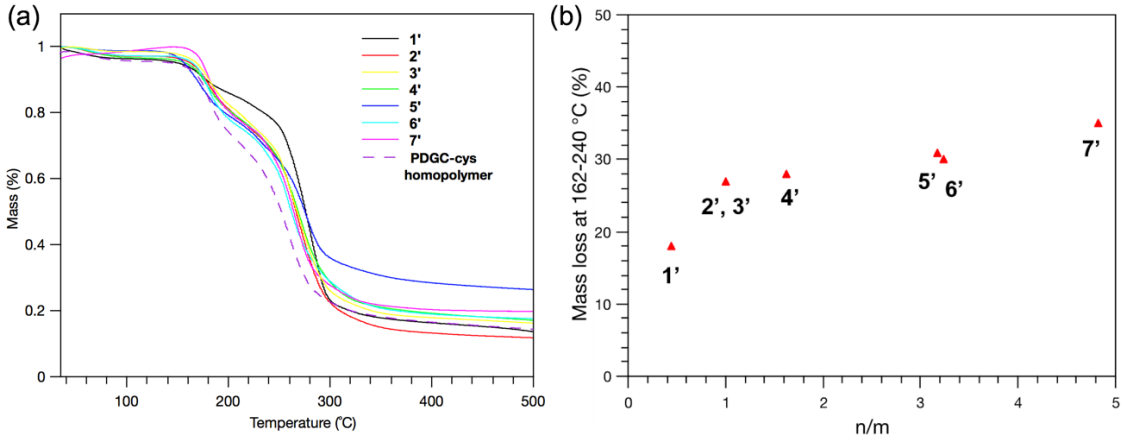

Figure IV.4 (a) TGA traces obtained under Ar atmosphere with a heating rate of 10 °C/min for copolymer **1'–7'**, and (b) Percentage mass loss of **1'-7'** between 162-240 °C as a function of the value n/m. Reprinted with permission from [48].

Crystallization-driven assembly of PLLA-*b*-PDGC-cys. To investigate the crystallization-driven assembly of PLLA-*b*-PDGC-cys, polymer solutions (0.05–0.1 mg/mL) were heated in nanopure water for 30 h at 65 °C to raise the solution temperature above the T_g of PLLA to aid dissolution, and then removed from heat and cooled to room

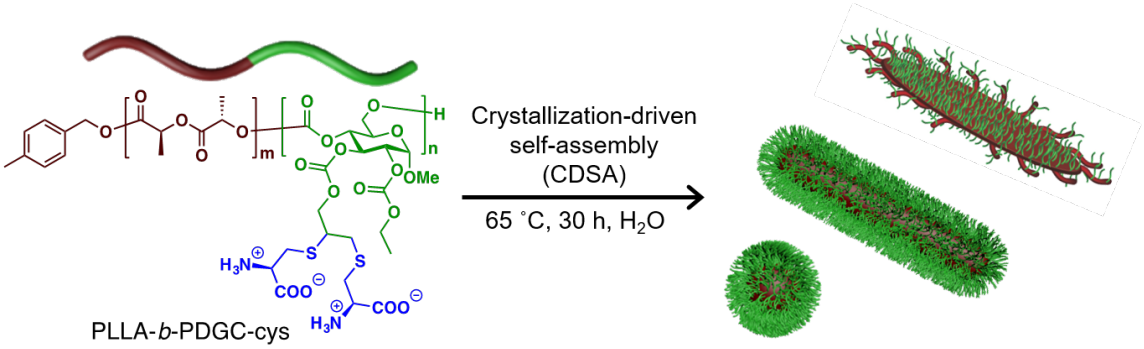

Figure IV.5 Crystallization-driven assembly of PLLA-b-PDGC-cys BCPs in aqueous solution into spherical, cylindrical, and 2D platelet-like bundled cylindrical nanostructures. Reprinted with permission from [48].

temperature (**Figure IV.5**).[147] The resulting assemblies were characterized by TEM and AFM.

PLLA-*b*-PDGC-cys nanostructure characterization by TEM and AFM. Following crystallization-driven assembly, TEM and AFM images (**Figure IV.6**) revealed spherical, cylindrical and 2D platelet-like bundled cylindrical micellar morphologies, depending on the weight percentage of PLLA in the diblock copolymers. The diblock copolymer with the highest PLLA weight percentage (34 wt%, polymer **1'**) yielded what appeared to be bundles of cylindrical nanostructures that were assembled into 2D platelets having average heights of 12 ± 2 nm (**Figure IV.7**), attributed to insufficient coronal repulsion. In contrast, strong repulsion between the hydrophilic PDGC-cys chains of polymers with low hydrophobic contents (<13 wt% PLLA, polymers **5'-7'**) promoted the formation of spherical micelles with high interfacial curvature upon aqueous crystallization-driven assembly. Polymers **2'-4'** with intermediate hydrophobic contents (13-19 wt% PLLA) assembled into cylinders with diameters ranging from 19–30 nm and a broad distribution of lengths; the distribution histograms are provided in **Figure IV.8**. Micelle dimensions were obtained using lengths and diameters measured from the TEM micrographs, while the heights were measured from AFM images. Polymers **2'** and **3',** synthesized with 19 wt% PLLA and different molecular weights (22.8 and 34.2 kDa overall, with PLLA DP_n values of 30 and 45, respectively) yielded cylinders with diameters of 21 ± 1 nm and 30 ± 3 nm, respectively. The assembly behaviors observed with these naturally-derived amphiphilic diblock copolymers are consistent with

previously published results for poly(acrylic acid) (PAA)-*b*-PLLA assemblies, where cylinders formed following crystallization-driven assembly in water from diblock copolymers with hydrophobic fractions exceeding 18 wt% and spherical micelles formed from polymers with lower hydrophobic fractions [161]. It is interesting that the number-averaged height of the bundled cylinders of polymer **1'** (12 ± 2 nm) was significantly less that the heights of the cylinders of **2'** and **3'** (18 ± 2 nm and 19 ± 2 nm) (**Figure IV.7**), even though the PLLA degree of polymerization was greater (72 *vs.* 30 *vs.* 45, respectively), which suggests partial reorganization and co-crystallization between the cores of individual cylinders. Further studies are underway to investigate these phenomena and gain control over the length and dispersity of the resulting nanostructures obtained from crystallization-driven assembly of these degradable amphiphilic diblock copolymers.

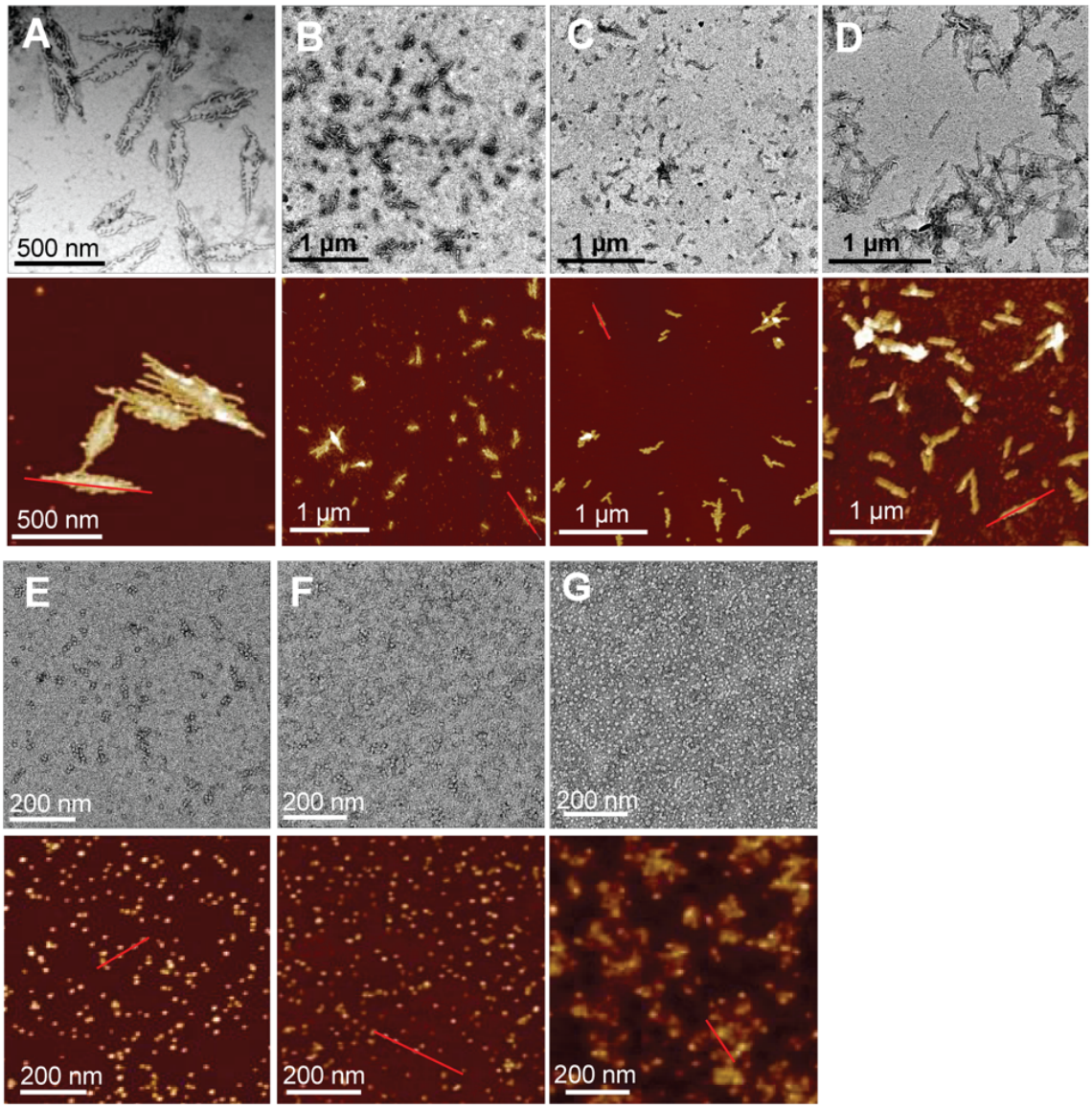

Figure IV.6 TEM micrographs (top) and AFM images (bottom) of assemblies from PLLA-b-PDGC-cys following crystallization-driven assembly. (A) Bundled cylinder platelets assembled from $PLLA_{72}$-*b*-$PDGC_{32}$-cys, polymer **1'**. (B) Cylinders assembled from $PLLA_{30}$-*b*-$PDGC_{30}$-cys, polymer **2'**: diameter (d) = 21 ± 1 nm. (C) Cylinders assembled from $PLLA_{45}$-*b*-$PDGC_{45}$-cys, polymer **3'**: d = 30 ± 3 nm. (D) Cylinders assembled from $PLLA_{32}$-*b*-$PDGC_{52}$-cys, polymer **4'**: d = 23 ± 1 nm. (E) Spheres assembled from $PLLA_{17}$-*b*-$PDGC_{54}$-cys, polymer **5'**: d = 15 ± 1 nm. (F) Spheres assembled from $PLLA_{26}$-*b*-$PDGC_{84}$-cys, polymer **6'**: d = 13 ± 1 nm. (G) Spheres assembled from $PLLA_{17}$-*b*-$PDGC_{82}$-cys, polymer **7'**: d = 14 ± 2 nm. Reprinted with permission from [48].

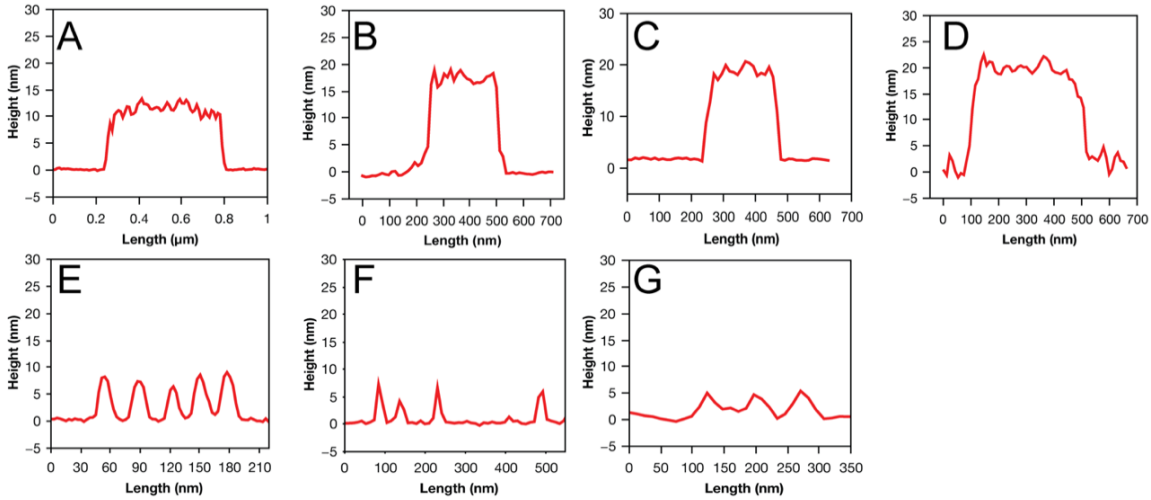

Figure IV.7 AFM height images of assemblies from PLLA-b-PDGC-cys following crystallization-driven assembly. (A) **Polymer 1'**: height (h) = 12 ± 2 nm. (B) **Polymer 2'**: h = 18 ± 2 nm. (C) **Polymer 3'**: h = 19 ± 2 nm. (D) **Polymer 4'**: h = 20 ± 1 nm. (E) **Polymer 5'**: h = 8 ± 1 nm. (F) **Polymer 6'**: h = 7 ± 1 nm. (G) **Polymer 7'**: h = 5 ± 1 nm. Reprinted with permission from [48].

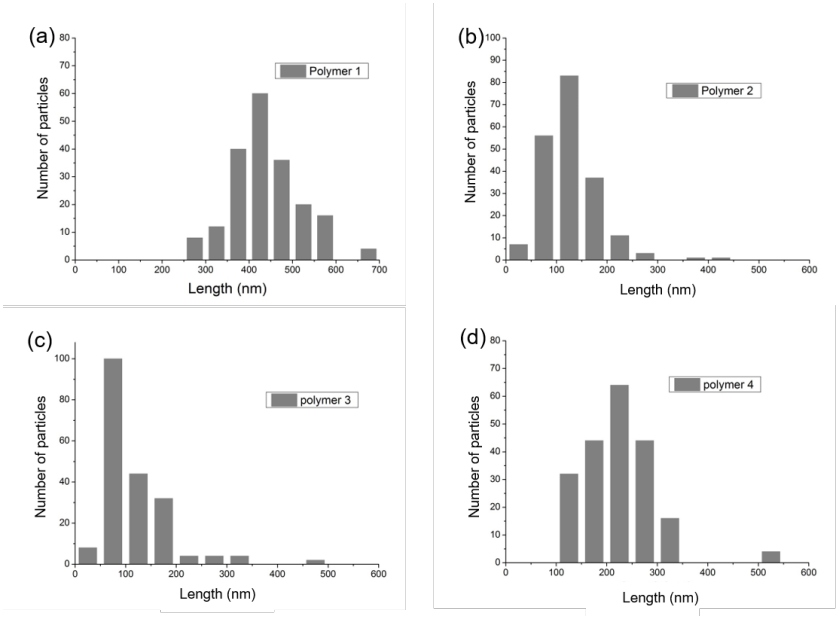

Figure IV.8 Histograms of the lengths of PLLA-*b*-PDGC-cys cylindrical (bundles) micelles (polymers **1'-4'**) as determined by TEM analysis. The average lengths of the cylinders assembled from polymers **1'** (bundles), **2'**, **3'**, and **4'** were determined to be 428 ± 77 nm, 114 ± 50 nm., 116 ± 56 nm, and 221 ± 70 nm, respectively. Reprinted with permission from [48].

WAXD characterization of PLLA-*b*-PDGC-cys. To determine the crystallinity of nanostructures formed following CDSA, WAXD was performed on assemblies of polymers **1'**, **2', 4'**, **6'**, and **7'** (**Figure IV.9**). The presence of the characteristic diffractions at 2θ = 16.6° and 19.1°, corresponding to the diffractions of (110)/(200) and (203) of the PLLA domains, respectively,[147, 161, 180] verified the crystalline nature of the micelle cores. The intensity of the peak decreased with decreasing PLLA weight fraction in the diblock copolymers, wherein WAXD of the cylindrical nanostructures formed from polymers **1'**, **2'** and **4'** showed an obvious peak, while almost no peak was observed for the spherical micelles formed from polymers **6'** and **7'**, having the lowest PLLA weight contents. These WAXD results provide strong evidence of the key influence of crystallization in the self-assembly process.

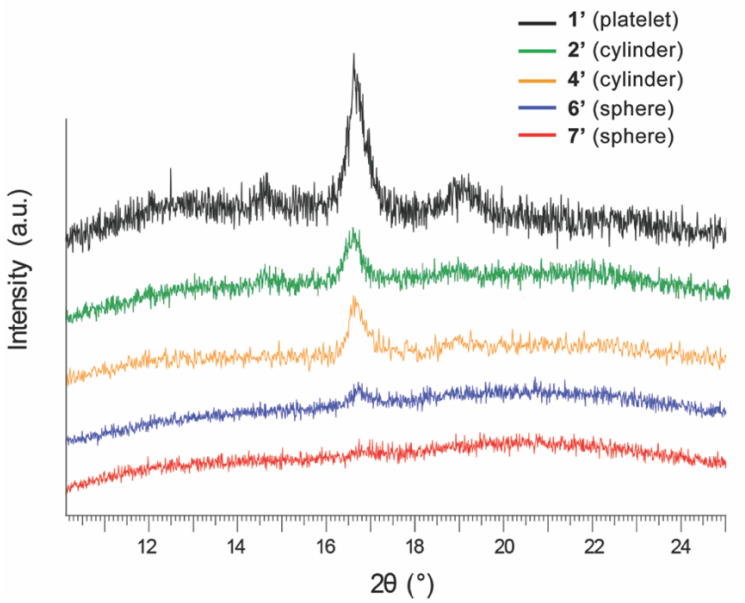

Figure IV.9 WAXD diffractograms of the nanostructures from polymers **1'**, **2'**, **4'**, **6'**, and **7'**. The peaks at 2θ = 16.6° and 19.1° correspond to the diffractions of (110)/(200) and (203) within crystalline regions of the PLLA nanostructure cores, respectively. Reprinted with permission from [48].

Hydrolytic degradation of PLLA-*b*-PDGC-cys. The ester and carbonate linkages of the PLLA and PDGC backbone segments, respectively, can be cleaved by spontaneous hydrolysis and/or enzymatic degradation [181-183]. Hydrolytic degradation of diverse polymers has been studied previously using NMR spectroscopy [183-184], SEC [184], dynamic light scattering (DLS) [183] and mass spectrometry [183]. In this work, the stability of the PLLA-*b*-PDGC-cys diblock copolymers was evaluated in aqueous solutions (pH 1 and 10) at 37 °C over 100 d by monitoring changes in the ^{1}H NMR spectra at δ 4.50–3.70, 3.50–2.50 and 1.13 ppm, corresponding to the proton resonances of L-cysteine-related moieties and D-glucose carbonate degradation products, and at δ 1.37 and 3.60 ppm, corresponding to L-lactide degradation products (**Figure IV.10**). Following NMR-based hydrolytic degradation studies, the solutions were analyzed by ESI and MALDI-TOF mass spectrometries (**Figure IV.11**).

Degradation of PLLA-*b*-PDGC-cys in aqueous solutions monitored by ^{1}H NMR spectroscopy. The PLLA-*b*-PDGC-cys diblock copolymers contain ester linkages in the PLLA segments and carbonate linkages in the PDGC-cys segments, which are potentially hydrolytically degradable. To evaluate the degradation of the ester and carbonate linkages along the polymer backbone and side chains, aqueous solutions (D_2O) in NMR tubes containing *ca.*5 mg/mL of PLLA-*b*-PDGC-cys **6'** at pH 1 and 10 were incubated at 37 °C, and degradation profiles were measured by ^{1}H NMR spectroscopy over 100 d. For each pH condition, sharp peaks appeared and increased in intensity with time, attributed to the production of small molecules and oligomers during polymer degradation (**Figure IV.10**). Specifically, the doublet at δ 1.37 ppm and the quartet at δ

3.60 ppm are attributed to the ^{1}H resonances of the degradation products of the PLLA segment, whereas the multiplets at δ 4.50–3.70, 3.50–2.65 ppm and the triplet at δ 1.13 ppm are attributed to hydrolytic degradation of the PDGC backbone and side chain carbonate linkages into glucose- and cysteine-based small molecules. Up- and down-field shifts of proton resonances corresponding to different protonation states of the carboxylic acid and amine groups of cysteine explain some of the differences between spectra acquired at pH 1 and pH 10. Precipitation of the polymer within 1 d upon incubation at 37 °C in aqueous solutions at either pH 7.4 (1X phosphate buffered saline) or pH 5.0 (sodium acetate/acetic acid buffer), attributed to interactions between the protonated amine and deprotonated carboxylic groups under neutral conditions, prevented the ability to conduct degradation studies at neutral pH [185]. Nevertheless, these NMR studies

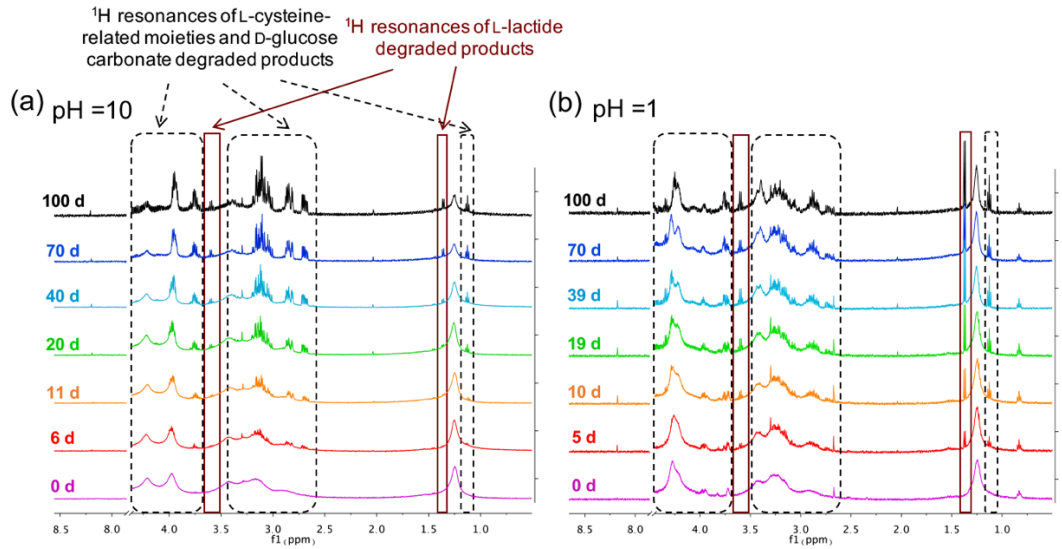

Figure IV.10 ^{1}H NMR (500 MHz) spectra of PLLA-*b*-PDGC-cys **6**' acquired in D_2O (*ca.* 5 mg/mL) adjusted to pH 10 (a) and 1 (b) during incubation at 37 ºC over 100 d. Reprinted with permission from [48].

confirmed the hydrolytic degradability of both segments of these amphiphilic diblock copolymers that were demonstrated to undergo CDSA into a variety of nanostructures.

Identification of PLLA-*b*-PDGC-cys degradation products by ESI mass spectrometry. The degradation products of the PLLA-*b*-PDGC-cys diblock copolymer **6'** were identified using ESI (**Figure IV.11**) and MALDI-TOF mass spectrometric analyses, following incubation at 37 °C in D_2O (*ca.* 5 mg/mL) adjusted to pH 1 and 10 for 100 d. By 100 d, the integration of the sharp peaks in the ^1H NMR spectra corresponding to small molecule degradation products no longer increased obviously in intensity. The hydrolytic degradation data suggested that the PDGC-cys segment was hydrolyzed into small molecules as the carbonate linkages in the PDGC backbone and side chains broke down, yielding methyl D-glucopyranoside and L-cysteine-related moieties. The hydrolytic degradability of the ester linkages of PLLA was confirmed by the presence of ESI mass spectrometry signals corresponding to the unimer and dimer of lactic acid, as well as of oligomers with a distribution of regularly spaced peaks at intervals of *m/z* 72 Da (corresponding to the molecular weight of a PLLA repeat unit). Two distributions of lactic acid oligomer peaks were observed, corresponding to oligomers with and without 4-methylbenzyl alcohol end groups. Finally, MALDI-TOF analysis of the mixture of degradation products confirmed the degradation of the polymers into small molecules and oligomers by the disappearance of high molecular weight peaks and appearance of lower molecular weight peaks (**Figure IV.12**).

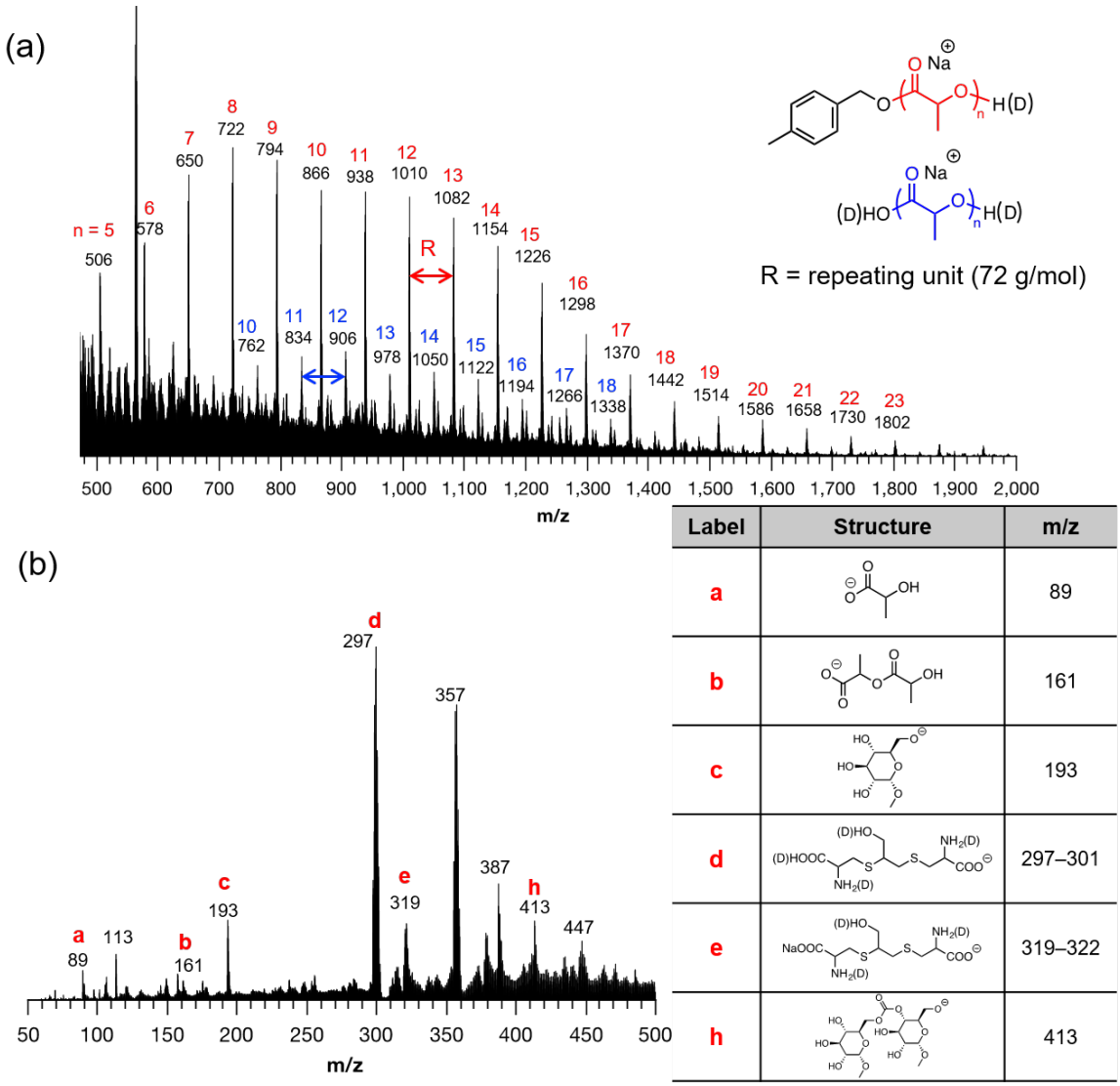

Label	Structure	m/z
a		89
b		161
c		193
d		297–301
e		319–322
h		413

Figure IV.11 ESI MS analysis of the degradation products of the polymer **6**'. Mass spectra acquired in positive ion mode, m/z range of 500–2000 (a), and in negative ion mode, m/z range of 50–500 (b). Reprinted with permission from [48].

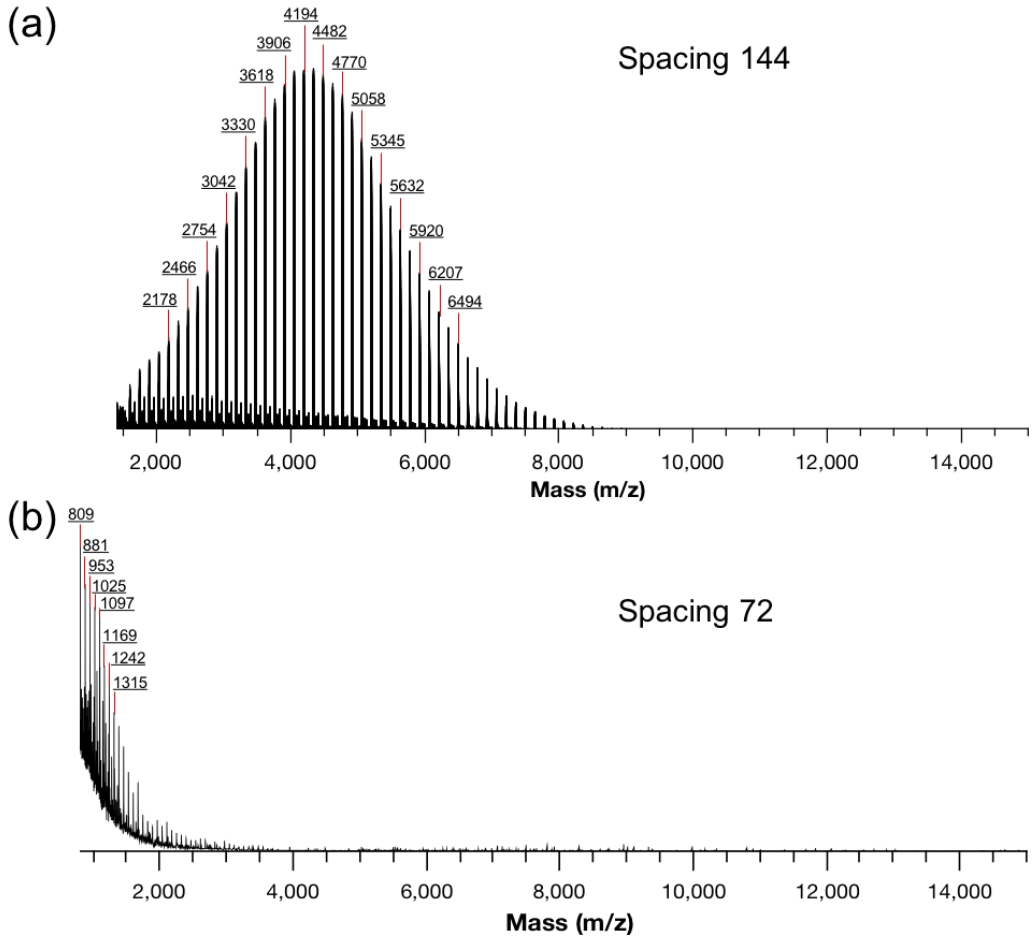

Figure IV.12 MALDI-TOF mass spectra of homopolymer aliquot PLLA (a), and polymer **6'** degradation products after 100 d in aqueous solution at pH 10 and 37 ˚C (b). Reprinted with permission from [48].

4.4 Conclusions

In summary, fully degradable, well-defined functional amphiphilic diblock copolymers synthesized from natural products were demonstrated to undergo crystallization-driven assembly in aqueous solution into a variety of nanostructures. Well-

defined diblock copolymers with alkyne-containing side chains were prepared by TBD-catalyzed sequential ROP of L-lactide and a bicyclic alkyne-substituted glucose carbonate. Subsequent modification of the alkyne side chain moieties with L-cysteine in a highly efficient UV-initiated thiol-yne reaction afforded amphiphilic semi-crystalline diblock copolymers with controlled molecular weights and compositions. Crystallization-driven assembly of the resulting polymers in aqueous solution afforded a series of nanoparticles, of which the morphology varied with PLLA content. AFM and TEM confirmed the successful formation of spherical and cylindrical nanostructures from PLLA-*b*-PDGC-cys. Importantly, the degradability of these micellar nanoparticles was demonstrated in comprehensive degradation studies involving ^{1}H NMR spectroscopy, and ESI and MALDI-TOF mass spectrometry measurements. Assembly procedures yielding control over nanostructure dimensions, and encapsulation and release of therapeutic agents using these functional, degradable micelles are under investigation.

CHAPTER V

MORPHOLOGIC DESIGN OF SILVER-BEARING SUGAR-BASED POLYMER NANOPARTICLES FOR UROEPITHELIAL CELL BINDING AND ANTIMICROBIAL DELIVERY

5.1 Introduction

Urinary tract infections (UTIs) are among the most common bacterial infections acquired in the community and in hospitals,[186-187] and recurrent UTIs can arise from re-emergence of bacterial colonies that are impervious to standard antibiotic treatment while they persist within epithelial cells lining the urinary bladder.[188-189] Globally increased antibiotic resistance among uropathogens further makes these recalcitrant UTIs challenging to treat.[190-191] An alternative strategy is to utilize biocides with low likelihood of resistance development; for example, silver cations (Ag^+), the predominant antimicrobial silver species, exert activity against a broad spectrum of bacteria and other microbes and rarely elicit bacterial resistance.[192-195]

For intracellular delivery of therapeutics, polymer nanocarriers offer capacity for encapsulating various antimicrobial agents and for optimizing nanoparticle (NP) cell binding and uptake, by installing targeting ligands or modulating NP physical and mechanical properties (*e.g.,* size, shape, chemical composition, surface chemistry, and modulus).[196-199] It is hypothesized that adherence and internalization of *E. coli* within epithelial cells is facilitated by multivalent adhesin-receptor binding interactions and by the elongated rod-like aspect ratio of these Gram-negative bacilli,[188, 200] features that can

both be leveraged in the chemical design of nanocarriers. Previous work demonstrated that shell crosslinked knedel-like (SCK) spherical NPs having dimensions of *ca.* 20-40 nm and functionalized with *E. coli* $FimH_A$, the type 1 pilus tip adhesin that mediates bacterial attachment to bladder epithelium,[201] readily bound cultured uroepithelial cells but were rarely internalized.[202-203] This result indicated that, despite specific interactions between NPs and cell-surface receptors, achieving epithelial internalization of NPs would require more than merely installing a targeting ligand. A logical next approach could rely on the optimization of NP size and shape to promote multivalent cell binding and improve internalization.[204-205]

Due in part to their anisotropic properties, rod-like NPs have attracted growing interest for multiple potential applications. Gratton *et al.* reported rapid and efficient internalization of rod-like, high-aspect-ratio hydrogel particles with dimensions as large as 3 μm by human cervical carcinoma epithelial (HeLa) cells.[206] Liu *et al.* elucidated the effect of aspect ratio of rod-like NPs on cellular uptake, showing that rods with aspect ratios of 4 and 8 were ingested much faster by both epithelial and endothelial cells than rods with an aspect ratio of 17.[207] Further, Agarwal *et al.* revealed that internalization of disc-shaped hydrophilic NPs into cultured mammalian cells was more efficient than nanorods made from similar materials.[208] Additionally, Decuzzi *et al.* have shown theoretically that non-spherical oblate-shaped particles bind more strongly and can withstand higher linear shear-flow forces than spherical NPs,[209] a consideration important in designing NPs for urinary tract use. These observations highlight the importance of NP morphology and dimension in creating optimized therapeutic carriers.

Here, we report the design of multifunctional, fully degradable synthetic zwitterionic block copolymers to afford micellar nanostructures of spherical, cylindrical, and platelet-like morphologies, and we evaluate the effect of NP morphology and dimension on cellular binding and internalization (**Figure V.1**). Biocompatibility of these nanocarriers was evaluated by measurement of cell viabilities and cytokine expression levels. Platelet-like nanostructures displayed optimal cell binding and internalization properties, compared to spherical and cylindrical NPs. Finally, loading capacity and sustained release of antimicrobial silver cations were quantified, and the *in vitro* antimicrobial activities of silver-loaded NPs against pathogenic bacteria were determined.

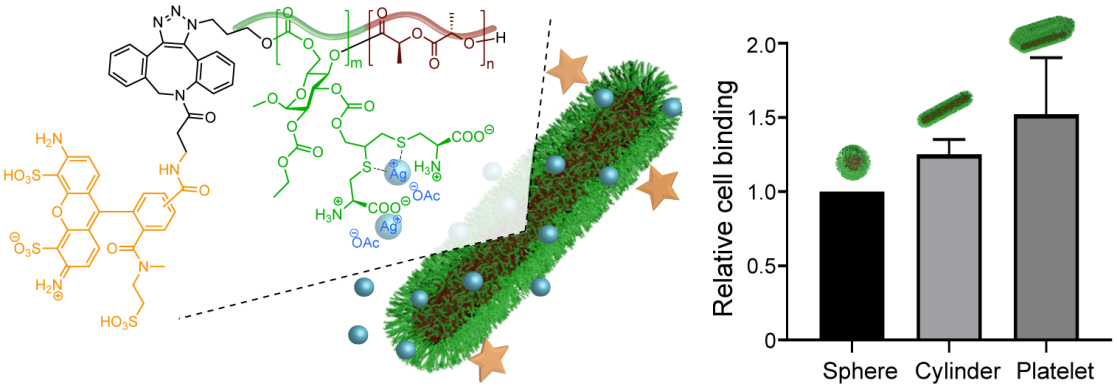

Figure V.1 Design of fluorescent nanocarriers with various morphologies for improvement of cell binding.

5.2 Materials and Methods

5.2.1 Materials

L-Lactide was purified by recrystallization from ethyl acetate. 1,5,7-Triazabicyclo[4.4.0]dec-5-ene (TBD) was used as received from TCI America (Portland, OR). The azide-reactive fluorescent label MB™ 488 DBCO was purchased from Click Chemistry Tools LLC (Scottsdale, AZ). Dichloromethane (DCM) was dried through a solvent purification system (J. C. Meyer Solvent Systems, Inc., Laguna Beach, CA). Nanopure water (18.2 MΩ·cm) was acquired through a Milli-Q water filtration system from Millipore Corp (Burlington, MA). All other chemicals were purchased from Sigma-Aldrich (St. Louis, MO) and used without further purification unless otherwise noted. Spectra/Por dialysis membranes (12-14 kDa molecular weight cut-off, MWCO) were purchased from Spectrum Laboratories, Inc. (Rancho Dominguez, CA). Slide-A-Lyzer dialysis cassettes (10 kDa MWCO) were purchased from Pierce Biotechnology (Rockford, IL). Dulbecco's Modified Eagle's Medium (DMEM) and Roswell Park Memorial Institute (RPMI) 1640 medium were obtained from the American Type Culture Collection (ATCC; Manassas, VA), with media additives (fetal bovine serum, penicillin/streptomycin) purchased from Sigma-Aldrich (St. Louis, MO). Cell culture 96-well round-bottom plates were purchased from Corning Costar Co. (Corning, NY).

5.2.2 Instrumentation

^{1}H, ^{13}C, and DOSY NMR spectra were recorded on Varian 500 MHz spectrometers, interfaced to a UNIX computer using VnmrJ software. Chemical shifts were referenced to solvent resonance signals. Fourier-transform infrared (FT-IR) spectra were recorded on an IR Prestige 21 system (Shimadzu Corp., Japan), equipped with an attenuated total reflectance (ATR) accessory, and analyzed using IRsolution v. 1.40 software. Size exclusion chromatography (SEC) with tetrahydrofuran (THF) elution was conducted on a Waters Chromatography (Milford, MA) system equipped with an isocratic pump (model 1515), a differential refractometer (model 2414), and a four-column set, including a 5 μm Guard column (50 × 7.5 mm), a PLgel 5 μm Mixed C column (300 × 7.5 mm, Agilent Technologies) and two Styragel® columns (500 Å and 104 Å, 300 × 7.5 mm, Waters Chromatography). The system was equilibrated at 40 °C in THF with the flow rate set to 1.0 mL/min. Data collection and analysis were performed with Waters Breeze™ software. Molar masses were determined relative to polystyrene standards (615-442800 Da) purchased from Polymer Laboratories (Amherst, MA). Polymer solutions were prepared at a concentration of *ca.* 3 mg/mL with *ca.* 0.05 vol% toluene added as a flow marker, and an injection volume of 200 μL was used. Thermogravimetric analysis (TGA) was performed under an Ar atmosphere using a Mettler-Toledo (Columbus, OH) model TGA2/1100/464 with a heating rate of 10 °C/min. Data were analyzed using Mettler-Toledo STAR^{e} v. 15.00a software. Glass transitions (T_g) were measured by differential scanning calorimetry (DSC) on a Mettler-Toledo DSC3/700/1190® under $N_{2(g)}$. Measurements were performed with heating and cooling rates of 10 °C/min and

analyzed using Mettler-Toledo Star^e v. 15.00a software. The T_g was taken as the midpoint of the inflection tangent of the third heating scan. Elemental analysis was performed at Midwest Microlab, LLC (Indianapolis, IN). Transmission electron microscopy (TEM) images were collected on a JEOL 1200EX operating at 100 kV and micrographs were recorded at calibrated magnifications using an SIA-15C CCD camera. The samples as aqueous solutions (8 μL) were deposited onto carbon-coated copper grids. Excess sample was wicked off using filter paper, and the grids were allowed to dry in air for 1 min. Where indicated, grids were stained with 8 μL of a 1% phosphotungstic acid (PTA) aqueous solution. After 30 s, excess stain solution was quickly wicked off using a piece of filter paper, and the samples were left to dry under ambient conditions prior to imaging. Ultraviolet-visible (UV-vis) spectroscopy measurements were performed on a Shimadzu UV-2550 spectrophotometer. Fluorescence spectroscopy was performed on a Shimadzu RF-5301pc Spectrofluorophotometer. Confocal images were collected with an LSM 880 Airyscan confocal microscope (Carl Zeiss, Thornwood, NY). Minimum inhibitory concentration (MIC) assays were read on a Synergy 2 microplate reader (Bio-Tek, Winooski, VT). All experiments were performed according to the Environmental Health and Safety guidelines of Texas A&M University and Washington University. Experiments involving mouse-derived cell lines (RAW 264.7) and HTB-9 human bladder carcinoma cell lines were performed according to guidelines provided by Texas A&M's Institutional Biosafety Committee for biosafety level 1 organisms (Protocol Approval Number IBC2014-075).

5.2.3 Synthetic procedures

Synthesis of N_3-PDGC-*b*-PLLA. A solution in anhydrous dichloromethane (DCM) of propargyl-containing D-glucose carbonate monomer (201 mg, 0.535 mmol) and 3-azido-1-propanol (0.10 mL, 9.8 mg/mL in DCM, 0.011 mmol) was prepared, and transferred to a vial equipped with a stir bar and a rubber septum in an argon-filled glovebox. The vial was then removed from the glovebox and connected to a Schlenk line. A solution of TBD in DCM (0.1 mL, 13.5 mg/mL, 0.012 mmol) was injected quickly into the vial at -78 °C. After stirring for 10 min, the reaction vial was taken out of the -78 °C dry ice bath, and a solution of L-lactide (77 mg, 0.54 mmol) in DCM (1.0 mL) was added *via* syringe to the reaction mixture. The reaction was stirred for an additional 3 min at *ca.* 0 °C and then quenched by addition of excess acetic acid. Size-exclusion chromatography (SEC) of the crude product showed negligible peak at 27-28 min, indicating quantitative conversions of both monomers. Precipitation from DCM into methanol three times, and drying under vacuum yielded **1**, N_3-$PDGC_{47}$-*b*-$PLLA_{44}$ as a white powder (yield: 78%). ^{1}H NMR (500 MHz, $CDCl_3$): δ 5.36 (t, J = 10 Hz), 5.16 (q, J = 7 Hz), 5.03 (d, J = 4 Hz), 4.89 (t, J = 10 Hz), 4.79 – 4.66 (m), 4.30 – 4.26 (m), 4.19 (tt, J = 7, 3 Hz), 4.01 (d, J = 10 Hz), 3.44 (s), 2.59 (q, J = 3 Hz), 1.95 (p, J = 7 Hz), 1.58 (d, J = 7 Hz), 1.30 (t, J = 7 Hz) ppm. ^{13}C NMR (126 MHz, $CDCl_3$): δ 169.76, 154.18, 154.19, 153.79, 153.69, 96.56, 77.07, 76.34, 74.28, 73.64, 72.34, 69.15, 66.78, 65.83, 64.93, 56.04, 55.91, 16.79, 14.27 ppm (**Figure V.2**). FT-IR: 3286, 2978, 2106, 1751, 1450, 1373, 1234, 1195, 1118, 1087, 1018, 987, 910, 879, 779, 663 cm^{-1} (**Figure V.3**). SEC (THF): M_n = 16.8 kDa, $Đ$ = 1.09. T_g = 110 °C. TGA in Ar: 250-390 °C, 75% mass loss; 20% mass remaining at 500 °C.

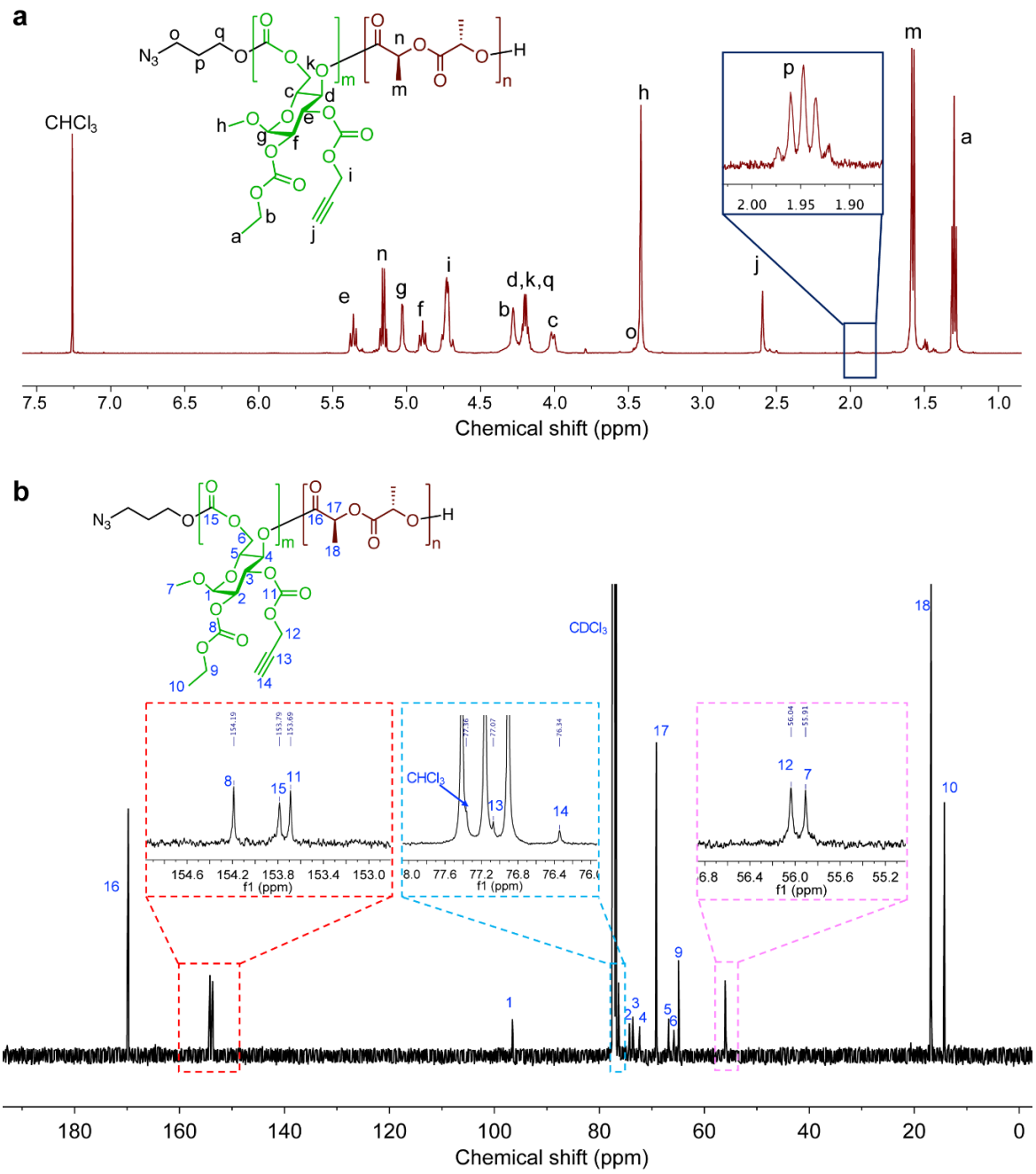

Figure V.2 (a) ^{1}H (500 MHz) and (b) ^{13}C NMR (126 MHz, $CDCl_3$) spectra of **1**, N_3-PDGC-*b*-PLLA (sample N_3-PDGC$_{39}$-*b*-PLLA$_{74}$).

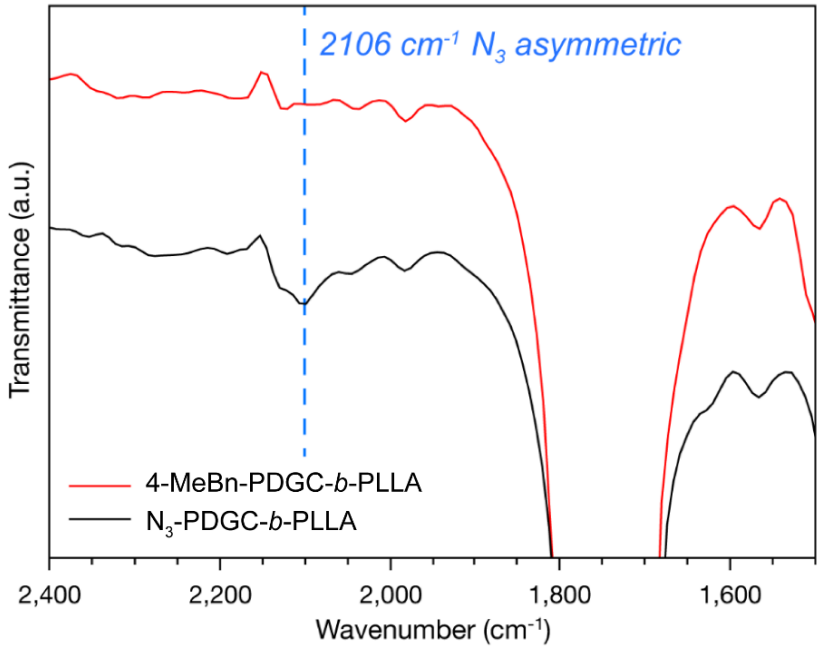

Figure V.3 FT-IR spectra of PDGC-*b*-PLLA prepared by initiation with 4-methylbenzyl alcohol and 3-azido-propa-1-ol to afford PDGC-*b*-PLLA with a 4-methylbenzyl alcohol chain end (red line) and N_3-PDGC-*b*-PLLA with a 3-azido-propa-1-ol chain end (black line).

General procedures for thiol-yne click reaction with cysteine. A solution of N_3-PDGC$_{47}$-*b*-PLLA$_{44}$ (50 mg, 0.098 mmol alkyne), L-cysteine (160 mg, 1.3 mmol), HCl (0.5 mL) and 2,2-dimethoxy-2-phenylacetophenone (DMPA; 10 mg, 0.04 mmol) was prepared in 5 mL of *N,N*-dimethylformamide (DMF), deoxygenated with bubbling $N_{2(g)}$ for 5 min, and irradiated at 365 nm (1000 μJ/cm^2) for 2 h. The DMF solution was transferred into dialysis tubing (MWCO 12–14 kDa) and dialyzed against nanopure water adjusted to pH 3 with HCl at 4 °C for 2 d. The resulting solution was then lyophilized to yield the cysteine-modified polymer **2**, N_3-PDGC(cys)$_{47}$-*b*-PLLA$_{44}$ as a white solid. Yield: 88%. ^{1}H NMR (500 MHz, DMSO-d_6): δ 5.19 (q, J = 7 Hz), 5.14 (s), 4.98 (s), 4.84

(br), 4.43 (br), 4.15 (br), 4.00 (br), 3.81 (br), 3.70 (br), 3.08 (s), 2.90 (b), 2.75 (br), 1.46 (d, J = 7 Hz), 1.21 (t, J = 7 Hz) ppm. ^{13}C NMR (126 MHz, DMSO-d_6): δ 169.46, 169.21, 153.83, 153.52, 118.90, 68.69, 64.65, 54.92, 52.21, 51.78, 40.43, 16.47, 13.99 ppm. FT-IR: 3680-2180, 1750, 1620, 1480, 1390, 1245, 1100, 1020, 880, 770, 630 cm^{-1}. T_g = 113 °C. TGA in Ar: 150-190 °C, 20% mass loss; 190-370 °C, 40% mass loss; 20% mass remaining at 500 °C.

General procedures for preparation of MB™ 488 DBCO labeled amphiphilic block copolymers. A solution of N_3-PDGC(cys)$_{47}$-*b*-PLLA$_{44}$ (15 mg, 0.42 μmol) was prepared by first dispersing polymers in 1 mL of water and followed by adding *ca.* 10 mL of DMSO. MB™ 488 DBCO (1.25 mg/mL, 500 μL, DMSO) was then added to the

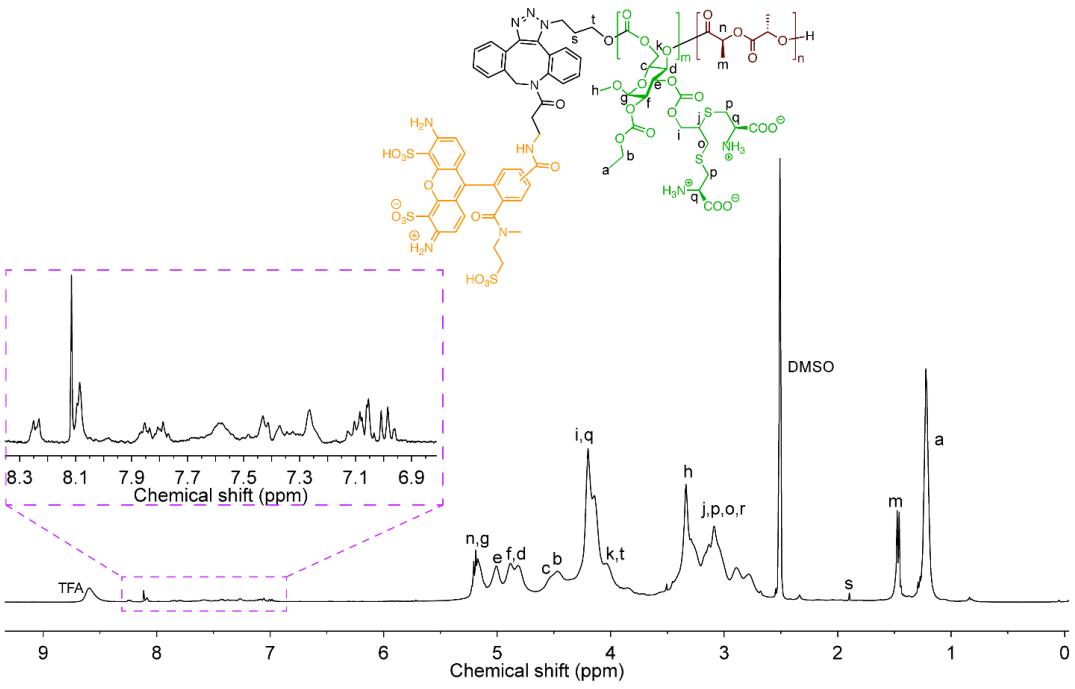

Figure V.4 ^{1}H NMR spectrum (500 MHz, DMSO-d_6 + TFA-*d*) of Polymer **3**.

solution, and the reaction mixture was allowed to stir at room temperature shielded from light for 30 h, followed by dialysis against nanopure water for 4 d to remove unconjugated dyes, yielding dye-labeled polymer solutions with a final concentration of *ca.* 0.2 mg/mL, 20 mL. The resulting solution was then lyophilized to yield the dye-labeled polymer **3**, dye-PDGC(cys)$_{47}$-*b*-PLLA$_{44}$, as a fluffy orange solid. Yield: 93%. ^{1}H NMR (500 MHz, DMSO-d_6 + TFA-*d*): δ 9.79 (br), 8.60 (s), 8.07 (s), 7.27 (q, J = 7 Hz), 7.19 (m), 7.00 (d, J = 8 Hz), 6.63 (d, J = 8 Hz), 5.20 (q, J = 7 Hz), 5.13 (m), 5.03 (m), 4.88 (br), 4.80 (br), 4.50 (br), 4.21 (br), 4.13 (br), 4.01 (m), 3.83 (br), 3.36 (br), 3.08 (br), 2.89 (b), 2.76 (br), 1.46 (d, J = 7 Hz), 1.21 (m) ppm (**Figure V.4**). ^{13}C NMR (126 MHz, DMSO-d_6 + TFA-*d*): δ 169.75, 169.63, 169.46, 169.21, 153.82, 119.23, 113.34, 95.96, 80.32, 68.69, 65.84, 55.24, 55.00, 52.18, 40.43, 16.64, 14.17 ppm. FT-IR: 3681-2154, 1753, 1622, 1492, 1452, 1382, 1242, 1091, 1031, 981, 881, 780, 640 cm^{-1}. T_g = 105 °C. TGA in Ar: 150-200 °C, 20% mass loss; 200-340, 32% mass loss; 25% mass remaining at 500 °C.

Self-assembly of PDGC(cys)-*b*-PLLA. Three polymer **2** samples N_3-PDGC(cys)-*b*-PLLA were dissolved in nanopure water (0.05-0.1 mg/mL). The solutions were heated to 65 °C for 30 h, and then allowed to cool to room temperature prior to characterizations and further experiments. For preparation of dye-containing nanostructures, the three polymer **2** samples N_3-PDGC(cys)-*b*-PLLA were allowed to react with *ca.* 20 mol% MB™ 488 DBCO and purified to yield fluorescent dye-labeled polymer, followed by the CDSA process.

Flow cytometry. 5637 bladder epithelial cells (ATCC HTB-9) were grown to confluence at 37 °C, 5% CO_2. Cells were liberated with trypsin/EDTA (Millipore Sigma,

St. Louis, MO) and transferred to FACS tubes. Cells were washed with 2 mL of RPMI medium with 10% FBS and centrifuged gently for 5 min, then resuspended with NP preparations (50 μg/mL polymer in RPMI with 10% FBS). Cells were incubated at 37 °C rocking for 1 h, then washed with FACS buffer, centrifuged at 1500 rpm for 5 min, and fixed with 3% paraformaldehyde (PFA) for 30 min at room temperature. After a final FACS buffer wash and centrifugation, cell pellets were resuspended in FACS buffer and

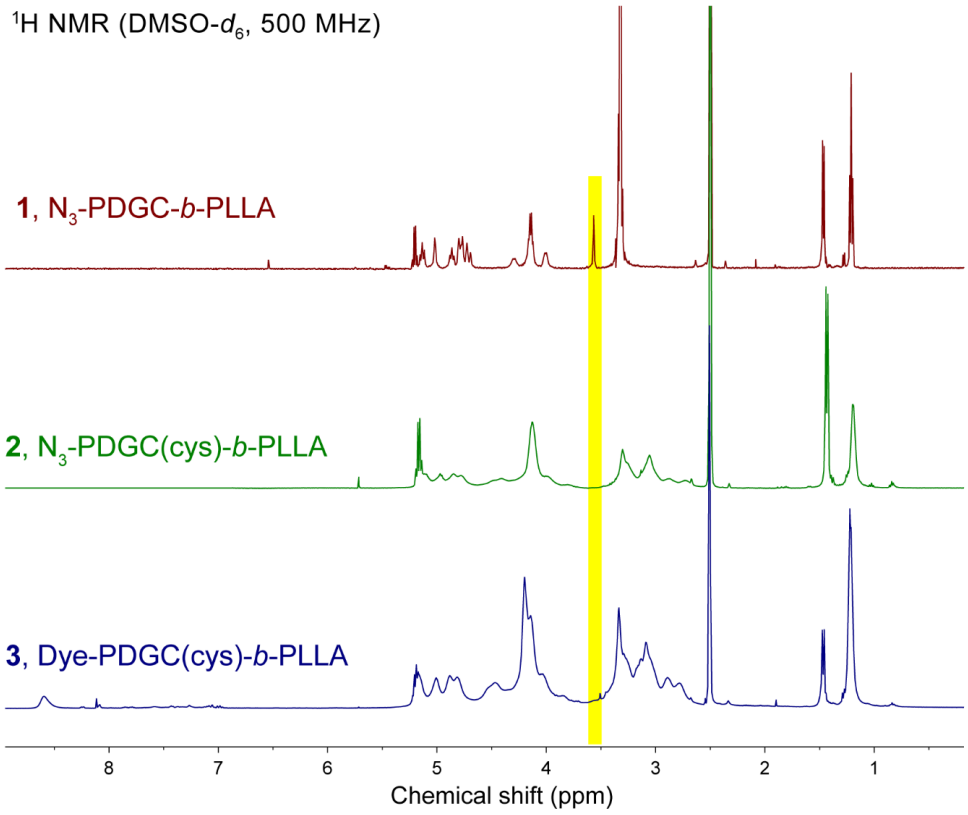

Figure V.5 ^{1}H NMR (500 MHz, DMSO-d_6) spectra of polymers **1**, N_3-PDGC-*b*-PLLA, **2**, N_3-PDGC(cys)-*b*-PLLA, and **3**, dye-PDGC(cys)-*b*-PLLA. The highlighted region showed the disappearance of PDGC alkyne proton resonance from **1** after thiol-yne reaction.

filtered through 44-μm nylon mesh. Samples were analyzed on the BD LSR Fortessa X-20 using the blue 488-nm laser and 530/30 filter.

Cell internalization. 5637 bladder epithelial cells were plated at 5×10^4 cells *per* well in a 24-well plate and grown overnight at 37 °C, 5% CO_2. The following day, cells were washed with PBS, overlaid with fresh RPMI with 10% FBS containing NPs (20 μg/mL polymer), and incubated at 37°C, 5% CO_2 for 1 h. Cells were washed thrice with PBS, then liberated with trypsin/EDTA, quenched with medium, and transferred to 1.5 mL tubes, then centrifuged at 3500 × *g* for 4 min. The pellet was resuspended in 3% PFA and fixed for 10 min at room temperature. After PBS washing and centrifugation, the cell pellet was resuspended in WGA 594 (Invitrogen, 1:5000 in PBS) and incubated for 3 min at room temperature in the dark. After PBS washing, centrifugation, and resuspension in PBS, cells were centrifuged onto poly(L-lysine)-coated glass slides (CytoPro, ELITech Biomedical Systems). Coverslips were mounted using ProLong Gold antifade reagent (Invitrogen).

Cytotoxicity assays. 5637 bladder epithelial cells (5×10^4 cells/well) were plated in 96-well plate in RPMI 1640 medium (with 10% fetal bovine serum [FBS] and 1% penicillin/streptomycin). Cells were incubated at 37 °C in a humidified atmosphere containing 5% CO_2 for 24 h. The culture medium was replaced by 100 μL of serial dilutions of the polymers in fresh medium (final concentrations ranged from 1.5-210 μg/mL). The cells were incubated with the NP formulations for 72 h; medium was then replaced with 100 μL of fresh medium prior to the addition of 20 μL of MTS combined reagent to each well (Cell Titer 96® Aqueous Non-Radioactive Cell Proliferation Assay,

Promega, Madison, WI). After further incubation for 2 h in the dark, absorbance at 490 nm was measured using a SpectraMax M5 instrument (Molecular Devices, Sunnyvale, CA). Cell viability was calculated based on absorbance relative to control untreated cells. The 0% and 100% cell viabilities were represented by control medium (no cells) and cells with no treatment, respectively.

Immunotoxicity and anti-biofouling assessment of polymer nanostructures. Zwitterionic N_3-PDGC(cys)$_{70}$-*b*-PLLA$_{18}$, N_3-PDGC(cys)$_{47}$-*b*-PLLA$_{44}$, N_3-PDGC(cys)$_{39}$-*b*-PLLA$_{74}$, anionic N_3-PDGC(COOH)$_{47}$-*b*-PLLA$_{44}$, and neutral PEGylated N_3-PDGC(PEG)$_{47}$-*b*-PLLA$_{44}$ diblock copolymers were dissolved in autoclaved, 0.2-μm filtered nuclease-free water at predetermined concentrations. The zwitterionic polymer solutions were heated at 65 °C for 30 h, followed by cooling to room temperature before use. All samples were adjusted to have a final concentration of 5 μg/mL. RAW 264.7 mouse macrophages (2×10^4 cells/well) were plated in a 96-well plate in DMEM with 10% fetal bovine serum and 1% penicillin/streptomycin and incubated at 37 °C with 5% CO_2 for 24 h. The medium was then replaced with fresh medium 1 h prior to the addition of 20 μL of each of the samples. After a 24 h incubation, the supernatants were collected and centrifuged for 10 min at 13000 rpm. The expression of 23 mouse cytokines [interleukin (IL)-1α, IL-1β, IL-2, IL-3, IL-4, IL-5, IL-6, IL-9, IL-10, IL-12 (P40), IL-12 (P70), IL-13, IL-17, eotaxin, granulocyte-colony-stimulating factor (G-CSF), granulocyte macrophage-colony stimulating factor (GM-CSF), interferon-γ (IFN-γ), keratinocyte-derived chemokine (KC), monocyte chemotactic protein (MCP)-1, macrophage inflammatory protein (MIP)-1α, MIP-1β, regulated upon activation normal T-cell

expressed and presumably secreted (RANTES) and tumor necrosis factor-α (TNF-α)] were measured immediately using a BioPlex 200 system, equipped with high-throughput fluidics (HTF) and a Pro II Wash station, and data were analyzed using BioPlex Data Pro software. Expression data upon treatment with NP formulations were compared to those in control (untreated) cells. Adsorption of cytokines onto N_3-PDGC(cys)-*b*-PLLA NPs of different morphologies and comparator NPs was calculated based on the apparent concentration of the cytokines measured after incubation with NPs, as compared to their concentrations in samples subject to the same procedures without NPs, as previously described.[210-211]

General procedure for the preparation of AgOAc-loaded polymeric NPs. A solution of AgOAc (60 μL, 4 mg/mL in nanopure water) was added dropwise to a solution of polymer assemblies of N_3-PDGC(cys)-*b*-PLLA (0.57 mg, polymer concentration = 0.1 mg/mL). The solution was shielded from light and allowed to stir overnight at room temperature to minimize light-induced reduction of Ag^+.[212] Unbound AgOAc was removed by centrifugal filtration (MWCO 30 kDa) several times (N>3). The resulting solution of Ag@polymer micelles was reconstituted to a final volume of *ca.* 3 mL, and the silver concentration was determined by ICP-MS. Aliquots of the solution of Ag@polymer micelles were used for TEM characterization.

Silver release. Solutions of silver-loaded N_3-PDGC(cys)-*b*-PLLA (3 mL) were transferred into presoaked dialysis cassettes (Slide-A-Lyzer, 10 kDa MWCO, Pierce Biotechnology, Rockford, IL). The dialysis cassettes were incubated in phosphate buffer (10 mM, pH 7.4) with 10 mM NaCl at 37 °C for 5 d. Aliquots (*ca.* 0.1 mL) from inside

of the dialysis cassettes were extracted at predetermined intervals, and [Ag^+] was measured by ICP-MS. Final results were obtained from triplicate experiments.

Antimicrobial activity. *E. coli* strains UTI89 and MG1655 were cultured in Luria-Bertani broth overnight at 37 °C. Strains were then subcultured into Mueller-Hinton broth and incubated with shaking at 37 °C until OD_{600nm} = 0.4. Silver-bearing NP preparations were serially diluted in a 96-well plate to yield [Ag^+] = 0.125 - 4 μg/mL; then bacteria were added at 2×10^4 colony-forming units per well. Plates were incubated statically at 37 °C in the dark for 24 h, and OD_{600nm} was recorded to determine bacterial growth *vs* inhibition.

5.3 Results and Discussion

Design of multifunctional polymeric nanocarriers with varied morphology. To construct nanocarriers of varied morphology from bio-based amphiphilic block polymers, synthetic building blocks were designed with tunable backbone chemical compositions and functional diversities rendered by side-chain and chain-end groups. Semicrystalline poly(L-lactide) (PLLA) was used as the hydrophobic segment due to its excellent performance in crystallization-driven self-assembly (CDSA), which facilitated the formation of high-aspect-ratio NPs.[162] Zwitterionic cysteine-modified poly(D-glucose carbonate) (PDGC)[48] served as the hydrophilic segment, because of its naturally-derived cysteine and glucose building blocks, versatile functionality and degradability into environmentally-benign molecules,[20, 29] potentially increasing biocompatibility and

minimizing toxicity.[213] Zwitterions in the PDGC block were introduced for hydrophilicity, biocompatibility, and capacity for antimicrobial metal chelation. In this study, the functional and degradable diblock copolymer N_3-PDGC(cys)-*b*-PLLA was designed to incorporate the features of a zwitterionic hydrophilic shell, semicrystalline hydrophobic core, and specially installed chain-end azido group for fluorescent labeling (**Figure V.1**). A series of fluorescently-labeled amphiphilic diblock copolymers having similar overall degrees of polymerization yet different hydrophilic-to-hydrophobic balances was readily prepared in three steps per each block polymer, from an azide-functionalized alcohol initiator, an alkyne-functionalized cyclic glucose carbonate monomer, L-lactide comonomer, cysteine and MB™ 488 DBCO, and then assembled into nanocarriers, loaded with silver cations and studied for their ability to inhibit *E. coli* growth. The morphological effects on epithelial cell binding and internalization were also investigated.

Synthesis and modification of multifunctional amphiphilic copolymers. The diblock copolymers were synthesized through sequential ring-opening polymerizations (ROP) of alkyne-functionalized cyclic D-glucose carbonate, followed by L-lactide. 3-Azido-1-propanol was utilized as the initiator to afford diblock copolymers with an azido group at the polymer α-chain end, capable of chemical conjugation of a fluorescent dye or targeting ligand. Of note, the monomer addition order is important to place the reactive azido group at the hydrophilic end of the chain to avail it for use in micelle surface functionalization. In a one-pot sequential ROP process, the cyclic carbonate of glucose was allowed to undergo polymerization at -78 °C in dichloromethane for 10 min, followed

by removal of the reaction mixture from the dry ice/acetone bath and the introduction of L-lactide and additional dichloromethane, with the polymerization being allowed to proceed for an additional 2-3 min before being quenched by addition of acetic acid. Allowing the temperature to increase from -78 °C to *ca.* 0 °C and decreasing the concentration of the reaction mixture from 0.45 M to 0.1 M for polymerization of the second L-lactide block were important to maintain narrow dispersity of the polymer, likely because reduced viscosity of the reaction mixture promoted better PLLA chain extension. Informed by our prior work,[48] we designed three different PDGC-to-PLLA ratios (4:1, 1:1 and 1:2) of polymer **1**, N_3-PDGC-*b*-PLLA, to achieve spherical, cylindrical, and platelet-like nanostructure morphologies, respectively. Size-exclusion chromatography (SEC) revealed unimodal molar mass distributions and low dispersities, demonstrating well-defined structures of the diblock copolymers (**Table V.1**). After purification of the polymers by precipitation into methanol, the degree of polymerization (DP_n) of each block was determined from ^{1}H NMR spectroscopy (**Figure V.2a**) by comparing the integration of the initiator $N_3CH_2C\boldsymbol{H}_2CH_2O$ central methylene proton resonance (1.95 ppm) with the integrations of the resonances of protons attached to the glucose anomeric carbons (5.03 ppm) in the PDGC segment and methine protons (5.16 ppm) from the PLLA segment, and the molar mass (M_n) values were then calculated. For the series of three polymer 1 samples, the DP_n values of PDGC *vs.* PLLA, m:n, were determined to be 70:18, 47:44, and 39:74, providing the desired 4:1, 1:1 and 1:2 proportions of PDGC-to-PLLA. Fourier-transform infrared (FT-IR) spectroscopy confirmed the presence of the azide functional group, by an azide stretching band observed at 2106 cm^{-1} (**Figure V.3**).

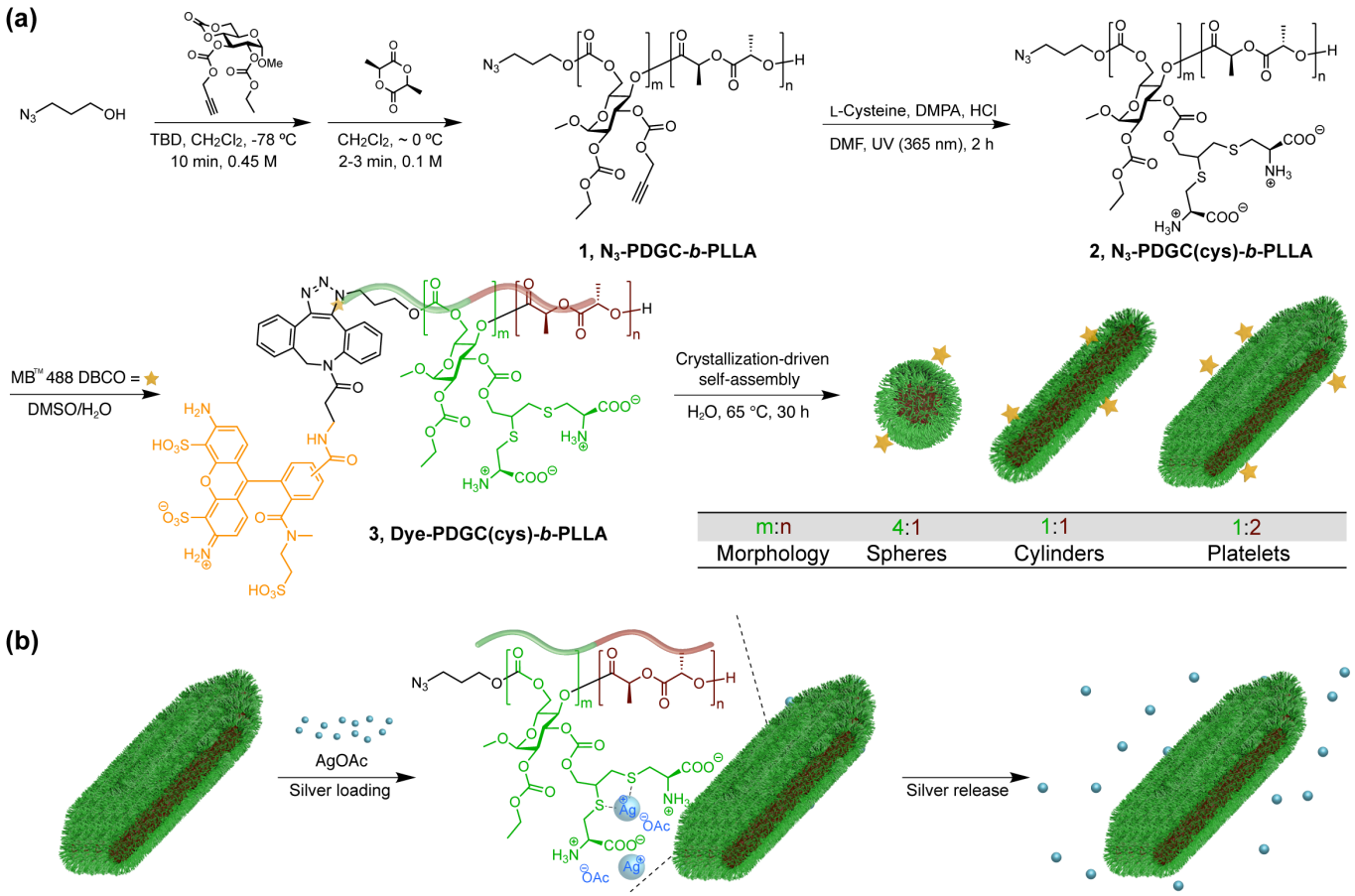

Figure V.6 Synthetic schemes. (a) Synthesis of polymer **1**, N_3-PDGC-*b*-PLLA, by ROP of glucose-carbonate and L-lactide monomers with an azido-containing initiator, followed by post-polymerization modification *via* thiol-yne reaction with cysteine to prepare the zwitterionic polymer **2**, N_3-PDGC(cys)-*b*-PLLA, and chain-end modification of polymer **2** with DBCO-functionalized fluorescent dye to afford dye-labeled polymer **3**, dye-PDGC(cys)-*b*-PLLA. (b), AgOAc loading into polymer nanostructures, through interactions with dithioether and carboxylate groups, and release.

Table V.1 Characterization of the N_3-PDGC-*b*-PLLA diblock copolymers.

	$M_{n,\,NMR}$[a] (kDa)	$M_{n,\,SEC}$[b] (kDa)	$Đ$[b]	Morphology after thiol-yne reaction and assembly[c]
N_3-PDGC$_{70}$-*b*-PLLA$_{18}$	28.7	19.0	1.12	Sphere
N_3-PDGC$_{47}$-*b*-PLLA$_{44}$	23.9	16.8	1.09	Cylinder
N_3-PDGC$_{39}$-*b*-PLLA$_{74}$	25.2	17.9	1.21	Platelet

[a] Determined by ^{1}H NMR (500 MHz) in $CDCl_3$.
[b] Estimated relative to polystyrene standards by SEC eluting in THF.
[c] After crystallization-driven self-assembly in nanopure water.

The three polymers **1** were then modified *via* photo-initiated thiol-yne click reaction with cysteine (10 equivalents to alkyne groups) under UV light (365 nm) in the presence of 2,2-dimethoxy-2-phenylacetophenone (DMPA) for 2 h, to facilitate quantitative conversion of the alkyne functional groups on the polymers and minimize polymer crosslinking. Dialysis against nanopure water (pH 3, adjusted with HCl) at 4 °C and lyophilization were performed to afford the series of three amphiphilic block copolymers 2 as white powders. The appearance of thioether proton resonances at 3.06 and 3.31 ppm and the disappearance of the alkyne proton signal resonating at 3.57 ppm (**Figure V.4–V.5**) indicated successful conjugation of cysteine side-chain substituents. FT-IR spectroscopy further supported the introduction of COO-H and N-H groups by showing a broad peak at 3600 – 2300 cm^{-1}, while indicating the carboxylate (COO-) characteristic of cysteine with a peak attributed to carboxylate C=O stretching at 1627 cm^{-1} (**Figure V.7**). Thermogravimetric analysis (TGA) of polymer **2** revealed two-

stage decomposition with different extents of mass loss for the different m:n values, but an overall trend of 10-20% mass loss at 160-190 °C and 30-50% mass loss at 220-320 °C, corresponding to the loss of cysteine moieties and decomposition of the polymer backbone, respectively, with *ca*. 20% mass remaining at 500 °C.

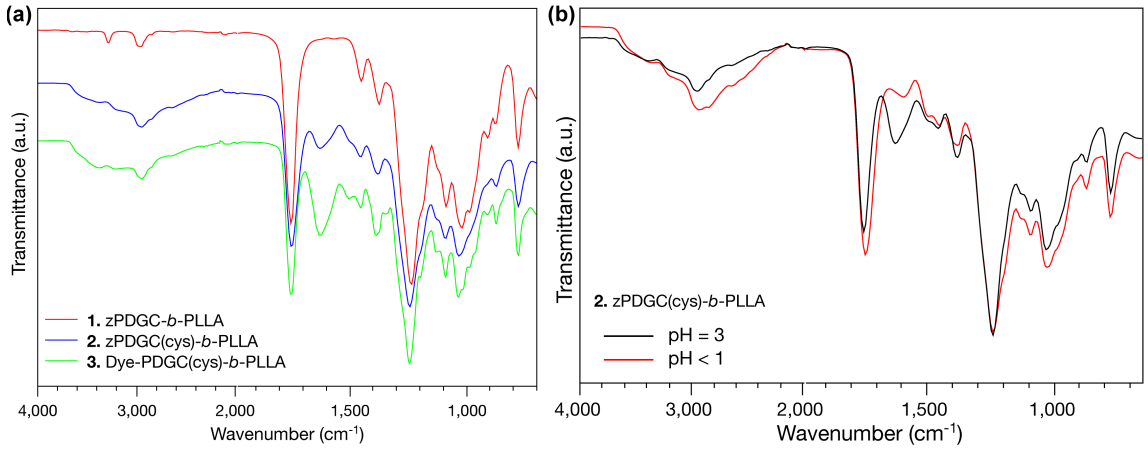

Figure V.7 FT-IR spectra of (a) polymers **1**, N_3-PDGC-*b*-PLLA, **2**, N_3-PDGC(cys)-*b*-PLLA, and **3**, dye-PDGC(cys)-*b*-PLLA; (b) polymer **2** powders prepared by lyophilization from solutions of pH = 3 and pH < 1.

The dye-functionalized polymers **3** were obtained by copper-free strain-promoted azide-alkyne cycloaddition of MB™ 488 DBCO with the azido group at the polymer chain-end. Polymer **2** and fluorescent dye MB™ 488 dibenzocyclooctyne (DBCO) were allowed to undergo reaction in a mixture of DMSO and H_2O (10:1) at room temperature, while wrapped with aluminum foil to avoid potential photobleaching. This chemistry would enable facile decoration of polymers **2** with dyes without UV irradiation, heat, or

applying metal catalysts,[214-215] thereby reducing potential toxicity caused by copper in traditional copper-catalyzed azide-alkyne cycloaddition, minimizing fluorescence quenching, and improving the cycloaddition reactivity. The appearance of resonances attributed to DBCO and dye protons in the aromatic region of 8.28-6.95 ppm indicated successful dye-polymer conjugation. Diffusion-ordered spectroscopic (DOSY-NMR) analysis of polymer **3** samples provided further evidence of the successful dye-polymer conjugation by showing the same diffusion efficiencies of the chain-end dye and polymer backbone protons at *ca.* 5×10^{-11} m^2/s, whereas free dye molecules in the presence of polymer (non-reactive chain end) displayed a different diffusion efficiency at *ca.* 4×10^{-10} m^2/s (**Figure V.8**). UV-Vis spectroscopy revealed a maximum absorption at 498 nm, and spectrophotometry of the dye-polymer conjugate showed an excitation maximum at 501 nm and emission maximum at 528 nm (**Figure V.9**).

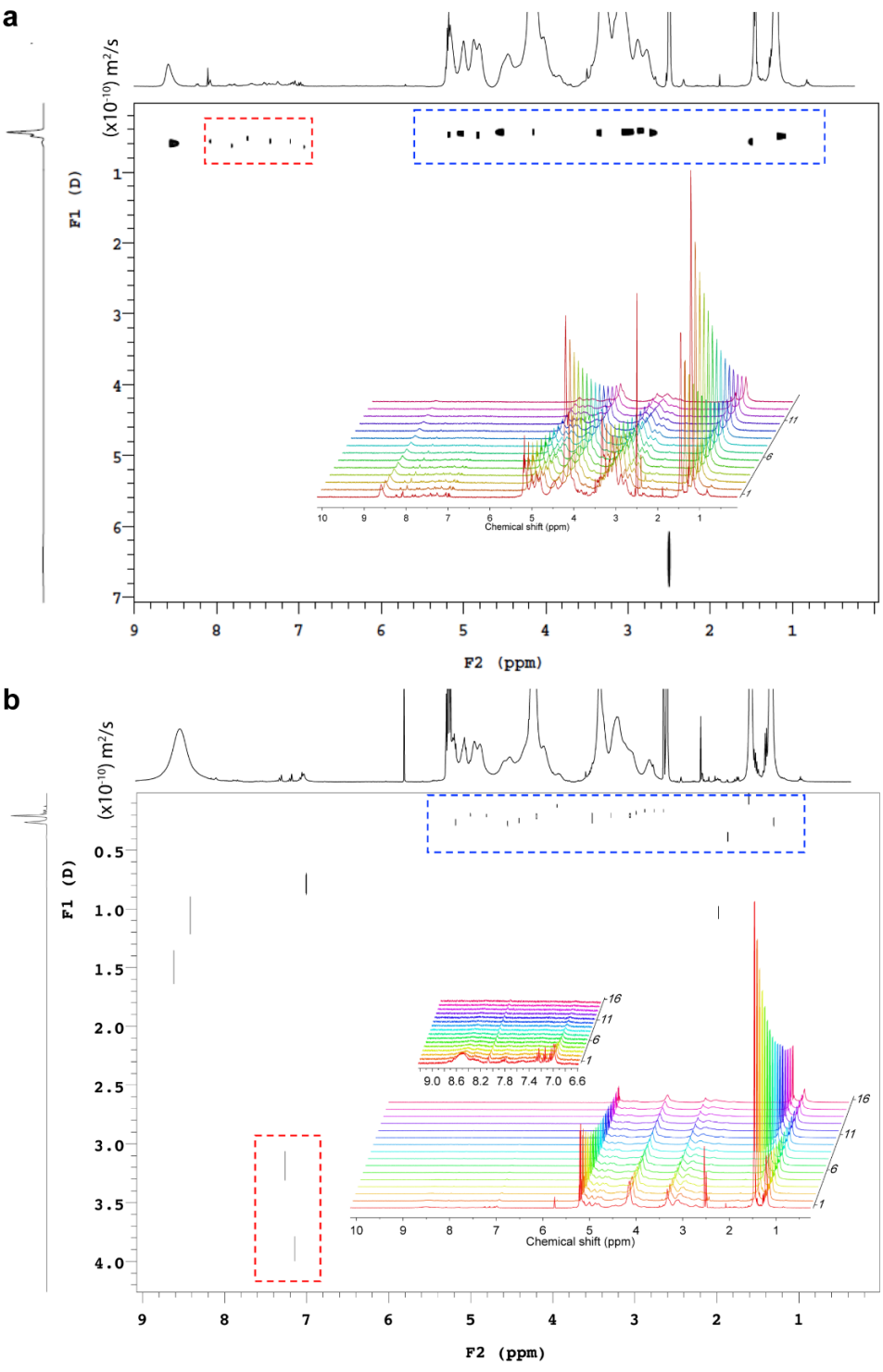

Figure V.8 DOSY NMR spectra (500 MHz, DMSO-d_6, TFA-*d*) of **a**, dye-polymer conjugate and **b**, dye and polymer mixture.

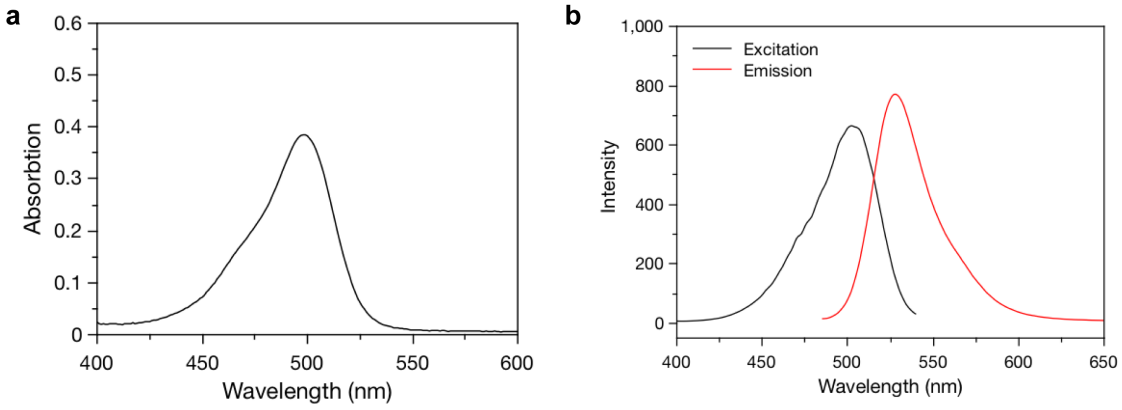

Figure V.9 **a**, UV-Vis spectrum (0.25 mg/mL in water) and **b**, Excitation and emission spectra ($\lambda_{ex,\,max}$ = 501 nm, $\lambda_{em,\,max}$ = 528 nm) of the dye-polymer conjugate.

Crystallization-driven Self-assembly (CDSA) into nanostructures with varied morphology. Self-assembly of the three polymer **3** samples was performed through CDSA,[161, 216-219] following previously described procedures,[48] to afford nanostructures of varied morphologies. Briefly, dispersions of dye-PDGC(cys)-*b*-PLLA in nanopure water (0.05 – 0.1 mg/mL) were allowed to undergo vortex, sonication, and then incubation at 65 °C for 30 h, followed by cooling to room temperature. Transmission electron microscopy (TEM) analysis (**Figure V.10**) of polymer **3** with hydrophilic-to-hydrophobic *DP* ratio at 70:18, 47:44, and 39:74 showed spheres (D_{av} = 11 ± 2 nm), cylinders (L_{av} = 220 ± 66 nm, D_{av} = 17 ± 4 nm), and platelet-like nanostructures (L_{av} = 620 ± 110 nm, W_{av} = 160 ± 35 nm), respectively. Polymers with the lowest PLLA content (*ca*. 6 *wt*%) yielded spherical micelles with measured diameters (*D*) of 6-14 nm. Elongated cylindrical nanostructures were obtained from polymers having PLLA contents of *ca.* 18 *wt*%, while the platelet-like nanostructures were formed by polymers with PLLA reaching *ca.* 30 *wt*% (m= 39, n = 74;

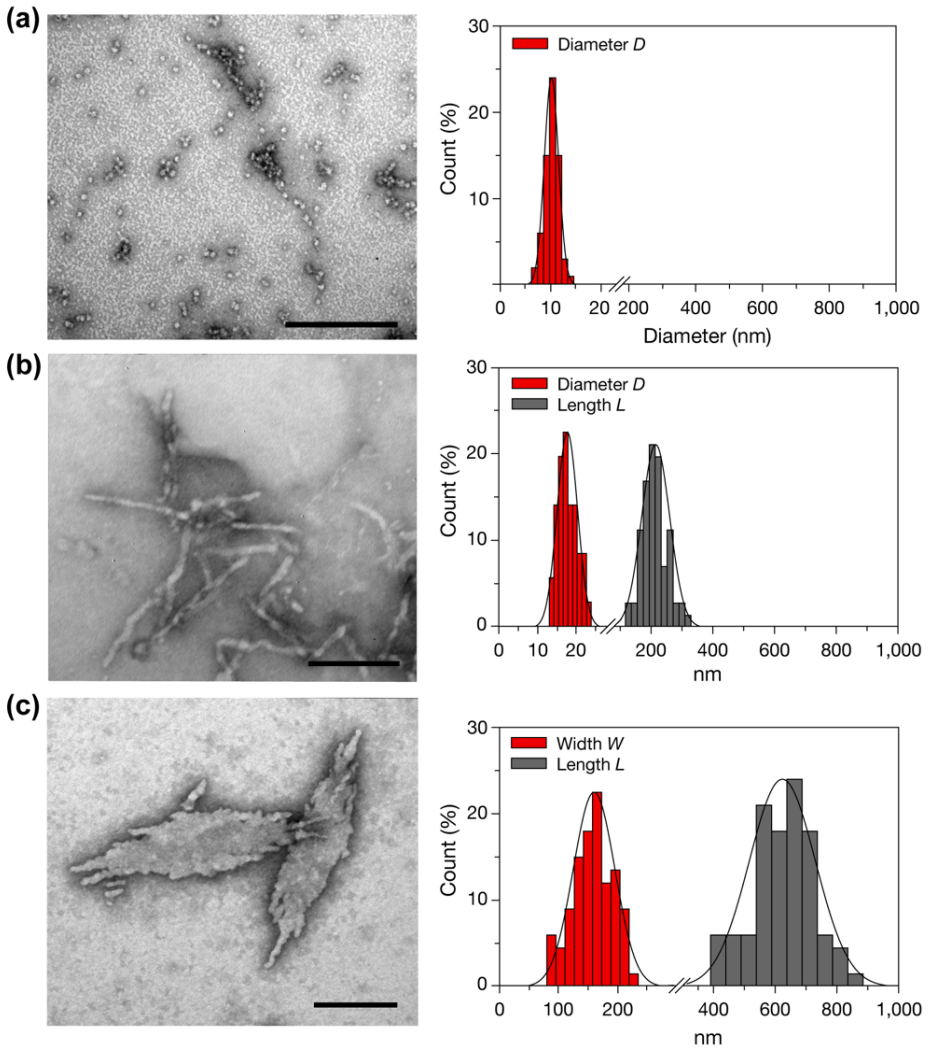

Figure V.10 Morphology characterization of nanostructures. TEM images (left) and histograms of nanostructure diameter/contour length/width distributions (right) crystallization-driven assembled from dye-containing block copolymers a, dye-PDGC(cys)$_{70}$-*b*-PLLA$_{18}$, b, dye-PDGC(cys)$_{47}$-*b*-PLLA$_{44}$, and c, dye-PDGC(cys)$_{39}$-*b*-PLLA$_{74}$ (scale bar, 200 nm).

1:2 of PDGC:PLLA). The cylindrical micelles had measured length (L) values from 150 – 350 nm, with D values of 13 – 24 nm. Platelet-like nanostructures (L = 400 – 900 nm) were found to be significantly longer than cylinders and exhibited widths (W) of 80 – 230

nm, revealing not only morphologic aspect ratio difference but also significant size differences between the cylinders and platelets. Additionally, only a small quantity of spherical nanoparticles was observed in cylinder and platelet samples by TEM (**Figure V.11**), indicating generally narrow-dispersed nanoparticle morphology within each sample, beneficial for studying the effects of morphology and size on performance. In total, these results demonstrated the feasibility of accessing diverse nanostructure morphologies of polymer **3** to enable investigation of nanostructure shape and dimension effects on uroepithelial binding and internalization.

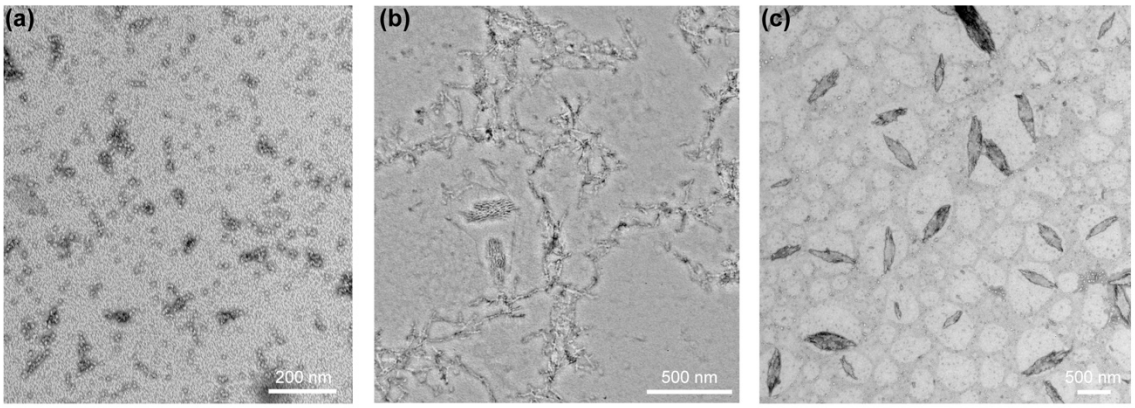

Figure V.11 TEM images of nanostructures assembled from (a) dye-PDGC(cys)$_{70}$-*b*-PLLA$_{18}$, (b) dye-PDGC(cys)$_{47}$-*b*-PLLA$_{44}$, and (c) dye-PDGC(cys)$_{39}$-*b*-PLLA$_{74}$.

Bladder epithelial cell binding and internalization. Flow cytometry and fluorescent confocal microscopy characterizations were carried out on the fluorescently labeled NPs derived from dye-PDGC(cys)$_{70}$-*b*-PLLA$_{18}$, dye-PDGC(cys)$_{47}$-*b*-PLLA$_{44}$, and

dye-PDGC$(cys)_{39}$-*b*-$PLLA_{74}$ to quantitatively determine their association with uroepithelial cells and visualize internalization, respectively. Cultured uroepithelial cells, either as sub-confluent adherent cells or in suspension, were treated with MB^{TM} 488-labeled NPs of various morphologies, using concentrations and exposure times established in our prior work.[202] Cellular association of the NPs was quantified by flow cytometry, and internalization was specified by confocal fluorescence microscopy after cell-surface staining with AlexaFluor 594-labeled wheat germ agglutinin (WGA). Shape-dependent differences in uroepithelial binding were observed using dilute (25 μg/mL polymer) suspensions of NPs. Specifically, treatment with NPs having the platelet morphology conferred the highest binding capacity, as reflected by both the proportion of cells bound (**Figure V.12a-b**) and the mean fluorescence intensity (*i.e.*, binding density; **Figure V.12c**). Furthermore, 3D-reconstructed z-stacks of confocal images were used to localize intracellular NPs, of which the platelet morphology was most often visualized (**Figure V.12d**). Of note, these methods did not permit precise enumeration of NPs attached to the cell surface *vs.* within the cells. Taken together, though, our results suggested that the enlarged and elongated dimensions offered by the platelet morphology confer improved and multivalent binding, favoring uroepithelial internalization despite their larger overall size.

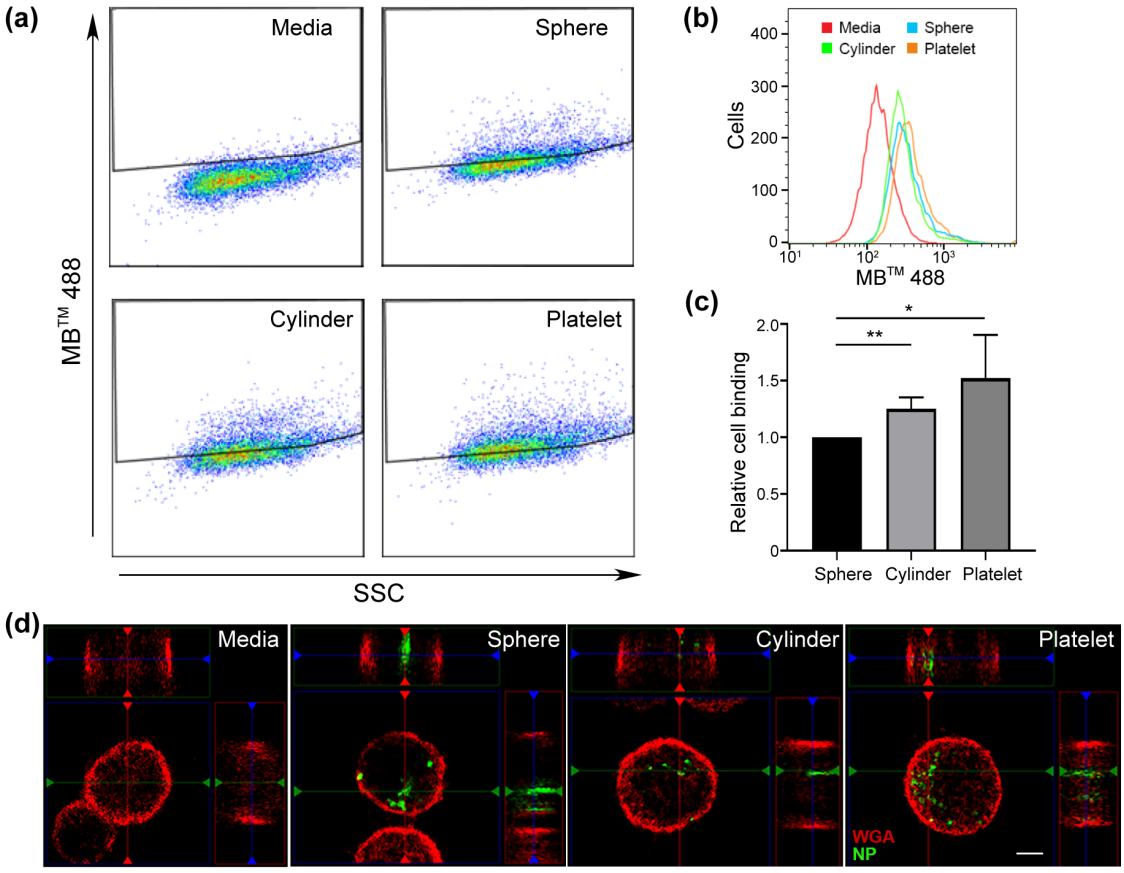

Figure V.12 Cell binding and internalization characterization. a, Flow cytometric analysis of cultured uroepithelial cells inoculated with MB™ 488-labeled PDGC(cys)-*b*-PLLA NPs having sphere, cylinder, or platelet morphologies. The proportions of cells bound/internalized with polymer NPs are shown. b, Histograms of fluorescence intensity of cells treated with NPs of varied morphologies. c, Binding efficiencies of NPs (sphere set to "1" as reference); cylinder and platelet were both statistically greater than sphere (*P<0.05 and **P<0.01). d, Confocal microscopy image with orthogonal projections showing multiple dye-labeled NPs internalized within uroepithelial cells (surfaces labeled with WGA 594); scale bar, 5 μm.

Evaluation of nanostructure toxicity. The affinity of polymer nanostructures to the epithelial cell surface could be mediated by interactions between nanostructure corona and cell-surface proteins. We therefore investigated their potential cytotoxicity, immunotoxicity, and cytokine adsorption activity, which are essential factors to consider for the development of materials in biomedical applications (**Figure V.13**). To gain further understanding of the effect of nanostructure morphology and whether their specific zwitterionic surface characteristics are beneficial in mitigating the nanostructure toxicity, measurements of these zwitterionic nanostructures were compared with spherical anionic (carboxylic acid-functionalized N_3-PDGC(COOH)-*b*-PLLA) and neutral (PEG-functionalized N_3-PDGC(PEG)-*b*-PLLA) nanoparticles. *In vitro* cytotoxicity was appraised by incubating nanostructures of different morphology and surface chemistry with cultured uroepithelial cells (5637; ATCC HTB-9). Three different morphologic zwitterionic NPs, as well as PEG-decorated neutral NPs, exhibited no observable cytotoxicity in uroepithelial cells over the tested concentration range (1.5-210 μg/mL), supporting the biocompatibility of these core-shell nanostructured polymeric micelles. In comparison, anionic NPs caused a reduction in cell viability at concentrations >60 μg/mL, consistent with previous results.[46]

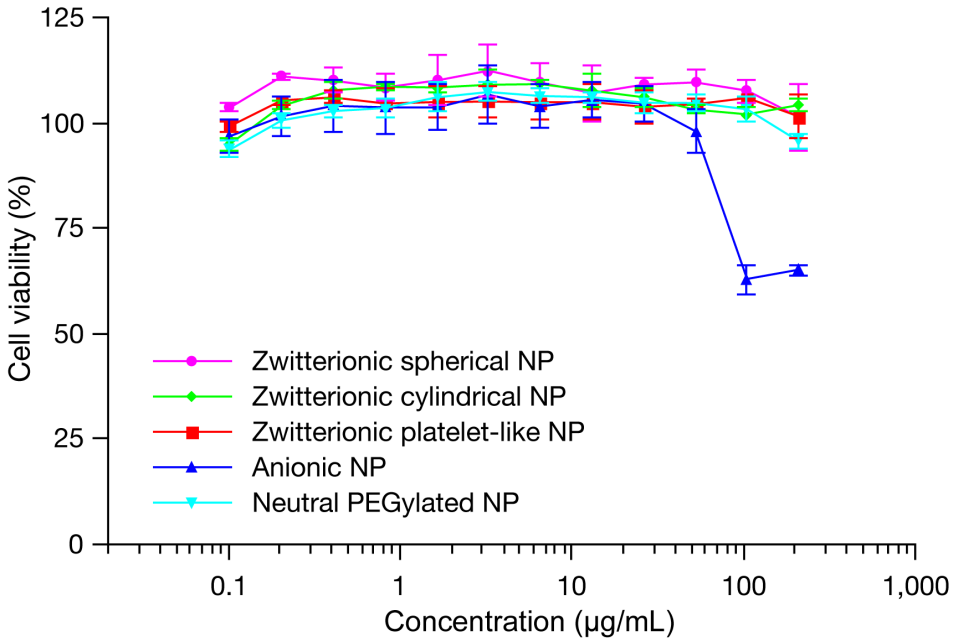

Figure V.13 Cytotoxicity assessment of zwitterionic nanostructures of different morphologies, in comparison with anionic and neutral polymer nanoparticles. Uroepithelial cell viabilities after treatment with polymer nanoparticles at concentrations ranging from 1.5-210 μg/mL for 72 h (triplicate experiments).

Immunotoxicity was evaluated by incubating RAW 264.7 mouse macrophages with various NP formulations for 24 h, then measuring the expression levels of 23 cytokines using a multiplex assay.[211] No significant overexpression of any of the tested cytokines was observed when compared to untreated cells (**Figure V.14a**). Independently, cytokine adsorption assay was performed by measuring the levels of 23 cytokine standards when premixed with polymer NPs of different morphologies and different surface chemistries (**Figure V.14b**), in comparison to the same biomarker concentrations in the absence of the test materials. This experiment was conducted for two purposes. First, cytokines may be adsorbed on surfaces and/or within internal regions of NPs, thereby

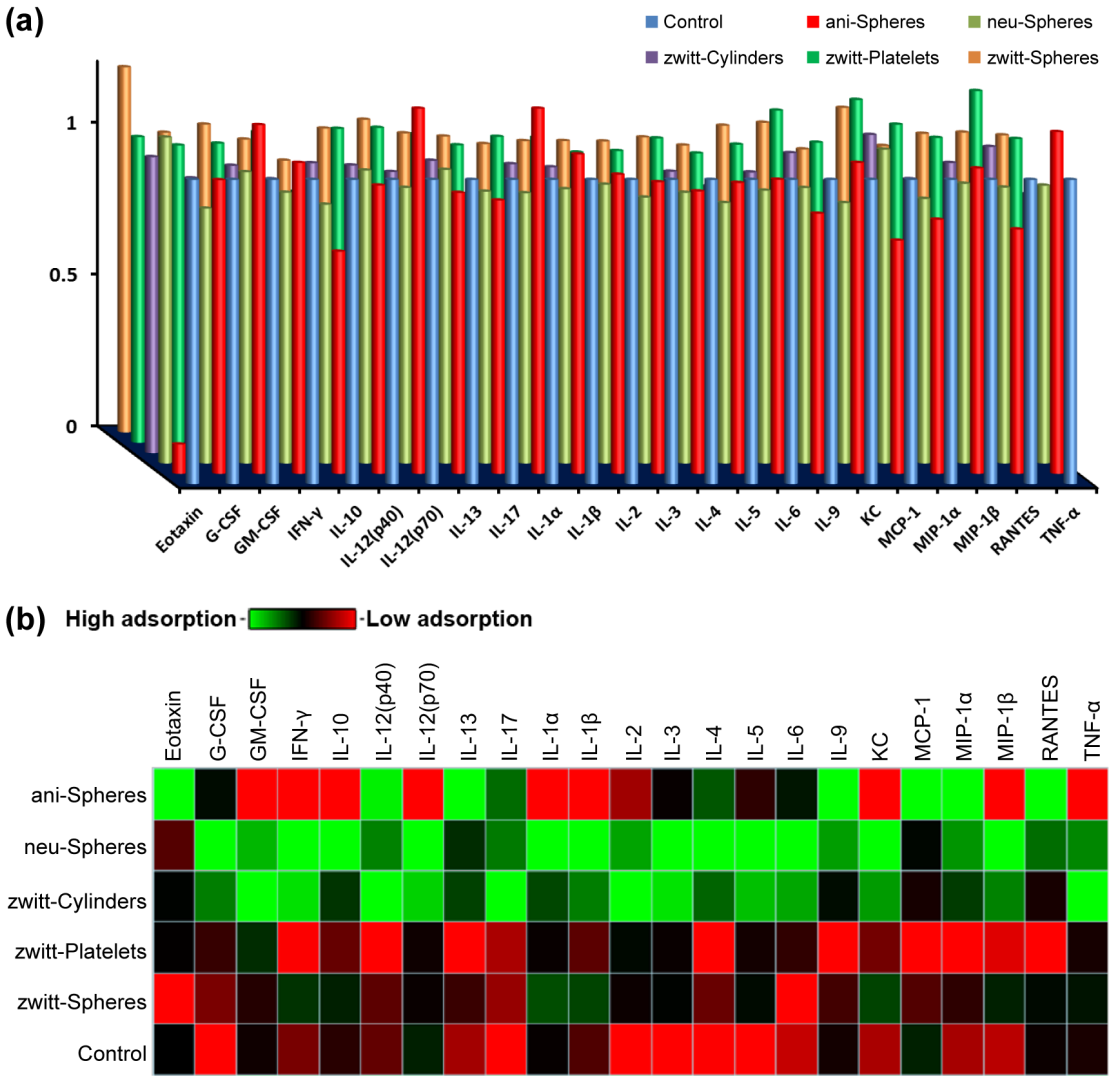

Figure V.14 Immunotoxicity and cytokine adsorption assessments of zwitterionic nanostructures of different morphologies, in comparison with anionic and neutral polymer nanoparticles. (a) Cytokine adsorption of different polymer nanoparticles was assessed by measuring the concentration of cytokines in supernatants after incubation of RAW cells, as compared to untreated samples. (b) Heat map for the cytokine adsorption assay showing the relative concentrations of various cytokines after incubation of cytokine standards with different polymer nanoparticles (control is cytokine standards without nanoparticles).

generating inaccurately low measurements of immunotoxic effect.[210-211] Second, the adsorption assay provides an indication of the adsorption of biomolecules (biofouling) onto the NPs. Spherical zwitterionic NPs showed much lower adsorption of cytokines compared to anionic and neutral NPs of the same spherical morphology. Among zwitterionic NPs of various morphologies, the least adsorption of the measured cytokines was observed with platelet-like NPs, while highest adsorption was observed for the zwitterionic cylindrical NPs. These results demonstrated that zwitterionic nanostructures have favorable anti-biofouling properties, supporting their viability as nanocarriers for biomedical delivery applications.[220-221] Opportunities exist for further study to understand the variations observed for levels of cytokine adsorption with different zwitterionic morphologies.

Preparation of silver-loaded nanostructures, silver release kinetics, and antibacterial activity. Silver cations were chosen as antibacterial cargo for their chemical compatibility, low propensity to elicit resistance,[222] and biocidal activity that does not require active bacterial replication or macromolecular synthesis. Encapsulation of silver into zwitterionic nanoparticles was achieved using silver acetate (40 *wt*%) *via* interactions with the cysteine carboxylate groups and dithioether moieties within the hydrophilic nanostructure corona. Total Ag loadings were 8-12 *wt*% and were generally independent of NP morphology, as determined by inductively coupled plasma mass spectrometry (ICP-MS) (**Figure V.15**). TEM revealed that the nanostructures retained their original morphologies after encapsulation of Ag (**Figure V.16**).

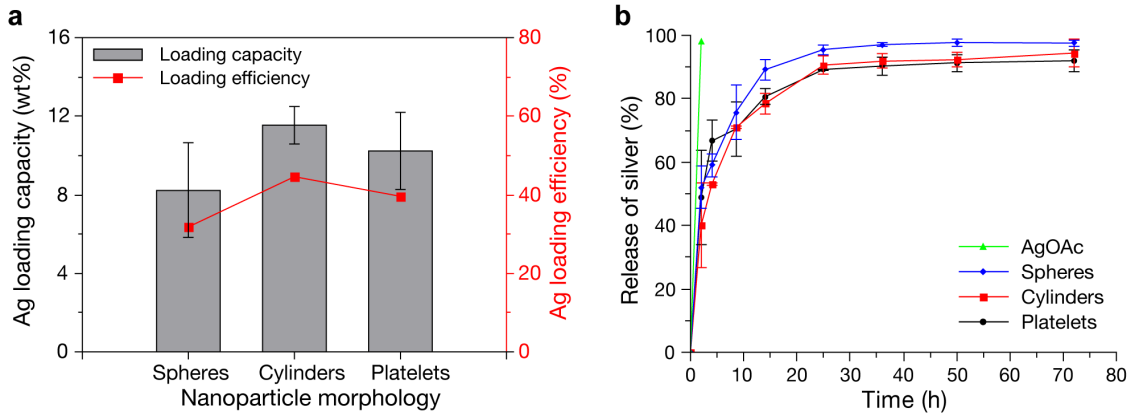

Figure V.15 Silver loading, release, and antimicrobial activity in nanostructures. **a**, Silver-loading capacities (wt%, left axis; bars) and efficiencies (%, right axis; lines and symbols) of AgOAc with 40 wt% feed. **b**, Release profiles of silver from dialysis cassettes containing solutions of silver-loaded NPs at 37 °C against phosphate buffer with 10 mM NaCl. Average values were calculated from triplicate experiments; error bars indicated the standard deviation.

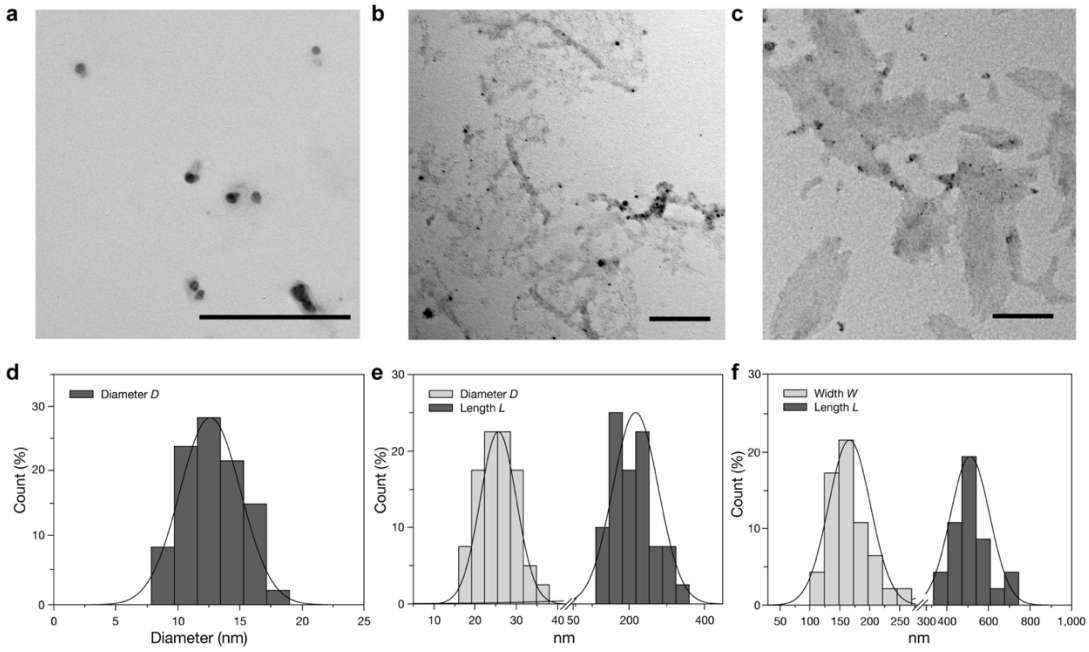

Figure V.16 TEM images (a, b, c) and histograms (d, e, f) of silver-bearing nanostructures of spherical (a, e; D_{av} = 13 ± 2 nm), cylindrical (b, e; L_{av} = 210 ± 60 nm, D_{av} = 25 ± 4 nm), and platelet-like (c, f; L_{av} = 515 ± 102 nm, W_{av} = 166 ± 35 nm) morphologies. No stain for TEM samples; scale bars, 200 nm.

Release of Ag from the nanostructures was determined by monitoring the decrease of [Ag] inside dialysis cassettes against 10 mM phosphate buffer with 10 mM NaCl (pH 7.4) at 37 °C, quantified by ICP-MS (**Figure V.15b**). As expected, compared to free unbound AgOAc, it was found that these zwitterionic nanostructures liberated silver in a sustained manner, with a release half-life ($t_{1/2}$) determined to be 3-5 h. Furthermore, the packaged silver cations were stable in aqueous solution for more than a week without visible precipitation, thus displaying colloidal stability needed for *in vitro* and *in vivo* applications. The release characteristics of these antimicrobial nanotherapeutics may be beneficial during local administration (*i.e.*, direct epithelial treatment).

The antimicrobial activity of Ag-loaded NPs was examined by measurement of minimum inhibitory concentrations (MICs) against two strains of *E. coli* (uropathogenic strain UTI89 and laboratory strain MG1655). The MICs of the silver-bearing NPs, expressed as μg/mL of Ag^+, were compared with silver acetate (**Table V.2**, averaged from n = 7 replicates). The silver-loaded NPs showed similar potencies against UTI89 and MG1655 as free silver acetate, with MICs ≤ 3.1 μg/mL, which were comparable to the values measured with earlier silver-bearing constructs (1-4 μg/mL Ag^+).[183, 223] The comparable antibacterial activities against *E. coli* indicated that the incorporated silver is available for antimicrobial activity, and demonstrated the suitability of using polymer nanostructure platforms for silver-based antimicrobial delivery.

Table V.2 MIC (μg/mL of Ag^+) of differently shaped silver-bearing micellar NPs (Ag@spheres, Ag@cylinders, and Ag@platelets), against *E. coli* strains.

Formulation		*E. coli* strains	
		UTI89	MG1655
Average MIC (μg/mL)	AgOAc*[183183]	2.1 ± 0.9	2.2 ± 1.1
	Ag@spherical NPs	3.1 ± 0.4	3.1 ± 0.4
	Ag@cylindrical NPs	1.7 ± 0.2	1.4 ± 0.3
	Ag@platelet NPs	2.1 ± 0.5	1.6 ± 0.2

*AgOAc MIC values from a prior study[183] are shown for comparison.

5.4 Conclusions

In summary, we have developed multifunctional polymer nanocarriers assembled from zwitterionic amphiphilic block copolymers and silver cation antimicrobials with high biocompatibility and morphology-dependent enhanced epithelial cell binding and internalization, thereby providing strategies to combat recurrent urinary tract infections. Well-defined natural product-based amphiphilic diblock copolymers of different hydrophilic-to-hydrophobic ratios were synthesized by sequential ROPs, followed by orthogonal "click" modifications to introduce zwitterionic hydrophilic moieties along the side chain and fluorescent dyes at the α-chain end. Well-defined nanostructures with tunable size and morphology were prepared *via* CDSA to afford spheres, cylinders, and platelets. The elongated cylindrical and platelet morphologies exhibited enhanced uroepithelial binding, and internalization was most evident with the platelet NPs. Cyto-

and immuno-toxicity assays both revealed negligible toxicities of the nanocarriers, confirming the biocompatibility of the zwitterionic assemblies. Silver cations as the antimicrobials were tested, and optimal loading capacities and sustained release profiles were attained. Inhibition of bacterial cell growth of the Ag-loaded NPs was demonstrated against two *E. coli* strains, confirming the availability of the incorporated silver for antimicrobial activity and comparable antimicrobial potencies as free Ag^{+}. Future directions include conjugation of *E. coli* adhesins ($FimH_A$) to the elongated nanostructures developed in this study, to enhance cell-particle interactions and cellular binding and internalization. This work emphasizes the use of multiple naturally-sourced building blocks to produce functional nanomaterials that have the potential to serve as therapeutic nanoscopic devices that then breakdown to regenerate the bioresorbable sugar, hydroxy acid and amino acid components. As such, this demonstration of the importance of morphology, in addition to composition, provides guidance on optimized nanocarrier design for the epithelial delivery of therapeutic agents.

5.5 Perspectives

Internalization of ~2 μm *E. coli* into the ~100 μm uroepithelial cells lining the bladder is known to occur *via* type 1 pilus adhesin domain ($FimH_A$; residues 1-160)-mediated bacterial attachment to mannose-decorated uroplakins that are assembled into 16-nm hexagonal arrays on the apical surfaces of uroepithelial cells. It is hypothesized that presentation of bacterial adhesin ligands on rod- or platelet-shaped NPs resembling

the aspect ratio of UPEC and capable of multivalent binding across uroplakin sites will facilitate targeted uroepithelial delivery of silver antimicrobials for eradication of these chronically-resident bacteria. Moreover, the direct uroepithelial administration approach proposed is anticipated to circumvent concerns of distribution, clearance, immunogenicity, and toxicity that accompany systemic NP administration. The *E.coli* reservoir eradication *in vivo* in mouse models of UTI by silver antimicrobials packaged within NPs equipped with $FimH_A$ is proposed, relative to treatments involving non-functionalized NPs or silver antimicrobials alone.

$FimH_A$-based targeting ligands to be conjugated to PGC(cys)-*b*-PLLA NPs can include the full-length $FimH_A$ domain (residues 1-160), a $FimH_A$ mutant with abrogated binding affinity (Q133K), and two small $FimH_A$-derived peptides conserved across UPEC $FimH_A$ mannose-binding pockets, namely RQTNNYNSDDF ($FimH_A$ residues 132-142) and CHNDYPETITD ($FimH_A$ residues 44-54).[224-225] These peptide sequences, with a cysteine residue added to the *N*-terminus of the former, will be prepared commercially, evaluated for their ability to bind mannose, and then attached to a heterobifunctional linker containing either an *N*-hydroxy succinimidyl (NHS) ester or a maleimide for reaction with the peptide *N*-terminus and DBCO with the polymer azides, as described in the aforementioned study. To avail $FimH_A$ cysteine for interaction with mannose, CHNDYPETITD will be coupled to DBCO containing an NHS ester, which reacts preferentially with amines over thiols.[226-227] Biolayer interferometry will be performed to gauge the ability of the peptides to bind mannose, employing conditions previously used to investigate FimH binding to mannose.[227] Since both peptide sequences are conserved

in the mannose binding pocket, these studies will be conducted for each peptide separately and together at a 1:1 ratio to inform the design of polymer NP surfaces. Relative to the full-length $FimH_A$, shorter peptides (if functional for binding mannose) are anticipated to allow flexibility in conjugation chemistries and ease of scaled-up production. Further, the smaller peptide sequences may enable higher surface coverage than is achieved with the full-length $FimH_A$, which may increase the probability and multivalence of mannose binding events. However, should the shorter peptides not bind mannose, we will proceed with NPs functionalized with the full $FimH_A$ domain, which we have already demonstrated to facilitate mannose-dependent binding to uroepithelial cells.[228]

In total, these studies promise the identification and development of optimized strategies for intravesical delivery of degradable NP-based agents to interrupt the cycle of recurrent UTI. The proposed work represents a significant step toward urgently needed strategies for treatment of common bacterial infections, which present an increasing threat due to rapidly spreading antibiotic resistance.

CHAPTER VI

CONCLUSIONS

Poly(D-glucose carbonate)s synthesized from natural resources, provides as a desirable alternative material for petrochemical-derived polymers, possessing synthetic feasibility, structural diversity, versatile functionality, and well-defined structures. This research dissertation discussed the fundamental studies and the application of biomedical nanocarrier of D-glucose-based polymers. Chapters II and III focused on the investigation of the chemical structure-dependent physicochemical property and polymerization regioselectivity. Chapters IV and V discussed the synthesis and preparation of multifunctional amphiphilic block copolymer-based nanoparticles of varied size and morphology, and potential applications of the nanoparticles in biological applications.

The fundamental aspects of PGCs were elucidated through the investigation of side-chain mediated polymer glass transition temperature and regioselectivity, as well as the effects of molar mass on the physicochemical property. Variation of T_g was studied as a function of the side-chain structure and molar mass for linear PGCs. A series of narrowly dispersed PGC homopolymers with nearly the same molar mass (15 – 16 kDa by SEC) were synthesized through ring-opening polymerization. A remarkable range of T_g values (38-125 °C), was accomplished with six different alkyloxycarbonyl side chains. The impact of molar mass on T_g was investigated for two series of polymers and discrete oligomers synthesized and fractionated with precise control over the degrees of polymerization. The T_g was found to be significantly influenced by a synergistic effect of

the flexibility and bulkiness of the repeating unit side chain, as well as the chain end relative free volume.

The structural details of the backbone regiochemistry for the PGCs were not explored sufficiently. Highly regioselective ROP was achieved using glucose carbonate monomers with carbonate-side-chains, whereas regioirregularity was observed for polymers having ether-type side-chain substituents. A comprehensive experimental and theoretical study was conducted to elucidate the mechanistic origins for the curious regiochemical differences in a series of PGCs, providing structural details for the ring-opening process. Unimers and dimers from ROP initiation and propagation processes, respectively, were isolated using chromatographic techniques and identified by a combination of 1D and 2D NMR analyses, and DFT calculations were carried out to understand the reactivity and regioselectivity of the reactions based on different monomer structures.

The utilization of functional PGC was studied as a building block for the construction of biocompatible silver-bearing multifunctional nanocarriers for bacterial infection treatment. Our synthetic polymeric nanoscopic scaffolds focus upon fully degradable and biocompatible cylindrical nanoparticles to enhance their cell binding and internalization, thereby providing effective treatment for recurrent bacterial infections. Herein, an antimicrobial delivery system with multi-functionality and optimized chemical compositions is presented. Polymer nanostructures of controlled morphology were constructed *via* CDSA method in aqueous solution. These nanoparticles exhibited negligible toxicity, while offering substantial silver loading capacity, extended-release,

and *in vitro* antimicrobial activity against uropathogenic *Escherichia coli*. In comparison to spherical analogs, cylindrical and platelet-like polymeric nanostructures engaged in significantly higher association (*i.e.* binding and internalization) with uroepithelial cells. This work establishes initial evidence of cylindrical and platelet-shaped nanostructures as versatile therapeutic carriers for bacterial infections.

To conclude, with straightforward chemical modifications, unique properties, and versatility of PGCs, fundamental understandings of the structure and property of novel PGCs was gained by studying the side-chain effects in the tuning of the polymer regioregularity and the glass transition temperature. Synthetic methodologies were also developed to control the size, shape, and composition of nanostructures and investigate their hierarchical assemblies. Furthermore, this research broadens the scope of self-assembly to functional, natural-product based degradable block copolymers, expands the types of discrete macromolecular nanoscale architectures that can be produced from the supramolecular assembly of programmed block copolymers. Finally, the well-defined and multifunctional polymers were successfully implemented as therapeutic nanomaterials aimed to address the increasing threats of bacterial infections by the development of biocompatible nanotherapeutics and the exciting findings of the influence of nanoparticle shape on epithelial cell interactions.

REFERENCES

(1) Yao, K.; Tang, C., Controlled Polymerization of Next-Generation Renewable Monomers and Beyond. *Macromolecules* **2013,** *46* (5), 1689-1712.

(2) Miller, S. A., Sustainable Polymers: Opportunities for the Next Decade. *ACS Macro Lett.* **2013,** *2* (6), 550-554.

(3) Holmberg, A. L.; Reno, K. H.; Wool, R. P.; Epps, T. H., 3rd, Biobased building blocks for the rational design of renewable block polymers. *Soft Matter* **2014,** *10* (38), 7405-24.

(4) Ragauskas, A. J.; Williams, C. K.; Davison, B. H.; Britovsek, G.; Cairney, J.; Eckert, C. A.; Frederick, W. J.; Hallett, J. P.; Leak, D. J.; Liotta, C. L.; Mielenz, J. R.; Murphy, R.; Templer, R.; Tschaplinski, T., The Path Forward for Biofuels and Biomaterials. *Science* **2006,** *311* (5760), 484-489.

(5) Williams, C. K.; Hillmyer, M. A., Polymers from renewable resources: A perspective for a special issue of polymer reviews. *Polym. Rev.* **2008,** *48* (1), 1-10.

(6) Gandini, A., Polymers from Renewable Resources: A Challenge for the Future of Macromolecular Materials. *Macromolecules* **2008,** *41* (24), 9491-9504.

(7) Mecking, S., Nature or petrochemistry?-biologically degradable materials. *Angew. Chem. Int. Ed. Engl.* **2004,** *43* (9), 1078-85.

(8) Zhu, Y.; Romain, C.; Williams, C. K., Sustainable polymers from renewable resources. *Nature* **2016,** *540* (7633), 354-362.

(9) Hillmyer, M. A.; Tolman, W. B., Aliphatic Polyester Block Polymers: Renewable, Degradable, and Sustainable. *Acc. Chem. Res.* **2014,** *47* (8), 2390-2396.

(10) Deming, T. J., Synthetic polypeptides for biomedical applications. *Prog. Polym. Sci.* **2007,** *32* (8), 858-875.

(11) Chen, W.; Meng, F. H.; Cheng, R.; Deng, C.; Feijen, J.; Zhong, Z. Y., Advanced drug and gene delivery systems based on functional biodegradable polycarbonates and copolymers. *J. Controlled Release* **2014,** *190*, 398-414.

(12) Wang, H. B.; Wang, Y.; Chen, Y. J.; Jin, Q.; Ji, J., A biomimic pH-sensitive polymeric prodrug based on polycarbonate for intracellular drug delivery. *Polym. Chem.* **2014,** *5* (3), 854-861.

(13) Kristufek, S. L.; Wacker, K. T.; Tsao, Y. T.; Su, L.; Wooley, K. L., Monomer design strategies to create natural product-based polymer materials. *Nat. Prod. Rep.* **2017,** *34* (4), 433-459.

(14) Pati, D.; Feng, X.; Hadjichristidis, N.; Gnanou, Y., Hydrophobic, Hydrophilic, and Amphiphilic Polyglycocarbonates with Linear and Macrocyclic Architectures from Bicyclic Glycocarbonates Derived from CO2 and Glucoside. *Macromolecules* **2017,** *50* (4), 1362-1370.

(15) Galbis, J. A.; García-Martín, M. d. G.; de Paz, M. V.; Galbis, E., Synthetic Polymers from Sugar-Based Monomers. *Chem. Rev.* **2016,** *116* (3), 1600-1636.

(16) Feng, X.; East, A. J.; Hammond, W. B.; Zhang, Y.; Jaffe, M., Overview of advances in sugar-based polymers. *Polym. Adv. Technol.* **2011,** *22* (1), 139-150.

(17) Rapi, Z.; Szolnoki, B.; Bakó, P.; Niedermann, P.; Toldy, A.; Bodzay, B.; Keglevich, G.; Marosi, G., Synthesis and characterization of biobased epoxy monomers derived from d-glucose. *Eur. Polym. J.* **2015,** *67*, 375-382.

(18) Desport, J. S.; Mantione, D.; Moreno, M.; Sardón, H.; Barandiaran, M. J.; Mecerreyes, D., Synthesis of three different galactose-based methacrylate monomers for the production of sugar-based polymers. *Carbohydr. Res.* **2016,** *432*, 50-54.

(19) López-Vidal, E. M.; Gregory, G. L.; Kociok-Köhn, G.; Buchard, A., Polymers from sugars and CS2: synthesis and ring-opening polymerisation of sulfur-containing monomers derived from 2-deoxy-d-ribose and d-xylose. *Polym. Chem.* **2018,** *9* (13), 1577-1582.

(20) Gregory, G. L.; Lopez-Vidal, E. M.; Buchard, A., Polymers from sugars: cyclic monomer synthesis, ring-opening polymerisation, material properties and applications. *Chem. Commun.* **2017,** *53* (14), 2198-2217.

(21) Xiao, R.; Zeng, J.; Grinstaff, M. W., Biologically Active Branched Polysaccharide Mimetics: Synthesis via Ring-Opening Polymerization of a Maltose-Based β-Lactam. *ACS Macro Lett.* **2018,** *7* (7), 772-777.

(22) Shearouse, W. C.; Lillie, L. M.; Reineke, T. M.; Tolman, W. B., Sustainable Polyesters Derived from Glucose and Castor Oil: Building Block Structure Impacts Properties. *ACS Macro Lett.* **2015,** *4* (3), 284-288.

(23) Mikami, K.; Lonnecker, A. T.; Gustafson, T. P.; Zinnel, N. F.; Pai, P. J.; Russell, D. H.; Wooley, K. L., Polycarbonates derived from glucose via an organocatalytic approach. *J. Am. Chem. Soc.* **2013,** *135* (18), 6826-9.

(24) McGuire, T. M.; López-Vidal, E. M.; Gregory, G. L.; Buchard, A., Synthesis of 5- to 8-membered cyclic carbonates from diols and CO2: A one-step, atmospheric pressure and ambient temperature procedure. *J. CO2 Util.* **2018,** *27*, 283-288.

(25) Gregory, G. L.; Kociok-Kohn, G.; Buchard, A., Polymers from sugars and CO2: ring-opening polymerisation and copolymerisation of cyclic carbonates derived from 2-deoxy-d-ribose. *Polym. Chem.* **2017,** *8* (13), 2093-2104.

(26) Gregory, G. L.; Jenisch, L. M.; Charles, B.; Kociok-Köhn, G.; Buchard, A., Polymers from Sugars and CO2: Synthesis and Polymerization of a d-Mannose-Based Cyclic Carbonate. *Macromolecules* **2016,** *49* (19), 7165-7169.

(27) Su, L.; Khan, S.; Fan, J. W.; Lin, Y. N.; Wang, H.; Gustafson, T. P.; Zhang, F. W.; Wooley, K. L., Functional sugar-based polymers and nanostructures comprised of degradable poly(D-glucose carbonate)s. *Polym. Chem.* **2017,** *8* (10), 1699-1707.

(28) Gustafson, T. P.; Lonnecker, A. T.; Heo, G. S.; Zhang, S.; Dove, A. P.; Wooley, K. L., Poly(D-glucose carbonate) Block Copolymers: A Platform for Natural Product-Based Nanomaterials with Solvothermatic Characteristics. *Biomacromolecules* **2013,** *14* (9), 3346-3353.

(29) Song, Y.; Ji, X.; Dong, M.; Li, R.; Lin, Y. N.; Wang, H.; Wooley, K. L., Advancing the Development of Highly-Functionalizable Glucose-Based Polycarbonates by Tuning of the Glass Transition Temperature. *J. Am. Chem. Soc.* **2018,** *140* (47), 16053-16057.

(30) Felder, S. E.; Redding, M. J.; Noel, A.; Grayson, S. M.; Wooley, K. L., Organocatalyzed ROP of a Glucopyranoside Derived Five-Membered Cyclic Carbonate. *Macromolecules* **2018,** *51* (5), 1787-1797.

(31) Osumi, S.; Felder, S. E.; Wang, H.; Lin, Y.-N.; Dong, M.; Wooley, K. L., Construction of nanostructures in aqueous solution from amphiphilic glucose-derived polycarbonates. *J. Polym. Sci., Part A: Polym. Chem.* **2019,** *57* (3), 432-440.

(32) Cheng, M.; Lobkovsky, E. B.; Coates, G. W., Catalytic Reactions Involving C1 Feedstocks: New High-Activity Zn(II)-Based Catalysts for the Alternating Copolymerization of Carbon Dioxide and Epoxides. *J. Am. Chem. Soc.* **1998,** *120* (42), 11018-11019.

(33) Cohen, C. T.; Chu, T.; Coates, G. W., Cobalt Catalysts for the Alternating Copolymerization of Propylene Oxide and Carbon Dioxide: Combining High Activity and Selectivity. *J. Am. Chem. Soc.* **2005,** *127* (31), 10869-10878.

(34) Darensbourg, D. J.; Yarbrough, J. C., Mechanistic Aspects of the Copolymerization Reaction of Carbon Dioxide and Epoxides, Using a Chiral Salen Chromium Chloride Catalyst. *J. Am. Chem. Soc.* **2002,** *124* (22), 6335-6342.

(35) Byrne, C. M.; Allen, S. D.; Lobkovsky, E. B.; Coates, G. W., Alternating Copolymerization of Limonene Oxide and Carbon Dioxide. *J. Am. Chem. Soc.* **2004,** *126* (37), 11404-11405.

(36) Wang, Y.; Darensbourg, D. J., Carbon dioxide-based functional polycarbonates: Metal catalyzed copolymerization of CO2 and epoxides. *Coord. Chem. Rev.* **2018,** *372*, 85-100.

(37) Dove, A. P., Organic Catalysis for Ring-Opening Polymerization. *ACS Macro Lett.* **2012,** *1* (12), 1409-1412.

(38) Kamber, N. E.; Jeong, W.; Waymouth, R. M.; Pratt, R. C.; Lohmeijer, B. G.; Hedrick, J. L., Organocatalytic ring-opening polymerization. *Chem. Rev.* **2007,** *107* (12), 5813-40.

(39) Simon, L.; Goodman, J. M., The mechanism of TBD-catalyzed ring-opening polymerization of cyclic esters. *J. Org. Chem.* **2007,** *72* (25), 9656-62.

(40) Thomas, C.; Bibal, B., Hydrogen-bonding organocatalysts for ring-opening polymerization. *Green Chem.* **2014,** *16* (4), 1687-1699.

(41) Dechy-Cabaret, O.; Martin-Vaca, B.; Bourissou, D., Controlled Ring-Opening Polymerization of Lactide and Glycolide. *Chem. Rev.* **2004,** *104* (12), 6147-6176.

(42) Lohmeijer, B. G. G.; Pratt, R. C.; Leibfarth, F.; Logan, J. W.; Long, D. A.; Dove, A. P.; Nederberg, F.; Choi, J.; Wade, C.; Waymouth, R. M.; Hedrick, J. L., Guanidine and Amidine Organocatalysts for Ring-Opening Polymerization of Cyclic Esters. *Macromolecules* **2006,** *39* (25), 8574-8583.

(43) Sanders, D. P.; Fukushima, K.; Coady, D. J.; Nelson, A.; Fujiwara, M.; Yasumoto, M.; Hedrick, J. L., A Simple and Efficient Synthesis of Functionalized Cyclic Carbonate Monomers Using a Versatile Pentafluorophenyl Ester Intermediate. *J. Am. Chem. Soc.* **2010,** *132* (42), 14724-14726.

(44) Tempelaar, S.; Mespouille, L.; Coulembier, O.; Dubois, P.; Dove, A. P., Synthesis and post-polymerisation modifications of aliphatic poly(carbonate)s prepared by ring-opening polymerisation. *Chem. Soc. Rev.* **2013,** *42* (3), 1312-1336.

(45) Iwasaki, Y.; Yamaguchi, E., Synthesis of well-defined thermoresponsive polyphosphoester macroinitiators using organocatalysts. *Macromolecules* **2010,** *43* (6), 2664-2666.

(46) Li, R.; Elsabahy, M.; Song, Y.; Wang, H.; Su, L.; Letteri, R. A.; Khan, S.; Heo, G. S.; Sun, G.; Liu, Y.; Wooley, K. L., Functional, Degradable Zwitterionic

Polyphosphoesters as Biocompatible Coating Materials for Metal Nanostructures. *Langmuir* **2019,** *35* (5), 1503-1512.

(47) Wang, H.; Dong, M.; Khan, S.; Su, L.; Li, R.; Song, Y.; Lin, Y.-N.; Kang, N.; Komatsu, C. H.; Elsabahy, M.; Wooley, K. L., Acid-Triggered Polymer Backbone Degradation and Disassembly to Achieve Release of Camptothecin from Functional Polyphosphoramidate Nanoparticles. *ACS Macro Lett.* **2018,** *7* (7), 783-788.

(48) Song, Y.; Chen, Y.; Su, L.; Li, R.; Letteri, R. A.; Wooley, K. L., Crystallization-driven assembly of fully degradable, natural product-based poly(L-lactide)-*block*-poly(α-D-glucose carbonate)s in aqueous solution. *Polymer* **2017,** *122*, 270-279.

(49) Gauthier, M. A.; Gibson, M. I.; Klok, H.-A., Synthesis of Functional Polymers by Post-Polymerization Modification. *Angew. Chem. Int. Ed.* **2009,** *48* (1), 48-58.

(50) Hall, D. J.; Van Den Berghe, H. M.; Dove, A. P., Synthesis and post-polymerization modification of maleimide-containing polymers by 'thiol-ene' click and Diels–Alder chemistries. *Polym. Int.* **2011,** *60* (8), 1149-1157.

(51) Easterling, C. P.; Kubo, T.; Orr, Zachary M.; Fanucci, G. E.; Sumerlin, B. S., Synthetic upcycling of polyacrylates through organocatalyzed post-polymerization modification. *Chem. Sci.* **2017,** *8* (11), 7705-7709.

(52) Kolb, H. C.; Finn, M. G.; Sharpless, K. B., Click Chemistry: Diverse Chemical Function from a Few Good Reactions. *Angew. Chem. Int. Ed. Engl.* **2001,** *40* (11), 2004-2021.

(53) Barner-Kowollik, C.; Du Prez, F. E.; Espeel, P.; Hawker, C. J.; Junkers, T.; Schlaad, H.; Van Camp, W., "Clicking" Polymers or Just Efficient Linking: What Is the Difference? *Angew. Chem. Int. Ed.* **2011,** *50* (1), 60-62.

(54) Meldal, M.; Tornøe, C. W., Cu-Catalyzed Azide−Alkyne Cycloaddition. *Chem. Rev.* **2008,** *108* (8), 2952-3015.

(55) Boren, B. C.; Narayan, S.; Rasmussen, L. K.; Zhang, L.; Zhao, H.; Lin, Z.; Jia, G.; Fokin, V. V., Ruthenium-Catalyzed Azide−Alkyne Cycloaddition: Scope and Mechanism. *J. Am. Chem. Soc.* **2008,** *130* (44), 14900-14900.

(56) Agard, N. J.; Prescher, J. A.; Bertozzi, C. R., A strain-promoted [3 + 2] azide-alkyne cycloaddition for covalent modification of biomolecules in living systems. *J. Am. Chem. Soc.* **2004,** *126* (46), 15046-7.

(57) Lowe, A. B., Thiol-ene "click" reactions and recent applications in polymer and materials synthesis. *Polym. Chem.* **2010,** *1* (1), 17-36.

(58) Lowe, A. B.; Hoyle, C. E.; Bowman, C. N., Thiol-yne click chemistry: A powerful and versatile methodology for materials synthesis. *J. Mater. Chem.* **2010,** *20* (23), 4745-4750.

(59) Lowe, A. B., Thiol-yne 'click'/coupling chemistry and recent applications in polymer and materials synthesis and modification. *Polymer* **2014,** *55* (22), 5517-5549.

(60) Nair, D. P.; Podgórski, M.; Chatani, S.; Gong, T.; Xi, W.; Fenoli, C. R.; Bowman, C. N., The Thiol-Michael Addition Click Reaction: A Powerful and Widely Used Tool in Materials Chemistry. *Chem. Mater.* **2014,** *26* (1), 724-744.

(61) Mather, B. D.; Viswanathan, K.; Miller, K. M.; Long, T. E., Michael addition reactions in macromolecular design for emerging technologies. *Prog. Polym. Sci.* **2006,** *31* (5), 487-531.

(62) Ulrich, S.; Boturyn, D.; Marra, A.; Renaudet, O.; Dumy, P., Oxime Ligation: A Chemoselective Click-Type Reaction for Accessing Multifunctional Biomolecular Constructs. *Chem. - Eur. J.* **2014,** *20* (1), 34-41.

(63) Collins, J.; Xiao, Z.; Müllner, M.; Connal, L. A., The emergence of oxime click chemistry and its utility in polymer science. *Polym. Chem.* **2016,** *7* (23), 3812-3826.

(64) Burmeister, D.; Ahrens, L.; Opitz, A.; Ligorio, G.; Hermerschmidt, F.; Jänsch, D.; Freudenberg, J.; Bunz, U. H. F.; Müllen, K.; List-Kratochvil, E. J. W., Utilizing Diels–Alder "click" chemistry to functionalize the organic–organic interface of semiconducting polymers. *J. Mater. Chem. C* **2020,** *8* (10), 3302-3307.

(65) Zhang, Y.; Chen, G.; Lin, Y.; Zhao, L.; Yuan, W. Z.; Lu, P.; Jim, C. K. W.; Zhang, Y.; Tang, B. Z., Thiol–bromo click polymerization for multifunctional polymers: synthesis, light refraction, aggregation-induced emission and explosive detection. *Polym. Chem.* **2015,** *6* (1), 97-105.

(66) Ashok Kothapalli, V.; Shetty, M.; de los Santos, C.; Hobbs, C. E., Thio-bromo "Click," post-polymerization strategy for functionalizing ring opening metathesis polymerization (ROMP)-derived materials. *J. Polym. Sci., Part A: Polym. Chem.* **2016,** *54* (1), 179-185.

(67) Chen, S.; Ströhl, D.; Binder, W. H., Orthogonal Modification of Polymers via Thio–Bromo "Click" Reaction and Supramolecular Chemistry: An Easy Method Toward Head-to-Tail Self-Assembled Supramolecular Polymers. *ACS Macro Lett.* **2015,** *4* (1), 48-52.

(68) Stuparu, M. C.; Khan, A., Thiol-epoxy "click" chemistry: Application in preparation and postpolymerization modification of polymers. *J. Polym. Sci., Part A: Polym. Chem.* **2016,** *54* (19), 3057-3070.

(69) Stuparu, M. C.; Khan, A., CHAPTER 6 Thiol-epoxy and Amine-epoxy 'Click' Polymerizations. In *Click Polymerization*, The Royal Society of Chemistry: 2018; pp 191-206.

(70) Mauri, M.; Tran, N.; Prieto, O.; Hjertberg, T.; Müller, C., Crosslinking of an ethylene-glycidyl methacrylate copolymer with amine click chemistry. *Polymer* **2017,** *111*, 27-35.

(71) Blanazs, A.; Armes, S. P.; Ryan, A. J., Self-Assembled Block Copolymer Aggregates: From Micelles to Vesicles and their Biological Applications. *Macromol. Rapid Commun.* **2009,** *30* (4-5), 267-277.

(72) Savić, R.; Eisenberg, A.; Maysinger, D., Block copolymer micelles as delivery vehicles of hydrophobic drugs: micelle–cell interactions. *J. Drug Targeting* **2006,** *14* (6), 343-355.

(73) Rösler, A.; Vandermeulen, G. W.; Klok, H.-A., Advanced drug delivery devices via self-assembly of amphiphilic block copolymers. *Adv. Drug Delivery Rev.* **2012,** *64*, 270-279.

(74) Tian, H. Y.; Tang, Z. H.; Zhuang, X. L.; Chen, X. S.; Jing, X. B., Biodegradable synthetic polymers: Preparation, functionalization and biomedical application. *Prog. Polym. Sci.* **2012,** *37* (2), 237-280.

(75) Ge, Z.; Liu, S., Functional block copolymer assemblies responsive to tumor and intracellular microenvironments for site-specific drug delivery and enhanced imaging performance. *Chem. Soc. Rev.* **2013,** *42* (17), 7289-325.

(76) Kumari, A.; Yadav, S. K.; Yadav, S. C., Biodegradable polymeric nanoparticles based drug delivery systems. *Colloids Surf., B* **2010,** *75* (1), 1-18.

(77) Kutikov, A. B.; Song, J., Biodegradable PEG-Based Amphiphilic Block Copolymers for Tissue Engineering Applications. *ACS Biomater. Sci. Eng.* **2015,** *1* (7), 463-480.

(78) Fan, J.; Zou, J.; He, X.; Zhang, F.; Zhang, S.; Raymond, J. E.; Wooley, K. L., Tunable mechano-responsive organogels by ring-opening copolymerizations of N-carboxyanhydrides. *Chem. Sci.* **2014,** *5* (2), 141-150.

(79) Lowe, A. B.; McCormick, C. L., Synthesis and solution properties of zwitterionic polymers. *Chem. Rev.* **2002,** *102* (11), 4177-89.

(80) Laschewsky, A., Structures and Synthesis of Zwitterionic Polymers. *Polymers* **2014,** *6* (5), 1544-1601.

(81) Maikawa, C. L.; Sevit, A.; Lin, B.; Wallstrom, R. J.; Mann, J. L.; Yu, A. C.; Waymouth, R. M.; Appel, E. A., Block copolymer composition drives function of self-assembled nanoparticles for delivery of small-molecule cargo. *J. Polym. Sci., Part A: Polym. Chem.* **2019,** *57* (12), 1322-1332.

(82) Alexandridis, P.; Lindman, B., *Amphiphilic block copolymers: self-assembly and applications*. Elsevier: 2000.

(83) Wang, X.; Guerin, G.; Wang, H.; Wang, Y.; Manners, I.; Winnik, M. A., Cylindrical Block Copolymer Micelles and Co-Micelles of Controlled Length and Architecture. *Science* **2007,** *317* (5838), 644-647.

(84) Liu, Y. F.; Abetz, V.; Muller, A. H. E., Janus cylinders. *Macromolecules* **2003,** *36* (21), 7894-7898.

(85) Cui, H.; Chen, Z.; Zhong, S.; Wooley, K. L.; Pochan, D. J., Block Copolymer Assembly via Kinetic Control. *Science* **2007,** *317* (5838), 647-650.

(86) Li, Z.; Hillmyer, M. A.; Lodge, T. P., Laterally nanostructured vesicles, polygonal bilayer sheets, and segmented wormlike micelles. *Nano Lett.* **2006,** *6* (6), 1245-9.

(87) Stoenescu, R.; Graff, A.; Meier, W., Asymmetric ABC-triblock copolymer membranes induce a directed insertion of membrane proteins. *Macromol. Biosci.* **2004,** *4* (10), 930-5.

(88) Crassous, J. J.; Schurtenberger, P.; Ballauff, M.; Mihut, A. M., Design of block copolymer micelles via crystallization. *Polymer* **2015,** *62*, A1-A13.

(89) Hudson, Z. M.; Boott, C. E.; Robinson, M. E.; Rupar, P. A.; Winnik, M. A.; Manners, I., Tailored hierarchical micelle architectures using living crystallization-driven self-assembly in two dimensions. *Nat. Chem.* **2014,** *6* (10), 893-898.

(90) Petzetakis, N.; Dove, A. P.; O'Reilly, R. K., Cylindrical micelles from the living crystallization-driven self-assembly of poly(lactide)-containing block copolymers. *Chem. Sci.* **2011,** *2* (5), 955-960.

(91) Elsabahy, M.; Wooley, K. L., Design of polymeric nanoparticles for biomedical delivery applications. *Chem. Soc. Rev.* **2012,** *41* (7), 2545-2561.

(92) Hauert, S.; Bhatia, S. N., Mechanisms of cooperation in cancer nanomedicine: towards systems nanotechnology. *Trends Biotechnol.* **2014,** *32* (9), 448-455.

(93) Sommerfeld, S. D.; Zhang, Z.; Costache, M. C.; Vega, S. L.; Kohn, J., Enzymatic Surface Erosion of High Tensile Strength Polycarbonates Based on Natural Phenols. *Biomacromolecules* **2014,** *15* (3), 830-836.

(94) Galbis, J. A.; García-Martín, M. d. G.; de Paz, M. V.; Galbis, E., Synthetic polymers from sugar-based monomers. *Chem. Rev.* **2015,** *116* (3), 1600-1636.

(95) Kristufek, S. L.; Wacker, K. T.; Tsao, Y.-Y. T.; Su, L.; Wooley, K. L., Monomer design strategies to create natural product-based polymer materials. *Nat. Prod. Rep.* **2017,** *34* (4), 433-459.

(96) Mikami, K.; Lonnecker, A. T.; Gustafson, T. P.; Zinnel, N. F.; Pai, P.-J.; Russell, D. H.; Wooley, K. L., Polycarbonates derived from glucose *via* an organocatalytic approach. *J. Am. Chem. Soc.* **2013,** *135* (18), 6826-6829.

(97) Lee, N. S.; Lin, L. Y.; Neumann, W. L.; Freskos, J. N.; Karwa, A.; Shieh, J. J.; Dorshow, R. B.; Wooley, K. L., Influence of nanostructure morphology on host capacity and kinetics of guest release. *Small* **2011,** *7* (14), 1998-2003.

(98) Yang, K.; Ma, Y.-Q., Computer simulation of the translocation of nanoparticles with different shapes across a lipid bilayer. *Nat Nano* **2010,** *5* (8), 579-583.

(99) Gratton, S. E.; Ropp, P. A.; Pohlhaus, P. D.; Luft, J. C.; Madden, V. J.; Napier, M. E.; DeSimone, J. M., The effect of particle design on cellular internalization pathways. *Proc. Natl. Acad. Sci. U. S. A.* **2008,** *105* (33), 11613-11618.

(100) Galbis, J.; García-Martín, M., Sugars as monomers. In *Monomers, polymers and composites from renewable resources*, Elsevier: 2008; pp 89-114.

(101) Dane, E. L.; Grinstaff, M. W., Poly-amido-saccharides: Synthesis via Anionic Polymerization of a β-Lactam Sugar Monomer. *J. Am. Chem. Soc.* **2012,** *134* (39), 16255-16264.

(102) Su, L.; Li, R.; Khan, S.; Clanton, R.; Zhang, F.; Lin, Y.-N.; Song, Y.; Wang, H.; Fan, J.; Hernandez, S.; Butters, A. S.; Akabani, G.; MacLoughlin, R.; Smolen, J.; Wooley, K. L., Chemical Design of Both a Glutathione-Sensitive Dimeric Drug Guest and a Glucose-Derived Nanocarrier Host to Achieve Enhanced Osteosarcoma Lung Metastatic Anticancer Selectivity. *J. Am. Chem. Soc.* **2018,** *140* (4), 1438-1446.

(103) Tee, B. C. K.; Wang, C.; Allen, R.; Bao, Z., An electrically and mechanically self-healing composite with pressure- and flexion-sensitive properties for electronic skin applications. *Nat. Nanotechnol.* **2012,** *7*, 825.

(104) Siepmann, J.; Peppas, N. A., Modeling of drug release from delivery systems based on hydroxypropyl methylcellulose (HPMC). *Adv. Drug Delivery Rev.* **2012,** *64*, 163-174.

(105) Yang, J.; Webb, A. R.; Pickerill, S. J.; Hageman, G.; Ameer, G. A., Synthesis and evaluation of poly(diol citrate) biodegradable elastomers. *Biomaterials* **2006,** *27* (9), 1889-1898.

(106) Fox, T. G.; Loshaek, S., Influence of molecular weight and degree of crosslinking on the specific volume and glass temperature of polymers. *Journal of Polymer Science* **1955,** *15* (80), 371-390.

(107) Liu, T.; Geng, X.; Nie, Y.; Chen, R.; Meng, Y.; Li, X., Hyperbranched polyethers with tunable glass transition temperature: controlled synthesis and mixing rules. *RSC Advances* **2014,** *4* (57), 30250-30258.

(108) Shi, Y.; Cao, X.; Luo, S.; Wang, X.; Graff, R. W.; Hu, D.; Guo, R.; Gao, H., Investigate the Glass Transition Temperature of Hyperbranched Copolymers with Segmented Monomer Sequence. *Macromolecules* **2016,** *49* (12), 4416-4422.

(109) Balizer, E.; Duffy, J. V., The effects of steric hindrance on sub-glass transitions in epoxy polymers. *Polymer* **1992,** *33* (10), 2114-2122.

(110) Liu, P.; Tan, Q.; Xiang, L.; Zhang, H., Steric hindrance effect on thermo‐responsive behaviors of well‐defined water‐soluble semi‐rigid polymers. *J. Polym. Sci., Part A: Polym. Chem.* **2013,** *51* (16), 3429-3438.

(111) Thorat, S. D.; Phillips, P. J.; Semenov, V.; Gakh, A., Physical properties of aliphatic polycarbonates made from CO_2 and epoxides. *J. Appl. Polym. Sci.* **2003,** *89* (5), 1163-1176.

(112) Wooley, K.; Hawker, C.; Pochan, J.; Frechet, J., Physical properties of dendritic macromolecules: a study of glass transition temperature. *Macromolecules* **1993,** *26* (7), 1514-1519.

(113) Kwei, T. K., The effect of hydrogen bonding on the glass transition temperatures of polymer mixtures. *Journal of Polymer Science: Polymer Letters Edition* **1984,** *22* (6), 307-313.

(114) Nielsen, L. E., Cross-linking–effect on physical properties of polymers. *Journal of Macromolecular Science, Part C* **1969,** *3* (1), 69-103.

(115) Nadgorny, M.; Gentekos, D. T.; Xiao, Z.; Singleton, S. P.; Fors, B. P.; Connal, L. A., Manipulation of Molecular Weight Distribution Shape as a New Strategy to Control Processing Parameters. *Macromol. Rapid Commun.* **2017,** *38* (19), 1700352.

(116) Rogers, S.; Mandelkern, L., Glass transitions of the poly-(*n*-alkyl methacrylates). *J. Phys. Chem.* **1957,** *61* (7), 985-991.

(117) Lavilla, C.; Alla, A.; De Ilarduya, A. M.; Benito, E.; García‐Martín, M. d. G.; Galbis, J.; Muñoz‐Guerra, S., Carbohydrate‐based copolyesters made from bicyclic acetalized galactaric acid. *J. Polym. Sci., Part A: Polym. Chem.* **2012,** *50* (8), 1591-1604.

(118) Lavilla, C.; Alla, A.; Martínez de Ilarduya, A.; Muñoz-Guerra, S. n., High T_g bio-based aliphatic polyesters from bicyclic D-mannitol. *Biomacromolecules* **2013,** *14* (3), 781-793.

(119) Besse, V.; Auvergne, R.; Carlotti, S.; Boutevin, G.; Otazaghine, B.; Caillol, S.; Pascault, J.-P.; Boutevin, B., Synthesis of isosorbide based polyurethanes: An isocyanate free method. *React. Funct. Polym.* **2013,** *73* (3), 588-594.

(120) Lonnecker, A. T.; Lim, Y. H.; Felder, S. E.; Besset, C. l. J.; Wooley, K. L., Four different regioisomeric polycarbonates derived from one natural product, D-glucose. *Macromolecules* **2016,** *49* (20), 7857-7867.

(121) Kempe, K.; Jacobs, S.; Lambermont-Thijs, H. M. L.; Fijten, M. M. W. M.; Hoogenboom, R.; Schubert, U. S., Rational Design of an Amorphous Poly(2-oxazoline) with a Low Glass-Transition Temperature: Monomer Synthesis, Copolymerization, and Properties. *Macromolecules* **2010,** *43* (9), 4098-4104.

(122) Beck, K. R.; Korsmeyer, R.; Kunz, R. J., An overview of the glass transition temperature of synthetic polymers. *J. Chem. Educ.* **1984,** *61* (8), 668.

(123) Lawrence, J.; Lee, S.-H.; Abdilla, A.; Nothling, M. D.; Ren, J. M.; Knight, A. S.; Fleischmann, C.; Li, Y.; Abrams, A. S.; Schmidt, B. V. K. J.; Hawker, M. C.; Connal, L. A.; McGrath, A. J.; Clark, P. G.; Gutekunst, W. R.; Hawker, C. J., A Versatile and Scalable Strategy to Discrete Oligomers. *J. Am. Chem. Soc.* **2016,** *138* (19), 6306-6310.

(124) Fox Jr, T. G.; Flory, P. J., Second‐order transition temperatures and related properties of polystyrene. I. Influence of molecular weight. *J. Appl. Phys.* **1950,** *21* (6), 581-591.

(125) Xie, Y.; Peng, C.; Gao, Y.; Liu, X.; Liu, T.; Joy, A., Mannose-based graft polyesters with tunable binding affinity to concanavalin A. *J. Polym. Sci., Part A: Polym. Chem.* **2017,** *55* (23), 3908-3917.

(126) Xiao, R.; Grinstaff, M. W., Chemical synthesis of polysaccharides and polysaccharide mimetics. *Prog. Polym. Sci.* **2017,** *74*, 78-116.

(127) Sopeña, S.; Laserna, V.; Guo, W.; Martin, E.; Escudero-Adán, E. C.; Kleij, A. W., Regioselective Organocatalytic Formation of Carbamates from Substituted Cyclic Carbonates. *Adv. Synth. Catal.* **2016,** *358* (13), 2172-2178.

(128) Uryu, T.; Koyama, Y.; Matsuzaki, K., Selective ring-opening polymerization of 3,5-anhydro-1,2-O-isopropylidene- α -D-xylofuranose synthesis of [3→5]-D-xylan. *Makromol. Chem.* **1984,** *185* (10), 2099-2107.

(129) Shen, Y. Q.; Chen, X. H.; Gross, R. A., Polycarbonates from sugars: Ring-opening polymerization of 1,2-O-isopropylidene-D-xylofuranose-3,5-cyclic carbonate (IPXTC). *Macromolecules* **1999,** *32* (8), 2799-2802.

(130) Frisch, M. J.; Trucks, G. W.; Schlegel, H. B.; Scuseria, G. E.; Robb, M. A.; Cheeseman, J. R.; Scalmani, G.; Barone, V.; Petersson, G. A.; Nakatsuji, H.; Li, X.; Caricato, M.; Marenich, A. V.; Bloino, J.; Janesko, B. G.; Gomperts, R.; Mennucci, B.; Hratchian, H. P.; Ortiz, J. V.; Izmaylov, A. F.; Sonnenberg, J. L.; Williams; Ding, F.; Lipparini, F.; Egidi, F.; Goings, J.; Peng, B.; Petrone, A.; Henderson, T.; Ranasinghe, D.; Zakrzewski, V. G.; Gao, J.; Rega, N.; Zheng, G.; Liang, W.; Hada, M.; Ehara, M.; Toyota, K.; Fukuda, R.; Hasegawa, J.; Ishida, M.; Nakajima, T.; Honda, Y.; Kitao, O.; Nakai, H.; Vreven, T.; Throssell, K.; Montgomery Jr., J. A.; Peralta, J. E.; Ogliaro, F.; Bearpark, M. J.; Heyd, J. J.; Brothers, E. N.; Kudin, K. N.; Staroverov, V. N.; Keith, T. A.; Kobayashi, R.; Normand, J.; Raghavachari, K.; Rendell, A. P.; Burant, J. C.; Iyengar, S. S.; Tomasi, J.; Cossi, M.; Millam, J. M.; Klene, M.; Adamo, C.; Cammi, R.; Ochterski, J. W.; Martin, R. L.; Morokuma, K.; Farkas, O.; Foresman, J. B.; Fox, D. J. *Gaussian 16 Rev. C.01*, Wallingford, CT, 2016.

(131) Chai, J.-D.; Head-Gordon, M., Long-range corrected hybrid density functionals with damped atom–atom dispersion corrections. *Phys. Chem. Chem. Phys.* **2008,** *10* (44), 6615-6620.

(132) Ditchfield, R.; Hehre, W. J.; Pople, J. A., Self‐consistent molecular‐orbital methods. IX. An extended Gaussian‐type basis for molecular‐orbital studies of organic molecules. *J. Chem. Phys.* **1971,** *54* (2), 724-728.

(133) Barone, V.; Cossi, M., Quantum Calculation of Molecular Energies and Energy Gradients in Solution by a Conductor Solvent Model. *J. Phys. Chem. A* **1998,** *102* (11), 1995-2001.

(134) Cossi, M.; Rega, N.; Scalmani, G.; Barone, V., Energies, structures, and electronic properties of molecules in solution with the C-PCM solvation model. *J. Comput. Chem.* **2003,** *24* (6), 669-681.

(135) Simon, L.; Goodman, J. M., The mechanism of TBD-catalyzed ring-opening polymerization of cyclic esters. *J. Org. Chem.* **2007,** *72* (25), 9656-9662.

(136) Chuma, A.; Horn, H. W.; Swope, W. C.; Pratt, R. C.; Zhang, L.; Lohmeijer, B. G. G.; Wade, C. G.; Waymouth, R. M.; Hedrick, J. L.; Rice, J. E., The Reaction Mechanism for the Organocatalytic Ring-Opening Polymerization of l-Lactide Using a Guanidine-

Based Catalyst: Hydrogen-Bonded or Covalently Bound? *J. Am. Chem. Soc.* **2008,** *130* (21), 6749-6754.

(137) Tsao, Y.-Y. T.; Smith, T. H.; Wooley, K. L., Regioisomeric Preference in Ring-Opening Polymerization of 3′,5′-Cyclic Phosphoesters of Functional Thymidine DNA Analogues. *ACS Macro Lett.* **2018,** *7* (2), 153-158.

(138) Jain, S.; Bates, F. S., On the Origins of Morphological Complexity in Block Copolymer Surfactants. *Science* **2003,** *300* (5618), 460-464.

(139) Holder, S. J.; Sommerdijk, N. A. J. M., New micellar morphologies from amphiphilic block copolymers: disks, toroids and bicontinuous micelles. *Polym. Chem.* **2011,** *2* (5), 1018-1028.

(140) Blanazs, A.; Madsen, J.; Battaglia, G.; Ryan, A. J.; Armes, S. P., Mechanistic Insights for Block Copolymer Morphologies: How Do Worms Form Vesicles? *J. Am. Chem. Soc.* **2011,** *133* (41), 16581-16587.

(141) Qiu, H.; Hudson, Z. M.; Winnik, M. A.; Manners, I., Multidimensional hierarchical self-assembly of amphiphilic cylindrical block comicelles. *Science* **2015,** *347* (6228), 1329-1332.

(142) Mai, Y.; Eisenberg, A., Self-assembly of block copolymers. *Chem. Soc. Rev.* **2012,** *41* (18), 5969-5985.

(143) Zhang, F.; Zhang, S.; Pollack, S. F.; Li, R.; Gonzalez, A. M.; Fan, J.; Zou, J.; Leininger, S. E.; Pavia-Sanders, A.; Johnson, R.; Nelson, L. D.; Raymond, J. E.; Elsabahy, M.; Hughes, D. M.; Lenox, M. W.; Gustafson, T. P.; Wooley, K. L., Improving paclitaxel delivery: in vitro and in vivo characterization of PEGylated polyphosphoester-based nanocarriers. *J. Am. Chem. Soc.* **2015,** *137* (5), 2056-66.

(144) Chai, J.; Buriak, J. M., Using Cylindrical Domains of Block Copolymers To Self-Assemble and Align Metallic Nanowires. *ACS Nano* **2008,** *2* (3), 489-501.

(145) Sun, L.; Pitto-Barry, A.; Thomas, A. W.; Inam, M.; Doncom, K.; Dove, A. P.; O'Reilly, R. K., Core functionalization of semi-crystalline polymeric cylindrical nanoparticles using photo-initiated thiol-ene radical reactions. *Polym. Chem.* **2016,** *7* (13), 2337-2341.

(146) Zhang, M.; Müller, A. H. E., Cylindrical polymer brushes. *J. Polym. Sci., Part A: Polym. Chem.* **2005,** *43* (16), 3461-3481.

(147) Petzetakis, N.; Walker, D.; Dove, A. P.; O'Reilly, R. K., Crystallization-driven sphere-to-rod transition of poly(lactide)-b-poly(acrylic acid) diblock copolymers: mechanism and kinetics. *Soft Matter* **2012,** *8* (28), 7408-7414.

(148) Petzetakis, N.; Dove, A. P.; O'Reilly, R. K., Cylindrical micelles from the living crystallization-driven self-assembly of poly (lactide)-containing block copolymers. *Chem. Sci.* **2011,** *2* (5), 955-960.

(149) Gilroy, J. B.; Gädt, T.; Whittell, G. R.; Chabanne, L.; Mitchels, J. M.; Richardson, R. M.; Winnik, M. A.; Manners, I., Monodisperse cylindrical micelles by crystallization-driven living self-assembly. *Nat. Chem.* **2010,** *2* (7), 566-570.

(150) Müllner, M.; Müller, A. H., Cylindrical polymer brushes–Anisotropic building blocks, unimolecular templates and particulate nanocarriers. *Polymer* **2016,** *98*, 389-401.

(151) Yuan, J.; Müller, A. H., One-dimensional organic–inorganic hybrid nanomaterials. *Polymer* **2010,** *51* (18), 4015-4036.

(152) Löbling, T. I.; Borisov, O.; Haataja, J. S.; Ikkala, O.; Gröschel, A. H.; Müller, A. H. E., Rational design of ABC triblock terpolymer solution nanostructures with controlled patch morphology. *Nat. Commun.* **2016,** *7*, 12097.

(153) Groschel, A. H.; Walther, A.; Lobling, T. I.; Schacher, F. H.; Schmalz, H.; Muller, A. H. E., Guided hierarchical co-assembly of soft patchy nanoparticles. *Nature* **2013,** *503* (7475), 247-251.

(154) Gröschel, A. H.; Schacher, F. H.; Schmalz, H.; Borisov, O. V.; Zhulina, E. B.; Walther, A.; Müller, A. H. E., Precise hierarchical self-assembly of multicompartment micelles. *Nat. Commun.* **2012,** *3*, 710.

(155) Geng, Y.; Dalhaimer, P.; Cai, S.; Tsai, R.; Tewari, M.; Minko, T.; Discher, D. E., Shape effects of filaments versus spherical particles in flow and drug delivery. *Nat. Nanotechnol.* **2007,** *2* (4), 249-255.

(156) Zhang, K.; Fang, H.; Chen, Z.; Taylor, J.-S. A.; Wooley, K. L., Shape Effects of Nanoparticles Conjugated with Cell-Penetrating Peptides (HIV Tat PTD) on CHO Cell Uptake. *Bioconjugate Chem.* **2008,** *19* (9), 1880-1887.

(157) Harada, A.; Kataoka, K., Supramolecular assemblies of block copolymers in aqueous media as nanocontainers relevant to biological applications. *Prog. Polym. Sci.* **2006,** *31* (11), 949-982.

(158) Hinde, E.; Thammasiraphop, K.; Duong, H. T.; Yeow, J.; Karagoz, B.; Boyer, C.; Gooding, J. J.; Gaus, K., Pair correlation microscopy reveals the role of nanoparticle shape in intracellular transport and site of drug release. *Nat. Nanotechnol.* **2017,** *12* (1), 81-89.

(159) Massey, J. A.; Temple, K.; Cao, L.; Rharbi, Y.; Raez, J.; Winnik, M. A.; Manners, I., Self-Assembly of Organometallic Block Copolymers: The Role of Crystallinity of the

Core-Forming Polyferrocene Block in the Micellar Morphologies Formed by Poly(ferrocenylsilane-b-dimethylsiloxane) in n-Alkane Solvents. *J. Am. Chem. Soc.* **2000,** *122* (47), 11577-11584.

(160) Cambridge, G.; Gonzalez-Alvarez, M. J.; Guerin, G.; Manners, I.; Winnik, M. A., Solution self-assembly of blends of crystalline-coil polyferrocenylsilane-block-polyisoprene with crystallizable polyferrocenylsilane homopolymer. *Macromolecules* **2015,** *48* (3), 707-716.

(161) Sun, L.; Petzetakis, N.; Pitto-Barry, A.; Schiller, T. L.; Kirby, N.; Keddie, D. J.; Boyd, B. J.; O'Reilly, R. K.; Dove, A. P., Tuning the Size of Cylindrical Micelles from Poly(L-lactide)-*b*-poly(acrylic acid) Diblock Copolymers Based on Crystallization-Driven Self-Assembly. *Macromolecules* **2013,** *46* (22), 9074-9082.

(162) Pitto-Barry, A.; Kirby, N.; Dove, A. P.; O'Reilly, R. K., Expanding the scope of the crystallization-driven self-assembly of polylactide-containing polymers. *Polym. Chem.* **2014,** *5* (4), 1427-1436.

(163) Sun, L.; Pitto-Barry, A.; Kirby, N.; Schiller, T. L.; Sanchez, A. M.; Dyson, M. A.; Sloan, J.; Wilson, N. R.; O'Reilly, R. K.; Dove, A. P., Structural reorganization of cylindrical nanoparticles triggered by polylactide stereocomplexation. *Nat. Commun.* **2014,** *5*, 5746.

(164) Inam, M.; Cambridge, G.; Pitto-Barry, A.; Laker, Z. P. L.; Wilson, N. R.; Mathers, R. T.; Dove, A. P.; O'Reilly, R. K., 1D vs. 2D shape selectivity in the crystallization-driven self-assembly of polylactide block copolymers. *Chem. Sci.* **2017**.

(165) Wang, J.; Zhu, W.; Peng, B.; Chen, Y., A facile way to prepare crystalline platelets of block copolymers by crystallization-driven self-assembly. *Polymer* **2013,** *54* (25), 6760-6767.

(166) Pratt, R. C.; Lohmeijer, B. G.; Long, D. A.; Waymouth, R. M.; Hedrick, J. L., Triazabicyclodecene: A simple bifunctional organocatalyst for acyl transfer and ring-opening polymerization of cyclic esters. *J. Am. Chem. Soc* **2006,** *128* (14), 4556-4557.

(167) Kiesewetter, M. K.; Shin, E. J.; Hedrick, J. L.; Waymouth, R. M., Organocatalysis: Opportunities and Challenges for Polymer Synthesis. *Macromolecules* **2010,** *43* (5), 2093-2107.

(168) Liang, L.; Astruc, D., The copper (I)-catalyzed alkyne-azide cycloaddition (CuAAC)"click" reaction and its applications. An overview. *Coord. Chem. Rev.* **2011,** *255* (23), 2933-2945.

(169) Hoyle, C. E.; Bowman, C. N., Thiol–ene click chemistry. *Angew. Chem. Int. Ed.* **2010,** *49* (9), 1540-1573.

(170) Halbes-Letinois, U.; Weibel, J.-M.; Pale, P., The organic chemistry of silver acetylides. *Chem. Soc. Rev.* **2007,** *36* (5), 759-769.

(171) Kikkawa, Y.; Abe, H.; Iwata, T.; Inoue, Y.; Doi, Y., Crystallization, Stability, and Enzymatic Degradation of Poly(l-lactide) Thin Film. *Biomacromolecules* **2002,** *3* (2), 350-356.

(172) Kiesewetter, M. K.; Scholten, M. D.; Kirn, N.; Weber, R. L.; Hedrick, J. L.; Waymouth, R. M., Cyclic Guanidine Organic Catalysts: What Is Magic About Triazabicyclodecene? *J. Org. Chem.* **2009,** *74* (24), 9490-9496.

(173) Tsao, Y.-Y. T.; Wooley, K. L., Synthetic, Functional Thymidine-Derived Polydeoxyribonucleotide Analogues from a Six-Membered Cyclic Phosphoester. *J. Am. Chem. Soc.* **2017,** *139* (15), 5467-5473.

(174) Elsabahy, M.; Zhang, S.; Zhang, F.; Deng, Z. J.; Lim, Y. H.; Wang, H.; Parsamian, P.; Hammond, P. T.; Wooley, K. L., Surface Charges and Shell Crosslinks Each Play Significant Roles in Mediating Degradation, Biofouling, Cytotoxicity and Immunotoxicity for Polyphosphoester-based Nanoparticles. *Sci. Rep.* **2013,** *3*, 3313.

(175) Appel, E. A.; Lee, V. Y.; Nguyen, T. T.; McNeil, M.; Nederberg, F.; Hedrick, J. L.; Swope, W. C.; Rice, J. E.; Miller, R. D.; Sly, J., Toward biodegradable nanogel star polymers via organocatalytic ROP. *Chem. Commun.* **2012,** *48* (49), 6163-6165.

(176) Jaffredo, C. G.; Carpentier, J.-F.; Guillaume, S. M., Organocatalyzed controlled ROP of [small beta]-lactones towards poly(hydroxyalkanoate)s: from [small beta]-butyrolactone to benzyl [small beta]-malolactone polymers. *Polym. Chem.* **2013,** *4* (13), 3837-3850.

(177) Lowe, A. B.; McCormick, C. L., Synthesis and solution properties of zwitterionic polymers. *Chem. Rev.* **2002,** *102* (11), 4177-4190.

(178) Zhang, S.; Zou, J.; Zhang, F.; Elsabahy, M.; Felder, S. E.; Zhu, J.; Pochan, D. J.; Wooley, K. L., Rapid and versatile construction of diverse and functional nanostructures derived from a polyphosphoester-based biomimetic block copolymer system. *J. Am. Chem. Soc.* **2012,** *134* (44), 18467-74.

(179) Lim, Y. H.; Heo, G. S.; Cho, S.; Wooley, K. L., Construction of a Reactive Diblock Copolymer, Polyphosphoester--Poly(L-lactide), as a Versatile Framework for Functional Materials that are Capable of Full Degradation and Nanoscopic Assembly Formation. *ACS Macro Lett.* **2013,** *2* (9), 785-789.

(180) Li, C.-H.; Wang, C.; Keplinger, C.; Zuo, J.-L.; Jin, L.; Sun, Y.; Zheng, P.; Cao, Y.; Lissel, F.; Linder, C.; You, X.-Z.; Bao, Z., A highly stretchable autonomous self-healing elastomer. *Nat. Chem.* **2016,** *8*, 618.

(181) Tokiwa, Y.; Calabia, B. P.; Ugwu, C. U.; Aiba, S., Biodegradability of Plastics. *International Journal of Molecular Sciences* **2009,** *10* (9), 3722-3742.

(182) Garlotta, D., A Literature Review of Poly(Lactic Acid). *J. Polym. Environ.* **2001,** *9* (2), 63-84.

(183) Lim, Y. H.; Tiemann, K. M.; Heo, G. S.; Wagers, P. O.; Rezenom, Y. H.; Zhang, S.; Zhang, F.; Youngs, W. J.; Hunstad, D. A.; Wooley, K. L., Preparation and in Vitro Antimicrobial Activity of Silver-Bearing Degradable Polymeric Nanoparticles of Polyphosphoester-block-Poly(L-lactide). *ACS Nano* **2015,** *9* (2), 1995-2008.

(184) Wang, H.; Su, L.; Li, R.; Zhang, S.; Fan, J.; Zhang, F.; Nguyen, T. P.; Wooley, K. L., Polyphosphoramidates That Undergo Acid-Triggered Backbone Degradation. *ACS Macro Lett.* **2017,** *6* (3), 219-223.

(185) Akbulut, H.; Yamada, S.; Endo, T., Preparation of a zwitterionic polymer based on l-cysteine for recovery application of precious metals. *RSC Advances* **2016,** *6* (110), 108689-108696.

(186) Foxman, B., Urinary Tract Infection Syndromes: Occurrence, Recurrence, Bacteriology, Risk Factors, and Disease Burden. *Infect. Dis. Clin. North Am.* **2014,** *28* (1), 1-13.

(187) Nielubowicz, G. R.; Mobley, H. L. T., Host-pathogen interactions in urinary tract infection. *Nat. Rev. Urol.* **2010,** *7* (8), 430-441.

(188) Flores-Mireles, A. L.; Walker, J. N.; Caparon, M.; Hultgren, S. J., Urinary tract infections: epidemiology, mechanisms of infection and treatment options. *Nat. Rev. Micro.* **2015,** *13* (5), 269-284.

(189) Kim, M.; Ashida, H.; Ogawa, M.; Yoshikawa, Y.; Mimuro, H.; Sasakawa, C., Bacterial Interactions with the Host Epithelium. *Cell Host & Microbe* **2010,** *8* (1), 20-35.

(190) Foxman, B., The epidemiology of urinary tract infection. *Nat. Rev. Urol.* **2010,** *7*, 653.

(191) Chen, Y.-H.; Ko, W.-C.; Hsueh, P.-R., Emerging resistance problems and future perspectives in pharmacotherapy for complicated urinary tract infections. *Expert Opin. Pharmacother.* **2013,** *14* (5), 587-596.

(192) Durán, N.; Durán, M.; de Jesus, M. B.; Seabra, A. B.; Fávaro, W. J.; Nakazato, G., Silver nanoparticles: A new view on mechanistic aspects on antimicrobial activity. *Nanomed. Nanotechnol. Biol. Med.* **2016,** *12* (3), 789-799.

(193) Wakshlak, R. B.; Pedahzur, R.; Avnir, D., Antibacterial activity of silver-killed bacteria: the "zombies" effect. *Sci. Rep.* **2015,** *5*, 9555.

(194) Jung, W. K.; Koo, H. C.; Kim, K. W.; Shin, S.; Kim, S. H.; Park, Y. H., Antibacterial activity and mechanism of action of the silver ion in *Staphylococcus aureus* and *Escherichia coli*. *Appl. Environ. Microbiol.* **2008,** *74* (7), 2171-2178.

(195) Silver, S., Bacterial silver resistance: molecular biology and uses and misuses of silver compounds. *FEMS Microbiol. Rev.* **2003,** *27* (2-3), 341-353.

(196) Elias, D. R.; Poloukhtine, A.; Popik, V.; Tsourkas, A., Effect of ligand density, receptor density, and nanoparticle size on cell targeting. *Nanomed. Nanotechnol. Biol. Med.* **2013,** *9* (2), 194-201.

(197) Gao, H.; Yang, Z.; Zhang, S.; Cao, S.; Shen, S.; Pang, Z.; Jiang, X., Ligand modified nanoparticles increases cell uptake, alters endocytosis and elevates glioma distribution and internalization. *Sci. Rep.* **2013,** *3*, 2534.

(198) Zhao, J.; Stenzel, M. H., Entry of nanoparticles into cells: the importance of nanoparticle properties. *Polym. Chem.* **2018,** *9* (3), 259-272.

(199) Tan, Z.; Jiang, Y.; Ganewatta, M. S.; Kumar, R.; Keith, A.; Twaroski, K.; Pengo, T.; Tolar, J.; Lodge, T. P.; Reineke, T. M., Block Polymer Micelles Enable CRISPR/Cas9 Ribonucleoprotein Delivery: Physicochemical Properties Affect Packaging Mechanisms and Gene Editing Efficiency. *Macromolecules* **2019,** *52* (21), 8197-8206.

(200) Young, K. D., The Selective Value of Bacterial Shape. *Microbiol. Mol. Biol. Rev.* **2006,** *70* (3), 660-703.

(201) Martinez, J. J.; Mulvey, M. A.; Schilling, J. D.; Pinkner, J. S.; Hultgren, S. J., Type 1 pilus-mediated bacterial invasion of bladder epithelial cells. *EMBO J.* **2000,** *19* (12), 2803-2812.

(202) Lin, L. Y.; Tiemann, K. M.; Li, Y.; Pinkner, J. S.; Walker, J. N.; Hultgren, S. J.; Hunstad, D. A.; Wooley, K. L., Synthetic Polymer Nanoparticles Conjugated with FimHA from *E. coli* Pili to Emulate the Bacterial Mode of Epithelial Internalization. *J. Am. Chem. Soc.* **2012,** *134* (9), 3938-41.

(203) Hannan, T. J.; Totsika, M.; Mansfield, K. J.; Moore, K. H.; Schembri, M. A.; Hultgren, S. J., Host–pathogen checkpoints and population bottlenecks in persistent and intracellular uropathogenic Escherichia coli bladder infection. *FEMS Microbiol. Rev.* **2012,** *36* (3), 616-648.

(204) Zhang, K.; Rossin, R.; Hagooly, A.; Chen, Z.; Welch, M. J.; Wooley, K. L., Folate-mediated cell uptake of shell-crosslinked spheres and cylinders. *J. Polym. Sci., Part A: Polym. Chem.* **2008,** *46* (22), 7578-7583.

(205) Sharma, G.; Valenta, D. T.; Altman, Y.; Harvey, S.; Xie, H.; Mitragotri, S.; Smith, J. W., Polymer particle shape independently influences binding and internalization by macrophages. *J. Control. Release* **2010,** *147* (3), 408-412.

(206) Gratton, S. E. A.; Ropp, P. A.; Pohlhaus, P. D.; Luft, J. C.; Madden, V. J.; Napier, M. E.; DeSimone, J. M., The effect of particle design on cellular internalization pathways. *Proc. Natl. Acad. Sci. U. S. A.* **2008,** *105* (33), 11613-11618.

(207) Liu, X.; Wu, F.; Tian, Y.; Wu, M.; Zhou, Q.; Jiang, S.; Niu, Z., Size Dependent Cellular Uptake of Rod-like Bionanoparticles with Different Aspect Ratios. *Sci. Rep.* **2016,** *6*, 24567.

(208) Agarwal, R.; Singh, V.; Jurney, P.; Shi, L.; Sreenivasan, S. V.; Roy, K., Mammalian cells preferentially internalize hydrogel nanodiscs over nanorods and use shape-specific uptake mechanisms. *Proc. Natl. Acad. Sci. U. S. A.* **2013,** *110* (43), 17247-17252.

(209) Decuzzi, P.; Ferrari, M., The adhesive strength of non-spherical particles mediated by specific interactions. *Biomaterials* **2006,** *27* (30), 5307-5314.

(210) Elsabahy, M.; Wooley, K. L., Reassessment of nanomaterials immunotoxicity. *Nano Today* **2018,** *20*, 10-12.

(211) Elsabahy, M.; Wooley, K. L.; Hendricksen, A.; Oh, K., Multiplexing techniques for measurement of the immunomodulatory effects of particulate materials: Precautions when testing micro- and nano-particles. *Methods* **2019,** *158*, 81-85.

(212) Li, R.; Wang, H.; Song, Y.; Lin, Y.-N.; Dong, M.; Shen, Y.; Khan, S.; Zhang, S.; Fan, J.; Zhang, F.; Su, L.; Wooley, K. L., In Situ Production of Ag/Polymer Asymmetric Nanoparticles via a Powerful Light-Driven Technique. *J. Am. Chem. Soc.* **2019,** *141* (50), 19542-19545.

(213) Maiti, S.; Manna, S.; Shen, J.; Esser-Kahn, A. P.; Du, W., Mitigation of Hydrophobicity-Induced Immunotoxicity by Sugar Poly(orthoesters). *J. Am. Chem. Soc.* **2019,** *141* (11), 4510-4514.

(214) Jewett, J. C.; Bertozzi, C. R., Cu-free click cycloaddition reactions in chemical biology. *Chem. Soc. Rev.* **2010,** *39* (4), 1272-1279.

(215) Ngo, J. T.; Adams, S. R.; Deerinck, T. J.; Boassa, D.; Rodriguez-Rivera, F.; Palida, S. F.; Bertozzi, C. R.; Ellisman, M. H.; Tsien, R. Y., Click-EM for imaging metabolically tagged nonprotein biomolecules. *Nat. Chem. Biol.* **2016,** *12* (6), 459-465.

(216) He, Y.; Eloi, J.-C.; Harniman, R. L.; Richardson, R. M.; Whittell, G. R.; Mathers, R. T.; Dove, A. P.; O'Reilly, R. K.; Manners, I., Uniform Biodegradable Fiber-Like Micelles and Block Comicelles via "Living" Crystallization-Driven Self-Assembly of Poly(l-lactide) Block Copolymers: The Importance of Reducing Unimer Self-Nucleation via Hydrogen Bond Disruption. *J. Am. Chem. Soc.* **2019,** *141* (48), 19088-19098.

(217) Cha, Y.; Jarrett-Wilkins, C.; Rahman, M. A.; Zhu, T.; Sha, Y.; Manners, I.; Tang, C., Crystallization-Driven Self-Assembly of Metallo-Polyelectrolyte Block Copolymers with a Polycaprolactone Core-Forming Segment. *ACS Macro Lett.* **2019,** *8* (7), 835-840.

(218) Pearce, S.; He, X.; Hsiao, M.-S.; Harniman, R. L.; MacFarlane, L. R.; Manners, I., Uniform, High-Aspect-Ratio, and Patchy 2D Platelets by Living Crystallization-Driven Self-Assembly of Crystallizable Poly(ferrocenyldimethylsilane)-Based Homopolymers with Hydrophilic Charged Termini. *Macromolecules* **2019,** *52* (16), 6068-6079.

(219) Li, Z.; Zhang, Y.; Wu, L.; Yu, W.; Wilks, T. R.; Dove, A. P.; Ding, H.-m.; O'Reilly, R. K.; Chen, G.; Jiang, M., Glyco-Platelets with Controlled Morphologies via Crystallization-Driven Self-Assembly and Their Shape-Dependent Interplay with Macrophages. *ACS Macro Lett.* **2019,** *8* (5), 596-602.

(220) Zhang, P.; Jain, P.; Tsao, C.; Yuan, Z.; Li, W.; Li, B.; Wu, K.; Hung, H.-C.; Lin, X.; Jiang, S., Polypeptides with High Zwitterion Density for Safe and Effective Therapeutics. *Angew. Chem. Int. Ed.* **2018,** *57* (26), 7743-7747.

(221) Liu, S.; Jiang, S., Zwitterionic polymer-protein conjugates reduce polymer-specific antibody response. *Nano Today* **2016,** *11* (3), 285-291.

(222) Elkrewi, E.; Randall, C. P.; Ooi, N.; Cottell, J. L.; O'Neill, A. J., Cryptic silver resistance is prevalent and readily activated in certain Gram-negative pathogens. *J. Antimicrob. Chemother.* **2017,** *72* (11), 3043-3046.

(223) Li, Y.; Hindi, K.; Watts, K. M.; Taylor, J. B.; Zhang, K.; Li, Z.; Hunstad, D. A.; Cannon, C. L.; Youngs, W. J.; Wooley, K. L., Shell crosslinked nanoparticles carrying silver antimicrobials as therapeutics. *Chem. Commun.* **2010,** *46* (1), 121-123.

(224) Hung, C.-S.; Bouckaert, J.; Hung, D.; Pinkner, J.; Widberg, C.; DeFusco, A.; Auguste, C. G.; Strouse, R.; Langermann, S.; Waksman, G.; Hultgren, S. J., Structural basis of tropism of Escherichia coli to the bladder during urinary tract infection. *Mol. Microbiol.* **2002,** *44* (4), 903-915.

(225) Schwartz, D. J.; Kalas, V.; Pinkner, J. S.; Chen, S. L.; Spaulding, C. N.; Dodson, K. W.; Hultgren, S. J., Positively selected FimH residues enhance virulence during urinary tract infection by altering FimH conformation. *Proc. Natl. Acad. Sci. U. S. A.* **2013,** *110* (39), 15530-15537.

(226) Spicer, C. D.; Davis, B. G., Selective chemical protein modification. *Nat. Commun.* **2014,** *5* (1), 4740.

(227) Kalkhof, S.; Sinz, A., Chances and pitfalls of chemical cross-linking with amine-reactive N-hydroxysuccinimide esters. *Anal. Bioanal. Chem.* **2008,** *392* (1), 305-312.

(228) Lin, L. Y.; Tiemann, K. M.; Li, Y.; Pinkner, J. S.; Walker, J. N.; Hultgren, S. J.; Hunstad, D. A.; Wooley, K. L., Synthetic Polymer Nanoparticles Conjugated with FimHA from E. coli Pili to Emulate the Bacterial Mode of Epithelial Internalization. *J. Am. Chem. Soc.* **2012,** *134* (9), 3938-3941.

APPENDIX A

CARTESIAN COORDINATES

INT1-a

Energy: -1378793.6260930

C	0.01551	-3.23076	-0.81336
O	-0.44744	-4.17220	0.00583
O	-0.60115	-2.04449	-0.88268
O	0.96418	-3.45619	-1.53070
O	1.42958	-1.65853	1.58432
H	2.22949	-1.83198	1.01666
H	2.07156	-1.75215	-1.59499
N	3.74279	-1.85896	0.11575
C	3.74143	-0.96389	-0.83713
N	2.62049	-0.89899	-1.63530
N	4.73829	-0.06589	-1.08257
C	4.88927	-1.91591	1.00797
C	1.13387	-0.27909	1.48491
H	0.31810	-0.08625	2.19405
H	0.76306	-0.03707	0.48013
C	2.29785	0.63811	1.79287
C	2.59412	1.69958	0.93901
C	3.08763	0.46681	2.93301
C	3.65889	2.55976	1.20089
H	1.98184	1.84781	0.05323
C	4.15238	1.32472	3.19576
H	2.87448	-0.35462	3.61295
C	4.46225	2.38153	2.33026
H	3.87420	3.37339	0.51067
H	4.75845	1.16876	4.08608
C	6.17559	-1.43385	0.34697
H	5.00470	-2.95120	1.34975
H	4.69608	-1.30613	1.90366
C	5.93227	-0.05639	-0.24775
C	4.70258	0.94539	-2.13371
C	2.65713	-0.22089	-2.91692
H	6.99435	-1.38613	1.07251
H	6.47025	-2.12934	-0.44905
H	6.77641	0.24801	-0.87723
H	5.81837	0.69621	0.54604
C	3.30882	1.13630	-2.71239

H	5.06263	1.88825	-1.70374
H	5.40681	0.65847	-2.92874
H	1.62876	-0.11671	-3.27467
H	3.21631	-0.79698	-3.67172
H	3.37652	1.68674	-3.65557
H	2.69767	1.72308	-2.02024
C	-1.59499	-1.71219	0.08575
C	-2.48835	-2.91841	0.31229
C	-2.39939	-0.52846	-0.41278
H	-1.08953	-1.45071	1.02067
C	-1.59810	-4.01150	0.86032
H	-2.94181	-3.23298	-0.63621
O	-3.48487	-2.60661	1.26212
C	-3.53775	-0.28935	0.57399
H	-2.78317	-0.71194	-1.41943
O	-1.57828	0.63802	-0.41399
H	-1.24241	-3.75673	1.86205
H	-2.09011	-4.98348	0.87553
C	-4.35201	-1.57379	0.81870
H	-5.05471	-1.43015	1.64642
O	-5.00852	-1.89553	-0.35739
C	-5.97940	-2.92687	-0.22009
H	-6.47204	-3.01718	-1.18833
H	-6.71748	-2.65853	0.54600
H	-5.50796	-3.87970	0.04349
C	5.64945	3.27481	2.59360
H	6.57501	2.80921	2.23178
H	5.54463	4.23851	2.08516
H	5.77696	3.46440	3.66453
H	-3.13029	0.04108	1.53364
O	-4.34727	0.74129	0.02031
C	-5.05417	1.48090	0.88469
O	-5.70425	2.40335	0.19782
O	-5.08282	1.31867	2.08616
C	-6.53820	3.30274	0.96589
H	-7.28418	2.70806	1.49962
H	-5.90796	3.81684	1.69614
C	-7.17486	4.26671	-0.00955
H	-7.81430	4.96339	0.54147
H	-6.41382	4.84454	-0.54248
H	-7.79227	3.73515	-0.73984
C	-1.21174	1.14863	-1.59721
O	-0.43194	2.19136	-1.35790
C	0.02839	2.92226	-2.51741

H	0.62443	2.24752	-3.13803
H	-0.84386	3.24494	-3.09157
C	0.83702	4.09786	-2.01713
H	1.69538	3.76844	-1.42348
H	1.21207	4.66499	-2.87462
H	0.22254	4.76256	-1.40289
O	-1.54087	0.73183	-2.68554

INT1-b

C	2.171031	-0.580958	3.612915
O	3.047578	-0.318602	2.636056
O	2.158216	0.107994	4.610363
O	1.389252	-1.655954	3.531446
O	0.545145	0.862655	1.977743
H	1.159591	1.659635	1.987589
N	2.078192	3.071095	1.907833
C	2.895482	3.579852	2.790236
N	3.266276	2.810598	3.855090
H	2.810672	1.909707	3.939924
N	3.447525	4.834400	2.704522
C	1.763731	3.881650	0.744663
C	1.645191	5.356774	1.109226
H	0.819541	3.518855	0.323914
H	2.535725	3.754274	-0.031822
C	2.949474	5.813463	1.742531
C	4.396712	5.368396	3.675733
C	4.014239	3.312643	4.987388
H	1.428809	5.971093	0.228927
H	0.818280	5.482104	1.817848
H	2.808616	6.765138	2.271007
H	3.716143	5.983522	0.973293
C	5.079247	4.267486	4.471367
H	5.139080	5.960437	3.125088
H	3.874039	6.057203	4.357120
H	4.463598	2.458337	5.500354
H	3.363408	3.831494	5.708697
H	5.641102	4.711572	5.298298
H	5.782665	3.717228	3.835583
C	2.862225	-0.937619	1.362122
C	2.624386	-2.420006	1.600681
C	4.082267	-0.709769	0.496037

H	1.985263	-0.482033	0.889737
C	1.329835	-2.517457	2.378705
H	3.453463	-2.835584	2.187588
O	2.488362	-3.113502	0.377875
C	3.932537	-1.570044	-0.760441
H	5.003284	-0.951884	1.031948
H	0.484508	-2.199154	1.762778
H	1.151995	-3.519102	2.769435
C	3.662477	-3.038352	-0.417513
H	3.423186	-3.607429	-1.322919
O	4.776899	-3.551715	0.225538
C	4.743300	-4.961239	0.415533
H	5.702882	-5.236278	0.853672
H	4.616147	-5.474865	-0.545632
H	3.932814	-5.248501	1.094029
C	-0.683760	1.256758	2.551614
H	-0.539969	1.573961	3.595545
H	-1.324026	0.367112	2.562434
C	-1.344825	2.372043	1.770676
C	-1.770029	2.155483	0.454284
C	-1.486801	3.649622	2.307476
C	-2.309995	3.190656	-0.300400
H	-1.661020	1.166346	0.014543
C	-2.033268	4.688944	1.551454
H	-1.148521	3.845815	3.322877
C	-2.448317	4.479354	0.235620
H	-2.629300	3.000855	-1.323365
H	-2.124096	5.679810	1.991553
C	-3.033744	5.595815	-0.593971
H	-2.471603	5.732374	-1.524846
H	-4.072084	5.378634	-0.870679
H	-3.022171	6.545007	-0.049470
O	4.123895	0.641839	0.040011
O	5.130517	-1.470637	-1.520532
H	3.092923	-1.203009	-1.356048
O	6.355511	-0.528325	-3.015620
C	5.107428	-0.670790	-2.598828
O	4.117818	-0.184733	-3.099662
C	6.572426	0.390352	-4.112663
H	7.527908	0.073629	-4.531584
H	5.785421	0.244834	-4.855512
C	6.625612	1.821744	-3.613644
H	6.850459	2.488811	-4.452366
H	5.667578	2.124337	-3.180975

H	7.408803	1.939863	-2.858318
O	4.950372	2.613367	-0.095555
C	5.021819	1.477299	0.577990
O	5.773596	1.222699	1.492760
C	5.801619	3.691226	0.347104
H	6.809404	3.302404	0.511796
H	5.401864	4.063839	1.294589
C	5.774627	4.748731	-0.734141
H	6.354874	5.616973	-0.406302
H	6.211383	4.369229	-1.663027
H	4.749914	5.074564	-0.938477

INT1-c

C	-1.003104	-0.992404	-2.997277
O	-1.444136	-0.219852	-3.986545
O	-1.609643	-0.963263	-1.803092
O	-0.058933	-1.729970	-3.169276
O	0.850214	1.321740	-1.662743
H	1.624862	0.697334	-1.703989
H	0.990097	-1.771776	-1.436787
N	1.517602	-1.885808	-0.579807
N	2.997384	-0.413732	-1.513718
C	2.725611	-1.250034	-0.543668
N	3.560898	-1.546377	0.497779
C	0.374201	1.316333	-0.331070
H	0.018248	0.314312	-0.055332
H	-0.484700	1.999069	-0.306868
C	1.389872	1.764457	0.696425
C	2.044847	2.993671	0.573103
C	1.683592	0.965854	1.801076
C	2.977940	3.400517	1.522301
H	1.827320	3.631729	-0.280388
C	2.616574	1.374450	2.753743
H	1.177961	0.010189	1.918144
C	3.286650	2.593277	2.625725
H	3.479713	4.358914	1.404935
H	2.833407	0.729197	3.602734
C	4.332580	0.158929	-1.521562
C	4.817108	0.489160	-0.112971
H	4.311570	1.065979	-2.135994

H	5.046303	-0.531239	-2.002838
C	4.772012	-0.767503	0.742194
C	3.207559	-2.475011	1.564432
C	0.996336	-2.716893	0.482895
H	5.838728	0.884343	-0.124622
H	4.163819	1.252644	0.318111
H	4.791960	-0.499356	1.806703
H	5.646175	-1.404811	0.546436
C	2.148633	-3.474616	1.125762
H	4.122471	-2.997195	1.868725
H	2.851744	-1.907391	2.438938
H	0.262754	-3.402824	0.050115
H	0.474154	-2.112549	1.239760
H	1.803618	-4.043316	1.994725
H	2.573296	-4.179626	0.401927
C	-2.809835	-0.207588	-1.635597
C	-2.670737	1.104502	-2.389621
C	-3.033531	0.055632	-0.160087
H	-3.646373	-0.792498	-2.037005
C	-2.496060	0.758414	-3.849590
H	-1.783567	1.638128	-2.030108
O	-3.833342	1.886958	-2.223346
C	-4.242825	0.975565	-0.024574
H	-2.155532	0.519431	0.290391
O	-3.301759	-1.180822	0.495355
H	-3.411876	0.331726	-4.267045
H	-2.180874	1.615059	-4.444337
C	-4.049875	2.249984	-0.867932
H	-4.966437	2.849184	-0.884745
O	-2.986396	2.953870	-0.326819
C	-2.795069	4.251239	-0.878889
H	-1.986533	4.710238	-0.309617
H	-3.707885	4.850722	-0.774839
H	-2.513132	4.192258	-1.935559
C	4.338111	3.014752	3.622128
H	4.323259	4.097458	3.785168
H	4.193864	2.520544	4.588089
H	5.340651	2.751513	3.262246
H	-5.147252	0.467378	-0.370000
O	-4.366447	1.280142	1.359409
O	-2.882662	-2.700889	1.960184
C	-2.518510	-1.503260	1.536235
C	-2.150250	-3.223279	3.093757
H	-2.286593	-2.539016	3.935304

H	-1.088796	-3.254998	2.834176
C	-2.699705	-4.600536	3.387919
H	-2.164794	-5.023769	4.243850
H	-3.764513	-4.553805	3.635111
H	-2.563378	-5.267683	2.531525
O	-1.634098	-0.815611	1.997499
O	-5.509250	1.823850	3.098742
C	-6.738724	2.165239	3.782963
H	-6.399763	2.693828	4.674349
H	-7.311604	2.848973	3.152983
C	-7.530180	0.922047	4.137413
H	-8.417801	1.212549	4.708957
H	-7.859376	0.393578	3.238075
H	-6.931525	0.242864	4.751945
C	-5.588499	1.611202	1.796663
O	-6.578154	1.701243	1.101614

INT1-d

C	0.513913	-2.902589	-2.158255
O	1.319226	-3.726835	-1.491652
O	0.603437	-1.586587	-1.911969
O	-0.233464	-3.313036	-3.014215
O	-1.139458	-2.997755	0.178151
H	-1.710282	-0.899460	-1.772770
H	-1.262629	-2.006691	0.305524
N	-2.046905	0.037124	-1.609638
C	-2.044245	0.422651	-0.303690
N	-1.487825	-0.377954	0.570045
N	-2.636979	1.613280	0.015930
C	-2.408384	-3.609338	0.307174
H	-2.752646	-3.568715	1.352317
H	-2.278109	-4.664898	0.043022
C	-3.448111	-2.969705	-0.587251
C	-3.407590	-3.165512	-1.972194
C	-4.420766	-2.116838	-0.067912
C	-4.310460	-2.518289	-2.809473
H	-2.644080	-3.812064	-2.397048
C	-5.327252	-1.469179	-0.907876
H	-4.461235	-1.938116	1.004723
H	-4.257253	-2.680242	-3.884531

H	-6.071270	-0.800918	-0.478846
C	-1.568791	0.033658	1.957261
C	-1.286806	1.525685	2.089935
H	-0.841032	-0.551159	2.528461
H	-2.564979	-0.192073	2.377886
C	-2.320101	2.291174	1.274411
C	-3.210562	2.480618	-1.003909
C	-2.648691	0.767746	-2.704349
H	-1.327483	1.855623	3.133636
H	-0.278914	1.722102	1.710008
H	-1.945531	3.294693	1.033289
H	-3.250448	2.415102	1.845302
C	-3.749192	1.672917	-2.172385
H	-4.017489	3.053760	-0.532547
H	-2.449506	3.196218	-1.348967
H	-3.052467	0.042672	-3.417512
H	-1.894257	1.368136	-3.234308
H	-4.098348	2.348281	-2.959404
H	-4.597058	1.064853	-1.839982
C	1.724861	-1.133967	-1.158210
C	1.807707	-1.939889	0.127384
C	1.559427	0.331686	-0.810427
H	2.631292	-1.277811	-1.760669
C	1.959466	-3.404372	-0.239135
H	0.897150	-1.771785	0.709809
O	2.951158	-1.543105	0.867643
C	2.762812	0.720989	0.048664
H	0.616966	0.486353	-0.278113
H	3.016088	-3.645183	-0.374097
H	1.515982	-4.058306	0.511449
C	2.894816	-0.190771	1.282328
H	3.853190	-0.017536	1.785408
C	1.908083	-0.559838	3.390978
H	1.100906	-0.145176	3.996262
H	2.871992	-0.347649	3.871264
H	1.777612	-1.643580	3.296992
C	-6.230410	-0.925829	-3.212791
H	-7.006849	-0.396568	-2.651624
H	-5.692668	-0.184841	-3.818022
H	-6.721653	-1.616136	-3.907400
C	-5.283839	-1.654317	-2.291285
O	1.828212	0.076846	2.124354
O	1.573127	1.083520	-2.024328
H	3.679020	0.624977	-0.541202

O	2.591931	2.081417	0.429109
C	3.702742	2.785404	0.670316
O	3.340869	4.022419	0.970649
O	4.834571	2.351037	0.623872
C	4.402920	4.970813	1.228280
H	3.923133	5.736863	1.838252
H	5.180215	4.476349	1.814774
C	4.947241	5.546380	-0.064271
H	5.700785	6.305762	0.169239
H	5.419815	4.770643	-0.673690
H	4.149278	6.019676	-0.644550
O	0.862088	2.643186	-3.325245
C	0.755061	2.141153	-2.101903
O	0.043983	2.562482	-1.219003
C	0.068315	3.819591	-3.594831
H	0.385799	4.613996	-2.913699
H	-0.980897	3.585858	-3.392753
C	0.291193	4.192167	-5.043124
H	-0.297404	5.084244	-5.279072
H	1.345619	4.413888	-5.233447
H	-0.026059	3.383185	-5.708102

TS1-a

Energy: -1378820.6515767

C	0.60008	-1.17478	-1.72416
O	0.76236	-2.42335	-1.23339
O	-0.63404	-0.61669	-1.64999
O	1.37717	-0.76918	-2.57416
O	1.31820	-0.26637	0.11836
H	2.65524	-0.90785	0.35671
H	3.10168	-0.92445	-1.81248
N	3.65450	-1.28417	0.56416
C	4.55574	-1.05242	-0.39361
N	4.10994	-0.90345	-1.65122
N	5.87566	-0.97894	-0.13585
C	4.04807	-1.27235	1.96442
C	1.34716	1.11553	-0.02865
H	0.39392	1.56820	0.30966
H	1.46785	1.39956	-1.09247
C	2.48717	1.73630	0.76092

C	3.72555	1.97996	0.16326
C	2.36415	1.98598	2.13077
C	4.81813	2.41199	0.91290
H	3.84030	1.80299	-0.90424
C	3.44954	2.43701	2.88083
H	1.40673	1.81438	2.61958
C	4.70128	2.63996	2.28822
H	5.77663	2.57311	0.42209
H	3.32579	2.62379	3.94586
C	5.43533	-1.87376	2.11368
H	3.30544	-1.84774	2.52399
H	4.03774	-0.24454	2.35123
C	6.39982	-1.10735	1.22371
C	6.85371	-0.66467	-1.17740
C	4.97250	-0.64262	-2.79073
H	5.77172	-1.81182	3.15233
H	5.41791	-2.93092	1.82434
H	7.36097	-1.62690	1.15736
H	6.58469	-0.10278	1.62879
C	6.21373	0.10165	-2.32404
H	7.63950	-0.06225	-0.71147
H	7.31414	-1.59409	-1.53760
H	4.40272	-0.05073	-3.51102
H	5.25591	-1.58473	-3.27825
H	6.92972	0.19910	-3.14436
H	5.94107	1.10890	-1.98998
C	-1.41026	-0.91312	-0.49667
C	-1.43464	-2.41866	-0.28343
C	-2.81792	-0.38699	-0.67798
H	-0.92986	-0.43347	0.36338
C	0.00175	-2.86462	-0.10334
H	-1.86878	-2.91326	-1.16188
O	-2.18489	-2.72736	0.87719
C	-3.63959	-0.82744	0.52892
H	-3.26267	-0.74874	-1.60798
O	-2.79019	1.04170	-0.68573
H	0.43188	-2.43312	0.80387
H	0.09482	-3.95094	-0.09194
C	-3.54345	-2.34742	0.75937
H	-3.99259	-2.61703	1.72180
O	-4.18995	-2.98070	-0.29261
C	-4.35631	-4.38084	-0.11188
H	-4.95362	-4.73244	-0.95355
H	-4.88576	-4.58697	0.82709

H	-3.38957	-4.89594	-0.10619
C	5.89291	3.06359	3.11178
H	5.59277	3.69801	3.95217
H	6.40875	2.18954	3.52931
H	6.61988	3.61653	2.50812
H	-3.26942	-0.32610	1.42734
O	-4.98328	-0.42339	0.28125
C	-5.75401	-0.20052	1.35143
O	-5.41075	-0.34772	2.50562
O	-6.94105	0.19585	0.92219
C	-7.92367	0.52968	1.93073
H	-8.87606	0.40875	1.41363
H	-7.85695	-0.20016	2.74042
C	-7.73542	1.94883	2.42945
H	-7.78699	2.66141	1.60062
H	-8.53268	2.18858	3.14073
H	-6.77470	2.06367	2.93963
O	-3.51886	1.13688	-2.83739
C	-3.14420	1.66751	-1.81408
O	-3.01432	2.96916	-1.60982
C	-3.34960	3.82606	-2.72484
H	-4.39243	3.64477	-2.99837
H	-2.71145	3.55713	-3.57072
C	-3.12285	5.25294	-2.27837
H	-3.36805	5.92983	-3.10281
H	-3.76066	5.50294	-1.42516
H	-2.07749	5.41432	-1.99839

TS1-b

C	1.931084	0.237638	3.789280
O	3.014416	0.294338	2.939080
O	1.979797	0.867670	4.830663
O	1.238406	-0.946495	3.778987
O	0.687779	1.256373	2.543331
H	0.161733	0.930386	0.773913
N	0.288447	1.095365	-0.233481
C	1.026774	2.177766	-0.523588
N	1.619627	2.808373	0.492965
H	1.400384	2.421769	1.432314

N	1.173845	2.592208	-1.790010
C	-0.457178	0.340382	-1.224491
C	-0.789886	1.246862	-2.399982
H	-1.365999	-0.031668	-0.745783
H	0.130560	-0.524255	-1.559929
C	0.481897	1.923839	-2.890244
C	2.092031	3.676888	-2.136695
C	2.503223	3.945281	0.307642
H	-1.232779	0.666858	-3.214007
H	-1.516442	2.003709	-2.082195
H	0.244140	2.688529	-3.635977
H	1.162662	1.197928	-3.353991
C	3.154549	3.853419	-1.064222
H	2.562219	3.410130	-3.088051
H	1.517000	4.600228	-2.286346
H	3.261227	3.912329	1.093539
H	1.941278	4.883487	0.410219
H	3.738422	4.755390	-1.268337
H	3.830329	2.995069	-1.080409
C	2.827310	-0.258052	1.653124
C	2.337735	-1.695531	1.771928
C	4.093346	-0.201508	0.830332
H	2.066752	0.319707	1.133192
C	1.038820	-1.652775	2.557802
H	3.081490	-2.304908	2.301357
O	2.079559	-2.236202	0.483595
C	3.720302	-0.802541	-0.525777
H	4.924237	-0.736720	1.294355
H	0.260417	-1.152940	1.972653
H	0.705233	-2.652040	2.842194
C	3.213905	-2.239403	-0.362595
H	2.849318	-2.631418	-1.319678
O	4.254878	-3.012276	0.133264
C	3.976593	-4.405786	0.169734
H	4.895693	-4.896493	0.491089
H	3.695112	-4.768149	-0.827348
H	3.172658	-4.628764	0.879359
C	-0.440923	1.668004	3.252652
H	-0.203257	2.496502	3.943182
H	-0.837524	0.841510	3.869411
C	-1.507085	2.114019	2.270947
C	-2.446930	1.208141	1.772901
C	-1.470714	3.395208	1.712267
C	-3.304057	1.560912	0.730843

H	-2.489773	0.202261	2.187496
C	-2.322194	3.747419	0.667944
H	-0.742158	4.115856	2.078765
C	-3.248826	2.832957	0.153315
H	-4.017097	0.831187	0.351683
H	-2.260668	4.745594	0.238336
C	-4.175193	3.216684	-0.974753
H	-4.451263	2.344534	-1.576615
H	-5.102909	3.658077	-0.590093
H	-3.710782	3.955091	-1.636829
O	4.460685	1.162465	0.618083
O	4.852275	-0.767878	-1.387660
H	2.917015	-0.211930	-0.973773
O	6.071607	0.239609	-2.848814
C	4.855967	0.189304	-2.328728
O	3.908220	0.875856	-2.644252
C	6.320148	1.293441	-3.809171
H	7.188610	0.939358	-4.365010
H	5.463881	1.365990	-4.482884
C	6.602744	2.606995	-3.105315
H	6.840337	3.373879	-3.849788
H	5.733586	2.942609	-2.531818
H	7.457086	2.506331	-2.428743
O	5.838646	2.802919	0.544871
C	5.721636	1.526256	0.875952
O	6.596748	0.817193	1.322752
C	7.141835	3.400764	0.709358
H	7.872342	2.799193	0.161503
H	7.399434	3.385061	1.771856
C	7.049567	4.810029	0.168436
H	8.019369	5.304755	0.279878
H	6.784109	4.803355	-0.893363
H	6.299850	5.389947	0.715322

TS1-c

C	-0.701331	-1.490875	-0.973475
O	-0.794623	-0.942446	-2.206538
O	-1.776058	-1.321003	-0.156111
O	0.015682	-2.467617	-0.792127

O	0.423761	0.098495	-0.215323
H	1.708017	0.080067	-0.953993
H	1.830729	-2.119486	-0.679197
N	2.849366	-2.076303	-0.593178
N	2.698332	0.058595	-1.408537
C	3.463969	-0.951093	-0.993601
N	4.807825	-0.874162	-0.979148
C	0.566539	-0.042921	1.158658
H	0.650049	-1.109448	1.444828
H	-0.327454	0.349155	1.682093
C	1.789866	0.684633	1.689880
C	1.841810	2.083043	1.685095
C	2.902253	-0.007462	2.169806
C	2.966560	2.761807	2.145326
H	0.985005	2.644930	1.317644
C	4.033557	0.670321	2.628163
H	2.887327	-1.095338	2.182921
C	4.086525	2.066040	2.620875
H	2.979289	3.850109	2.134647
H	4.887729	0.102458	2.992231
C	3.286186	1.324131	-1.815236
C	4.577834	1.579138	-1.051644
H	2.549243	2.105291	-1.609077
H	3.476578	1.321219	-2.896916
C	5.505716	0.388059	-1.227988
C	5.655071	-2.009570	-0.616060
C	3.565531	-3.211133	-0.042012
H	5.074328	2.483014	-1.416724
H	4.347704	1.716972	0.009315
H	6.338624	0.444957	-0.518778
H	5.930252	0.366632	-2.240470
C	4.910716	-3.329720	-0.743704
H	6.528154	-1.995181	-1.276943
H	6.013003	-1.867598	0.412777
H	2.953904	-4.101850	-0.200634
H	3.711486	-3.091379	1.040611
H	5.509909	-4.127426	-0.296644
H	4.752211	-3.573010	-1.800189
C	-2.770296	-0.405892	-0.590145
C	-2.120061	0.835993	-1.186194
C	-3.622944	-0.002251	0.596736
H	-3.398487	-0.894350	-1.347827
C	-1.276637	0.401418	-2.371961
H	-1.485661	1.310010	-0.434993

O	-3.132545	1.731559	-1.628214
C	-4.617103	1.063064	0.147276
H	-2.992191	0.370890	1.406989
O	-4.364773	-1.134272	1.053740
H	-1.886009	0.385288	-3.278930
H	-0.413658	1.054430	-2.510364
C	-3.909089	2.233630	-0.559423
H	-4.642354	2.896658	-1.032468
O	-3.157176	2.913646	0.389929
C	-2.563063	4.111497	-0.090497
H	-2.101076	4.594475	0.771101
H	-3.324739	4.775094	-0.520071
H	-1.798459	3.897980	-0.845510
C	5.323603	2.805524	3.067590
H	5.067938	3.731687	3.593090
H	5.937139	2.191733	3.734733
H	5.945058	3.079770	2.205545
H	-5.332687	0.627820	-0.555651
O	-5.307277	1.494757	1.316998
O	-4.945227	-2.591214	2.524414
C	-4.166240	-1.541857	2.313279
C	-4.869868	-3.185525	3.840285
H	-5.131916	-2.423468	4.578925
H	-3.839456	-3.506241	4.015165
C	-5.834921	-4.349481	3.863426
H	-5.801252	-4.823488	4.849421
H	-6.859314	-4.013128	3.676909
H	-5.565241	-5.097295	3.111594
O	-3.409334	-1.039076	3.115184
O	-7.021495	2.302493	2.334984
C	-8.371495	2.821762	2.376903
H	-8.404402	3.381316	3.312230
H	-8.509170	3.509132	1.539530
C	-9.389687	1.698711	2.361877
H	-10.394401	2.122853	2.460036
H	-9.344431	1.137722	1.423952
H	-9.222195	1.011900	3.197120
C	-6.536688	1.991666	1.143718
O	-7.092229	2.131884	0.074429

TS1-d

C	0.415797	-2.776884	-1.935480
O	1.342596	-3.596692	-1.361617
O	0.696357	-1.432995	-1.836044
O	-0.216101	-3.165292	-2.905003
O	-0.904869	-2.747129	-0.402470
H	-1.593682	-1.039464	-1.989206
H	-1.316696	-1.316670	0.089979
N	-2.051373	-0.138428	-1.918161
C	-2.136559	0.378397	-0.686403
N	-1.588093	-0.311528	0.314805
N	-2.756731	1.551068	-0.476192
C	-1.908249	-3.703299	-0.534017
H	-2.010547	-4.291866	0.397027
H	-1.653342	-4.413578	-1.339252
C	-3.247259	-3.063609	-0.863712
C	-3.703918	-2.972520	-2.179497
C	-3.999574	-2.436098	0.134997
C	-4.864557	-2.262836	-2.491324
H	-3.125161	-3.437424	-2.974780
C	-5.150259	-1.716976	-0.174441
H	-3.661931	-2.490643	1.168702
H	-5.191934	-2.198769	-3.527448
H	-5.706142	-1.222300	0.620300
C	-1.766576	0.114551	1.687391
C	-1.645874	1.629746	1.739423
H	-0.990036	-0.364093	2.287531
H	-2.745098	-0.208402	2.073434
C	-2.681723	2.248654	0.809836
C	-3.300996	2.322593	-1.589588
C	-2.568293	0.499417	-3.112559
H	-1.806450	1.999676	2.755932
H	-0.637008	1.917126	1.426033
H	-2.424948	3.292987	0.601107
H	-3.677336	2.234060	1.271325
C	-3.724360	1.411269	-2.731377
H	-4.162067	2.880473	-1.208450
H	-2.546091	3.047095	-1.923683
H	-2.900573	-0.287073	-3.794913
H	-1.774274	1.070128	-3.612250
H	-4.026762	2.016992	-3.589914
H	-4.580444	0.802757	-2.421825

C	1.766620	-1.060397	-0.990211
C	1.721377	-1.855655	0.308943
C	1.650756	0.415141	-0.660886
H	2.718922	-1.254885	-1.504072
C	1.808295	-3.335144	-0.032593
H	0.785346	-1.645767	0.829908
O	2.826627	-1.487469	1.126255
C	2.769283	0.782332	0.307142
H	0.671076	0.622806	-0.225440
H	2.852870	-3.656604	-0.020711
H	1.221116	-3.936933	0.663071
C	2.770025	-0.138798	1.541529
H	3.681999	0.011503	2.130380
C	1.596249	-0.494327	3.554677
H	0.743736	-0.075272	4.091220
H	2.515783	-0.299115	4.121219
H	1.462651	-1.575532	3.438113
C	-6.856916	-0.844196	-1.825273
H	-6.913603	-0.612625	-2.893877
H	-7.754273	-1.417306	-1.561806
H	-6.899378	0.099490	-1.269730
C	-5.602217	-1.616492	-1.496405
O	1.638208	0.155680	2.292403
O	1.811156	1.171374	-1.864096
H	3.737707	0.681020	-0.190797
O	2.567325	2.145583	0.671640
C	3.644108	2.831996	1.066573
O	3.261297	4.071263	1.331027
O	4.766351	2.382190	1.166031
C	4.291291	5.000838	1.741869
H	3.744611	5.764583	2.295921
H	4.978611	4.487000	2.417312
C	5.008564	5.587788	0.542233
H	5.733846	6.332598	0.886113
H	5.548033	4.814473	-0.012234
H	4.300318	6.081088	-0.130446
O	1.208096	2.664176	-3.291754
C	0.916341	2.132283	-2.113561
O	-0.002770	2.459714	-1.394704
C	0.342822	3.733521	-3.733559
H	0.387791	4.541378	-2.998168
H	-0.682681	3.355342	-3.775057
C	0.832743	4.177649	-5.093316
H	0.195681	4.990062	-5.456707

H	1.862106	4.544403	-5.038237
H	0.788014	3.355047	-5.813359

INT2-a

Energy: -1378886.3622536

C	0.80485	-0.76984	-1.37914
O	0.83072	-2.19811	-1.27154
O	-0.56207	-0.31945	-1.48862
O	1.50746	-0.35521	-2.36279
O	1.28500	-0.34700	-0.06660
H	2.93875	-1.21462	0.00830
H	3.13623	-0.39162	-2.03158
N	3.93565	-1.42738	0.09670
C	4.72778	-0.77838	-0.78006
N	4.17349	-0.30454	-1.89510
N	6.04253	-0.63757	-0.54052
C	4.39812	-1.77010	1.43361
C	1.33259	1.06643	0.12228
H	0.35560	1.41504	0.48324
H	1.54332	1.55169	-0.83644
C	2.41943	1.37294	1.11973
C	3.65317	1.86986	0.69866
C	2.24045	1.10836	2.48060
C	4.69447	2.06501	1.60401
H	3.80481	2.09121	-0.35482
C	3.27657	1.31518	3.38822
H	1.28247	0.73119	2.83188
C	4.52640	1.78251	2.96308
H	5.65166	2.43970	1.24689
H	3.11597	1.10139	4.44266
C	5.84899	-2.21082	1.35019
H	3.76063	-2.57387	1.80926
H	4.29602	-0.90897	2.10624
C	6.66563	-1.10713	0.69846
C	6.91542	0.08613	-1.46669
C	4.93121	0.39198	-2.92207
H	6.24443	-2.41189	2.34927
H	5.92416	-3.13213	0.76191
H	7.66629	-1.46925	0.44381
H	6.77802	-0.25398	1.38119

C	6.12902	1.08897	-2.29560
H	7.67011	0.59983	-0.86396
H	7.43436	-0.63449	-2.11168
H	4.25899	1.11047	-3.39745
H	5.26373	-0.31656	-3.69161
H	6.77437	1.50747	-3.07229
H	5.79195	1.91291	-1.65721
C	-1.40599	-0.79343	-0.46621
C	-1.41680	-2.31815	-0.48357
C	-2.81373	-0.26646	-0.66230
H	-1.04319	-0.45928	0.51732
C	0.01142	-2.78991	-0.27407
H	-1.77441	-2.66888	-1.45994
O	-2.25251	-2.81457	0.55302
C	-3.71531	-0.89779	0.39124
H	-3.17676	-0.48004	-1.67008
O	-2.81835	1.14835	-0.44396
H	0.35463	-2.52062	0.73320
H	0.09586	-3.87146	-0.40388
C	-3.60230	-2.43368	0.39205
H	-4.11942	-2.85315	1.26294
O	-4.16028	-2.90210	-0.79184
C	-4.28032	-4.31613	-0.85335
H	-4.81804	-4.54176	-1.77482
H	-4.84978	-4.69277	0.00636
H	-3.29566	-4.79589	-0.87544
C	5.66512	1.94311	3.93910
H	5.30984	2.29451	4.91319
H	6.17194	0.98362	4.10202
H	6.41164	2.65266	3.56905
H	-3.42745	-0.53913	1.38324
O	-5.04795	-0.47505	0.10659
C	-5.89932	-0.42527	1.13520
O	-5.63959	-0.73789	2.27856
O	-7.06216	0.01524	0.68086
C	-8.12280	0.18193	1.65040
H	-9.03239	0.12242	1.05186
H	-8.09463	-0.65691	2.34917
C	-8.00951	1.51597	2.36170
H	-8.02171	2.34113	1.64309
H	-8.86135	1.63577	3.03923
H	-7.09073	1.57122	2.95274
O	-3.45988	1.57953	-2.58244
C	-3.13339	1.94065	-1.47218

O	-3.02999	3.19633	-1.05973
C	-3.33657	4.21514	-2.03721
H	-4.36536	4.07001	-2.37766
H	-2.66321	4.09067	-2.88939
C	-3.14973	5.55561	-1.36219
H	-3.37475	6.35266	-2.07780
H	-3.82280	5.66050	-0.50584
H	-2.11829	5.68096	-1.01899

INT2-b

C	1.733232	-0.125181	3.307419
O	2.919141	-0.049281	2.488626
O	1.903430	0.473652	4.422373
O	1.365261	-1.497746	3.485377
O	0.738565	0.486664	2.428845
H	1.628429	2.042386	2.001326
N	2.068961	2.931418	1.753789
C	2.802815	3.541935	2.689659
N	3.010421	2.921925	3.853365
H	2.583070	1.982706	4.019477
N	3.330792	4.759665	2.448403
C	1.703053	3.545405	0.488449
C	1.663414	5.055526	0.657047
H	0.720527	3.156229	0.208382
H	2.423816	3.261184	-0.288259
C	2.978225	5.529519	1.254734
C	4.216678	5.419297	3.407978
C	3.788898	3.513800	4.928394
H	1.504805	5.543475	-0.308267
H	0.833569	5.327327	1.317810
H	2.905447	6.579756	1.554246
H	3.787577	5.449204	0.518952
C	4.867510	4.407923	4.337535
H	4.975908	5.961284	2.833887
H	3.642740	6.160253	3.980105
H	4.225067	2.697213	5.508185
H	3.139243	4.093677	5.597308
H	5.406190	4.934518	5.129658
H	5.588337	3.795741	3.783463

C	2.817734	-0.714721	1.253230
C	2.542510	-2.190326	1.520792
C	4.096403	-0.559433	0.458452
H	1.991443	-0.297766	0.660879
C	1.241118	-2.276136	2.304139
H	3.355839	-2.605006	2.129651
O	2.432494	-2.907166	0.297986
C	3.973724	-1.415150	-0.799414
H	4.970118	-0.845420	1.048674
H	0.406131	-1.924202	1.682850
H	1.038940	-3.300452	2.625624
C	3.624912	-2.870855	-0.460029
H	3.396929	-3.429705	-1.375757
O	4.706823	-3.431062	0.208536
C	4.590032	-4.830237	0.424927
H	5.533424	-5.156237	0.864091
H	4.426804	-5.353976	-0.525923
H	3.767661	-5.057255	1.112084
C	-0.555956	0.656678	2.996208
H	-0.457879	0.804392	4.076656
H	-1.153160	-0.246161	2.812719
C	-1.176118	1.864019	2.343377
C	-1.807201	1.762929	1.101118
C	-1.043715	3.128105	2.921761
C	-2.281614	2.899149	0.448499
H	-1.916680	0.786952	0.633011
C	-1.523689	4.262403	2.271771
H	-0.541191	3.228449	3.881494
C	-2.144137	4.168332	1.021684
H	-2.760927	2.798659	-0.522852
H	-1.403675	5.237771	2.738713
C	-2.666621	5.396730	0.318961
H	-2.561227	5.306474	-0.767002
H	-3.731306	5.548677	0.534187
H	-2.132794	6.296308	0.641595
O	4.244250	0.795522	0.013131
O	5.207631	-1.379254	-1.512470
H	3.180283	-1.017951	-1.437075
O	6.539182	-0.528292	-2.970231
C	5.272050	-0.579494	-2.585439
O	4.336585	-0.018702	-3.113176
C	6.852496	0.377192	-4.053543
H	7.788195	-0.011790	-4.456227
H	6.073041	0.302420	-4.814561

C	7.009695	1.795380	-3.538947
H	7.306715	2.450765	-4.364350
H	6.069165	2.169994	-3.124111
H	7.782356	1.842244	-2.765254
O	5.175783	2.729679	-0.027017
C	5.155629	1.564070	0.611493
O	5.856081	1.253402	1.549712
C	6.139403	3.699702	0.432617
H	7.065363	3.183698	0.694533
H	5.735484	4.169986	1.334126
C	6.354635	4.698406	-0.683342
H	7.039802	5.479424	-0.339290
H	6.795513	4.212187	-1.558682
H	5.416075	5.172235	-0.986402

INT2-c

C	-0.453387	-1.081854	-0.736953
O	-0.692520	-0.575831	-2.045934
O	-1.700470	-1.097191	-0.006227
O	0.105771	-2.231819	-0.738362
O	0.362368	-0.025027	-0.131602
H	1.868150	0.028607	-1.165513
H	1.763687	-2.137808	-0.637642
N	2.805658	-2.132343	-0.515170
N	2.832129	-0.057025	-1.498965
C	3.507258	-1.096003	-0.975996
N	4.849799	-1.090910	-0.936614
C	0.617200	-0.187820	1.257702
H	0.807612	-1.244496	1.478424
H	-0.270242	0.125660	1.823403
C	1.812656	0.650394	1.631681
C	1.795281	2.036552	1.444939
C	2.960549	0.068469	2.169051
C	2.897359	2.813941	1.787745
H	0.908776	2.509948	1.028583
C	4.063114	0.848851	2.517756
H	2.996537	-1.008031	2.318630
C	4.051764	2.233032	2.329414
H	2.862462	3.890397	1.633954

H	4.946695	0.370279	2.934576
C	3.501472	1.141083	-1.983622
C	4.788356	1.361230	-1.203657
H	2.812283	1.978139	-1.852514
H	3.712726	1.042324	-3.055697
C	5.634334	0.100145	-1.268396
C	5.618401	-2.259071	-0.503531
C	3.444453	-3.275152	0.112860
H	5.353813	2.198987	-1.620999
H	4.544409	1.593909	-0.162582
H	6.458120	0.156242	-0.549129
H	6.070171	-0.029072	-2.267563
C	4.784991	-3.529952	-0.560982
H	6.491203	-2.340280	-1.159618
H	5.981800	-2.080216	0.516937
H	2.774035	-4.130248	0.003943
H	3.587123	-3.095680	1.187274
H	5.323161	-4.337983	-0.058519
H	4.620283	-3.826456	-1.602757
C	-2.687203	-0.195695	-0.450116
C	-2.068314	1.105334	-0.959346
C	-3.627385	0.124806	0.700092
H	-3.266356	-0.649312	-1.269570
C	-1.160676	0.767507	-2.137494
H	-1.497690	1.576877	-0.154046
O	-3.093100	1.992745	-1.396396
C	-4.642327	1.167121	0.250555
H	-3.061540	0.481928	1.563468
O	-4.347593	-1.056639	1.065413
H	-1.739878	0.822490	-3.063926
H	-0.317279	1.463549	-2.199441
C	-3.946523	2.400955	-0.350028
H	-4.679531	3.063109	-0.825150
O	-3.276322	3.056524	0.677564
C	-2.712189	4.302651	0.295950
H	-2.315429	4.754818	1.205611
H	-3.479471	4.958335	-0.136057
H	-1.902271	4.164931	-0.429105
C	5.260743	3.074679	2.653438
H	4.971337	4.064298	3.021452
H	5.889287	2.596444	3.411068
H	5.877839	3.225274	1.758446
H	-5.297133	0.742325	-0.515027
O	-5.418257	1.509522	1.398229

O	-4.905910	-2.636868	2.411251
C	-4.169825	-1.540391	2.297537
C	-4.847566	-3.312914	3.686702
H	-5.170210	-2.614764	4.463730
H	-3.809953	-3.598567	3.879317
C	-5.757019	-4.518114	3.599086
H	-5.735147	-5.054463	4.552980
H	-6.789119	-4.216397	3.396319
H	-5.426917	-5.201717	2.811050
O	-3.465379	-1.062832	3.161539
O	-7.217045	2.201787	2.353448
C	-8.583190	2.677220	2.340754
H	-8.691112	3.180386	3.302195
H	-8.693231	3.407786	1.536453
C	-9.561858	1.527979	2.199727
H	-10.583885	1.916526	2.259249
H	-9.442004	1.023894	1.236391
H	-9.422702	0.798915	3.003800
C	-6.651149	1.974761	1.178121
O	-7.149195	2.158144	0.086924

INT2-d

C	0.178060	-2.275749	-1.304677
O	1.273743	-3.142037	-1.022051
O	0.603573	-0.901032	-1.095952
O	-0.289368	-2.461532	-2.479667
O	-0.789956	-2.404807	-0.221622
H	-1.303793	-1.148008	-2.810119
H	-1.645013	-0.627954	-0.674963
N	-1.935636	-0.371285	-3.111844
C	-2.580097	0.337190	-2.183702
N	-2.290070	0.127773	-0.895640
N	-3.485366	1.274704	-2.531236
C	-1.664770	-3.529271	-0.325076
H	-1.732346	-3.957144	0.681463
H	-1.229405	-4.277319	-0.993905
C	-3.033087	-3.106635	-0.808739
C	-3.381075	-3.187231	-2.159217
C	-3.954091	-2.547362	0.079296

C	-4.600003	-2.690407	-2.610628
H	-2.671713	-3.610893	-2.864124
C	-5.167036	-2.032949	-0.375726
H	-3.708982	-2.485715	1.138088
H	-4.848840	-2.765392	-3.667470
H	-5.859552	-1.583345	0.333064
C	-2.916161	0.830570	0.209155
C	-3.378201	2.201181	-0.256761
H	-2.174896	0.920871	1.006856
H	-3.763647	0.246585	0.591128
C	-4.206029	2.050599	-1.522455
C	-3.862594	1.487694	-3.927995
C	-2.223243	-0.270654	-4.532896
H	-3.982485	2.678340	0.519539
H	-2.505575	2.831233	-0.453324
H	-4.417304	3.031799	-1.957656
H	-5.166974	1.562492	-1.307834
C	-3.643808	0.226964	-4.747387
H	-4.918755	1.772067	-3.940820
H	-3.285620	2.327383	-4.339371
H	-2.085046	-1.263900	-4.968388
H	-1.506485	0.407017	-5.014973
H	-3.816296	0.440226	-5.805614
H	-4.357298	-0.541000	-4.431211
C	1.833562	-0.727639	-0.450968
C	1.945238	-1.635812	0.767273
C	1.947151	0.715560	0.005227
H	2.663025	-0.953901	-1.138973
C	1.806844	-3.084896	0.296085
H	1.151091	-1.383667	1.478786
O	3.218237	-1.441759	1.382068
C	3.276409	0.892914	0.718641
H	1.119705	0.973048	0.670267
H	2.798226	-3.541671	0.234816
H	1.184984	-3.666090	0.985102
C	3.408028	-0.130828	1.868066
H	4.428813	-0.125211	2.266898
C	2.621186	-0.520865	4.054909
H	1.916317	-0.087870	4.765562
H	3.641599	-0.434595	4.450822
H	2.380905	-1.577935	3.896672
C	-6.780330	-1.464119	-2.245432
H	-6.589232	-0.467506	-2.664022
H	-7.225328	-2.070735	-3.041168

H	-7.519587	-1.349491	-1.446483
C	-5.501751	-2.078801	-1.732542
O	2.488568	0.221187	2.851292
O	1.897829	1.562800	-1.147397
H	4.105492	0.735423	0.023508
O	3.318586	2.232359	1.208070
C	4.527100	2.751736	1.440615
O	4.362731	3.997442	1.858761
O	5.582164	2.170164	1.295271
C	5.562016	4.758065	2.134555
H	5.226398	5.527070	2.831099
H	6.282879	4.107544	2.634474
C	6.130774	5.363919	0.866541
H	6.997595	5.982680	1.121095
H	6.457266	4.586461	0.169831
H	5.388156	5.997473	0.371981
O	0.723192	2.659391	-2.588131
C	0.774263	2.266862	-1.322843
O	-0.050755	2.517303	-0.471028
C	-0.440700	3.428447	-2.961666
H	-0.427584	4.371009	-2.407096
H	-1.333445	2.866054	-2.674073
C	-0.376821	3.649813	-4.456014
H	-1.246106	4.236198	-4.770399
H	0.527731	4.198681	-4.734842
H	-0.389857	2.696588	-4.993338

INT3-a

C	-0.266350	-1.463999	-1.652758
O	-0.547712	-2.864852	-1.403869
O	-1.515942	-0.769286	-1.838577
O	0.496266	-1.326725	-2.670457
O	0.286171	-1.040019	-0.393316
H	1.291824	-3.334079	-1.041427
H	2.064060	-1.665140	-2.251035
N	3.046344	-1.834107	-1.926448
N	2.216890	-3.590089	-0.693747
C	3.240968	-2.771614	-1.001544
N	4.436008	-2.929409	-0.407464

C	0.788261	0.275843	-0.372968
H	-0.009987	0.980282	-0.092522
H	1.136116	0.552036	-1.376226
C	1.937341	0.373845	0.603598
C	2.641669	1.576586	0.724330
C	2.340375	-0.709671	1.380726
C	3.731779	1.680592	1.582850
H	2.342244	2.438048	0.130228
C	3.435200	-0.603311	2.239708
H	1.799480	-1.646373	1.297757
C	4.155863	0.587061	2.350367
H	4.269546	2.623876	1.652675
H	3.733388	-1.466983	2.830829
C	2.278634	-4.523521	0.418030
C	3.680801	-5.106356	0.483196
H	1.532944	-5.301596	0.241430
H	2.027489	-4.023211	1.364083
C	4.687208	-3.971669	0.588119
C	5.543022	-2.001912	-0.648361
C	4.086386	-0.903820	-2.333454
H	3.783581	-5.762580	1.351229
H	3.873198	-5.699408	-0.417553
H	5.703151	-4.344177	0.423039
H	4.656221	-3.517844	1.587635
C	5.047732	-0.666545	-1.179001
H	6.057089	-1.859388	0.307830
H	6.251892	-2.467052	-1.345632
H	3.596109	0.025863	-2.633340
H	4.622982	-1.297626	-3.206496
H	5.901473	-0.069321	-1.510820
H	4.536459	-0.119991	-0.381807
C	-2.422758	-0.936570	-0.774091
C	-2.751436	-2.418481	-0.617958
C	-3.695733	-0.158273	-1.043193
H	-1.980857	-0.572455	0.164757
C	-1.454437	-3.161487	-0.348706
H	-3.192209	-2.791840	-1.551077
O	-3.653653	-2.610223	0.462552
C	-4.692804	-0.464197	0.067865
H	-4.109950	-0.408537	-2.022406
O	-3.407501	1.242873	-0.992182
H	-1.039033	-2.865959	0.622988
H	-1.605802	-4.243524	-0.362145
C	-4.898759	-1.979822	0.248776

H	-5.475736	-2.179819	1.159127
O	-5.561586	-2.456925	-0.875914
C	-5.977746	-3.810884	-0.769694
H	-6.565735	-4.025455	-1.662663
H	-6.599796	-3.954209	0.123477
H	-5.116825	-4.486933	-0.725420
C	5.365722	0.695141	3.245416
H	5.340878	1.614706	3.840123
H	5.429141	-0.153849	3.933178
H	6.289071	0.714760	2.653666
H	-4.323108	-0.059947	1.014176
O	-5.913477	0.188433	-0.277839
O	-7.779894	1.138159	0.213248
C	-6.725924	0.524562	0.728344
O	-6.522992	0.295349	1.902546
C	-8.775188	1.622702	1.144513
H	-8.908966	0.879465	1.933436
H	-9.684407	1.680096	0.545174
C	-8.388445	2.978156	1.702676
H	-9.191415	3.342142	2.352135
H	-7.470966	2.913790	2.294800
H	-8.242259	3.702767	0.895821
O	-3.216635	3.207221	-1.842726
C	-3.578895	1.959477	-2.106313
O	-3.994489	1.547089	-3.167903
C	-3.332985	4.147549	-2.933475
H	-2.718473	3.791165	-3.764422
H	-4.377361	4.176541	-3.255616
C	-2.863590	5.490814	-2.420965
H	-1.820581	5.442550	-2.093620
H	-2.938958	6.228552	-3.226033
H	-3.481875	5.829058	-1.583893

INT3-b

C	0.617734	-1.895039	1.235678
O	1.577366	-2.852647	1.703740
O	1.325366	-0.620264	1.073492
O	-0.345482	-1.756380	2.069014
O	0.276407	-2.313055	-0.098021

H	-0.387227	0.000496	2.530332
H	-2.068699	-1.034544	1.993862
N	-2.724242	-0.248630	2.054744
N	-0.835888	0.925626	2.597352
C	-2.112591	0.939261	2.203981
N	-2.768089	2.090285	1.998348
C	-1.084467	-2.425246	-0.441063
H	-1.665495	-2.703812	0.446800
H	-1.150047	-3.257694	-1.150409
C	-1.686104	-1.183549	-1.071701
C	-1.192968	0.097871	-0.819410
C	-2.816297	-1.309127	-1.884757
C	-1.832844	1.217801	-1.344601
H	-0.310866	0.221127	-0.198682
C	-3.454752	-0.184807	-2.407281
H	-3.214867	-2.298285	-2.103848
C	-2.976908	1.101961	-2.139745
H	-1.429031	2.205575	-1.134178
H	-4.337999	-0.311834	-3.029778
C	-0.020891	2.121909	2.717044
C	-0.589910	3.218197	1.830579
H	0.996160	1.860373	2.415892
H	0.008232	2.453345	3.762322
C	-2.078674	3.377471	2.095290
C	-4.158511	2.117449	1.541765
C	-4.040240	-0.358276	1.446135
H	-0.078509	4.164316	2.023960
H	-0.439881	2.952887	0.778808
H	-2.526256	4.040596	1.348992
H	-2.258826	3.814107	3.085747
C	-4.881935	0.826606	1.892669
H	-4.644484	2.973167	2.019938
H	-4.168099	2.282698	0.456097
H	-4.483088	-1.302089	1.772325
H	-3.956269	-0.377296	0.352542
H	-5.853802	0.810858	1.392511
H	-5.054260	0.774552	2.973487
C	2.424847	-0.690650	0.200777
C	3.440103	-1.669370	0.785421
C	3.063087	0.671428	0.011210
H	2.099981	-1.056234	-0.783806
C	2.748230	-3.016990	0.921020
H	3.745918	-1.318965	1.779559
O	4.575419	-1.789256	-0.061376

C	4.322665	0.476444	-0.833937
H	3.295448	1.148262	0.966206
O	2.144831	1.493393	-0.724316
H	2.508484	-3.419067	-0.072145
H	3.380639	-3.732627	1.452005
C	5.263534	-0.567593	-0.217595
H	6.087355	-0.788939	-0.907203
O	5.743922	-0.059752	0.984535
C	6.762515	-0.851175	1.579448
H	7.109249	-0.302412	2.455697
H	7.597513	-0.993596	0.881031
H	6.374914	-1.828519	1.887248
C	-3.644547	2.326815	-2.715002
H	-3.140096	2.654284	-3.632392
H	-4.692247	2.131537	-2.964803
H	-3.612053	3.164749	-2.009890
H	4.035706	0.128893	-1.829317
O	5.021438	1.713404	-0.955061
C	4.997359	2.327678	-2.144264
O	5.650749	3.472754	-2.015899
O	4.473746	1.905879	-3.152980
C	5.677407	4.340113	-3.173029
H	6.552782	4.968531	-3.006504
H	5.833645	3.731620	-4.066140
C	4.407828	5.164307	-3.262938
H	4.265367	5.753600	-2.351754
H	4.482869	5.852997	-4.110832
H	3.533493	4.524825	-3.417633
C	2.036750	2.781418	-0.396029
O	2.622084	3.346129	0.503371
O	1.159791	3.334361	-1.225572
C	0.946076	4.756641	-1.091085
H	0.836044	5.001256	-0.032664
H	1.831874	5.268656	-1.476979
C	-0.296093	5.101975	-1.881270
H	-1.178155	4.607926	-1.461530
H	-0.458493	6.183540	-1.841476
H	-0.191405	4.805457	-2.929158

INT3-c

C	-0.144194	0.087889	0.467226
O	-0.390203	0.128670	-0.962807
O	-1.436437	-0.055379	1.111241
O	0.647380	-0.865535	0.772774
O	0.283339	1.423500	0.812219
H	1.207448	-0.270275	-1.798784
H	2.081143	-1.121095	-0.005197
N	3.002319	-1.293276	-0.470887
N	2.063836	-0.375579	-2.349513
C	3.155492	-0.820135	-1.706463
N	4.353903	-0.840725	-2.324427
C	1.480329	1.551556	1.543187
H	1.658259	0.649740	2.137502
H	1.323234	2.388095	2.235354
C	2.695782	1.842027	0.684050
C	3.977917	1.657169	1.211366
C	2.582762	2.338154	-0.612248
C	5.111388	1.945626	0.457902
H	4.091798	1.271541	2.223068
C	3.720017	2.633427	-1.365174
H	1.595881	2.484145	-1.040222
C	5.002498	2.437751	-0.849177
H	6.097478	1.783271	0.889031
H	3.605370	3.027603	-2.373180
C	2.107451	0.292888	-3.639427
C	3.274418	-0.247803	-4.449172
H	2.206159	1.377419	-3.501755
H	1.157696	0.104360	-4.145929
C	4.543490	-0.178452	-3.613531
C	5.553646	-1.203924	-1.573288
C	4.098956	-1.786118	0.346392
H	3.078635	-1.286131	-4.738629
H	3.404597	0.340611	-5.361231
H	4.842524	0.865751	-3.450203
H	5.366105	-0.686049	-4.124442
C	5.229666	-2.275727	-0.543929
H	6.291908	-1.568752	-2.292172
H	5.966578	-0.311972	-1.082864
H	3.713635	-2.595242	0.972305
H	4.454402	-0.986444	1.007605
H	6.116923	-2.487876	0.058522

H	4.936595	-3.199595	-1.055109
C	-2.561916	0.279386	0.337767
C	-2.296420	1.537357	-0.489213
C	-3.745149	0.526512	1.257961
H	-2.814593	-0.544549	-0.348414
C	-1.156800	1.222563	-1.454526
H	-2.022061	2.357259	0.182005
O	-3.452339	1.896021	-1.240176
C	-4.932452	1.010600	0.436158
H	-3.482845	1.253878	2.029198
O	-4.119093	-0.708177	1.878885
H	-1.574245	0.891364	-2.409661
H	-0.522226	2.098538	-1.623022
C	-4.557789	2.225522	-0.428454
H	-5.365359	2.459229	-1.132241
O	-4.311458	3.298617	0.420612
C	-4.116391	4.533699	-0.252902
H	-4.029517	5.298030	0.520057
H	-4.974164	4.760731	-0.899438
H	-3.201792	4.515545	-0.855854
C	6.234687	2.737299	-1.667213
H	6.777662	1.818272	-1.921370
H	5.977561	3.240388	-2.604732
H	6.930458	3.380182	-1.116918
O	-5.974685	1.325879	1.358588
H	-5.270450	0.213730	-0.231657
O	-8.043822	1.529567	1.909533
C	-9.463368	1.454099	1.642214
H	-9.903772	2.108704	2.395035
H	-9.655856	1.865288	0.648948
C	-9.970603	0.031495	1.774523
H	-9.517898	-0.620331	1.021740
H	-9.752005	-0.367441	2.769759
H	-11.055920	0.021462	1.629453
C	-7.229133	1.237919	0.907333
O	-7.550404	0.947073	-0.226084
O	-4.492823	-1.987882	3.564428
C	-4.557292	-2.250711	4.983407
H	-3.568999	-2.069902	5.414441
H	-5.269716	-1.553391	5.432462
C	-4.992180	-3.689087	5.154917
H	-4.274269	-4.373204	4.692436
H	-5.051741	-3.921353	6.222906
H	-5.977691	-3.856440	4.709802

C	-4.120165	-0.764882	3.213006
O	-3.834114	0.137495	3.970802

INT3-d

C	-0.208428	-1.890469	-0.728819
O	0.654493	-2.910939	-1.255131
O	0.593828	-1.138026	0.274733
O	-0.662607	-1.151624	-1.667832
O	-1.156169	-2.515370	0.132713
H	-0.311180	0.320832	0.799038
H	-0.720116	0.485784	-1.375118
N	-0.905728	1.508595	-1.247105
N	-0.831376	1.173666	1.020475
C	-1.241247	1.910884	-0.017957
N	-1.940837	3.042699	0.180239
C	-2.508534	-2.531163	-0.303581
H	-2.900596	-3.513799	-0.019483
H	-2.553088	-2.432641	-1.391022
C	-3.328407	-1.444239	0.356293
C	-3.687488	-0.284867	-0.329655
C	-3.744482	-1.581205	1.685880
C	-4.435500	0.713628	0.296286
H	-3.363818	-0.157673	-1.359607
C	-4.491751	-0.586814	2.309141
H	-3.481225	-2.480992	2.238271
C	-4.848752	0.581684	1.623705
H	-4.704468	1.610891	-0.257898
H	-4.803304	-0.716404	3.343641
C	-1.281538	1.406361	2.381201
C	-1.414406	2.905534	2.595978
H	-0.533951	0.979959	3.053331
H	-2.237524	0.899572	2.559220
C	-2.310197	3.499973	1.520512
C	-2.557999	3.782015	-0.924596
C	-1.248613	2.296937	-2.418479
H	-1.846082	3.116336	3.577940
H	-0.422081	3.365487	2.559687
H	-2.244060	4.593308	1.526359
H	-3.358470	3.228892	1.701409

C	-2.598783	2.967626	-2.208761
H	-3.571953	4.052514	-0.610268
H	-2.000317	4.714932	-1.078065
H	-1.268454	1.620731	-3.275505
H	-0.472922	3.051482	-2.602927
H	-2.839067	3.628784	-3.045663
H	-3.379350	2.201953	-2.149930
C	1.971122	-1.236660	0.032516
C	2.374308	-2.645836	0.446246
C	2.771644	-0.226135	0.823304
H	2.186275	-1.087107	-1.034227
C	1.457053	-3.612645	-0.319202
H	2.217204	-2.756212	1.525568
O	3.753605	-2.867297	0.156321
C	4.250660	-0.540825	0.587175
H	2.524811	-0.250780	1.887263
O	2.499332	1.079488	0.298843
H	2.057458	-4.317031	-0.899917
H	0.825093	-4.173790	0.377405
C	4.589444	-2.007619	0.902627
H	5.608448	-2.237440	0.567960
O	4.465616	-2.191802	2.276052
C	4.922618	-3.456948	2.731727
H	4.859281	-3.435777	3.820217
H	5.964414	-3.623136	2.427730
H	4.296716	-4.267513	2.342627
C	-5.647950	1.660079	2.312770
H	-6.598666	1.267614	2.690835
H	-5.101129	2.065661	3.172795
H	-5.871520	2.488453	1.632966
H	4.491358	-0.357510	-0.462863
O	5.052578	0.307647	1.405664
O	6.290849	2.028038	1.756179
C	6.978068	3.228479	1.333854
H	7.676288	3.427657	2.147285
H	7.537950	3.012589	0.421542
C	6.001127	4.372634	1.143403
H	5.300446	4.159886	0.330370
H	5.437619	4.555801	2.063617
H	6.554305	5.282870	0.889831
C	5.707640	1.310644	0.807337
O	5.758510	1.516672	-0.385976
C	2.267334	2.078301	1.154276
O	2.254379	1.996000	2.363955

O	2.059289	3.172610	0.434397
C	1.900913	4.422012	1.138806
H	1.527875	4.220556	2.144286
H	2.892616	4.875897	1.219978
C	0.949320	5.283606	0.339345
H	-0.026384	4.795887	0.256704
H	0.817567	6.246168	0.843329
H	1.334817	5.468342	-0.667802

TS2-a

C	-0.107837	-0.079152	-1.343251
O	-0.033954	-1.965589	-0.611409
O	-1.448118	-0.095452	-1.590025
O	0.666496	-0.141976	-2.293959
O	0.169950	0.594442	-0.192809
H	1.237470	-2.877391	-0.662472
H	2.100434	-1.307036	-1.922809
N	3.055373	-1.642587	-1.781704
N	2.160686	-3.406526	-0.619641
C	3.241058	-2.718831	-1.003550
N	4.483141	-3.098546	-0.655467
C	1.410804	1.290678	-0.107550
H	1.159031	2.299708	0.233002
H	1.841885	1.366809	-1.110065
C	2.399527	0.656018	0.842263
C	3.497841	1.406321	1.275193
C	2.278436	-0.661351	1.275025
C	4.467128	0.838092	2.097276
H	3.602849	2.443425	0.962138
C	3.252263	-1.225305	2.099257
H	1.432475	-1.250502	0.935265
C	4.367387	-0.495109	2.514996
H	5.316640	1.438233	2.416247
H	3.142487	-2.258778	2.421687
C	2.253655	-4.510677	0.320218
C	3.562299	-5.253146	0.102419
H	1.397013	-5.167822	0.150359
H	2.189563	-4.144301	1.354603
C	4.718296	-4.269368	0.188596

C	5.657328	-2.289794	-0.985857
C	4.132811	-0.762087	-2.204674
H	3.690822	-6.032967	0.857693
H	3.553895	-5.732750	-0.882829
H	5.646447	-4.738240	-0.152512
H	4.872151	-3.936791	1.224481
C	5.275336	-0.835185	-1.204995
H	6.353757	-2.375509	-0.146101
H	6.148661	-2.708421	-1.873876
H	3.726434	0.250431	-2.266915
H	4.479523	-1.047151	-3.206214
H	6.141310	-0.281154	-1.577285
H	4.963407	-0.389349	-0.255387
C	-2.329134	-0.305708	-0.493890
C	-2.345413	-1.786387	-0.108720
C	-3.713624	0.139934	-0.929777
H	-2.010163	0.294864	0.365075
C	-0.966099	-2.217219	0.381548
H	-2.615333	-2.382919	-0.989479
O	-3.301562	-1.988000	0.930590
C	-4.718241	-0.205922	0.159960
H	-3.990672	-0.331264	-1.875551
O	-3.713109	1.561926	-1.090622
H	-0.750503	-1.662447	1.318365
H	-1.005807	-3.288609	0.648014
C	-4.624015	-1.689042	0.552364
H	-5.228156	-1.888176	1.445457
O	-5.069792	-2.445862	-0.526751
C	-5.184662	-3.833268	-0.247033
H	-5.630586	-4.292104	-1.130181
H	-5.835317	-3.999439	0.621669
H	-4.203002	-4.280987	-0.056253
C	5.446198	-1.126233	3.359686
H	5.812515	-0.433437	4.124592
H	5.082696	-2.028797	3.860982
H	6.305291	-1.413903	2.740910
H	-4.518259	0.393439	1.052308
O	-6.008726	0.125386	-0.351002
O	-8.063674	0.716016	-0.117976
C	-6.959181	0.408503	0.544288
O	-6.821399	0.378724	1.749455
C	-9.216487	1.092198	0.670649
H	-9.271765	0.439715	1.544653
H	-10.060011	0.884119	0.011582

C	-9.160501	2.556519	1.059316
H	-10.076521	2.820974	1.597864
H	-8.307486	2.758831	1.713443
H	-9.087405	3.191210	0.170908
O	-3.944404	3.377449	-2.217742
C	-4.017120	2.056372	-2.294446
O	-4.308379	1.414132	-3.280521
C	-4.242402	4.102554	-3.431605
H	-3.542080	3.781027	-4.207081
H	-5.257673	3.847118	-3.746601
C	-4.102393	5.576004	-3.120937
H	-3.084200	5.813535	-2.798176
H	-4.322637	6.155560	-4.022956
H	-4.802220	5.879387	-2.336363

TS2-b

C	1.380749	-3.345671	0.191652
O	0.502914	-4.349839	-0.077650
O	0.269787	-1.879182	-0.573603
O	2.420011	-3.298357	-0.469924
O	1.318640	-2.964829	1.500626
H	1.190008	-0.858034	-1.537518
H	3.163228	-1.742632	-0.817794
N	3.659945	-0.867096	-1.022543
N	1.745758	-0.165975	-2.085436
C	3.000329	0.085344	-1.687704
N	3.600272	1.255192	-1.972359
C	2.515890	-2.508015	2.126704
H	3.374548	-2.917457	1.584751
H	2.499781	-2.954181	3.125371
C	2.644776	-1.004085	2.235997
C	1.887253	-0.124101	1.464816
C	3.610332	-0.476431	3.097502
C	2.113421	1.247870	1.532366
H	1.144581	-0.519837	0.779495
C	3.835656	0.898630	3.159073
H	4.207222	-1.143367	3.717323
C	3.096315	1.785255	2.369216
H	1.506736	1.911929	0.920100

H	4.599885	1.284679	3.830199
C	1.015082	0.785416	-2.905386
C	1.378360	2.200306	-2.481475
H	-0.050555	0.588588	-2.774943
H	1.255128	0.633158	-3.965596
C	2.883424	2.376074	-2.583867
C	4.990703	1.535252	-1.605627
C	4.935375	-0.611318	-0.378449
H	0.879638	2.940932	-3.112352
H	1.063034	2.358783	-1.445137
H	3.198431	3.287601	-2.064890
H	3.195242	2.463525	-3.632418
C	5.769128	0.265173	-1.300007
H	5.448594	2.078807	-2.438641
H	4.987588	2.201038	-0.732396
H	5.415985	-1.575355	-0.199136
H	4.783023	-0.118934	0.591008
H	6.718463	0.531590	-0.827868
H	5.988627	-0.278741	-2.225145
C	-0.936003	-1.851128	0.087819
C	-1.631456	-3.204629	-0.120242
C	-1.869577	-0.713098	-0.340896
H	-0.792349	-1.721741	1.180620
C	-0.795786	-4.312122	0.507491
H	-1.730444	-3.387375	-1.198006
O	-2.911892	-3.272768	0.505682
C	-3.227096	-0.903231	0.332263
H	-1.966815	-0.660267	-1.427858
O	-1.285626	0.509634	0.149090
H	-0.728265	-4.172185	1.591295
H	-1.235368	-5.289223	0.298679
C	-3.804118	-2.290682	0.041615
H	-4.727761	-2.445827	0.613472
O	-4.048714	-2.381218	-1.326339
C	-4.740172	-3.559850	-1.710824
H	-4.942444	-3.467217	-2.778544
H	-5.688558	-3.647393	-1.164285
H	-4.132364	-4.453129	-1.528515
C	3.329972	3.275322	2.417358
H	2.446594	3.800550	2.799230
H	4.177238	3.527915	3.062430
H	3.535282	3.673374	1.416744
H	-3.109136	-0.805024	1.414002
O	-4.162568	0.076705	-0.123785

C	-4.529529	1.035708	0.730870
O	-5.375484	1.836417	0.098053
O	-4.156429	1.149212	1.879640
C	-5.852556	2.988415	0.829602
H	-6.776040	3.257025	0.315689
H	-6.083916	2.685375	1.852981
C	-4.843841	4.119753	0.789191
H	-4.608292	4.390127	-0.244919
H	-5.265854	4.998432	1.287944
H	-3.921566	3.842072	1.308179
C	-1.463468	1.637326	-0.533026
O	-2.020996	1.757509	-1.604093
O	-0.897830	2.619760	0.162558
C	-0.988026	3.950732	-0.388225
H	-0.798625	3.905925	-1.463037
H	-2.006650	4.315007	-0.229828
C	0.036043	4.800426	0.331089
H	1.050061	4.430702	0.146280
H	-0.026769	5.830088	-0.034433
H	-0.144254	4.803792	1.410281

TS2-c

C	-0.438463	-1.270335	0.325245
O	-0.209835	-0.850912	-1.593385
O	-1.753275	-1.621233	0.237752
O	0.400662	-2.153632	0.489774
O	-0.315292	-0.023839	0.875322
H	1.195639	-0.698571	-2.222306
H	1.984536	-1.698286	-0.446280
N	2.954076	-1.458083	-0.665686
N	2.175893	-0.536943	-2.613658
C	3.191334	-0.741784	-1.777434
N	4.437994	-0.303334	-2.051828
C	0.881888	0.290935	1.572595
H	1.412437	-0.635751	1.811867
H	0.557472	0.746489	2.513976
C	1.790710	1.244719	0.831713
C	2.991272	1.622509	1.444940
C	1.490522	1.769931	-0.420961

C	3.878567	2.481318	0.807712
H	3.239280	1.231956	2.430538
C	2.378811	2.643867	-1.051386
H	0.578149	1.467388	-0.922396
C	3.588632	3.005901	-0.458878
H	4.811833	2.749204	1.298882
H	2.123681	3.045129	-2.029928
C	2.291053	0.268543	-3.817623
C	3.721659	0.243356	-4.330617
H	1.980814	1.300694	-3.608464
H	1.601235	-0.138958	-4.561873
C	4.668354	0.583734	-3.190039
C	5.499761	-0.395110	-1.052121
C	3.933312	-1.666493	0.388262
H	3.962247	-0.750807	-4.723736
H	3.845739	0.967213	-5.140567
H	4.539936	1.628564	-2.877375
H	5.708137	0.452367	-3.501701
C	5.331850	-1.647769	-0.205943
H	6.452816	-0.419675	-1.587485
H	5.487625	0.504972	-0.421538
H	3.717296	-2.627928	0.860263
H	3.839106	-0.883481	1.151759
H	6.078539	-1.654296	0.592556
H	5.488770	-2.536766	-0.826916
C	-2.719592	-0.699773	-0.260090
C	-2.171863	0.400235	-1.174333
C	-3.512879	-0.039885	0.861771
H	-3.399326	-1.320509	-0.855247
C	-1.249653	-0.184292	-2.233364
H	-1.613767	1.130220	-0.585600
O	-3.294143	1.051512	-1.767560
C	-4.608484	0.820307	0.241171
H	-2.856259	0.553656	1.500533
O	-4.155531	-1.049484	1.646197
H	-1.838373	-0.856526	-2.886158
H	-0.885141	0.643896	-2.871021
C	-4.052975	1.780031	-0.827950
H	-4.871771	2.223421	-1.406415
O	-3.317457	2.765614	-0.176586
C	-2.841208	3.790908	-1.035675
H	-2.397092	4.552234	-0.393360
H	-3.667705	4.229970	-1.609839
H	-2.083169	3.406748	-1.727669

C	4.562028	3.930006	-1.147725
H	5.543460	3.454234	-1.261625
H	4.206589	4.213432	-2.143443
H	4.712830	4.848997	-0.569706
O	-5.234392	1.526425	1.312076
H	-5.346312	0.173738	-0.242308
O	-6.907846	2.522986	2.225368
C	-8.275570	2.993514	2.242905
H	-8.268411	3.782157	2.996037
H	-8.510165	3.427083	1.268355
C	-9.233908	1.878319	2.612164
H	-9.229485	1.088009	1.855965
H	-8.970508	1.445705	3.582183
H	-10.248912	2.283668	2.679327
C	-6.497102	1.917876	1.121451
O	-7.140667	1.747351	0.106902
O	-4.474077	-2.181335	3.446051
C	-4.214454	-2.474252	4.836962
H	-3.153260	-2.712782	4.947775
H	-4.437501	-1.580732	5.426171
C	-5.097664	-3.639466	5.223621
H	-4.869044	-4.522145	4.618747
H	-4.924599	-3.887514	6.275566
H	-6.155239	-3.388406	5.097688
C	-3.785956	-1.176188	2.923481
O	-2.971239	-0.492302	3.505657

TS2-d

C	-0.147933	-1.946258	-1.696013
O	0.817847	-2.934298	-1.647257
O	0.412160	-0.871889	-0.304835
O	-0.168581	-1.223286	-2.699456
O	-1.308964	-2.437195	-1.131674
H	-0.272540	0.422164	0.733891
H	-0.263945	0.602831	-1.356385
N	-0.836526	1.452100	-1.361748
N	-0.677949	1.349300	0.920615
C	-1.169407	1.952070	-0.169001
N	-1.952558	3.039038	-0.070669

C	-2.470638	-1.637315	-1.263045
H	-3.242861	-2.279789	-1.703170
H	-2.279188	-0.821916	-1.966520
C	-2.961767	-1.098785	0.061516
C	-3.933655	-0.095603	0.070809
C	-2.520513	-1.607375	1.281934
C	-4.452087	0.387367	1.269368
H	-4.297470	0.311183	-0.870472
C	-3.049542	-1.130247	2.480932
H	-1.752181	-2.373963	1.290201
C	-4.020498	-0.124471	2.497656
H	-5.205103	1.172773	1.248915
H	-2.689758	-1.540808	3.422224
C	-0.975302	1.771384	2.278542
C	-1.276846	3.260753	2.283558
H	-0.099140	1.552763	2.893652
H	-1.825662	1.205967	2.671422
C	-2.335336	3.572546	1.236378
C	-2.569360	3.654520	-1.248208
C	-1.266530	2.036168	-2.617817
H	-1.638374	3.567225	3.268628
H	-0.362544	3.825193	2.070656
H	-2.455799	4.654427	1.124084
H	-3.307051	3.150835	1.527424
C	-2.626812	2.688734	-2.423143
H	-3.579379	3.962527	-0.961260
H	-2.007856	4.558703	-1.517425
H	-1.308602	1.231025	-3.354512
H	-0.532432	2.776712	-2.961845
H	-2.920916	3.233551	-3.323947
H	-3.380089	1.917033	-2.234700
C	1.761824	-1.109686	-0.138203
C	1.914997	-2.495362	0.487586
C	2.486955	-0.092908	0.735586
H	2.284902	-1.115280	-1.110847
C	1.137333	-3.493838	-0.375454
H	1.492442	-2.482434	1.499944
O	3.295942	-2.862561	0.570060
C	3.938367	-0.552481	0.879543
H	2.014688	0.017965	1.715358
O	2.449132	1.166065	0.046320
H	1.752670	-4.371183	-0.584617
H	0.222284	-3.811746	0.129637
C	4.026206	-1.994615	1.404423

H	5.063063	-2.349708	1.353327
O	3.569062	-2.000178	2.721221
C	3.753804	-3.239290	3.388230
H	3.449502	-3.083118	4.423935
H	4.809146	-3.541160	3.357814
H	3.138658	-4.027125	2.939336
C	-4.543564	0.436383	3.796584
H	-4.452259	-0.289024	4.611116
H	-3.978846	1.331973	4.088200
H	-5.595573	0.727659	3.712018
H	4.425444	-0.516379	-0.097903
O	4.646993	0.294102	1.785540
O	5.918220	1.957783	2.268270
C	6.756350	3.082465	1.918003
H	7.300182	3.295365	2.838863
H	7.462741	2.769464	1.146004
C	5.923947	4.270692	1.475571
H	5.397836	4.056175	0.540944
H	5.192597	4.539091	2.244251
H	6.581954	5.129873	1.308537
C	5.452167	1.225796	1.265982
O	5.713207	1.369054	0.090322
C	2.266050	2.280129	0.753571
O	2.227988	2.363347	1.963425
O	2.145507	3.281684	-0.110352
C	2.012989	4.620754	0.409844
H	1.805437	4.568458	1.479960
H	2.978558	5.111743	0.261508
C	0.906890	5.318965	-0.351770
H	-0.049280	4.813025	-0.188849
H	0.817824	6.352029	-0.000661
H	1.116106	5.333708	-1.425713

INT4-a

C	-0.232552	0.140007	-1.801240
O	-0.099908	-2.667019	-0.923736
O	-1.447934	-0.399414	-1.863940
O	0.526116	0.079389	-2.743721
O	0.001485	0.766330	-0.650132

H	0.745020	-3.149218	-0.644668
H	1.928846	-1.888387	-1.948341
N	2.915421	-2.043525	-1.796261
N	2.257604	-3.702661	-0.355784
C	3.223752	-2.945487	-0.815477
N	4.522761	-3.000855	-0.402387
C	1.232025	1.491347	-0.504106
H	0.943860	2.507679	-0.225232
H	1.735873	1.521655	-1.473410
C	2.115421	0.869234	0.547040
C	3.136075	1.637507	1.115964
C	1.988095	-0.463815	0.925841
C	4.026014	1.070523	2.023324
H	3.244163	2.684676	0.841065
C	2.875483	-1.022442	1.844262
H	1.213070	-1.083542	0.486997
C	3.915537	-0.274883	2.397672
H	4.818414	1.682772	2.448173
H	2.761449	-2.067688	2.118313
C	2.569241	-4.660751	0.689651
C	3.995722	-5.187071	0.574299
H	1.852275	-5.486504	0.621365
H	2.429203	-4.212160	1.687271
C	4.952720	-4.006099	0.560753
C	5.536762	-2.029539	-0.798926
C	3.850754	-1.079404	-2.345841
H	4.241192	-5.850843	1.409410
H	4.101541	-5.759988	-0.355042
H	5.962493	-4.329289	0.281401
H	5.018117	-3.551327	1.560902
C	4.912047	-0.742012	-1.310098
H	6.155577	-1.821014	0.081994
H	6.191774	-2.472155	-1.563920
H	3.283600	-0.191218	-2.635594
H	4.327352	-1.480362	-3.252039
H	5.688400	-0.109581	-1.751237
H	4.456434	-0.196572	-0.478634
C	-2.252898	-0.604737	-0.696668
C	-2.361708	-2.110447	-0.414023
C	-3.619171	-0.006335	-1.001865
H	-1.813370	-0.096035	0.163507
C	-1.065220	-2.733972	0.089915
H	-2.676667	-2.624398	-1.331009
O	-3.318976	-2.313394	0.622526

C	-4.604480	-0.364033	0.098144
H	-3.981642	-0.361441	-1.969260
O	-3.480353	1.415364	-1.039681
H	-0.743205	-2.200236	0.999830
H	-1.286183	-3.773014	0.374220
C	-4.625371	-1.882237	0.315665
H	-5.221404	-2.140129	1.198640
O	-5.140700	-2.475037	-0.829371
C	-5.379034	-3.870268	-0.700007
H	-5.856802	-4.189842	-1.626522
H	-6.047879	-4.069391	0.147125
H	-4.441657	-4.420092	-0.561022
C	4.907120	-0.898959	3.347628
H	5.135842	-0.229911	4.183933
H	4.527762	-1.840641	3.756596
H	5.852586	-1.115953	2.835322
H	-4.311897	0.112056	1.037820
O	-5.875764	0.133618	-0.311525
O	-7.850908	0.886361	0.088066
C	-6.755476	0.410324	0.657252
O	-6.567673	0.242052	1.843837
C	-8.924782	1.289691	0.970238
H	-9.005054	0.562082	1.780668
H	-9.813202	1.228508	0.340948
C	-8.705142	2.696413	1.490852
H	-9.564866	2.992274	2.101032
H	-7.807579	2.750966	2.113665
H	-8.609177	3.405850	0.663257
O	-3.611295	3.341287	-1.985419
C	-3.821321	2.047402	-2.170063
O	-4.243483	1.526622	-3.179307
C	-3.918026	4.202528	-3.105755
H	-3.308403	3.890289	-3.957777
H	-4.973118	4.073728	-3.361197
C	-3.609266	5.620254	-2.679945
H	-2.552461	5.729775	-2.418354
H	-3.831981	6.299890	-3.508461
H	-4.219260	5.912959	-1.820011

INT4-b

C	0.011469	-3.024056	0.402895
O	1.112810	-3.147760	1.136534
O	0.857195	-0.198254	0.996617
O	-1.082683	-3.229016	0.886545
O	0.239314	-2.728749	-0.873957
H	0.066465	1.182598	1.334509
H	-0.949765	-0.606804	1.401888
N	-1.836161	-0.229256	1.756922
N	-0.752704	1.783794	1.623752
C	-1.878309	1.104719	1.852468
N	-3.021781	1.739217	2.182040
C	-0.906908	-2.647951	-1.746465
H	-1.542044	-3.520689	-1.577253
H	-0.460551	-2.721006	-2.740363
C	-1.695490	-1.370495	-1.599376
C	-1.067902	-0.123103	-1.620848
C	-3.086435	-1.416820	-1.502750
C	-1.814592	1.046765	-1.529950
H	0.012378	-0.056135	-1.690064
C	-3.833676	-0.242923	-1.425037
H	-3.594745	-2.378263	-1.477725
C	-3.209214	1.007613	-1.428688
H	-1.296972	2.003114	-1.534326
H	-4.917453	-0.302561	-1.348651
C	-0.662633	3.203688	1.901758
C	-1.972082	3.868337	1.504242
H	0.182321	3.609948	1.346223
H	-0.463806	3.374999	2.969658
C	-3.111117	3.198263	2.257489
C	-4.245218	0.991777	2.462508
C	-2.974221	-1.092809	2.022106
H	-1.956492	4.935093	1.744376
H	-2.120710	3.763000	0.423332
H	-4.077876	3.493076	1.835342
H	-3.106605	3.502017	3.312738
C	-3.919129	-0.396808	2.988411
H	-4.814976	1.561327	3.202946
H	-4.851746	0.926605	1.547871
H	-2.593467	-2.025080	2.440687
H	-3.491004	-1.333587	1.087028
H	-4.841102	-0.975066	3.093563

H	-3.454443	-0.315349	3.977966
C	1.964339	-0.385285	0.225344
C	2.897297	-1.454909	0.846261
C	2.730739	0.933347	-0.011289
H	1.724627	-0.753002	-0.795761
C	2.414917	-2.885188	0.600529
H	2.977182	-1.257622	1.922968
O	4.208462	-1.502673	0.262563
C	4.095640	0.702267	-0.627604
H	2.812577	1.498674	0.918850
O	1.938522	1.685345	-0.954084
H	2.434042	-3.100780	-0.469268
H	3.074676	-3.583840	1.118369
C	4.894210	-0.280470	0.228175
H	5.860939	-0.508662	-0.238422
O	5.076153	0.284212	1.488848
C	5.939230	-0.462744	2.332196
H	6.062129	0.119255	3.246439
H	6.917666	-0.606333	1.854714
H	5.507564	-1.440289	2.574975
C	-4.019888	2.273143	-1.307817
H	-3.475751	3.137448	-1.701392
H	-4.969811	2.193443	-1.846404
H	-4.258253	2.483294	-0.258159
H	3.991309	0.271022	-1.626350
O	4.762425	1.965165	-0.730811
C	5.641843	2.108912	-1.723369
O	6.119232	3.344855	-1.669530
O	5.949468	1.253013	-2.527496
C	7.063762	3.726241	-2.695249
H	7.619259	4.549126	-2.243909
H	7.742249	2.890082	-2.877639
C	6.351407	4.163031	-3.960518
H	5.663901	4.988833	-3.753162
H	7.091636	4.505613	-4.691169
H	5.790514	3.334741	-4.403083
C	1.722330	2.974921	-0.735616
O	2.171704	3.646646	0.171045
O	0.898228	3.415529	-1.683262
C	0.522243	4.806021	-1.612498
H	0.099051	5.006862	-0.624256
H	1.420356	5.417276	-1.738059
C	-0.488346	5.051500	-2.710662
H	-1.376328	4.427236	-2.570296

H	-0.798284	6.100915	-2.688882
H	-0.059839	4.837092	-3.694295

INT4-c

C	-0.621007	-2.164581	0.874174
O	-0.278197	-2.327472	-2.337335
O	-1.777173	-2.403258	0.254523
O	-0.022109	-3.062259	1.422021
O	-0.227519	-0.894821	0.818018
H	0.443646	-1.632769	-2.394833
H	2.053229	-2.018387	-0.787891
N	2.911156	-1.529044	-0.997169
N	1.590948	-0.399298	-2.488318
C	2.727471	-0.466438	-1.854438
N	3.786966	0.381776	-2.032824
C	0.823868	-0.526506	1.723126
H	1.564075	-1.330357	1.750679
H	0.376998	-0.440145	2.719045
C	1.457653	0.768031	1.289984
C	2.564188	1.225740	2.013550
C	1.005319	1.523986	0.212462
C	3.214389	2.399853	1.651705
H	2.926843	0.653374	2.865223
C	1.664320	2.699092	-0.147763
H	0.143115	1.198179	-0.357201
C	2.782976	3.152055	0.552178
H	4.078288	2.730706	2.223800
H	1.304479	3.269923	-1.001153
C	1.360389	0.719236	-3.384988
C	2.646160	1.232845	-4.022048
H	0.877864	1.542955	-2.835698
H	0.651372	0.401829	-4.158028
C	3.651799	1.529504	-2.920881
C	4.908309	0.417837	-1.100502
C	3.968834	-1.589954	-0.002559
H	3.053709	0.472561	-4.699244
H	2.459625	2.139753	-4.606204
H	3.343670	2.415871	-2.347686
H	4.639526	1.739070	-3.345873
C	5.230705	-0.975591	-0.584227

H	5.768074	0.832319	-1.636468
H	4.680631	1.093857	-0.263035
H	4.126857	-2.638565	0.263613
H	3.691657	-1.046141	0.912449
H	6.006928	-0.914541	0.184193
H	5.607442	-1.598213	-1.403733
C	-2.587730	-1.401651	-0.372355
C	-1.948524	-0.719877	-1.590449
C	-3.125945	-0.377188	0.627676
H	-3.435010	-1.991019	-0.736382
C	-1.488492	-1.700490	-2.671597
H	-1.092877	-0.109411	-1.291714
O	-2.952769	0.108691	-2.176497
C	-4.062895	0.575354	-0.097780
H	-2.318832	0.173432	1.111876
O	-3.909924	-1.051890	1.617563
H	-2.247830	-2.476365	-2.823883
H	-1.402558	-1.128495	-3.607375
C	-3.393303	1.161097	-1.348541
H	-4.126158	1.707875	-1.952451
O	-2.362118	1.995858	-0.936412
C	-1.825697	2.800534	-1.976785
H	-1.073469	3.441778	-1.516093
H	-2.610119	3.422866	-2.425923
H	-1.361427	2.183525	-2.754100
C	3.532312	4.385512	0.116326
H	4.423254	4.110284	-0.462588
H	2.911841	5.027246	-0.516826
H	3.870267	4.973574	0.975877
O	-4.417144	1.592441	0.836242
H	-4.963608	0.042770	-0.415089
O	-5.745165	3.100390	1.604773
C	-6.971636	3.868559	1.591496
H	-6.722970	4.762357	2.164494
H	-7.197274	4.151060	0.561001
C	-8.108773	3.094918	2.228997
H	-8.345906	2.195784	1.653013
H	-7.855467	2.806159	3.253606
H	-9.001498	3.728233	2.259658
C	-5.579310	2.221121	0.630008
O	-6.333605	2.013911	-0.297249
O	-4.223875	-1.910349	3.564921
C	-3.779984	-2.269489	4.894402
H	-2.905120	-2.918194	4.800880

H	-3.487657	-1.355886	5.418427
C	-4.932545	-2.969247	5.578617
H	-5.219377	-3.874773	5.035616
H	-4.628052	-3.255192	6.590270
H	-5.802726	-2.310185	5.653368
C	-3.340262	-1.287031	2.804421
O	-2.210540	-0.979142	3.122400

INT4-d

C	-0.146078	-2.651855	-1.806435
O	0.936525	-3.046628	-1.150881
O	0.519238	-0.388375	0.954866
O	-0.086601	-2.319179	-2.972443
O	-1.257344	-2.693064	-1.073128
H	-0.082331	1.060553	1.863461
H	-0.151744	0.663926	-0.079522
N	-0.727613	1.497184	-0.386172
N	-0.690443	1.895284	1.860535
C	-1.207872	2.178797	0.653174
N	-2.147908	3.127907	0.507067
C	-2.475197	-2.233886	-1.672301
H	-3.033374	-3.115754	-2.001168
H	-2.230750	-1.638084	-2.555696
C	-3.264870	-1.428136	-0.671386
C	-4.608531	-1.148030	-0.945874
C	-2.690327	-0.910110	0.486816
C	-5.354442	-0.345805	-0.089033
H	-5.073804	-1.551673	-1.842985
C	-3.453131	-0.119757	1.348925
H	-1.639292	-1.085632	0.708148
C	-4.786029	0.187250	1.076059
H	-6.394466	-0.131823	-0.325745
H	-2.987613	0.272551	2.249720
C	-1.170981	2.486296	3.094663
C	-1.717706	3.879001	2.813675
H	-0.332215	2.529626	3.794235
H	-1.952885	1.860269	3.547160
C	-2.708652	3.829063	1.660655
C	-2.781901	3.361178	-0.791689
C	-1.265334	1.626571	-1.728324
H	-2.216273	4.272483	3.703395
H	-0.899344	4.561056	2.562790
H	-2.963376	4.842764	1.337046
H	-3.638279	3.330830	1.967036
C	-2.704465	2.120096	-1.669032
H	-3.826691	3.623718	-0.600152
H	-2.303299	4.220401	-1.279689
H	-1.206209	0.646284	-2.208555
H	-0.647925	2.320013	-2.314177
H	-3.065244	2.360552	-2.672891

H	-3.346514	1.337667	-1.251938
C	1.741847	-0.819687	0.526975
C	1.988963	-2.297440	0.892841
C	2.900101	0.001454	1.114432
H	1.851702	-0.745668	-0.576371
C	0.957078	-3.218416	0.281971
H	1.903408	-2.409256	1.983627
O	3.284282	-2.741687	0.468680
C	4.241985	-0.552910	0.671540
H	2.833360	0.030471	2.204280
O	2.788966	1.340125	0.603864
H	1.215204	-4.263958	0.463830
H	-0.019731	-2.992995	0.704201
C	4.350787	-2.032775	1.048301
H	5.257921	-2.475332	0.617745
O	4.370968	-2.128303	2.439194
C	4.630762	-3.437683	2.920170
H	4.704510	-3.361816	4.005793
H	5.577677	-3.818310	2.514476
H	3.820509	-4.126098	2.654562
C	-5.595019	1.069862	1.993763
H	-5.030662	1.329126	2.895229
H	-5.877494	2.003102	1.491745
H	-6.522275	0.576143	2.305302
H	4.347982	-0.467013	-0.412159
O	5.302516	0.170872	1.304297
O	6.791156	1.719495	1.374059
C	7.561127	2.791609	0.785523
H	8.402782	2.913037	1.468335
H	7.931174	2.467218	-0.189451
C	6.737261	4.061154	0.684590
H	5.889903	3.927695	0.005680
H	6.361502	4.358257	1.668613
H	7.365218	4.869697	0.295867
C	5.973638	1.057712	0.564534
O	5.865703	1.219960	-0.632404
C	2.472163	2.316512	1.448570
O	2.453795	2.247831	2.660743
O	2.189832	3.395386	0.725869
C	1.806312	4.582525	1.443730
H	1.274461	4.286031	2.350030
H	2.718665	5.112660	1.733696
C	0.939041	5.411516	0.521105
H	0.041193	4.855126	0.231039

H	0.628345	6.326021	1.036849
H	1.483928	5.694088	-0.384709